THE EFFECT OF LOAD ON THE AIR-GAP FIELD AND FORCES IN INDUCTION MACHINES

A thesis presented for the degree of

DOCTOR OF PHILOSOPHY

of the

UNIVERSITY OF SOUTHAMPTON

in the

FACULTY OF ENGINEERING AND APPLIED SCIENCE

DEPARTMENT OF ELECTRICAL ENGINEERING

by

PETER ANDREW KAHAN

MAY 1980

UNIVERSITY OF SOUTHAMPTON

ABSTRACT

FACULTY OF ENGINEERING AND APPLIED SCIENCE

ELECTRICAL ENGINEERING

Doctor of Philosophy

THE EFFECT OF LOAD ON THE AIR-GAP FIELD AND FORCES IN INDUCTION MACHINES

by Peter Andrew Kahan

An accurate method is given for the determination, under load conditions, of the tooth-ripple flux and force pulsations produced by the relative motion of the slotted stator and rotor surfaces in induction machines. These pulsations are obtained using a conformal transformation field solution and the Maxwell stress function. When using conformal transformation to solve the field in the air-gap region, or in any region having a complicated polygonal boundary, it is necessary to evaluate integrals containing singularities numerically. A number of quadrature methods for performing this process are reviewed and two methods are described for the evaluation of Cauchy Principal Values which arise with boundaries having parallel sides.

The tooth-ripple flux and force pulsations are computed, for a given stator slot number, and a range of rotor slot numbers and rotor positions. The results are presented graphically. In order to assess the influence of slot combination on these pulsations, the peak to peak values of the largest flux, normal and tangential force pulsations are used as defining quantities. A number of simple equations are derived relating these quantities to the slot pitch difference, and these equations are used to determine the conditions under which the flux and force pulsations into a stator or rotor tooth are minimal. Furthermore, conclusions are drawn about the choice of slot combination.

In addition, the fundamental tooth-ripple components of torque are computed for the same slot combinations as the flux and force pulsations. The influence of slot combination on this torque component is examined. Conclusions of practical value are drawn from the results obtained.

ACKNOWLEDGEMENTS

I would like to express my gratitude to my supervisor, Dr. K. J. Binns, for his close involvement and interest in the research, and without whose help and guidance this thesis would not have been possible.

My particular thanks go to Miss J. E. Sutton for typing this thesis, and to Mr. J. P. Whitehorn for reading the manuscript.

I would also like to thank Professor P. Hammond, the members of the Department of Electrical Engineering of Southampton University, and my family and friends for their help and encouragement during the research and the writing of this thesis.

Finally, I would like to acknowledge the Science Research Council for their financial support.

LIST OF SYMBOLS

All quantities are measured in S.I. units.

ω_x carrier frequency

ω_y modulating signal frequency

μ_{cir} circumferential permeability

P_q specific slot permeance of a real machine

P_q' specific slot permeance of a machine with slots having parallel sides

$\underline{H}$ magnetic field strength

$\underline{J}$ current density

q number of phase belts per pole

N_S number of stator slots

N_R number of rotor slots

P pole pairs

$B_\Delta'R$ rotor difference field with respect to the stator m.m.f. slot harmonic having $(N_S + P)$ pole pairs

$B_\Delta'S$ stator difference field with respect to the rotor m.m.f. slot harmonic having $(N_R - P)$ pole pairs

$B_\Delta' = B_\Delta'S + B_\Delta'R$

$B_\Delta"R$ rotor difference field with respect to the stator m.m.f. slot harmonic having $(N_S - P)$ pole pairs

$B_\Delta"S$ stator difference field with respect to the rotor m.m.f. slot harmonic having $(N_R + P)$ pole pairs

$B_\Delta" = B_\Delta"R + B_\Delta"S$

n_S synchronous speed

$n_{rs} = n_S/(N_S + P)$

R radial component in cylindrical co-ordinates

θ tangential component in cylindrical co-ordinates

m,n harmonic orders

$\underline{D}$ electric flux density

$\underline{B}$ magnetic flux density

μ_o primary magnetic constant ($4\pi \times 10^{-7}$)

μ_r relative permeability

V scalar potential

grad nabla operator ($\underline{i}\frac{\partial}{\partial x} + \underline{j}\frac{\partial}{\partial y} + \underline{k}\frac{\partial}{\partial z}$)

$\nabla^2 = \frac{\partial^2}{\partial x^2} + \frac{\partial^2}{\partial y^2} + \frac{\partial^2}{\partial z^2}$

$\mu = \mu_o \mu_r$

t,z,u,v complex variables

Φ flux function

ψ potential function

W complex potential function

$\underline{Q}$ magnetic pole

$\underline{I}$ current

$\underline{m}$ dipole moment

$\underline{F}$ force

H_N normal component of field strength

H_T tangential component of field strength

F_N normal component of force

S_m sum of squares function

F_T	tangential component of force
E_r	error function
$\underline{x}$	vector of variables
$\underline{h}$	vector of constants
$\underline{G}$	vector of gradients
$\underline{y}$	the values of the vector of variables at the minimum
w_i	weights
X_i	nodes
a	lower limit of integration
b	upper limit of integration
A_i	coefficients of Gauss-Jacobi quadrature formulae
w(t)	weighting function
f(t)	continuous function
v(x)	transformed weighting function
g(x)	transformed continuous function
c_j	coefficients of Chebyshev series
$T_j(x)$	Chebyshev polynomials
S	slot width of the slot in singly-slotted region
S_A	slot width of upper slot in doubly-slotted region
S_B	slot width of lower slot in doubly-slotted region
g	air-gap width
I_1	current in slot in singly-slotted region and current in upper slot in doubly-slotted region
I_2	current in lower slot in doubly-slotted region

I_3 effective current in the air-gap

$\bar{\Phi}_A$, $\bar{\Phi}_B$ fluxes in teeth A and B

$\phi_{d1}, \phi_{d2}, \phi_{d3}, \phi_{d4}$ flux components in doubly-slotted region

$\phi_{s1}, \phi_{s2}, \phi_{s3}$ flux components in singly-slotted region

ϕ_n flux component in region containing no slots

F_{NA} normal force on tooth A

H_I magnetic field strength in iron

H_A magnetic field strength in air

L_i mean length of iron path

L_A mean length of air path

I_{NL} peak no-load current per phase

n_C number of turns per coil side

$I = n_C I_{NL}$

N_p number of poles

P_S stator slot pitch

P_R rotor slot pitch

$\bar{\Phi}_{TP}$ peak to peak value of the largest flux pulsation

$\bar{\Phi}_{FP}$ peak value of fundamental flux wave

K_{dn} distribution factor associated with n^{th} harmonic

K_{pn} pitch factor associated with n^{th} harmonic

K_d distribution factor

K_p pitch factor

T_{end} a tooth at the end of a phase belt

T_{middle}	a tooth contained within a phase belt
F_{NP}	peak to peak value of the largest normal force pulsation
B	flux density in the air-gap
L	axial length of the bore
F_{TP}	peak to peak value of the largest tangential force pulsation
T_m	useful torque produced by an induction motor
T_S	Peak value of fundamental tooth-ripple component of torque

LIST OF FIGURES

Figure 2.1 Heteropolar field in machine air-gap.

Figure 2.2 Homopolar field in machine air-gap.

Figure 2.3 Simplified air-gap geometry containing region Q where no-load boundary conditions are defined.

Figure 2.4 Simplified air-gap geometry containing region U where load boundary conditions are defined.

Figure 2.5 The mapping of a curve from the t to z planes.

Figure 2.6 Uniform field in t and w planes.

Figure 2.7 Simplified air-gap geometry used to calculate tooth forces.

Figure 2.8 Tooth force calculations using a conformal transformation field solution.

Figure 3.1 The mapping of the general polygonal boundary in the z-plane from the real axis of the t-plane using the Schwarz-Christoffel transformation equation.

Figure 3.2 General polygonal boundary with parallel sides.

Figure 3.3 An illustration of Powell's method showing a possible path from the guessed starting point to the minimum of the function.

Figure 3.4 The Simplex method in which a simplex first surrounds the minimum and is then shrunk until the solution is obtained to the desired accuracy.

Figure 4.1 A complicated boundary with four right-angled vertices.

Figure 4.2 The four types of integrand associated with the definite integral evaluated in Chapter 4.

Figure 4.3 Configuration in w-plane used to evaluate I_0 when $\alpha + \beta = 0$.

Figure 4.4 Configuration in w-plane used to evaluate I_0 when $\alpha + \beta < 0$.

Figure 4.5 A pair of semi-closed slots shown in the z-plane.

Figure 4.6 A pair of semi-closed slots and a possible equivalent open slot configuration.

Figure 5.1 Some typical induction motor slot profiles.

Figure 5.2 The slot leakage flux pattern of a high voltage and normal induction machine.

Figure 5.3 A representation of the slotted-boundary of an induction machine.

Figure 5.4 Representation of the singly-slotted boundary in the z-plane and its relationship with the complex t-plane.

Figure 5.5 Representation of the doubly-slotted boundary in the complex z-plane and its relationship with the complex t-plane.

Figure 5.6 Two doubly-slotted boundaries having a positive and negative displacement, d. A simple relationship exists between these two sets of transformation constants.

Figure 5.7 The most complicated section of the slotted air-gap boundary in which the flux in a tooth has been calculated.

Figure 5.8 A region containing no slots.

Figure 5.9 The singly-slotted region showing the correct boundary conditions.

Figure 5.10 The separate boundary conditions on the singly-slotted boundary used to determine the direction of flux.

Figure 5.11 The doubly-slotted region showing the correct boundary conditions.

Figure 5.12 The tangential force on two consecutive teeth.

Figure 5.13 The section of slotted air-gap boundary used to illustrate the calculation of the total normal force on a tooth.

Figure 5.14 A simplified block diagram of the computer program which calculates the total flux in any tooth and the total tangential and normal forces.

Figure 6.1 A section of the slotted air-gap boundary showing the path of integration taken to obtain part of the m.m.f. distribution.

Figure 6.2 A typical m.m.f. distribution, the current carrying conductors in the slot have been replaced by point current sources as is the case in conformal transformation.

Figure 6.3 The stator current distribution on no-load at the instant when the current in phase A is zero.

Figure 6.4 The m.m.f. distribution associated with the current distribution shown in Figure 6.3.

Figure 6.5 The tooth-ripple flux pulsations in a rotor tooth at a load level of 2.5 : 1.

Figure 6.6 The tooth-ripple flux pulsations in a rotor tooth at a load level of 5 : 1.

Figure 6.7 The stator current distribution on load at the same instant in time as the current distribution in Figure 6.3.

Figure 6.8 The m.m.f. distribution associated with the current distribution shown in Figure 6.7.

Figure 6.9 The smoothed m.m.f. waveform used to calculate the rotor m.m.f.

Figure 6.10 An approximate rotor m.m.f. distribution for the slot combination N_S= 36, N_R = 32, rotor displacement d = 0.0.

Figure 6.11 A section of the slotted air-gap boundary illustrating the two conditions discussed in Section 6.5.

Figure 6.12 The complete stator and rotor current and air-gap m.m.f. distributions for the slot combination N_S = 36, N_R = 32, rotor displacement d = 0.0.

Figure 7.1 The stator and rotor flux distributions for the slot combination N_S = 36, N_R = 30 and d/g = 5.0.

Figure 7.2 The time history of the tooth-ripple flux in a rotor tooth for the slot combination N_S = 36, N_R = 24.

Figure 7.3 The time history of the tooth-ripple flux in a rotor tooth for the slot combination N_S = 36, N_R = 28.

Figure 7.4 The time history of the tooth-ripple flux in a rotor tooth for the slot combination N_S = 36, N_R = 30.

Figure 7.5 The time history of the tooth-ripple flux in a rotor tooth for the slot combination N_S = 36, N_R = 32.

Figure 7.6 The time history of the tooth-ripple flux in a rotor tooth for the slot combination N_S = 36, N_R = 36.

Figure 7.7 The time history of the tooth-ripple flux in a rotor tooth for the slot combination N_S= 36, N_R = 40.

Figure 7.8 The time history of the tooth-ripple flux in a rotor tooth for the slot combination N_S = 36, N_R= 42.

Figure 7.9 The time history of the tooth-ripple flux in a rotor tooth for the slot combination N_S = 36, N_R = 44.

Figure 7.10 The time history of the tooth-ripple flux in a rotor tooth for the slot combination N_S = 36, N_R = 48.

Figure 7.11 The time history of the tooth-ripple flux in a rotor tooth for the slot combination N_S = 36, N_R = 60.

Figure 7.12 The variation in the peak to peak value of the largest flux pulsation as a fraction of the fundamental flux with the difference in slot pitches for the rotor.

Figure 7.13 The time history of the tooth-ripple flux in a stator tooth (T_{end}) for the slot combination $N_S = 36$, $N_R = 24$.

Figure 7.14 The time history of the tooth-ripple flux in a stator tooth (T_{end}) for the slot combination $N_S = 36$, $N_R = 28$.

Figure 7.15 The time history of the tooth-ripple flux in a stator tooth (T_{end}) for the slot combination $N_S = 36$, $N_R = 30$.

Figure 7.16 The time history of the tooth-ripple flux in a stator tooth (T_{end}) for the slot combination $N_S = 36$, $N_R = 32$.

Figure 7.17 The time history of the tooth-ripple flux in a stator tooth (T_{end}) for the slot combination $N_S = 36$, $N_R = 36$.

Figure 7.18 The time history of the tooth-ripple flux in a stator tooth (T_{end}) for the slot combination $N_S = 36$, $N_R = 42$.

Figure 7.19 The time history of the tooth-ripple flux in a stator tooth (T_{end}) for the slot combination $N_S = 36$, $N_R = 48$.

Figure 7.20 The time history of the tooth-ripple flux in a stator tooth (T_{middle}) for the slot combination $N_S = 36$, $N_R = 24$.

Figure 7.21 The time history of the tooth-ripple flux in a stator tooth (T_{middle}) for the slot combination $N_S = 36$, $N_R = 28$.

Figure 7.22 The time history of the tooth-ripple flux in a stator tooth (T_{middle}) for the slot combination $N_S = 36$, $N_R = 30$.

Figure 7.23 The time history of the tooth-ripple flux in a stator tooth (T_{middle}) for the slot combination $N_S = 36$, $N_R = 32$.

Figure 7.24 The time history of the tooth-ripple flux in a stator tooth (T_{middle}) for the slot combination $N_S = 36$, $N_R = 36$.

Figure 7.25 The time history of the tooth-ripple flux in a stator tooth (T_{middle}) for the slot combination $N_S = 36$, $N_R = 42$.

Figure 7.26 The time history of the tooth-ripple flux in a stator tooth (T_{middle}) for the slot combination $N_S = 36$, $N_R = 48$.

Figure 7.27 The variation in the peak to peak value of the largest tooth flux pulsation as a fraction of the fundamental flux with the difference in slot pitches for the stator.

Figure 8.1 The distribution of normal forces acting on the rotor teeth for the slot combination $N_S = 36$, $N_R = 48$ and $d/g = 0.0$.

Figure 8.2 The distribution of tangential forces acting on the rotor teeth for the slot combination $N_S = 36$, $N_R = 48$ and $d/g = 0.0$.

Figure 8.3 The variation in the normal force acting on a rotor tooth with displacement of the rotor for the slot combination $N_S = 36$, $N_R = 24$.

Figure 8.4 The variation in the normal force acting on a rotor tooth with displacement of the rotor for the slot combination $N_S = 36$, $N_R = 28$.

Figure 8.5 The variation in the normal force acting on a rotor tooth with displacement of the rotor for the slot combination $N_S = 36$, $N_R = 30$.

Figure 8.6 The variation in the normal force acting on a rotor tooth with displacement of the rotor for the slot combination $N_S = 36$, $N_R = 32$.

Figure 8.7 The variation in the normal force acting on a rotor tooth with displacement of the rotor for the slot combination $N_S = 36$, $N_R = 36$.

Figure 8.8 The variation in the normal force acting on a rotor tooth with displacement of the rotor for the slot combination $N_S = 36$, $N_R = 40$.

Figure 8.9 The variation in the normal force acting on a rotor tooth with the displacement of the rotor for the slot combination $N_S = 36$, $N_R = 42$.

Figure 8.10 The variation in the normal force acting on a rotor tooth with displacement of the rotor for the slot combination $N_S = 36$, $N_R = 44$.

Figure 8.11 The variation in the normal force acting on a rotor tooth with dispalcement of the rotor for the slot combination $N_S = 36$, $N_R = 48$.

Figure 8.12 The variation in the normal force acting on a rotor tooth with displacement of the rotor for the slot combination $N_S = 36$, $N_R = 60$.

Figure 8.13 The variation in the peak to peak value of the largest normal force pulsation acting on a rotor tooth with the difference in slot pitches.

Figure 8.14 The variations in the normal force acting on the two stator teeth, T_{end} and T_{middle}, with the displacement of the rotor for the slot combination $N_S = 36$, $N_R = 24$.

Figure 8.15 The variations in the normal force acting on the two stator teeth, T_{end} and T_{middle}, with the displacement of the rotor for the slot combination $N_S = 36$, $N_R = 28$.

Figure 8.16 The variations in the normal force acting on the two stator teeth, T_{end} and T_{middle}, with the displacement of the rotor for the slot combination $N_S = 36$, $N_R = 30$.

Figure 8.17 The variations in the normal force acting on the two stator teeth, T_{end} and T_{middle}, with the displacement of the rotor for the slot combination $N_S = 36$, $N_R = 32$.

Figure 8.18 The variations in the normal force acting on the two stator teeth, T_{end} and T_{middle}, with the displacement of the rotor for the slot combination $N_S = 36$, $N_R = 36$.

Figure 8.19 The variations in the normal force acting on the two stator teeth, T_{end} and T_{middle}, with the displacement of the rotor for the slot combination $N_S = 36$, $N_R = 40$.

Figure 8.20 The variations in the normal force acting on the two stator teeth, T_{end} and T_{middle}, with the displacement of the rotor for the slot combination $N_S = 36$, $N_R = 42$.

Figure 8.21 The variations in the normal force acting on the two stator teeth, T_{end} and T_{middle}, with the displacement of the rotor for the slot combination $N_S = 36$, $N_R = 44$.

Figure 8.22 The variations in the normal force acting on the two stator teeth, T_{end} and T_{middle}, with the dispalcement of the rotor for the slot combination $N_S = 36$, $N_R = 48$.

Figure 8.23 The variations in the normal force acting on the two stator teeth, T_{end} and T_{middle}, with the displacement of the rotor for the slot combination $N_S = 36$, $N_R = 60$.

Figure 8.24 The variations in the peak to peak values of the largest normal force pulsations acting on the two stator teeth (T_{end}, T_{middle}) with the difference in slot pitches.

Figure 8.25 The variation in the tangential force acting on a rotor tooth with displacement of the rotor for the slot combination $N_S = 36$, $N_R = 28$.

Figure 8.26 The variation in the tangential force acting on a rotor tooth with displacement of the rotor for the slot combination $N_S = 36$, $N_R = 30$.

Figure 8.27 The variation in the tangential force acting on a rotor tooth with displacement of the rotor for the slot combination $N_S = 36$, $N_R = 36$.

Figure 8.28 The variation in the tangential force acting on a rotor tooth with displacement of the rotor for the slot combination $N_S = 36$, $N_R = 42$.

Figure 8.29 The variation in the tangential force acting on a rotor tooth with displacement of the rotor for the slot combination $N_S = 36$, $N_R = 48$.

Figure 8.30 The variation in the peak to peak value of the largest tangential force pulsation acting on a rotor tooth with the difference in slot pitches.

Figure 8.31 The variations in the tangential force acting on the two stator teeth, T_{end} and T_{middle}, with displacement of the rotor for the slot combination $N_S = 36$, $N_R = 28$.

Figure 8.32 The variations in the tangential force acting on the two stator teeth, T_{end} and T_{middle}, with displacement of the rotor for the slot combination $N_S = 36$, $N_R = 30$.

Figure 8.33 The variations in the tangential force acting on the two stator teeth, T_{end} and T_{middle}, with displacement of the rotor for the slot combination $N_S = 36$, $N_R = 36$.

Figure 8.34 The variations in the tangential force acting on the two stator teeth, T_{end} and T_{middle}, with displacement of the rotor for the slot combination $N_S = 36$, $N_R = 42$.

Figure 8.35 The variations in the tangential force acting on the two stator teeth, T_{end} and T_{middle}, with displacement of the rotor for the slot combination $N_S = 36$, $N_R = 48$.

Figure 8.36 The variations in the peak to peak values of the largest tangential force pulsationsacting on the two stator teeth (T_{end}, T_{middle}) with the difference in slot pitches.

Figure 9.1 The variation in torque with displacement of the rotor for the slot combination $N_S = 36$, $N_R = 24$.

Figure 9.2 The variation in torque with dispalcement of the rotor for the slot combination $N_S = 36$, $N_R = 28$.

Figure 9.3 The variation in torque with displacement of the rotor for the slot combination $N_S = 36$, $N_R = 30$.

Figure 9.4 The variation in torque with displacement of the rotor for the slot combination $N_S = 36$, $N_R = 32$.

Figure 9.5 The variation in torque with displacement of the rotor for the slot combination $N_S = 36$, $N_R = 36$.

Figure 9.6 The variation in torque with displacement of the rotor for the slot combination $N_S = 36$, $N_R = 40$.

Figure 9.7 The variation in torque with displacement of the rotor for the slot combination $N_S = 36$, $N_R = 42$.

Figure 9.8 The variation in torque with displacement of the rotor for the slot combination $N_S = 36$, $N_R = 44$.

Figure 9.9 The variation in torque with displacement of the rotor for the slot combination $N_S = 36$, $N_R = 48$.

Figure 9.10 The variation in torque with displacement of the rotor for the slot combination $N_S = 36$, $N_R = 60$.

Figure 9.11 The tangential force pulsations acting on the stator teeth of the slot combination $N_S = 36$, $N_R = 36$, showing clearly that most of the pulsations are in phase with each other.

Figure 9.12 The tangential force pulsations acting on the stator teeth of the slot combination $N_S = 36$, $N_R = 30$, showing that the pulsations are not in phase with each other.

CONTENTS

Page No.

ABSTRACT

ACKNOWLEDGEMENTS

LIST OF SYMBOLS i.

LIST OF FIGURES vi.

CHAPTER 1 INTRODUCTION 1

1. Introduction 2

1.1 Tooth-Ripple Fluxes 3

1.2 Tooth-Ripple Forces 5

1.3 Harmonic Tooth-Ripple Torques 6

1.4 Numerical Methods in Conformal Transformation 7

1.5 Literature Review 8

1.5.1 Tooth-Ripple Fluxes and Forces 8

1.5.2 Harmonic Tooth-Ripple Torques 10

1.5.3 Layer Theory 19

1.6 Scope of the Work 22

1.7 Breakdown of the Subject 22

1.8 References 25

CHAPTER 2 THE CALCULATION OF MAGNETIC FIELDS AND FORCES IN THE AIR-GAP REGION OF AN INDUCTION MOTOR 28

2. Introduction 29

2.1 The Air-Gap Field in an Induction Motor 29

2.2 A Comparison of Some Two-Dimensional Field Methods 30

2.3 Two-Dimensional Field Solutions 34

2.3.1 Derivation of Boundary Conditions for No-Load and Load Cases 36

2.4 Conformal Transformation 41

2.5 The Calculation of Magnetic Forces 45

2.5.1 The Calculation of Tooth Forces Under Load Conditions 47

2.6 References 50

Figures 2.1 - 2.8 51

Page No.

CHAPTER 3 THE APPLICATION OF CONFORMAL TRANSFORMATION METHODS TO COMPLICATED POLYGONAL BOUNDARY PROBLEMS 59

3. Introduction 60

3.1 Schwarz-Christoffel Transformation 61

3.2 The Constant Finding Process 62

3.2.1 Definite Integral 63

3.2.2 Residues 63

3.2.3 Improper Integral 65

3.3 Simple Description of Direct-Search Methods 67

3.3.1 Peckham's Method 69

3.4 References 72

Figures 3.1 - 3.4 73

CHAPTER 4 THE ANALYTICAL AND NUMERICAL EVALUATION OF INTEGRALS ENCOUNTERED IN CONFORMAL TRANSFORMATION PROBLEMS 77

4. Introduction 78

4.1 Limitations of Analytical Methods 79

4.2 Quadrature Methods 81

4.3 Methods for the Solution of Integrals with End-Point Singularities 84

4.3.1 Integrals Associated with Boundaries having Right-Angle Vertices 85

4.3.2 Integrals Associated with a General Boundary Shape 86

4.3.3 Displacing the Singularity 86

4.3.4 The Change of Variable Method 88

4.3.5 Gauss-Jacobi Method 89

4.3.6 The Method of Branders and Piessens 90

4.3.7 A Comparison of the Different Forms of Quadrature 92

4.4 The Evaluation of Cauchy Principal Values 92

4.4.1 Evaluation of the Integral using the Chebyshev Series 93

4.4.2 Evaluation of C_r 95

4.4.3 Cases where I_0 and I_1 can be Evaluated Analytically 95

4.4.4 The Evaluation of the Improper Integral by Subtracting Out the Singularity 98

Page No.

4.4.5 A Comparison of the Two Methods 99

4.5 A Further Problem 102

4.6 Conclusions 104

4.7 References 105

Figures 4.1 - 4.6 107

CHAPTER 5 THE CALCULATION OF THE TOTAL FLUX ENTERING ANY TOOTH AND THE TANGENTIAL AND NORMAL FORCES ACTING ON IT 113

5. Introduction 114

5.1 List of Assumptions 115

5.2 Division of Air-gap into Regions 117

5.3 The Transformation Equations of the Singly and Doubly-Slotted Boundaries 117

5.3.1 Singly-Slotted Boundary 117

5.3.2 Doubly-Slotted Boundary 119

5.4 The Calculation of Flux in a Tooth 124

5.4.1 The Calculation of the Flux Components in the Singly-Slotted Region 126

5.4.2 The Calculation of the Flux Components in the Doubly-Slotted Region 127

5.5 The Relationship between Field and Force Distributions 130

5.6 The Tangential Force Acting on a Tooth 131

5.7 The Normal Force Acting on a Tooth 133

5.8 The Computer Program 135

5.9 References 137

Figures 5.1 - 5.14 138

CHAPTER 6 A METHOD FOR CALCULATING THE APPROXIMATE ROTOR CURRENT AND AIR-GAP M.M.F. DISTRIBUTIONS 154

6. Introduction 155

6.1 The Concept of a Distributed M.M.F. 156

6.2 Assumptions 158

6.3 The Calculation of the Peak Value of the Fundamental No-Load M.M.F. 161

Page No.

6.4 The Calculation of an Approximate Rotor Current Distribution on Load. 162

6.5 The Calculation of the Air-gap M.M.F. in the Conformal Transformation Model 165

6.6 References 168

Figures 6.1 -6.12 169

CHAPTER 7 AN EXAMINATION OF THE TOOTH-RIPPLE FLUX PULSATIONS ON LOAD 181

7. Introduction 182

7.1 Flux Distribution 183

7.2 The Tooth-Ripple Flux Pulsations in a Rotor Tooth 183

7.3 The Tooth-Ripple Flux Pulsations in Two Stator Teeth, One Contained Within and One at the End of a Phase Belt 187

7.4 Conclusions 190

7.5 References 192

Figures 7.1 - 7.27 193

CHAPTER 8 AN EXAMINATION OF THE NORMAL AND TANGENTIAL TOOTH-RIPPLE FORCE PULSATIONS UNDER LOAD 220.

8. Introduction 221

8.1 The Normal Force Pulsations acting on a Rotor Tooth Tooth 222

8.2 The Normal Force Pulsations acting on a Stator Tooth 223

8.3 The Tangential Force Pulsations acting on a Rotor Tooth 224

8.4 The Tangential Force Pulsations acting on a Stator Tooth 225

8.5 Conclusions 226

8.5.1 Normal Force Pulsations 226

8.5.2 Tangential Force Pulsations 227

8.5.3 General Conclusions 227

8.6 References 228

Figures 8.1 - 8.36 229

Page No.

CHAPTER 9 HARMONIC TOOTH-RIPPLE TORQUES ON LOAD 265.

9. Introduction 266

9.1 Discussion of Results 266

9.2 Conclusions 269

Figures 9.1 - 9.12 271

CHAPTER 10 CONCLUSIONS 283

10. Introduction 284

10.1 Summary of Detailed Conclusions 289

10.1.1 Numerical Evaluation of the Integrals Associated with Conformal Transformation 289

10.1.2 Tooth-Ripple Flux Pulsations 290

10.1.3 Normal Tooth-Ripple Force Pulsations 291

10.1.4 Tangential Tooth-Ripple Force Pulsations 292

10.1.5 General Conclusions Relating to the Force Pulsations 293

10.1.6 Harmonic Tooth-Ripple Torques 293

10.2 Discussion 294

10.3 Suggestion for Further Work 296

10.4 Reference 297

APPENDIX 1 THE ANALYTICAL SOLUTION OF AN ELLIPTIC INTEGRAL 298

BIBLIOGRAPHY 301

CHAPTER 1

INTRODUCTION

1. Introduction

1.1 Tooth-Ripple Fluxes

1.2 Tooth-Ripple Forces

1.3 Harmonic Tooth-Ripple Torques

1.4 Numerical Methods in Conformal Transformation

1.5 Literature Review

1.5.1 Tooth-Ripple Fluxes and Forces

1.5.2 Harmonic Tooth-Ripple Torques

1.5.3 Layer Theory

1.6 Scope of the Work

1.7 Breakdown of the Subject

1.8 References

1. Introduction

The polyphase induction motor is a very simple and robust machine. It is manufactured in a wide range of sizes with power outputs ranging from a few watts to many megawatts. Although its design is now largely routine, there is scope for additional research into problems relating to parasitic harmonic fluxes, forces and torques. These phenomena arise as a result of the distributed windings and the slotted nature of the stator and rotor. They cause such problems as stray losses, magnetic noise and crawling (stable running at low speeds). These parasitic effects will always be present in induction motors to some extent because of the nature of their construction. It is the designer's responsibility to contain them within acceptable limits. Over the last fifty years a number of rules have been developed to reduce these effects[1.1, 1.2, 1.3]. However, these rules should not be regarded as hard and fast because if they are rigorously applied, they often lead to the conclusion that no design is acceptable, rather than help the designer find the best compromise. Also, in applying a certain set of rules to minimise one effect, another effect can be made too large. Any new information which helps the designer to make machines quieter and more efficient is welcome.

It has long been known that the performance of an induction motor is highly dependent on the number of stator and rotor slots (the slot combination). With one slot combination the machine may have a satisfactory performance whilst a slightly different combination can display some undesirable effect such as crawling, cogging, or be extremely noisy. The designer has only a limited range of stator slot numbers to choose from. The choice of a particular stator slot number is governed

mainly by the number of poles but is also closely related to the suppression of the harmonics in the m.m.f. wave of the stator winding. In practice, the machine designer has essentially only to choose a suitable number of rotor slots. It is because the choice of slot combination, or more particularly rotor slot number, is so important in avoiding undesirable effects, that its influence on parasitic fluxes and forces is considered here.

The work presented in this thesis is a continuation of a previous investigation into parasitic fluxes, forces and torques in induction motors. At the beginning of this research, it was decided to calculate these parasitic effects under no-load and load conditions. This distinction was mainly made because designers wish to distinguish between effects that occur on no-load and effects that occur on load. Binns and Rowlands-Rees[1.4, 1.5] have examined the no-load case and determined a set of relationships between the flux and force pulsations and the air-gap dimensions (slot widths and pitches). From these relationships a number of design rules have been obtained.

In this thesis, the parasitic fluxes, forces and torques are calculated under load conditions. The main purpose of this research is to determine the relationships between slot combination and the parasitic fluxes and forces on load. In addition, the variation of torque with rotor displacement over a rotor slot pitch is determined for a number of slot combinations. From these torque variations, the high frequency components of torque, periodic in a rotor slot pitch, or a fraction of a slot pitch, can be obtained. It is then possible to assess the influence of slot combination on such torque components.

1.1 Tooth-Ripple Fluxes

The stator or rotor tooth-ripple flux is that component of flux

in a stator or rotor tooth, periodic in a rotor or stator slot pitch, or sub-multiples of these pitches, which arises as a result of the relative motion of the two slotted surface.

Binns and Schmid[1.6] show that the stator and rotor tooth-ripple fluxes are important components of stray loss. Furthermore, they define a modulation process in which these high frequency flux components are modulated by the low frequency m.m.f. harmonics. This modulation process is now briefly described.

The basic modulation process is conveniently expressed in terms of two sinusoidal waves, $x = X\cos w_x t$ and $y = Y\cos w_y t$. The product of these two waves, z, called the modulated signal, can be expanded to give

$$z = \frac{XY}{2}\left[\cos (w_x + w_y)t + \cos (w_x - w_y)\, t\right] \qquad (1.1)$$

where y is arbitrarily chosen to be the modulating signal and x is the carrier. Equation (1.1) shows that the resultant product is equivalent to the sum of two sine waves shifted in angular frequency from the carrier frequency w_x by $\pm w_y$. In the case of the air-gap field, the modulating signal is the m.m.f. However, as is shown shortly, this signal is not a pure sine wave, and there is a series of such functions each representing an m.m.f. harmonic. For each of these m.m.f. harmonics, a separate modulation process applies, and so the upper side-band has a frequency $w_x + mw_y$, where m is the order of the m.m.f. harmonic, and the lower side-band has frequency $w_x - mw_y$. The high frequency carrier signal represents the influence of the boundaries (tooth-ripple flux) and it also has harmonic components. Therefore, the modulation process applies not only to the fundamental tooth-ripple component but to all its harmonics, and, in practice, the variation due to slotting is sufficiently non-sinusoidal for the second and third

harmonics to be appreciable.

Binns and Schmid used an experimental approach, involving the use of search coils, to measure the tooth-ripple fluxes in a particular machine. In this thesis, the tooth-ripple flux components associated with the stator and rotor teeth are computed, using a numerical conformal transformation, for a number of slot combinations. The influence of slot combination on the amplitude of these flux components is then examined.

1.2 Tooth-Ripple Forces

The stator or rotor tooth-ripple force is defined as that component of force acting on an individual stator or rotor tooth periodic in a rotor or stator slot pitch, or sub-multiples of these slot pitches, which arise as a result of the relative motion of the two slotted surfaces. It is convenient, for the purpose of analysis, to separate the tooth-ripple forces into their tangential and normal components. These force pulsations are of particular importance in the study of noise and vibration in electrical machines.

This study involves a detailed consideration of the various sources of noise in induction machines. A comprehensive review of the various sources of noise in electrical machines is given by Ellison and Moore[1.2]. One important source which they identify is the flux distribution in the air-gap. It is normal when examining noise from this source to calculate the radial force distribution associated with the air-gap field. The tangential force distribution can also be calculated and its effect studied[1.2]. The normal force distribution can be resolved into an infinite number of force waves revolving around the air-gap of the machine. The force waves which are most important in the production of noise and vibration are those for which the number of poles are small, since the stator and rotor are least stiff to these modes of

vibration. In practice, only stator core vibration is normally considered as the rotor is usually sufficiently stiff to all but a 2-pole force wave. Therefore, stator core vibration is investigated by applying the simple force waves to a model representing the core. Such an analytical model usually consists of a combination of thick and thin annular cores of homogenous material and reveals the appropriate resonances. However, practical cores respond significantly to most force harmonics to which they are subjected. Tests on machines reveal that the combined structure consisting of stator core, frame and winding does not simply vibrate at a few discrete frequencies corresponding to the resonances of a particular model, but the response of the structure is of a very complex nature and is distributed over the whole frequency spectrum. An important part of the reduction of noise is the minimisation of the amplitude of the tooth-ripple normal force carrier. This force carrier has been computed for a number of slot combinations in this thesis.

In addition to stator core vibration, the resonant frequencies of the teeth of large machines come within the audible range[1.2], so that it is possible that such resonances will be excited and sound radiated directly from the teeth.

1.3 Harmonic Tooth-Ripple Torques

These harmonic torques are defined as the components of the torque, periodic in a rotor slot pitch, or sub-multiples of a rotor slot pitch.

As in the case of the tooth-ripple fluxes and forces, these harmonic torques are computed under steady state conditions. However, if these torque components are large under these conditions, it is reasonable to assume that they will also be large under starting

conditions, for the same slot combination, especially as the stator and rotor currents are larger. Such harmonic torques can give rise to crawling in a machine.

1.4 Numerical Methods in Conformal Transformation

The study of tooth-ripple phenomena has involved the use of conformal transformation methods. The reasons this method has been chosen in preference to other methods for calculating magnetic fields is explained in the next chapter.

The method of conformal transformation is a powerful analytical method and has been used widely in both engineering and physics. The range of problems that can be treated has greatly increased since the introduction of the digital computer to solve numerical optimisation problems.

The first of any problem involving conformal transformation consists of finding a number of constant terms contained in the transformation equation. To find these constant terms, it is necessary to formulate and solve a set of non-linear equations. These equations are found by integrating the transformation equation between specific limits and relating these integrals to the dimensions of the geometry under consideration. For simple boundaries the equations can be solved analytically, but for complicated ones a numerical method must be used.

With a numerical approach there are two problems to overcome.

(i) The solution of a set of non-linear simultaneous equations. These are implicit equations and the constant terms have to be found using a numerical optimisation method.

(ii) The numerical evaluation of the associated integrals.

In the last two decades, there has been a rapid development in methods of optimisation suitable for use with the digital computer.

There are, therefore, a number of methods available for solving the non-linear equations that arise with conformal transformation.

The integrals that arise in conformal transformation are usually definite, but have integrands with critical points at both limits of integration. These critical points can present difficulties, since they can be either poles, in which case the integrand has an infinite value at the limits of integration, or they can be zeroes, in which case the integrand has an infinite first derivative, or a mixture of the two. A number of methods are available for the evaluation of this type of integral and these are discussed in detail later.

There is another type of integral that arises when dealing with boundaries having parallel sides which meet at infinity. This is an improper integral which in addition to having critical points at both limits of integration has a simple pole within the range of integration. This type of integral is known as a 'Cauchy Principal Value'. Previous to this research, there were no methods available which could be used to give results of sufficient accuracy. This stimulated an investigation by Binns, Rowlands-Rees and the present author into the evaluation of this type of integral and two methods have been developed for its evaluation.

1.5 Literature Review

1.5.1 Tooth-Ripple Fluxes and Forces

Apart from the previous work by Binns and Rowlands-Rees[1.4,1.5], other work on the computation of tooth-ripple phenomena is very limited.

A number of researchers have used two-dimensional field solutions in conjunction with the Maxwell stress function to calculate the forces on various machine members. For example, a number of authors, including Carpenter[1.7], have calculated the force which aligns two salient

poles. Lehmann[1.8] discusses the calculation of magnetic attraction between two bodies by using flux plots, and takes as an example the attraction between a salient pole and the armature of an electrical machine. Carter[1.9] used the conformal transformation field solution of a singly-slotted boundary to calculate the forceson teeth, as has Dvoracek[1.10]. Binns[1.11] has calculated the centring forces on a displaced ventilating duct in a machine, using the conformal transformation solution of a doubly-slotted boundary in conjunction with the Maxwell stress function. Whilst this earlier work differs in practical application from the work on the no-load flux and force pulsations and from the present work, it does form the basis for much of this later work.

Liebmann[1.12] has also calculated the forces which tend to align two doubly-slotted boundaries. The method used to calculate the forces differs from that used by Binns; the force in this method is given as the product of the rate of change of flux and the magnetic potential. The total change in flux was obtained experimentally using a resistive network analogue and the rate of change of flux was calculated from the experimental results. However, difficulties arise in obtaining an accurate result because the change in total flux is small. Furthermore, once the approximate variation of the flux with displacement has been determined, numerical differentiation greatly increases any inaccuracies.

It was thought advantageous to consider a boundary integral method, developed by Trowbridge and Simkin[1.13], and compare this with the method of conformal transformation. The boundary integral method depends upon a direct application of Green's Theorem and has been used in a number of harmonic problems[1.14], including those arising in magnetostatic. Magnetic problems involving finite permeability and distributed conductors can be solved by subdividing the boundaries

into line elements. The boundary integral method and conformal transformation have been used to compute the fluxes entering and the normal and tangential forces acting on several teeth of an induction motor. The Maxwell stress function is also used to determine the forces in the boundary integral method. A comparison of the two methods reveals that the method of conformal transformation is of the order of one hundred times faster than the boundary integral method[1.15]. Further details about both methods are given in Chapter 2.

The finite element method has become a very popular method in the solution of two and three dimensional field problems and can be used in the treatment of saturable magnetic field problems[1.16]. A complete review of this method is given by Norrie and Vries[1.17] and by Jabbar[1.18]. This method has not been used in the present research because hundreds of field solutions are required to investigate the parameters of interest and it would simply be too costly in computer time and storage to use finite elements.

1.5.2 Harmonic Tooth-Ripple Torques

A number of authors, including Liwschitz[1.19], Oberretl[1.20] and Alger[1.3], have published work on parasitic torques in induction motors. However, some of these authors[1.19, 1.20] have entirely ignored the effects of the slotted stator and rotor on the torque. Others[1.3] do allow for the effectsof slotting but use a method to calculate the air-gap field which can only be regarded as giving an approximate solution of this field. To fully understand this, it is necessary to briefly review these methods.

The methods most commonly used to calculate the air-gap field in induction motors are based on the well-known approach of representing the flux distribution by a family of harmonic flux waves. Each

of these harmonic flux components varies sinusoidally in both time and space and is associated with a pole number appropriate to its harmonic order. The most important of these flux waves is the fundamental which rotates at synchronous speed (n_s) and produces the useful torque of the machine. The remaining flux components are regarded as parasitic and can be divided into those components which travel in the same direction as the fundamental and those which travel in the opposite direction. The speed at which these harmonic flux waves rotate lies between zero and synchronous speed and are dependent on their harmonic orders. Each flux wave is normally associated with either the stator or rotor surfaces. There are essentially two approaches available for calculating these flux waves. Both approaches can be used to obtain a quantative analysis of the useful and parasitic torques produced by a motor. Before describing these approaches, it is necessary to briefly discuss the concept of a distributed m.m.f. This subject will be discussed in greater detail in Chapter 6.

The basis of the m.m.f. distribution is the relation curl $\underline{H} = \underline{J}$. The m.m.f. is obtained by integrating the current distribution from an arbitrary origin and can be considered to have a distribution around the air-gap in θ, the angle subtended at the centre of the machine. It is easily shown[1.3 , 1.21] that, as the stator currents alternate, the m.m.f. of the stator currents is equivalent to a family of waves, each harmonic component of which varies sinusoidally in space and time, and is associated with a pole number appropriate to its harmonic order.

In the first approach used to calculate the air-gap field, the production of the flux wave is exclusively attributed to the effects of the stator and rotor windings. The permeance of the air-gap is assumed uniform, that is, the stator and rotor are assumed to have

smooth surfaces. The stator and rotor current distributions are analysed in terms of m.m.f. waves and it is assumed that the flux waves are proportional to these m.m.f. waves. This method is described in detail in the book by Liwschitz-Garik and Whipple[1.22]. The authors describe the construction of tables of stator and rotor m.m.f. harmonic pole pairs. Each harmonic pole pair has either a positive or negative sign attached to it, depending on whether it is travelling in the same direction as the fundamental flux wave or in the opposite direction, when the rotor is stationary. These tables can be used to predict the occurrence of such parasitic torque phenomena as asynchronous crawling, synchronous crawling and cogging.

Oberretl[1.20, 1.23] takes this analysis a stage further and assumes that the flux waves produced by the rotor m.m.f. waves induce currents in the stator windings which in turn produce more stator m.m.f. waves, and sometimes extends this up to a fourth order of reaction. He has also considered the currents in the individual slots to be distributed over the width of the slot rather than concentrated at points. The rotor currents are calculated by solving a series of linear simultaneous equations which relate these currents to the terminal voltages and machine inductances. The torque is then obtained from these quantities. A numerical and experimental example is given, but it is for the rather impractical machine having 2 poles, 6 stator slots and 7 rotor slots.

It is important to emphasise that in the methods just discussed, the slotted stator and rotor are replaced by a stator and rotor having smooth surfaces. Therefore, although there are m.m.f. and consequently flux harmonics having a wavelength of a similar order to the wavelengths of the stator and rotor slot pitches or sub-multiples of these pitches, there are no additional field harmonics due to slotting alone.

Furthermore, it is not possible to assess the influence of slotting on the torque characteristic of an induction machine. In fact, the stator and rotor slots considerably modify the flux distribution in the air-gap and should, therefore, be taken into account in any analysis.

The second approach to the calculation of the air-gap field does take into account the effect of slotting and involves the use of permeance waves. It is necessary at this point to consider the concept of a permeance distribution. This distribution is taken to be the flux density along an arbitrary line, say, the centre of the air-gap. This distribution has harmonic components periodic in stator and rotor slot pitches and in submultiples of these. As the rotor rotates, this distribution has some harmonic components that are stationary and others that revolve. It is then assumed that the flux density distribution, under load conditions, is given by the harmonic series for the m.m.f. and the harmonic series for the permeance distribution. Robinson[1.24] employs this technique in his general discussion of harmonics in a.c. machines.

Alger[1.3] uses this technique to determine the conditions that cause crawling, cogging and noise in a machine. In his analysis, Alger assumes that only certain of the m.m.f. harmonics have significant values. These harmonics are: the fundamental m.m.f. wave, the phase belt harmonics of order $2q - 1$ and $2q + 1$ (where q = the number of phase belts per pole) and the two m.m.f. slot harmonics of order $(N_S/P) - 1$ and $(N_S/P) + 1$. The phase belt harmonics have a wavelength of a similar order to the length of a phase belt and the two m.m.f. slot harmonics have wavelengths of a similar order to the length of the stator slot pitch. In addition, he also takes into account the two rotor m.m.f. slot harmonics of order $(N_R/P) - 1$ and $(N_R/P) + 1$. Alger obtains an expression for the product of the m.m.f. and permeance wave series and identifies five terms as

being significant in producing crawling and cogging torques. For example, with regard to asynchronous crawl, he shows that the forward rotating phase-belt and m.m.f. slot harmonic terms produce magnetic fields having $(2q + 1)$ P and $(N_S + P)$ pole pairs, their m.m.f.s being in direct proportion to the stator currents. These harmonic fields produce induced voltages in the rotor winding, which in turn produces rotor currents and torques. When the rotor, during its period of acceleration from standstill, reaches the synchronous speed of one of these harmonic fields, that is, $P/(N_S + P)$ or $1/(2q + 1)$ times the synchronous speed, the corresponding harmonic torque falls to zero and at higher speeds reverses, thereby acting as a brake on the rotor. This gives the characteristic dip in the torque-speed curve. Alger also uses this analysis to predict conditions for synchronous crawling and cogging. The rules relating to cogging are discussed by Rowlands-Rees in his thesis[1.25].

Heller and Jokl[1.26] also use the m.m.f. andpermeance wave method to examine parasitic torque effects. The authors particularly concentrate on the effects of slotting on the torque produced by an induction machine. They begin their analysis by considering the m^{th} order stator m.m.f. harmonic and show that the air-gap permeance introduced by the slotted stator and rotor surfaces generates additional harmonic flux-density waves, which they call slot harmonics and which have $(N_S \pm P)$ and $(N_R \pm P)$ pole pairs. It should be noted that the m.m.f. harmonic series is defined in terms of a 2-pole fundamental field which is commonly done in this form of analysis. At a given point on the slotted stator surface, the stator slot harmonic pulsates in time with the frequency of the exciting m.m.f. harmonic (ω'), whilst on the rotor surface, the rotor slot harmonic pulsates with frequency $(\omega' \pm N_R \omega_r)$ where ω_r is the rotor frequency. Furthermore, it is shown that the

stator m.m.f. slot harmonics, defined previously, have the same number of poles and angular velocity as the slot harmonics. They can, therefore, be summed together. However, this is only strictly correct under no-load conditions, since, under load, the stator m.m.f. slot harmonics are a function of the stator current, whilst the slot harmonics are generated by the fundamental flux wave and are, therefore, a function of the no-load current. On load, they must be added in correct phase.

The authors were particularly interested in the effect of the stator and rotor slotting on the field produced by the stator and rotor m.m.f. slot harmonics with $(N_S \pm P)$ and $(N_R \pm P)$ pole pairs. For example, the rotor slot harmonic flux density wave produced by the stator m.m.f slot harmonic having $(N_S + P)$ pole pairs comprises of two waves, the first is a wave of long wavelength having $(N_R - (N_S + P))$ pole pairs and the second is a wave of short wavelength having $(N_R + (N_S + P))$ pole pairs. The most important of these waves, as regards the production of parasitic torques, is the wave of long wavelength. This field is referred to as the rotor difference field $B\Delta'R$ with respect to the stator m.m.f. slot harmonic having $(N_S + P)$ pole pairs.

Similarly, the rotor m.m.f. slot harmonic having $(N_R - P)$ pole pairs generates the stator difference field $B\Delta'S$. This field is also a wave of long wavelength having $(N_R - (N_S + P))$ pole pairs. The two fields $B\Delta'R$ and $B\Delta'S$ are summed together to give the combined difference field $B\Delta'$.

In a similar manner, the interaction of the stator m.m.f. slot harmonic having $(N_S - P)$ pole pairs with the rotor slotting produces the rotor difference field B "R. This field is a wave of long wavelength having $(N_R - (N_S - P))$ pole pairs. The rotor m.m.f. slot

harmonic $(N_R + P)$ pole pairs produces the stator difference field $B\Delta"S$, which is also a wave of long wavelength, having $(N_R - (N_S - P))$ pole pairs. The two fields, $B\Delta"R$ and $B\Delta"S$, are also summed together to give the total difference field $B\Delta"$.

In their paper, Heller and Jokl were particularly interested in the parasitic torques produced by the stator m.m.f. slot harmonics having $(N_S \pm P)$ pole pairs. They first consider the calculation of torques associated with these m.m.f. harmonics in the absence of slotting and then go on to show how slotting modifies the values of these torques.

A strong additional torque, due to slotting, may be produced if the stator harmonic field has a small number of pole pairs. Under these conditions, if the number of bars per pole exceeds a certain minimum value, large currents will flow in the squirrel cage. This situation occurs for the difference fields having $(N_R - (N_S + P))$ pole pairs which, of course, are present in the air-gap.

Consider the differences field $B\Delta'$ having $(N_R - (N_S + P))$ pole pairs. This field is in synchronism with the rotor at a speed

$$n_{rs} = \frac{n_s}{(N_S + P)}$$

where n_s = synchronous speed.

This is the same angular velocity as the stator step harmonic of $(N_S - P)$ pole pairs.

The action of this particular difference field on a rotor having N_R rotor bars is to induce an additional current distribution in the rotor. This current in turn generates an additional rotor m.m.f. distribution. The m.m.f. slot harmonic of this m.m.f. distribution has $(N_S + P)$ pole pairs and an angular velocity $n_S/(N_S + P)$ and it pulsates

with the stator frequency. Furthermore, this rotor field increases the value of the maximum torque at the speed $n_S/(N_S + P)$. Therefore the maximum torque at this speed associated with stator m.m.f. slot harmonic having $(N_S + P)$ pole pairs is given by

$$M_T = M_o \cdot K_o$$

where M_o is the maximum torque in the absence of slotting and K_o is the factor by which the torque is increased due to slotting. The equations for K_o are given in the paper. A similar argument can be applied to the stator m.m.f. slot harmonic having $(N_S - P)$ pole pairs at the speed $- n_S/(N_S - P)$.

From the analysis, it is apparent that slotting has a considerable effect on the parasitic torques of the stator m.m.f. slot harmonics. The largest increase occurs when $N_R > N_S$. The increase is much smaller when $N_R < N_S$ and, under certain conditions, slotting can either decrease parasitic torques or eliminate them altogether. It follows that motors in which $N_R < N_S$ are preferable from the point of view of additional harmonic torques.

In order to obtain satisfactory results the coefficients of the air-gap permenace must be calculated with due regard to saturation of the tooth-tips of the motor, that is, a fictitious increase in the slot openings must be introduced to account for saturation. This assumption, which is also used in this analysis, is discussed in Chapters 2, 4 and 5.

The occurrence of synchronous cusp can generally be anticipated if the number of rotor teeth is given by

$$N_R = 6.P.c + 2\,P \quad , \quad c = 1, 2, \ldots$$

Cogging may also occur if

$$N_R = 6.P.c \quad , \quad c = 1, 2, \ldots$$

It is shown earlier[1.27] that the motor has a 90% chance of passing through a synchronous cusp if the accelerating torque is larger than 72.5% of the synchronous torque. The effects of parallel windings on parasitic torques are also considered in some detail.

The general conclusions arrived at are that the ratio of the number of rotor to stator slots should be below 1.25 in unskewed machines and below 1.15 in skewed machines having uninsulated cages. It is beneficial to choose the number of rotor slots to be less than the number of stator slots.

It is important to clarify the assumptions underlying the use of the m.m.f. and permeance wave approach. This approach, and the previous one in which the gap permeance was assumed uniform, involve essentially only a consideration of the radial component of the air-gap field. This is a one-dimensional view of the air-gap field[1.6]. Such a field can be calculated using homopolar field conditions[1.3]. However, the complex air-gap field in the vicinity of the current carrying conductors in the stator and rotor slots is in reality a heteropolar field[1.28] and requires a two-dimensional field solution. This subject is discussed in more detail in the next chapter. It is, however, worth noting that some of the flux harmonics can be found to a good approximation using the m.m.f. and permeance wave approach. This is the case when the m.m.f. and permeance harmonics are significantly different in wavelength. Under these conditions, it is very reasonable to use a homopolar field solution, so long as the relevant m.m.f. harmonic is nearly constant over several slot pitches. This approximation is no longer valid, however, if the permeance and m.m.f. harmonics are of similar wavelengths, as the field bears no relation to the homopolar field from which the permeance harmonics have been calculated.

In contrast, the complex heteropolar field in the vicinity of the current carrying conductors in the slots can be accurately calculated using conformal transformation[1.28], since this is a two-dimensional field method. Furthermore, this method can be used in conjunction with the Maxwell stress function to obtain the tangential force on each tooth[1.4]. At any instant, these tangential forces can be summed to give the instantaneous torque produced by the machine. It is also possible, as shown later, to examine the variation of torque with rotor position. Therefore, the effects of slotting on the torque produced by an induction machine can be accurately determined using a conformal transformation field solution of the air-gap field.

1.5.3 Layer Theory

The multi-regional field analysis method, or layer theory, presents an alternative approach to the calculation of fields in induction motors. In this method, a model is used consisting of a number of laminar regions which are infinite in length in the plane of lamination and have an arbitrary thickness[1.29, 1.30]. The material properties of each region are dependent on the part of the machine they have replaced. For example, some of the regions may be conducting and/or ferromagnetic. The regions may also be assumed to be isotropic, or they may be allowed to be anisotropic[1.30]. The model is subjected to a travelling field produced by a current sheet which is located at the interface of two layers. This current sheet has a sinusoidal distribution in the plane of lamination and flow is normal to the direction of motion. Maxwell's equations can be solved in all layers of the model with the appropriate matching at the boundaries.

The layer theory model has been used extensively in the analysis of linear induction motors[1.31, 1.32]. It has the advantage that the idealised model quite closely resembles the linear motor it models,

especially in the case of the rotor. Furthermore, using this method, the air-gap field in a linear motor can be explicitly determined, which permits the study of three-dimensional forces and stability.

However, until recently, the layer theory model has not in general been used in the calculation of fields in rotating induction motors. The reason for this is that it is difficult to model the slotted region, and, in particular, to model the rotor. In the layer theory model, the squirrel-cage and its adjacent teeth are replaced by a homogenous layer of uniform thickness and conductivity. Therefore, the slot-harmonics, which are produced by the discrete bar currents, are simply not present. Furthermore, the effect of skewing the rotor is lost when a homogenous current sheet is used to represent the rotor. Also, concern has been expressed about the ability of layer theory models to account for the effects of slot leakage. Eastham and Williamson[1.33,1.34] have overcome these limitations by using techniques which 'borrow heavily' from the equivalent circuit method. However, the resulting model has to be simplified considerably to incorporate these modifications.

In a recent paper[1.35], Williamson and Smith introduced a new form of analysis which allows the discrete nature of the rotor currents to be taken into account. Subsequently, this new theory has been extended to include the effects of rotor skew[1.34]. The new theory takes account of all impedances due to the flux which enters the air-gap and in addition includes slot leakage directly. This analysis can be applied to both cage and slip-ring motors. The effects of saturation may be taken into account by modifying the permeabilities in the appropriate regions using an iterative technique.

The main difficulty with this method lies in the calculation of radial, circumferential and axial permeabilities in the layers.

Williamson[1.36] calculates these permeabilities using a model consisting of a number of alternate rectangular sections of two different materials. However, this model can only be regarded as giving approximate values of these permeabilities. In a more recent paper[1.34], Williamson and Smith show how the appropriate choice of circumferential permeability, in a slotted region, may be made. For a typical region (say the q^{th} region) the appropriate choice of circumferential permeability is given by

$$\mu_{cir} = \mu_o \left(\frac{P_q}{P_q'} \right) \tag{1.2}$$

where μ_{cir} is the circumferential permeability, P_q is the specific slot permeance of that part of the slot which the q^{th} region models and P_q' is the specific slot permeance for the q^{th} region of a machine having slots with parallel sides (open slots). The slot widths of the machine with parallel sided slots are equal to the widths of the slot mouths in the real machine.

The development of the new layer theory model is too recent to have been considered in the study of parasitic flux and force pulsations. Whilst the discrete nature of the current conductors can now be accounted for in the model proposed by Williamson and Smith, there are still problems in replacing the discrete nature of the slotted boundaries by layers. In particular, the model is unable to account for the influence of the tooth corners on the flux density distribution, whereas conformal transformation can treat these sharp corners successfully. Clearly, in order to calculate the flux and force pulsations associated with a tooth, it is important to be able to calculate the flux distribution and the forces acting on a tooth accurately and in this regard conformal transformation is a particularly suitable method.

1.6 Scope of the Work

The aim of the investigation into tooth-ripple fluxes, forces and harmonic torques is to determine the relationships between these phenomena and slot combination and to determine conditions under which these problems are minimised.

In this study, an experimental approach has not been used because of the difficulties in obtaining results for a wide range of slot combinations. Furthermore, economic considerations also make this impossible. Instead, a numerical approach is adopted in which the air-gap field, under load conditions, is accurately calculated using conformal transformation. The normal and tangential components of force are calculated using the Maxwell stress function.

1.7 Breakdown of the Subject

In Chapter 2, a number of methods suitable for the calculation of the air-gap field are reviewed and it is shown that conformal transformation is best suited to the requirements of the present research. This is followed by a simple description of the air-gap field which gives a useful insight into the production of parasitic fluxes and forces. A brief review of the method of conformal transformation is presented and a description of a method suitable for calculating magnetic forces on machine teeth under no-load and load conditionsis given.

Chapter 3 is concerned with the application of conformal transformation to field problems with polygonal boundaries. Such problems involve the use of an intermediate transformation known as the Schwarz-Christoffel transformation. This transformation equation contains a number of constant terms which have to be found before it can be used. For complicated boundaries, this involves the use of a numerical method

and a description of a general method for finding the constants is given.

In Chapter 4, a general outline is given of the analytical solution of integrals that occur in conformal transformation problems and it is shown that such analytical solutions have their limitations. The rest of the chapter is concerned with the numerical evaluation of the two types of integral described in Section 1.2. Two new methods are described and compared for the evaluation of Cauchy Principal Values.

In Chapter 5, the slotted air-gap boundary is separated into three distinct regions. The solution of the field and the computation of the forces in each of these regions are then described. The separate solutions are then combined to give the flux in, and the tangential and normal forces acting on, any tooth in an induction motor. This is followed by a description of a computer program which has been used to determine the distributions of flux in, and the forces acting on, the teeth over a double pole pitch.

Chapter 6 is concerned with the calculation of the stator and rotor current distributions and the air-gap m.m.f. under load. It is shown that it is not practical or necessary to consider all types of stator winding in the examination of tooth-ripple phenomena. Consideration is also given to the damping action of the cage and the choice of load current level.

In Chapters 7 and 8, the results of the examination into tooth-ripple fluxes and forces are presented. From these results a number of design rules for the choice of slot combination are obtained. A comparison is made of the conditions which give rise to low pulsations under no-load and load conditions.

In Chapter 9, the tangential forces computed for each tooth are summed to give the torque of the machine. The variations of torque

with a rotor displacement of one rotor slot pitch are presented in graphic form for a range of slot combinations. The useful torque and fundamental tooth-ripple torques are obtained from these graphs by Fourier analysis. The magnitude of the two torque components are then compared.

Finally, in Chapter 10 the results and conclusions are drawn together, and suggestions made for future research.

1.8 References

1.1 SCHWARZ, K. K. : 'Survey of basic stray losses in squirrel cage induction motors', Proc. IEE, 1964, 111, (9), pp.1565-1574.

1.2 ELLISON, A. J. and MOORE, C. J. : 'Acoustic noise and vibration of rotating electric machines', Proc. IEE, 115, (11), pp.1633-1640.

1.3 ALGER, P. L. : 'The nature of induction machines', (Gordon and Breach, 1965).

1.4 BINNS, K. J. and ROWLANDS-REES, G. : 'Main flux pulsations and tangential tooth-ripple forces in induction motors', Proc. IEE, 1975, 122, (3), pp.273-277.

1.5 BINNS, K. J. and ROWLANDS-REES, G. : 'Radial tooth-ripple forces in induction motors due to the main flux', Proc. IEE, 1978, 125, (11), pp.1227-1231.

1.6 BINNS, K. J. and SCHMID, E. : 'Some concepts involved in the analysis of the magnetic field in cage induction machines', Proc. IEE, 1975, 122, (2), pp.169-175.

1.7 CARPENTER, C. J. : 'Surface-integral methods of calculating forces on magnetised iron parts', Proc. IEE, 1960, 107C, pp.19-28.

1.8 LEHMANN, T. H. : 'The calculation of magnetic attraction', Trans. A.I.E.E., 1926, 45, pp.383-394.

1.9 CARTER, F. W. : 'Magnetic noise in dynamo-electric machines', Engineering, 1932, pp.548-551.

1.10 DVORACEK, A. I. : 'Forces on the teeth in d.c. machines', Trans. A.I.E.E., 1962-63, 81, pp.1054-1061.

1.11 BINNS, K. J. : 'The magnetic field and centring force of displaced ventilating ducts in machine cores', Proc. I.E.E., 1961, 108C, pp.64-70.

1.12 LIEBMANN, G. : 'The change in air-gap flux in electrical machines due to the displacement of opposed slots', Proc. I.E.E., 1957, 104C, pp.102-118.

1.13 SIMKIN, J. and TROWBRIDGE, C. W. : 'Magnetostatic fields computed using an integral equation derived from Green's theorem', Proc. Compumag, Oxford, 1976.

1.14 JAWSON, M. A. : 'Integral equation methods in potential theory 1' Proc. Roy. Soc. A., 1963, 275, pp.23-32.

1.15 BINNS, K. J., KAHAN, P. A., REES, G. R., SIMKIN, J. and TROWBRIDGE, C. W. : 'A comparison of two methods of field solution for slotted boundary shapes in two dimensions, Proc. Compumag, Oxford, 1978.

1.16 SILVESTER, P. and CHARI, M. V. K. : 'Finite element solution of saturable magnetic field problems', I.E.E.E. Trans., 1970, PAS-89, pp.1642-1651.

1.17 NORRIE, D. H. and VRIES, G. : 'The finite element method', (Academic Press, 1973).

1.18 JABBAR, M. A. : 'Analysis of the performance of a permanent-magnet a.c. machine', Ph.D. thesis, University of Southampton, 1977.

1.19 LIWSCHITZ, M. M. : 'Field harmonics in induction motors', Trans. A.I.E.E., 1942, 61, pp.797-803.

1.20 OBERRETL, K. : 'New facts about parasitic torques in induction motors', Bulletin Oerlikon, 1962, 348, pp.130-155.

1.21 RICHTER, R. : 'Elektrische Maschinen, Vol. 4-Die Induktions machinen', (Verlag Birkhaüser, 1954).

1.22 LIWSCHITZ-GARIK, M. M. and WHIPPLE, C. : 'A.c. machines', (Von Nostrand, 1961, 2nd Edition).

1.23 OBERRETL, K. : 'The field harmonic theory of the squirrel-cage motor, taking multiple armature reaction and parallel winding branches into account', Arch. Elektrotech, 1965, 49, pp.343-364 (in German).

1.24 ROBINSON, A. C. : 'Harmonics in a.c. rotating machines', Proc. I.E.E., 1962, 109C, pp.380-387.

1.25 ROWLANDS-REES, G. : 'Analysis of no-load force pulsations and cogging torques in induction machines', Ph.D. thesis, University of Southampton, 1978.

1.26 HELLER, B. and JOKL, A. L. : 'Tangential forces in squirrel-cage induction motors', I.E.E.E. Trans., 1969, PAS-88, pp.484-492.

1.27 HELLER, B. and HAMATA, V. : 'Additional fields, forces and losses in the induction machine', Publishing House of the Czechoslovakia Academy of Science, NCSAV, 1961.

1.28 BINNS, K. J. : 'Calculation of some basic flux quantities in induction and other doubly slotted machines', Proc. I.E.E., 1964, 111, (11), pp.1847-1858.

1.29 STOLL, R. L. and HAMMOND, P. : 'Calcualtion of the magnetic field of rotating machines - Pt. 4, Approximate determination of the field and losses associated with eddy currents in conducting surfaces', Proc. I.E.E., 1965, 112, (11), pp.2083-2094.

1.30 FREEMAN, E. M. : 'Travelling waves in induction machines; input impedance and equivalent circuits', Proc. I.E.E., 115, (12), 1968, pp.1772-1776.

1.31 FREEMAN, E. M. and LOWTHER, D. A. : 'Normal force in single sided linear induction motors', Proc. I.E.E., 1973, 120, (12), pp.1499-1505.

1.32 EASTHAM, J. F. and BALCHIN, M. J. : 'Pole-change windings for linear induction motors', Proc. I.E.E., 1975, 122, (2), pp.154-160.

1.33 EASTHAM, J. F. and WILLIAMSON, S. : 'Generalised theory of induction motors with asymmetrical air-gaps and primary windings', Proc. I.E.E., 1973, 120 (7), pp.767-775.

1.34 WILLIAMSON, S. and SMITH, A. C. : 'A field analysis for rotating induction machines and its relationship to the equivalent circuit method',Proc. I.E.E.,1980,127,Pt.B, 2, pp.83-90.

1.35 WILLIAMSON, S. and SMITH, A. C. : 'Layer theory analysis for integral-bar induction devices', 2nd Compumag Conference, Grenoble, Sept. 1978.

1.36 WILLIAMSON, S. : 'The anisotropic layer theory of induction machines and induction devices, J. Inst. Maths. Applics., 1976, 17, No. 1, pp.69-84.

CHAPTER 2

THE CALCULATION OF MAGNETIC FIELDS AND FORCES IN THE AIR-GAP REGION OF AN INDUCTION MOTOR

2. Introduction

2.1 The Air-Gap Field in an Induction Motor

2.2 A Comparison of Some Two-Dimensional Field Methods

2.3 Two-Dimensional Field Solutions

2.3.1 Derivation of the Boundary Conditions for No-Load and Load Cases

2.4 Conformal Transformation

2.5 The Calculation of Magnetic Forces

2.5.1 The Calculation of Tooth Forces under Load Conditions

2.6 References

2. Introduction

In Section 2.1 a description is given of the air-gap field and it is shown that this field is axially uniform over most of the bore length and can, therefore, be examined in a two-dimensional cross-section of the machine. This is followed, in Section 2.2, by a comparison of some methods for the solution of the two-dimensional air-gap field and it is shown why the method of conformal transformation has been chosen in preference to other methods. A brief historical review of the use of conformal transformation in the analysis of the air-gap field is also given in Section 2.2. In Section 2.3, the three cateogries under which all two-dimensional field solutions lie are listed. The method of conformal transformation lies under the category involving the solution of a partial differential equation.

More specifically, the methods in this category involve finding a potential function which satisfies Laplace's equation. The air-gap field strength is then found by differentiating this potential function. To solve Laplace's equation, it is necessary to specify the boundary conditions of the problem and this is the subject of Section 2.3.1, where suitable conditions are derived both for no-load and load cases. The method of conformal transformation is briefly described in Section 2.4. Finally, in Section 2.5, a method is described for the calculation of forces on machine members. Section 2.5.1 deals with the specific case of the calculation of electromagnetic forces on the teeth of induction machines under load condition.

2.1 The Air-Gap Field in an Induction Motor

The air-gap field in an induction motor is complicated and three-dimensional in reality. It is produced by the time-varying currents

in both stator and rotor windings, and by the magnetising effect that these have on the iron boundaries. The field varies in time and space in a complicated manner.

In this analysis the rotor is assumed to be unskewed. A number of manufacturers do not skew their rotors. From a practical point of view skewing smothers certain phenomena associated with the air-gap field. It is best to analyse the field without the extra complication introduced by skewing. Furthermore, the choice of slot combination is not critically dependent on skewing. That is, if a slot combination is bad as regards a certain phenomenon when the machine rotor is skewed, it will also be bad when the machine rotor is unskewed.

In cylindrical induction motors, the air-gap field is resolved into its three cylindrical components, namely, radial, tangential and axial. In unskewed machines, it is reasonable to assume that the axial field is uniform over most of the bore length, this assumption only breaking down in the end regions. However, for the phenomena under investigation, the significance of the contributions from the end regions is small and can be neglected. Hence, the field can be examined in a two-dimensional cross-section of the machine.

2.2 A Comparison of Some Two-Dimensional Field Methods

There are a number of methods currently available for solving the two-dimensional air-gap field. In this section some of these methods are reviewed and it is shown why the method of conformal transformation is preferred to other methods.

As mentioned in Chapter 1, in recent years the finite element method has become very popular in the solution of two and three-dimensional field problems. This method can handle complicated boundary conditions and finite values of permeability in iron[2.1], but at the expense of both computer storage and time. It is because this method is so

costly in computer resources that it has not been used in this work, where hundreds of field solutions are required to investigate properly the parameters of interest.

A boundary integral method, developed by Trowbridge and Simkin[2.2], was considered in the computation of the air-gap field. This method can handle complicated boundary conditions and a fixed finite permeability in the iron. However, this fixed finite value of permeability introduces an unknown amount of core-back reluctance into the computation of the air-gap field. Since the core-back reluctance cannot be specified precisely using this method, it is just as reasonable to have an infinite permeability and to neglect the unknown reluctance, as in conformal transformation. The boundary integral method and conformal transformation were used to calculate the flux values in, and the forces acting on, some of the teeth of an induction machine. The results obtained were found to be in close agreement[2.2]. The flux values found by conformal transformation were slightly higher because the core-back reluctance had been neglected. However, the boundary integral method was of the order of one hundred times slower than conformal transformation and has, therefore, not been pursued further.

A popular numerical method for solving Laplace's equation (it will be shown that the air-gap field is a Laplacian field) is the finite difference method. Full details of this method are given by Binns and Lawrenson[2.3] in their book, so that, this method will not be described here. It is, however, worth mentioning that this method tends to be expensive in computer time because a large number of simultaneous equations often have to be solved. Furthermore, because a continuous medium is replaced by a finite set of points, a discretisation error is introduced by this method.

A numerical conformal transformation is particularly suitable for the solution of the air-gap field because in this method a continuous

potential distribution is retained. It does not, therefore, suffer from the discretisation errors associated with other methods. Furthermore, as will be shown later, it is a particularly convenient method for treating the slotted air-gap boundary as it can cope with the sharp corner associated with such a boundary with relative ease. This method has formed the basis for a program of research conducted by K. J. Binns, G. Rowlands-Rees and the present author. Some of the important aspects of this research are now reviewed.

The earliest work, done by Binns, was the calculation of centring forces on displaced ventilating ducts[2.4]. This involved the first use of numerical conformal transformation techniques in the treatment of doubly-slotted boundaries. These techniques have since been developed more rigorously by Binns, Rowlands-Rees and Kahan[2.5]. The Maxwell stress function was used to obtain the centring forces and has subsequently been used in calculating normal and tangential force pulsations under no-load conditions.

In another paper[2.6], Binns dealt with the calculation of some basic flux quantities in induction motors. It was shown in this paper how the complex magnetic field in the air-gap of an induction motor can be 'synthetised' from the field of a single current in a slot. The current has its return path along the other side of the coil. Treating the field in this way, it is possible to consider it in two parts, the field in the vicinity of the current carrying conductor being a heteropolar or leakage field, while remote from the slot the field is homopolar. These two types of field will be discussed in more detail later in this chapter when it will be shown that the homopolar field closely resembles the field of an induction motor under no-load conditions, whilst a combination of the two types of field are required to represent the field under load conditions.

In the same paper, Binns derived an equation for the gap extension factor which is believed to be the most accurate equation now available. He also obtained, using the homopolar field solution, an accurate equation for the flux pulsations into the slots of an induction motor. Also obtained, using an electrolytic tank, was an empirical relation for the flux pulsations into the teeth. However, a probable error of 25% is quoted for this formula, so that it can only be regarded as a guide. Subsequently, a more accurate equation has been derived for the flux pulsations into the teeth under no-load conditions[2.7], and the calculation of such pulsations under load conditions is one of the main subjects of the present work.

In the early paper on basic flux quantities, another important subject considered was the air-gap leakage flux. A definition of air-gap leakage was given based upon the heteropolar field solution. This definition is very convenient because it allows the winding reactance to be calculated to a high accuracy by synthesis of basic field elements. Also, this definition is more precise than the one given by Alger in his book[2.8], which divides the air-gap leakage into several components. Unfortunately, there is no general agreement as to the precise definition of these components. Furthermore, the definition given in the above paper gives a clearer insight into the actual path of the air-gap leakage flux.

From the calculation of the air-gap leakage field, Binns was able to investigate the variation of leakage permeance with slot position, deriving some simple equations for the permeance. He later used these results in his work on cogging torques in induction motors[2.9]. The air-gap leakage field arises as a direct result of an induction motor operating under load and must, therefore, be included in the calculation of the air-gap field under load conditions.

Binns and Rowlands-Rees[2.7] have calculated the no-load tangential force pulsations acting on the teeth of induction motors, and have shown that a clear relationship exists between these and the main flux pulsations entering the teeth under no-load conditions. They have also derived equations which show the relationship between these pulsations and the air-gap dimensions. Using these equations, they have derived a number of rules for the minimisation of the flux and force pulsations into both and stator and rotor teeth.

In another paper[2.10], the normal force pulsations, under no-load conditions, acting on the stator and rotor teeth have been calculated. As in the case of the tangential force pulsations, equations have been derived which show the relationship between the air-gap dimensions and the normal force pulsations, and, from these equations, rules have been derived for the minimisation of these pulsations.

2.3 Two-Dimensional Field Solutions

In his thesis[2.11], Rowlands-Rees outlines the three basic categories under which all two-dimensional field solutions may be listed. These are:

a) the solution of a variation problem;

b) the solution of the integral equation;

c) the solution of the partial differential equation.

The method of conformal transformation lies in the third category, so that, only this category, which will be called the differential approach, will be considered here. The starting point

for all methods in the differential approach is Maxwell's equations, that is,

$$\text{curl } \underline{H} = \underline{J} + \frac{d\underline{D}}{dt} \tag{2.1}$$

At power frequency the displacement current is negligible and so equation (2.1) becomes

$$\text{curl } \underline{H} = \underline{J} \tag{2.2}$$

and

$$\text{div } \underline{B} = 0 \tag{2.3}$$

Additionally, for a field in air

$$\underline{B} = \mu_0 \underline{H} \tag{2.4}$$

and in iron

$$\underline{B} = \mu_0 \mu_r \underline{H} \tag{2.5}$$

Where there is no current, as in the air-gap region, there is no curl field, and equation (2.2) becomes

$$\text{curl } \underline{H} = 0 \tag{2.6}$$

It should be noted that in calculating the flux entering an individual tooth, the flux contribution due to the current conductors in the slots on either side of the tooth can be added to the flux calculated in the air-gap region, providing it is assumed that the flux crossing the slot remote from the slot opening is uniform. Returning to the air-gap field, since the current density in this region is zero, the magnetic

field described by equation (2.6) is irrotational. This is important because it allows the vector field to be calculated from a scalar potential function. This subject is discussed in detail by Hammond[2.13]. Let this scalar potential function be denoted by V, then

$$\underline{H} = - \text{grad } V \tag{2.7}$$

By suitably rearranging this equation using equations (2.3) and (2.4), it can be shown that V obeys the equation

$$\nabla^2 V = 0 \tag{2.8}$$

which is, of course, the well known Laplace equation.

Therefore, the differential approach to calculating the magnetic field in the air-gap involves finding a scalar potential function which satisfies Laplace's equation. The field can then be found by solving equation (2.7). There are, however, two problems in using this approach:

(i) It is often difficult, if not impossible, to specify the boundary conditions with complete accuracy;

(ii) Given a set of boundary conditions, it may be difficult to obtain an accurate solution to the equation.

In practice, a compromise is sought between these two factors, depending largely on the nature of the problem. In general, simplified boundary conditions are used which give solutions that are substantially correct in a limited region.

2.3.1 Derivation of the Boundary Conditions for the No-Load and Load Cases

The choice of suitable boundary conditions for the calculation of the air-gap field under no-load and load conditions will now be considered. The machine designer wishes to distinguish between effects which occur under no-load and load conditions. Under no-load the air-gap field is main flux dominated, whilst under load there are

additional leakage flux components which can be superimposed on the main flux providing saturation is neglected. The analysis developed by Binns, Rowlands-Rees and the present author distinguishes between the no-load and load conditions and is, therefore, exceedingly valuable. Before considering the boundary conditions associated with these two operating conditions, certain assumptions which are common to the two must first be examined.

For the investigation of tooth-ripple flux and force pulsations under no-load and load conditions, it is sufficient to analyse the field quasistatically. The reason for this is that, at present, the main interest lies in the variation of these phenomena with the displacement of stator and rotor surfaces, and not in their variation with time.

It is common in many analytical methods of analysis to assume that the permeability of the iron parts is infinite. It is inherent in such an assumption that all flux crosses the iron boundaries normal to their surfaces. Binns and Lawrenson[2.3] have discussed this assumption of flux crossing normal to the surface and have shown that it is still valid for quite low values of permeability, quoting typical errors of less than 5 per cent for $\mu > 40$, and less than 0.5 per cent for $\mu > 400$. Furthermore, the optimum slot combination is not critically dependent upon the flux level and neither is the exact value of the permeability of the iron important providing it is reasonably high.

The assumption of infinite permeability not only allows the method of conformal transformation to be applied to induction machine field problems, but also results in simple expressions for the Maxwell stress function and, therefore, greatly reduces the computation required.

However, under load conditions, in regions of the machine where there are heavy currents flowing in the conductors in the slots, the tooth tips enclosing the conductors become saturated. These saturated

tooth tips obviously effect the flux-density distribution locally. To overcome this difficulty, and to retain the assumption of infinite permeability, an equivalent slot opening is used, the width of which lies between that of the actual slot opening and slot width.

As mentioned earlier, in assuming an infinite permeability, the core-back reluctance of both the stator and rotor is neglected. Accordingly,any tooth fluxes calculated will tend to have too high a value. This point is confirmed by the comparison of the boundary integral method with conformal transformation, the former method giving flux values lower than the latter. The reason for preferring an infinite permeability when considering the core-back reluctance has already been discussed.

In Section 2.1 it was stated that the air-gap field under load conditions can be synthetised from the field of a single current-carrying conductor in a typical slot. This current has its return path along the other side of the coil. It is, as mentioned in Section 2.1, possible to consider the field of the slot conductor in two parts. In the vicinity of the conductor the field is a heteropolar or leakage field, and the flux crosses the current-carrying slot between adjacent teeth or crosses the air-gap twice (See Figure 2.1). Remote from the slot, the field is homopolar, the flux passing across the air-gap between the two slotted surface at constant magnetic potential (see Figure 2.2). The homopolar field is independent of the actual position of the current, providing that the current is reasonably remote. In fact, the field in the region of the slot adjacent to the one carrying the current is virtually homopolar. Binns[2.6] has computed the error in assuming this, and has found that there is a negligible error in this assumption for practical air-gap dimensions. Hence over the

region where the teeth overlap, the heteropolar field merges into the homopolar field. By superposition, the fields due to the currents in individual coils can be combined to give the field due to both stator and rotor windings.

The treatment of the field in this way gives rise then to two basic field solutions, and, providing it is assumed that the iron boundaries have infinite permeability, simple boundary conditions can be defined for these two solutions.

The boundary conditions in a simplified section of the slotted boundary are now considered first for the no-load case and then for the load case. The following remarks apply to all induction machines in the integral K.W. range and to all machines in the fractional K.W. range above 200 Watts. It is interesting to note that induction machines below 50 Watts are not usually polyphase except for control applications. A consideration of such machines lies outside the scope of this thesis.

Under no-load conditions only a small current flows in the stator winding. This current may be resolved into two components, a magnetising and core-loss component. The former component magnetises the iron parts of the machine, whilst the latter flows because of the eddy current losses in the core. Almost all the flux crosses the air-gap and links the rotor circuits. There are only small components of stator and rotor leakage flux. In fact, since the e.m.f. induced in the rotor circuits is small, so are the resulting rotor currents. These currents are just sufficient to produce the necessary torque to overcome friction and windage. It is quite common in analysis to neglect the rotor currents; both Say[2.12] and Alger[2.8] make this remark in their books. Furthermore, if the stator currents are neglected, which is reasonable

since they give rise to only small leakage fields, the air-gap field, under no-load conditions, is dominated by the main flux. The distribution of this can be derived by assuming a simple magnetic potential difference to exist across the air-gap. Under this assumption, the air-gap field in any particular region of a machine is, of course, homopolar and corresponds to the first of the field solutions discussed earlier.

In calculating the air-gap field under both no-load and load conditions, it is usual to simplify the air-gap geometry and to solve Laplace's equation in a region Q, see Figure 2.3., for which the boundary conditions can be defined. It will be noted that the simplificationin Figure 2.3 involves the use of open rather than closed slots. In this figure, the dotted lines indicate that the sections of the iron surfaces from A to B and C to D are coincident with equipotentials and have a potential difference of ψ. Such boundary conditions are referred to as Dirichlet boundary conditions. The lines from A to D and B to C coincide with flux lines and hence the Neumann boundary conditions hold, that is,the normal derivative of the potential is zero along them. With the boundary condition specified everywhere in the region, a unique solution of Laplace's equation is guaranteed for all points within the region bounded by the dotted lines.

When an induction machine is loaded, the rotor slows, increasing the slip. The e.m.f. induced in the rotor circuits rises in magnitude and frequency, producing more current and torque. This process is only limited by the leakage reactance of the rotor. The larger rotor currents flowing in the cage give rise to an m.m.f. which, in turn, causes an extra component of current to flow in the stator winding to balance this rotor m.m.f. If the main flux level in the machine remains

constant, the two m.m.f.s will cancel each other out, leaving only the no-load m.m.f. which, of course, produces the main flux. However, this is not strictly the case, because the main flux level drops as part of it becomes leakage flux.

The magnetic field in region U of the air-gap geometry (see Figure 2.4) consists of the main field crossing the air-gap and the leakage fields associated with the two current-carrying conductors in the slots. The air-gap field can be calculated using a combination of the two basic field solutions discussed earlier. The appropriate boundary conditions for region U are now derived. It should be noted that the current-carrying conductors are included in this figure, but do not lie in the air-gap region where Laplace's equation is to be solved. In Figure 2.4, the iron surfaces AB, CD, EF and GH coincide with equipotentials, but there is now a potential difference across both slots as well as the air-gap. The lines BC, DE, FG and HA coincide with flux lines for which the Neumann boundary conditions hold. Thus, again, a unique solution exists for Laplace's equation within the region enclosed by the dotted lines.

The method of separation of variables cannot be used to solve Laplace's equation in regions Q and U. Conformal transformation is the only analytical method capable of solving Laplace's equation in these two regions.

2.4 Conformal Transformation

Conformal transfromation is a very powerful method for the analytical solution of Laplace's equation although, in problems with complicated boundaries, numerical methods are required to solve the integrals that arise. The transformation method is capable of handling boundaries of greater complexity than other analytical methods. Furthermore,

although the magnetic fields and boundaries being considered are often complicated, the resulting solution of the field is usually simple and functions of the field such as permeance and force are readily obtainable. The main limitation of the method, for most problems, is that boundaries have to coincide with equipotentials (which implies an infinite permeability) or to be coincident with flux lines, or a combination of these two conditions.

The method of conformal transformation is discussed in great detail by both Binns and Lawrenson[2.3] and Gibbs[2.14] in their books. However, a brief description of that part of the method relevant to the calculation of the air-gap field is included here for the sake of completeness.

Consider the complex function

$$z = f(t) = x(u,v) + jy(u,v) \qquad (2.9)$$

which describes a relationship between the two sets of complex variables $t = u + jv$ and $z = x + jy$. A particular value described by the point $t = u + jv$ in the complex t-plane can, through equation (2.9), describe a value (or values) represented by a point (or points) $z = x + jy$ in the complex z-plane. Furthermore, this concept can be extended to a succession of pairs of points in the two complex planes, so that a curve tt' in the t-plane can, through equation (2.9), describe a curve zz' in the z-plane, see Figure 2.5. Another way of describing this process is to say that the curve t t' has been transformed or mapped onto zz'. This definition is, however, general and in engineering field problems particular interest lies in those transformations for which each point in the t-plane maps into one, and only one, point in the z-plane. This means that for a given function

$$z = f(t) \qquad (2.10)$$

describing a mapping between the t and z planes, there exists an inverse function

$$t = g(z) \qquad (2.11)$$

which describes the reverse mapping between the z and t planes.

The term 'conformal' is applied to those transformations which are analytic in a given region and whose derivatives do not vanish. The first condition is satisfied if the real and imaginary functions of equation (2.9) obey the well known Cauchy-Riemann equations. That is:

$$\frac{\partial x(u,v)}{\partial u} = \frac{\partial y(u,v)}{\partial v} \quad , \quad \frac{\partial x(u,v)}{\partial v} = \frac{-\partial y(u,v)}{\partial u} \qquad (2.12)$$

The two functions x(u,v) and y(u,v) are called conjugate functions, since they obey the Cauchy-Riemann equations, and the curves defined by the equation u = constant and v = constant are orthogonal to each other. It can also be shown[2.3] that if any two curves cross at a given angle in one plane, the two transformed curves cross at the same angle in the other plane and in such a way that the sense of the two angles is preserved. An important property of conjugate functions is that they are solutions of Laplace's equation and this is another powerful reason for using transformation methods. Thus, any conformal transformation describes a relationship between two Laplacian fields, so that, given a Laplacian field with a complex boundary, conformal transformation can be used to transfrom this boundary to a simpler one where the field can be solved. Thus, the transformation method consists, in the first instance, of finding a mapping function which relates the complex boundary to the simpler one.

It is now necessary to introduce the complex potential function to explain how the field is found once the complex boundary has been mapped into the simpler one. Consider the simple Laplacian field in the t-plane of Figure 2.6. The figure shows a uniform field in which the lines u = constant are flux lines and the lines v = constant are equipotentials. Let the gradient of the potential function be K at all points. Then, if the axis v = 0 is taken as an arbitrary reference, a function describing the potential at any point (u,v) is given by $\psi = Kv$. Similarly,

if the vertical axis described by the equation $u = 0$ is taken as reference for the flux lines, a function describing the flux at any point is given by $\phi = Ku$. It is important to note that the two functions, ψ and ϕ, are proportional to the potential and flux respectively. Accordingly, the two separate functions can be combined to give one complex function

$$w = \phi + j\psi = K(u + jv) \tag{2.13}$$

or

$$w = Kt \tag{2.14}$$

and it is the complex function w that is called the complex potential function. It is convenient to regard the complex potential function as representing another plane and equation (2.14) as describing a mapping function between the t- and w-planes. Hence, for any field, the process of transformation involves deriving an equation of the form

$$w = h(z) \tag{2.15}$$

which relates points in the z-plane to those in the w-plane. With simple problems, the potential and flux functions can be expressed directly as functions of the z-plane variables, x and y. However, with more complicated problems, the complex boundary in the z-plane has first to be transformed into a simpler one in the t-plane and the field found by mapping on to the third plane, the w-plane. Thus, the t-plane acts as an intermediate plane in the transformation process. A good example of this process is the Schwarz-Christoffel transformation which will be discussed in the next chapter.

It is important to note that when the actual flux or potential is obtained from the flux or potential function, only one of these quantities is in the correct S.I. units. Which of these quantities this is depends on the way the problem is defined. To obtain the other quantity in the correct units, the appropriate function has to be multiplied by a suitable constant.

Finally, as shown by Binns and Lawrenson[2.3], a simple relationship exists for calculating the flux density and is given by

$$|\underline{B}| = \left|\frac{dw}{dt}\right| \qquad (2.16)$$

This equation will be used in conenction with the calculation of forces on machine members.

2.5 The Calculation of Magnetic Forces

Having chosen an appropriate method for the calculation of the two-dimensional air-gap field, it is now necessary to examine methods for the calculation of forces on magnetised iron boundaries. This subject has been reviewed in detail by Rowlands-Rees[2.11], so that only those details relevant to the calculation of forces under load conditions will be described here.

The main method for calculating forces considered by Rowlands-Rees was the boundary equation method. In physical terms this method consists of replacing the region of magnetised iron, on which the force is to be calculated, by an equivalent set of magnetic sources which, to an external observer, produce an effect indistinguishable from the iron they have replaced. Accordingly, the total force can be calculated by summing together the effect the external field sources have on the sources that represent the magnetised iron. The sources which replace the iron can be made up of magnetic poles, dipoles or electric currents, although often the iron is considered to be a collection of either dipoles or current loops. The basic equations associated with the magnetic poles, currents and dipoles are:

$$\underline{F} = Q \, . \, \underline{H} \qquad (2.17)$$

for the force acting on a magnetic pole Q ,

$$\underline{F} = \underline{I} \times \underline{B} \qquad (2.18)$$

for the force on a current $\underline{I}$,

and

$$\underline{F} = (\underline{m} \cdot \nabla) \cdot \underline{H} \qquad (2.19)$$

for the force on a bar magnetic with a dipole moment $\underline{m}$.

For a given configuration, it would be possible to use an infinite number of source combinations to give the same effect to the external observer as the original iron that has been replaced. In practice, however, force equations have been developed for only a limited number of combinations. These combinations have been listed by Rowlands-Rees[2.11], the most important combination in the calculation of tooth-ripple forces being a surface layer of poles combined with a surface layer of currents.

This method will now be described in detail. It consists of totally enclosing the iron region by a surface in air on which a distribution of both poles and currents are postulated. The distributions are defined in such a way that the total field external to the surface is constant, whilst the field inside the surface is zero at every point. There are two stresses that occur with this arrangement; the first is a tension along the line of the field of magnitude $\frac{1}{2}\mu_0\underline{H}^2$, and the second is a stress of equal pressure perpendicular to the first stress. For a surface, inclined to the field, the two stresses can be resolved into two components, the first normal to the surface and given by the equation

$$F_N = \tfrac{1}{2}\mu_0 (H_N^2 + H_T^2) \qquad (2.20)$$

and the second, a tangential component, given by

$$F_T = \mu_0 H_N \cdot H_T \qquad (2.21)$$

The total force acting on a body can be calculated by integrating these stresses around the surface enclosing the body.

An important feature of this method of calculating forces is that is may be used irrespective of both saturation or hysteresis; all that is required is a knowledge of the field over the surface surrounding the

magnetised body. A further advantage of this method is that there is complete freedom of choice in the selection of a suitable surface. Both Hammond[2.13] and Carpenter[2.15] give examples in which a discrete choice of surfaces leads to the formulation of the problem in such a way that forces can be easily calculated.

2.5.1 The Calculation of Tooth Forces Under Load Conditions

The boundary equation method, discussed in the previous section, is now applied to the calculation of the forces acting on the teeth of induction motors under load conditions. The same application of the method is made as that by Rowlands-Rees when calculating tooth forces under no-load conditions. It consists of substituting the conformal transformation solution of the air-gap field, under load conditions, into a Maxwell stress integral evaluated over the surface of the teeth. It is convenient, in this analysis, to separate the normal and tangential components of force and calculate them separately.

The tangential component of force acting on a tooth can be calculated by integrating the stress around the surface ABCD, shown in Figure 2.7. A simplified air-gap geometry is used to make the calculation of the force tractable. This assumption will be discussed in detail in a later chapter. The planes AB, BC and CD coincide with the three faces of the teeth, while the plane AD, crossing the tooth, is an indefinitely small air-gap introduced to close the surface. This air-gap is a prerequesite of applying the boundary integral method. Under the assumption of infinite permeability, all forces act normal to the surface, so that there is no contribution from sides BC and AD. The tangential force acting on the tooth can be calculated by integrating the stress contributions over the surfaces AB and CD alone. Accordingly, under the assumption of infinite permeability, equation (2.20) becomes

$$F_N = \tfrac{1}{2}\,\mu_0\,H_N^2 \qquad (2.22)$$

and equation (2.21) is zero.

The normal component of force on the tooth can be calculated in a similar manner by integrating the stresses around the surface EFGH shown in Figure 2.7. As in the previous case, a fictitious air-gap is introduced into the tooth to give a closed surface. If again the iron is assumed infinitely permeable, the sides EF and GH make no contribution to the normal force on the tooth. Hence, the normal force may be calculated by integrating the stresses over the surfaces FG and EH. However, the field at the surface FG is zero, since it lies outside the machine, so that the only contribution to the normal component of force on the tooth comes from integrating the stresses over the surface EH. The normal component of force on the tooth is thus obtained by integrating equation (2.22) over this surface.

In the two cases just considered, the fictitious air-gap, introduced to form the closed surface around the tooth, makes no contribution to either the tangential or normal components of force. Furthermore, since these air-gaps are indefinitely small, their presence has no effect on the field distribution. For these reasons, the normal and tangential component of force may be calculated by integrating the stresses over the surface JKLM in Figure 2.7.

In using conformal transformation field solutions, the slots are assumed to be infinitely deep and the current conductors are replaced by point current sources at an infinite distance down the slot. This assumption will be discussed in detail in Chapter 5. This gives rise to a field solution in which the flux crossing the slot becomes uniform at a distance remote from the slot opening. The method of calculating the tangential and normal components of force consist of integrating the stress function around the surface ABCD in Figure 2.8. The points A and D are found by finding a distance z, far enough down the slot for

the flux to have become uniform. To the tangential force component calculated over the surfaces AB and CD are added the contributions associated with the uniform flux crossing the slots, calculated to the required depth of tooth, z'. This presents a slightly different approach to that described above but leads to the same results, as a conformal transformation solution is used. Interestingly, the first approach was used when calculating the tangential and normal components of force on a tooth in the boundary integral method, except that a finite permeability was used which gave rise to a small tangential stress. However, a comparison of the results obtained for the tangential and normal forces on a tooth revealed a close agreement between this method and conformal transformation.(2.2)

2.6 References

2.1 SILVESTER, P. and CHARI, M. V. K. : 'Finite element solution of saturable magnetic field problem', I.E.E. Trans., 1970, PAS-89, pp. 1642-1651.

2.2 BINNS, K. J., KAHAN, P. A., REES, G. R., SIMKIN, J. and TROWBRIDGE, C. W. : 'A comparison of two methods of field solution for slotted boundary shapes in two dimensions', Proc. Compumag, Oxford, 1978.

2.3 BINNS, K. J. and LAWRENSON, P. J. : 'Analysis and computation of electric and magnetic field problems', (Pergamon, 1973).

2.4 BINNS, K. J. : 'The magnetic field and centring force of displaced ventilating ducts in machine cores', Proc. I.E.E., 1961, 108C, pp. 64-70.

2.5 BINNS, K. J., ROWLANDS-REES, G. and KAHAN, P. A. : 'The evaluation of improper integrals encountered in the use of conformal transformation', Journal of Numerical Methods in Engineering, Vol. 14, pp. 567-580, 1979.

2.6 BINNS, K. J. : 'Calculation of some basic flux quantities in induction and other doubly-slotted electrical machines', Proc. I.E.E., 1964, 111, (11), pp. 1847-1858.

2.7 BINNS, K. J. and ROWLANDS-REES, G. R. : 'Main flux pulsations and tangential tooth-ripple forces in induction motors', Proc. I.E.E., 1975, 122, (3), pp. 273-277.

2.8 ALGER, P. L. : 'The nature of induction machines', (Gordon and Breach, 1965).

2.9 BINNS, K. J. : 'Cogging torques in induction machines', Proc. I.E.E., 1968, 115, (12), pp. 1783-1790.

2.10 BINNS, K. J. and ROWLANDS-REES, G. : 'Radial tooth-ripple forces in induction motors due to the main flux', Proc. I.E.E., 1978, 125, (11), pp. 1227-1231.

2.11 ROWLANDS-REES, G. : 'Analysis of no-load force pulsations and cogging torques in induction machines', Ph.D. Thesis, University of Southampton, 1978.

2.12 SAY, M. G. : 'Alternating current machines', (Pitman, 1976).

2.13 HAMMOND, P. :'Applied electromagnetism', (Pergamon Press, 1971).

2.14 GIBBS, W. J. : 'Conformal transformation in electrical engineering',(Chapman and Hall, 1958).

2.15 CARPENTER, C. J. : 'Surface-integral methods of calculating forces on magnetised iron parts', Proc. I.E.E., 1960, 107C, pp. 19-28.

FIG 2.1

HETEROPOLAR FIELD IN MACHINE AIR-GAP

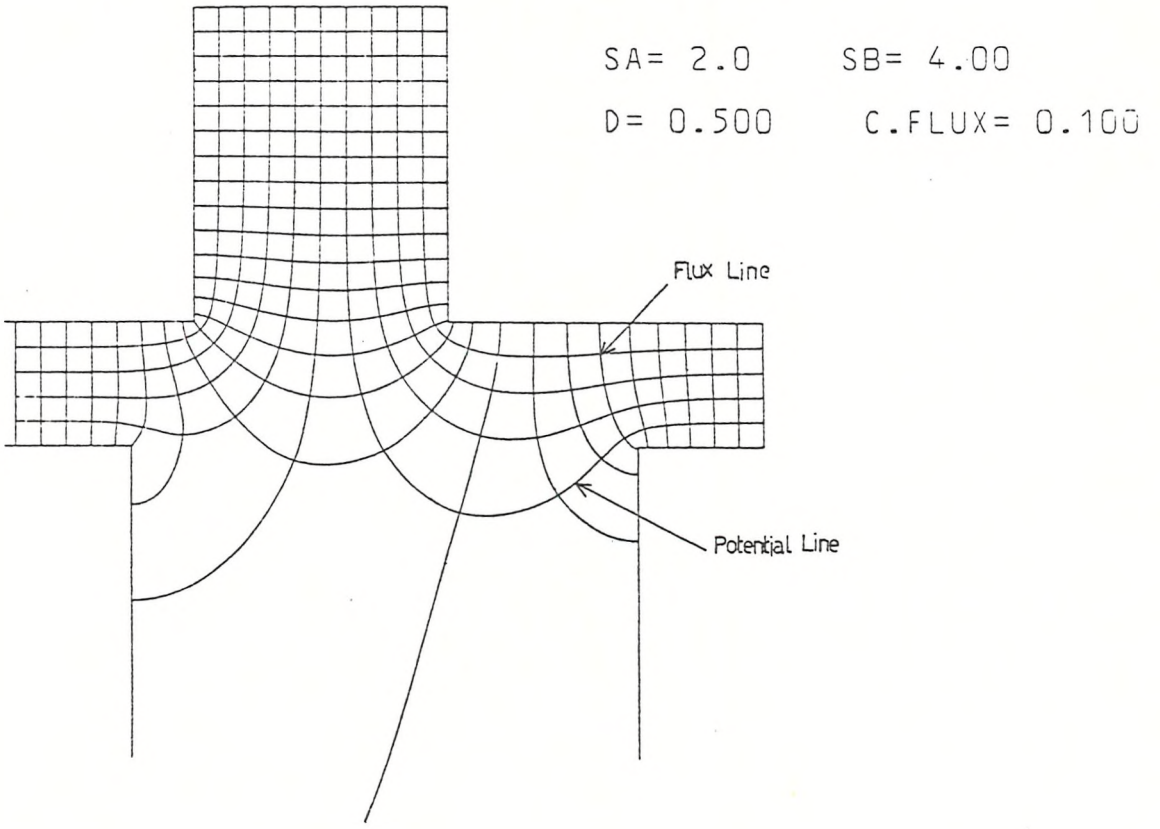

FIG 2.2

HOMOPOLAR FIELD IN MACHINE AIR-GAP

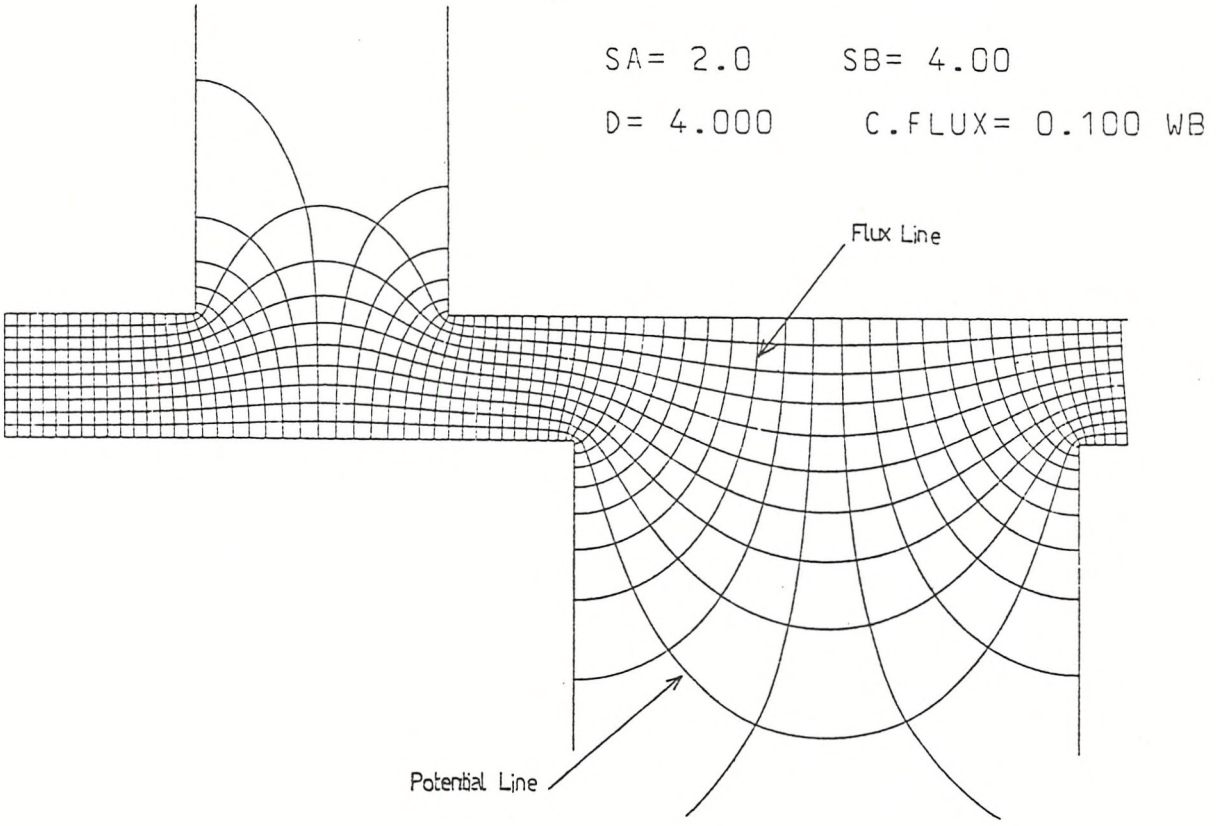

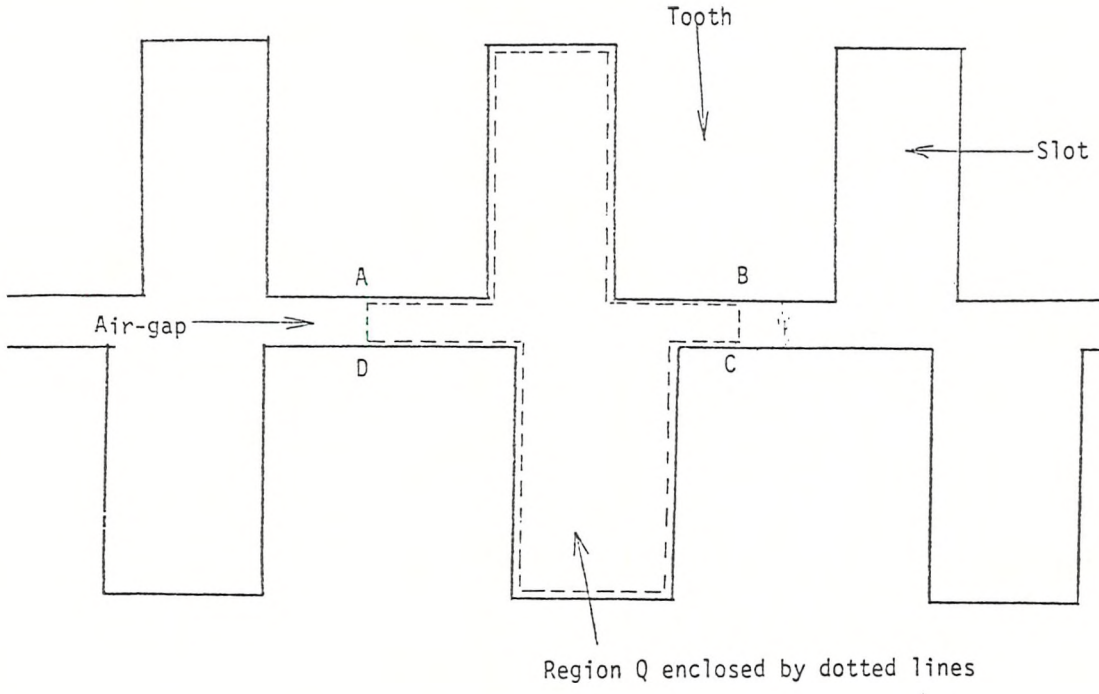

Figure 2.3 Simplified air-gap geometry containing region Q where no-load boundary conditions are defined.

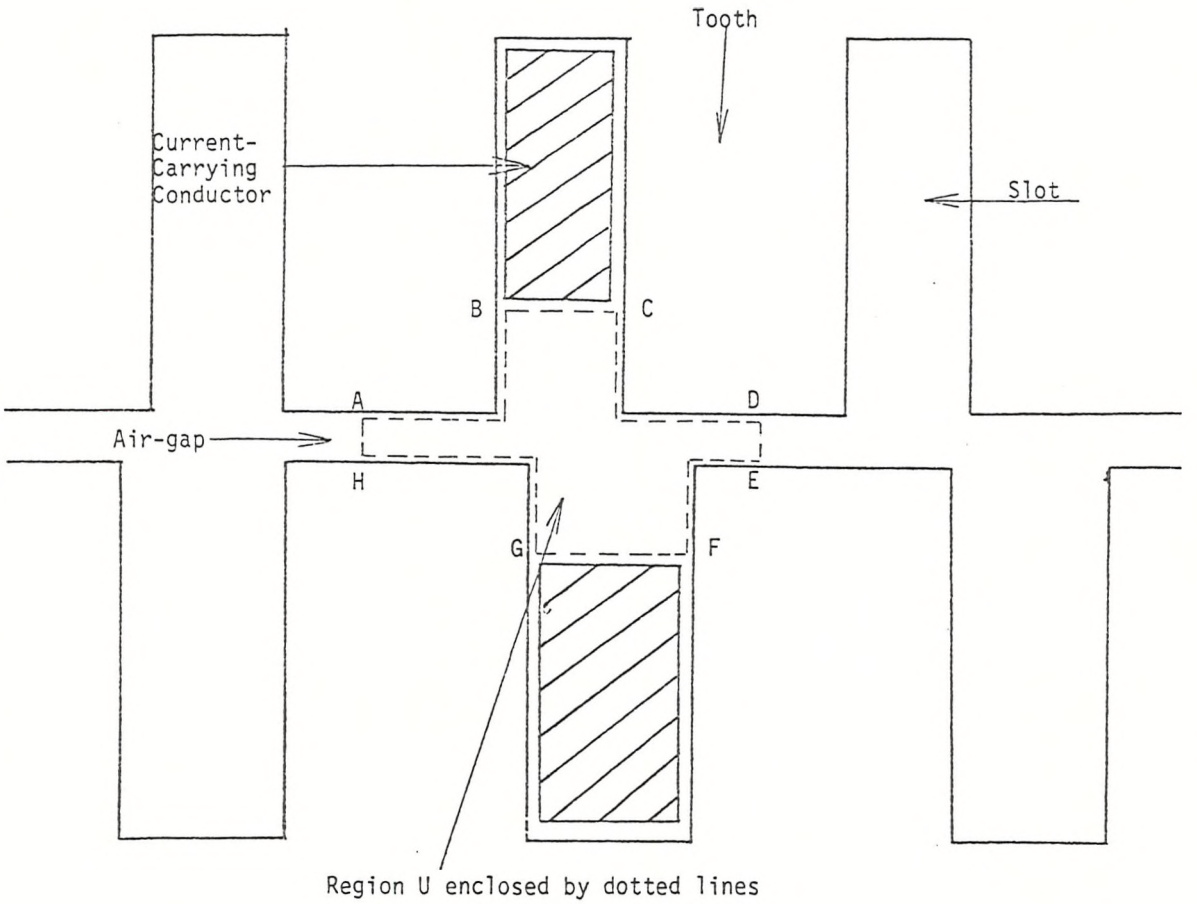

Figure 2.4 Simplified air-gap geometry containing region U where load boundary conditions are defined

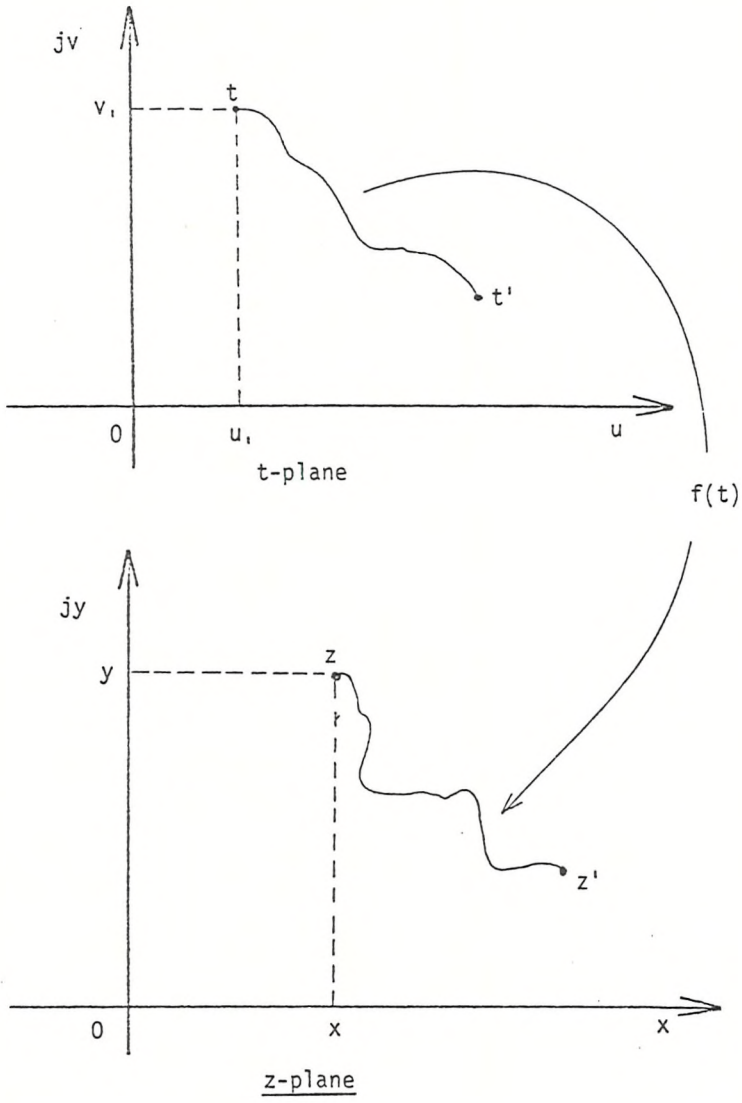

Figure 2.5 The mapping of a curve from the t to z planes

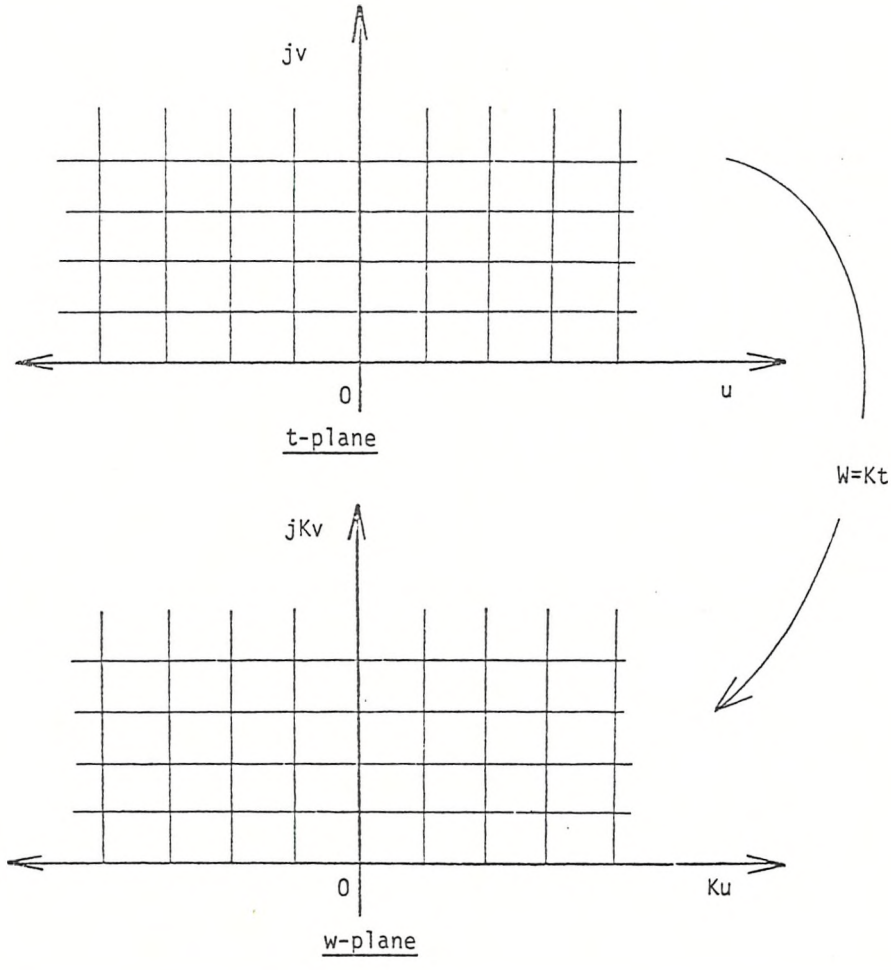

Figure 2.6 Uniform field in t and w planes

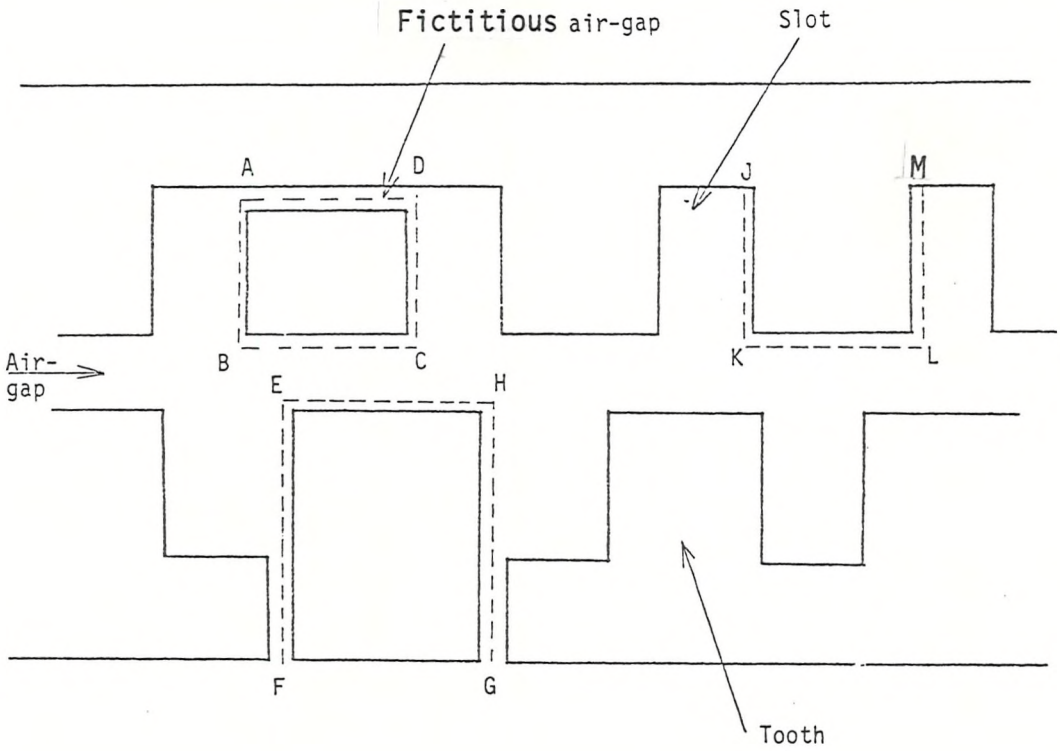

Figure 2.7 Simplified air-gap geometry used to calculate tooth forces

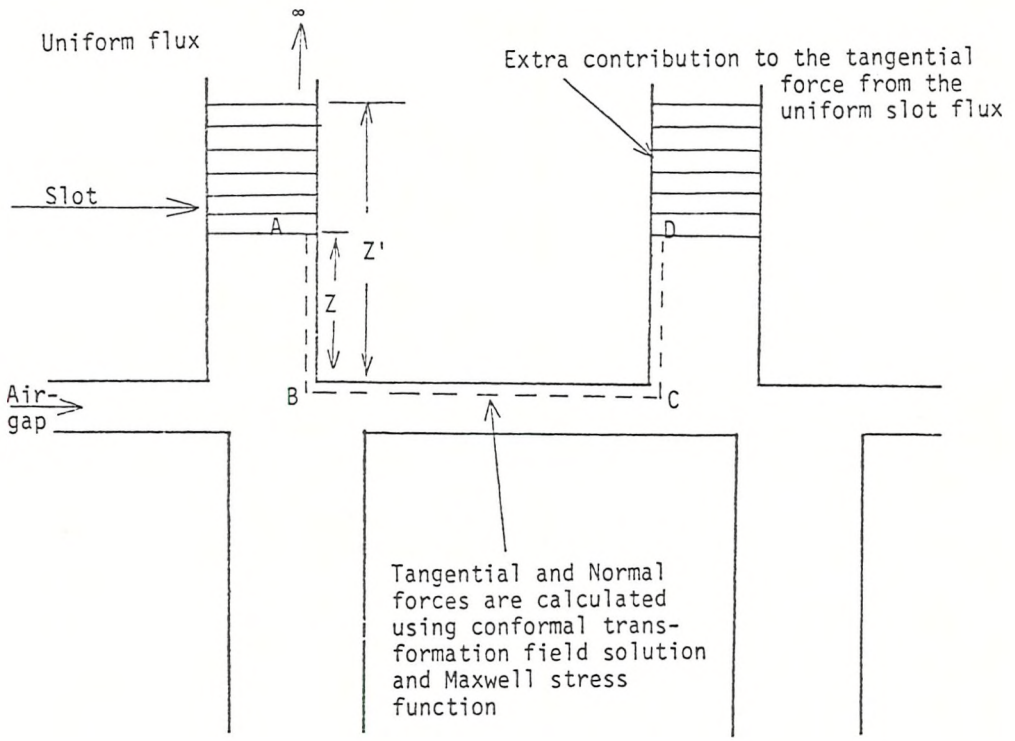

Figure 2.8 Tooth force calculations using a conformal transformation field solution

CHAPTER 3

THE APPLICATION OF CONFORMAL TRANSFORMATION METHODS TO COMPLICATED POLYGONAL BOUNDARY PROBLEMS

3. Introduction

3.1 Schwarz-Christoffel Transformation

3.2 The Constant Finding Process

3.2.1 Definite Integral

3.2.2 Residues

3.2.3 Improper Integral

3.3 Simple Description of Direct-Search Methods

3.3.1 Peckham's Method

3.4 References

3. Introduction

In Chapter 2, methods for calculating the magnetic field and forces in the air-gap region of an induction machine were reviewed, and a numerical conformal transformation was found to be the most suitable. The air-gap geometry, with its slotted boundaries, is a good example of a polygonal boundary, for which a transformation using an intermediate mapping function involving the Schwarz-Christoffel equation is particularly suitable. The main advantages of this transformation equation are that it can handle the sharp corners that occur in the air-gap geometry and it is able to cope with problems in which the vertices of the polygonal boundary meet at infinity. The transformation equation establishes a relationship which can be used to map the real axis of the t-plane onto the polygonal boundary in the z-plane. This transformation equation is defined in Section 3.1.

In Section 3.1, it will be shown that the Schwarz-Christoffel transformation equation is a differential equation containing a number of constant terms. With problems that have only simple boundaries in the z-plane, it is possible to integrate the transformation equation analytically. Furthermore, the constants of the transformation equation can easily be found, as Binns and Lawrenson[3.1] show when considering a number of simple examples. However, when the boundary in the z-plane is more complicated, a numerical integration method is required to evaluate the transformation equation. Furthermore, numerical methods are also required to find the constants of the transformation equation. This constant finding process involves formulating a set of simultaneous equations by relating the constants to the dimensionsof the z-plane boundary. These equations are then evaluated using a numerical optimisation method. This is an important process because unless the

constants can be found to a high accuracy, any field calculation will be subject to error. A further consideration is the time the constant finding process takes to compute the values of the constants to a sufficiently high accuracy. This depends on two factors; firstly, the accuracy and efficiency with which the equations containing integrals of the Schwarz-Christoffel transformation equation can be evaluated, and, secondly, on the particular method of numerical optimisation used. Both G. Rowlands-Rees and the present author have spent much time in developing the constant finding process. Whilst their main interest lies in the calculation of flux and force pulsations in induction machine teeth, their research has led to the development of two new methods for the evaluation of a particular type of improper integral and to the formulation of a general constant finding process suitable for use with complicated boundaries. This type of improper integral also occurs when calculating the electromagnetic forces on teeth.

Such is the importance of the constant finding process that the whole of this chapter is devoted to it. In Section 3.2, a set of non-linear equations is derived from which the constants of a general polygonal boundary can be found. These equations are expressed in the form of integrals, of which there are three different types. The evaluation of one type of integral is explained in this section whilst methods for the evaluation of the other two types are left to Chapter 4. In Section 3.3, a simple description is given of a numerical method suitable for use in finding the constant of a general polygonal boundary.

3.1 Schwarz-Christoffel Transformation

The transformation equation which relates the real axis of the t-plane to the general polygonal boundary of the z-plane (see Figure 3.1) in such a way that the interior of the polygon transforms into the upper

half of the t-plane is given by

$$\frac{dz}{dt} = K.f(t) = K.(t-t_1)^{\frac{\alpha_1}{\pi}-1}(t-t_2)^{\frac{\alpha_2}{\pi}-1}\ldots(t-t_{i-1})^{\frac{\alpha_{i-1}}{\pi}-1}(t-t_i)^{\frac{\alpha_i}{\pi}-1}(t-t_{i+1})^{\frac{\alpha_{i+1}}{\pi}-1}\ldots(t-t_n)^{\frac{\alpha_n}{\pi}-1} \quad (3.1)$$

or more concisely by

$$\frac{dz}{dt} = K.f(t) = K\prod_{i=1}^{n}(t-t_i)^{\frac{\alpha_i}{\pi}-1} \quad (3.2)$$

This is the well known Schwarz-Christoffel differential equation, in which K is a constant of scale and rotation, α_i is the interior angle of the polygon at any vertex i, and t_i is the point on the real axis of the t-plane corresponding to the vertex i of the polygon in the z-plane. Use of equation (3.2) ensures a transformation giving the required vertex angles of the polygon, but before the transformation can be usefully employed, it is necessary to find the values of the constants.

3.2 The Constant Finding Process

In general, two values of t_i can be chosen arbitrarily, as discussed by Binns and Lawrenson[3.1]. The remaining constants have to be found by formulating and solving a set of n-1 equations. As explained previously, these equations are obtained by relating the constants of the transformation equation to the dimensions of the z-plane boundary. These equations will now be derived using the general polygonal boundary shown in Figure 3.2. They can be considered in two categories

(i) where the transformation equation, and therefore the constants, can be related to a finite length of the polygonal boundary, such as the dimension $z_{i-2,i-1}$ in Figure 3.2; this relationship gives rise to a definite integral.

(ii) where those parts of the boundary having parallel sides are used to obtain equations relating the dimensions S and d to the constants of the transformation equation, giving rise to two further types of integral.

3.2.1 Definite Integral

The relationship between the dimension $z_{i-2,\ i-1}$ and the Schwarz-Christoffel transformation equation is given by

$$\left|z_{i-2,i-1}\right| = \left| K\int_{t_{i-2}}^{t_{i-1}} f(t)\ dt \right| \qquad (3.3)$$

Using equation 3.1, this integral may be expressed in the following form

$$\left|z_{i-2,i-1}\right| = \left| K \int_{t_{i-2}}^{t_{i-1}} (t-t_{i-2})^{\alpha}\ (t_{i-1}-t)^{\beta}\ H(t)\ dt \right| \qquad (3.4)$$

where

$$\alpha = \frac{\alpha_{i-2}}{\pi} - 1\ , \quad \beta = \frac{\alpha_{i-1}}{\pi} - 1$$

$$H(t) = \prod_{j=1}^{j=i-3} (t-t_j)^{\frac{\alpha_j}{\pi}-1} \prod_{j=i}^{n} (t_j-t)^{\frac{\alpha_j}{\pi}-1}$$

and the function H(t) is well-behaved in $(t_{i-2},\ t_{i-1})$. In this and the following sections, a well-behaved function may be taken to be one that is continuous and bounded in the region under consideration, and its derivatives are also continuous and bounded in the same region. Clearly, the number of equations of this form is equal to the number of finite dimensions available on the z-plane boundary.

3.2.2 Residues

Consider first the derivation of equations which relate the constants to the dimension S. This involves, in particular, the constant t_i which, as it will be shown, is related to S. It is clear from

Figure 3.2 that the constant t_i corresponds to the point at infinity in the z-plane where the parallel sides meet. There are two possible cases:

a) the point t_i has a finite value,

b) the point t_i is infinite

Consider first case (a). To derive an equation in this case, for the dimension S, it is convenient to express the transformation equation in the following form:

$$\frac{dz}{dt} = \frac{k\,F(t)}{t-t_i} \tag{3.5}$$

In the orientation shown in Figure 3.2, the dimension S may be obtained as the imaginary part of the complex integral

$$\int_c k\,\frac{F(t)}{t-t_i}\,dt \tag{3.6}$$

taken around the semi-circular contour shown in the t-plane of Figure 3.2. To simplify this integral, let $t-t_i = Re^{j\theta}$, then equation (3.6) becomes

$$jS = I_m \int_0^{\pi} k \cdot \frac{F(Re^{j\theta} + t_i)}{Re^{j\theta}}\; j\,Re^{j\theta}\,d\theta \tag{3.7}$$

To obtain the desired relationship, the radius R is shrunk to zero, so that equation (3.7) becomes

$$jS = I_m \lim_{R\to 0} \int_0^{\pi} k\,F(Re^{j\theta} + t_i)\,j\,d\theta \tag{3.8}$$

$$= k\,F(t_i)\,\pi\,j \tag{3.9}$$

or $$S = k\,F(t_i)\,\pi \tag{3.10}$$

The term $F(t_i)$ is the residue of the transformation equation at the simple (or 1st order) pole at the point $t = t_i$. A more general equation for S, which includes all orientations of the geometry, is

given by

$$S = |k \pi F(t_i)| \tag{3.11}$$

In case (b), where $t_i = \infty$, an even simpler equation can be derived for the dimension S. In this case the transformation equation is expressed in its original form (see equation (3.1)) and the dimension S is obtained as the imaginary part of the complex integral

$$\int_C k\, f(t)\, dt \tag{3.12}$$

integrated around the semi-circular contour centred at the origin.

The imaginary part of this integral is given by

$$jS = I_m \int k\, f(t)\, dt \tag{3.13}$$

In this case let $t = Re^{j\theta}$, then equation (3.13) becomes

$$jS = I_m \int_0^{\pi} k\, f(Re^{j\theta})\, j\, Re^{j\theta}\, d\theta \tag{3.14}$$

Now as R approaches infinity $t \gg t_1, t_2, \ldots t_n$

and $\lim_{R\to\infty} f(Re^{j\theta}) = (Re^{j\theta})^{k'}$

where $k' = \sum_{i=1}^{n} (\frac{\alpha_i}{\pi} - 1) = -1$

Hence $jS = \lim_{R\to\infty} \int_0^{\pi} k.f(Re^{j\theta})\, j\, Re^{j\theta}\, d\theta = j.k.\pi$ (3.15)

and $S = k \pi$ (3.16)

As in the previous case, the residue of the transformation equation has been evaluated, although in this case at the point $t_i = \infty$. Equation (3.16) can be generalised to include all orientations of the geometry. This equation is then given by

$$S = |k \pi| \tag{3.17}$$

Obviously, the number of equations of this form, and of the form of equation (3.11), are the same as the number of parallel sides of the boundary in the z-plane.

3.2.3 Improper Integral

The remaining dimension for which it may be necessary to find an expression is d. Rewriting equation (3.1), so that it is in a suitable form in the interval (t_{i-1}, t_{i+1}), and assuming t_i finite

$$\frac{dz}{dt} = (-1)^{\lambda} \frac{k\,(t-t_{i-1})^{\alpha}\,(t_{i+1}-t)^{\beta}\,G(t)}{(t-t_i)} \qquad (3.18)$$

where $\alpha = \frac{\alpha_i}{\pi} - 1$, $\beta = \frac{\alpha_{i+1}}{\pi} - 1$ $(\alpha, \beta > -1)$

$$\lambda = \sum_{j=i+1}^{n} \left(\frac{\alpha_j}{\pi} - 1 \right) \text{ and } G(t) = \prod_{j=1}^{i-2} (t-t_j)^{\frac{\alpha_j}{\pi}-1} \prod_{j=i+2}^{n} (t_j-t)^{\frac{\alpha_j}{\pi}-1}$$

where $G(t)$ is a well-behaved function in (t_{i-1}, t_{i+1}). Then

$$d = \left| \lim_{\substack{\varepsilon\to 0 \\ \varepsilon>0}} \left((-1)^{\lambda} \int_{t_i+\varepsilon}^{t_{i+1}} \frac{k\,(t-t_{i-1})^{\alpha}(t_{i+1}-t)^{\beta}}{t-t_i}\,G(t)\,dt \right.\right.$$

$$\left.\left. - (-1)^{\lambda} \int_{t_i-\varepsilon}^{t_{i-1}} \frac{k\,(t-t_{i-1})^{\alpha}\,(t_{i+1}-t)^{\beta}}{t-t_i}\,G(t)\,dt \right) \right| \qquad (3.19)$$

which reduces to

$$\lim_{\substack{\varepsilon\to 0 \\ \varepsilon>0}} \left(\int_{t_{i-1}}^{t_i-\varepsilon} \frac{k\,(t-t_{i-1})^{\alpha}\,(t_{i+1}-t)^{\beta}}{t-t_i}\,G(t)\,dt + \int_{t_i+\varepsilon}^{t_{i+1}} \frac{k\,(t-t_{i-1})^{\alpha}\,(t_{i+1}-t)^{\beta}}{t-t_i}\,G(t)\,dt \right) \qquad (3.20)$$

The limit of this improper integral is the Cauchy Principal Value, denoted by

$$d = P \int_{t_{i-1}}^{t_{i+1}} |K| \frac{(t-t_{i-1})^{\alpha}\,(t_{i+1}-t)^{\beta}}{t-t_i}\,G(t)\,dt \qquad (3.21)$$

A formal definition of the Cauchy Principal Values is given in Appendix 1 of the thesis by Rowlands-Rees[3.2] and in the book by Cohen[3.3].

Thus, three types of integrals have been defined, namely, definite, residue and improper. Each of these integrals relate the constants K and t_i (for all values of i) to the dimensions of the z-plane boundary. Using them, it is possible to derive the n-1 equations necessary to find

the constants of the transformation equation. With some simple geometries the constants can be found analytically, but with more complicated geometries a numerical method is required. The explicit relationships, obtained by relating the distance between parallel sides to the value of the residue at the appropriate poles, can either be solved directly or by an iterative process to give some of the constants. The remaining implicit relationships, where a formal numerical integration is required to relate the chosen dimensions to the t-plane constants, are rearranged to form a set of equations, elements of which tend to zero at the required solution. A typical element, F_j, is given by

$$F_j = \left|Z_{i,i+1}\right| - \left|K \int_{t_i}^{t_{i+1}} f(t)\, dt\right| \qquad (3.22)$$

An error function, composed of the elements of F_j is defined as

$$E_r = \sum_j F_j^2 \qquad (3.23)$$

Initial values of the unknown constants t_1, t_2, etc. are chosen and are varied by a direct-search program until E_r has been made sufficiently small. The choice of a suitable computer program is the subject of the next section.

3.3 Simple Description of Direct-Search Methods

Since the advent of the digital computer, a number of numerical methods have been developed to find the n variables of a set of n non-linear equations. Essentially, these methods minimise a function which is formulated from the set of equations. The function E_r, defined in the previous section, is an example of such a function. It has been shown[3.4] that a function expressed as a sum of squares function can be minimised more efficiently than a general function. It is for this reason that the function E_r is defined as a sum of squares function.

Numerical methods of optimisation may be categorised under two headings:

(i) gradient methods,

(ii) direct-search methods.

In general, the first methods are more efficient because gradients of the functions are calculated and used to determine the best direction of search for the minimum of the function. However, these methods have not been applied to the minimisation of the function E_r, because it is very difficult to calculate the gradients associated with this function. Thus the function E_r has been minimised using direct-search methods.

Of the direct-search methods currently available, the most suitable are those devised by Powell[3.5] and Peckham[3.4]. Lawrenson and Gupta[3.6] propose the use of Powell's method to find the constants of the transformation equation of a general polygonal boundary. This method is iterative, the n-dimensional search is broken down into a sequence of one-dimensional linear searches. One iteration consists of a linear search along each of the co-ordinate directions of the n-variables. At each iteration a new conjugate direction is generated and used to replace one of the current direction, so that a path is found from the "guessed" starting point to the minimum. This principle is illustrated in Figure 3.3 for a problem in two-dimensional space. A possible path from the starting point to the minimum is shown.

Binns, Rowlands-Rees and Kahan[3.7] have used Peckham's method. This method is based on the simplex method in which the minimum is enclosed in a n-dimensional region called a simplex. As an example of a simplex, such a region in two-dimensional space would be an equilateral triangle. The simplex is reduced in size around the minimum until it has been calculated to the desired accuracy. The principle of this

method is illustrated in Figure 3.4, where again the problem of finding a minimum in two-dimensional space is shown. Clearly, to obtain the most rapid solution, the simplex should surround the minimum. However, even if the simplex does not, it is still possible to obtain a solution because the program based on Peckham's method used here will generate new points so that a simplex is obtained which does surround the minimum.

The author has chosen Peckham's method in preference to Powell's mainly because it requires fewer function evaluations per iteration, which is clearly an advantage when evaluating functions containing definite and improper integrals which have to be evaluated numerically. It should be noted, however, that Peckham's method requires a greater number of numerical operations per iteration.

3.3.1 Peckham's Method

The method devised by Peckham determines the vector of variables $\underline{x} = x_1, x_2, \ldots x_n$ which minimises the sum of squares function

$$S_m = \sum_{k=1}^{m} \left(f_k (x) \right)^2 \qquad (3.24)$$

A linear approximation to the f_ks are given by

$$f_k = h_k + \sum_{i=1}^{n} g_{ki} x_i \qquad (3.25)$$

where h_k is the constant and the g_{ki}s are the gradients associated with the function f_k. In matrix notation

$$\underline{f} = \underline{h} + \underline{G}.\underline{x} \qquad (3.26)$$

The value of $\underline{x}$ at the minimum $\underline{y}$ is given by

$$\underline{G}^T \underline{G}.\underline{y} = -\underline{G}^T.\underline{h} \qquad (3.27)$$

If the values of the gradients are available, these equations can be solved for $\underline{y}$. However, the functions f_k are not generally linear, so that $\underline{y}$ is not the true minimum, but may be used as a starting point

for the next iteration. Peckham combined the above equation with the simplex method to obtain an efficient method for the minimisation of a sum of squares function. His method is now available as a subroutine package in the Nottingham Algorithms Library (N.A.G.) and a description of this routine now follows.

The user of the subroutine submits an initial estimate of the values of $\underline{x}$, from which a set of at least n+1 points (denoted x_{n+1}) are generated. The corresponding function values f_{n+1} are then calculated. A linear approximation to these function values is obtained by minimising the weighted sum of squares, over the point set $\underline{x}_{n+1}$, of the difference between the linear approximation and the function values. That is, $\underline{h}$ and $\underline{G}$ are chosen to minimise the m expressions

$$\sum_{\ell=1}^{n+1} \omega_\ell{}^2 (h_k + \sum g_{ki}\, x_{i\ell} - f_{k\ell})^2 \qquad (3.28)$$

where $k = 1, 2, \ldots m$ and the w_ℓs are the weighting factors. The values of $\underline{h}$ and $\underline{G}$ which minimise equation (3.28) are given by

$$\underline{X}' . \underline{X}'^{T}\, \underline{G}^{T} = \underline{X}'\, \underline{F}'^{T} \qquad (3.29)$$

and

$$\underline{h} = \frac{1}{\Omega}\, \underline{F}'\, w \qquad (3.30)$$

where matrix notation has been used and $\Omega = \sum_{\ell=1}^{n+1} w_\ell{}^2$

Once the coefficients of the linear approximation have been calculated, they are then used to obtain a set of equations for y. An equation for $\underline{y}$ in terms of $\underline{X}$ and $\underline{F}$ is given by

$$\underline{y} = \frac{-1}{\Omega} (\underline{X}'\, \underline{X}'^{T})\, (\underline{X}'\, \underline{F}'^{T}\, \underline{F}'\, \underline{X}'^{T})^{-}\, (\underline{X}'\, \underline{F}'^{T}\, \underline{F}'\, w) \qquad (3.31)$$

Thesesets of equations for $\underline{y}$ are evaluated using orthogonal transformations. One iteration consists, therefore, of replacing that point of

the current point set $\underline{x}_{n+1}$, which has the largest sum of squares by the estimated solution of the previous iteration. The set of equations derived from this new set is then solved to obtain a new estimate of the solution. This process continues until S_m has been minimised to the required accuracy.

The value of the weights in equation (3.28) are chosen to give function values nearer the minimum more weight in determining h and G

$$\omega_i^2 = \frac{1}{S_i} \quad \text{where} \quad S_i = \sum_{k=1}^{m} (f_{ki}) \tag{3.32}$$

To ensure convergence, the step made in any one iteration is limited. Also no point is accepted if the value of S_m for this point is greater than all those in the set x_{n+1}. If a point $\underline{x}_i$ is unacceptable, a new point x_i' may be generated by

$$\underline{x}_i' = \frac{w_i \underline{x}_i + w_o \underline{x}_o}{w_i + w_o} \tag{3.33}$$

where x_o is the point with the smallest value of S_m. This rule may have to be applied several times to obtain an acceptable point.

In the routine, the number of points generated at the start of the program (denoted P) is, in fact, greater than n+1 and becomes equal to the largest integer less than $n+3+\frac{1}{3}n$. The extra points are obtained by repeated application of equation (3.31) and each new point replaces the point of the set with the largest value of S_m. The upper bound for P is chosen empirically. These additional points are included to reduce the probability of the n+1 points collapsing in a sub-space of less than n-dimensions. However, this may still happen if the functions f_k are linear in one variable. In this case equation (3.31) will be ill-conditioned and the routine will not attempt to obtain a solution. Instead a new point in the region of the point with the smallest value of S_m will be generated using a pseudo-random number generator.

Obviously, it is important to ensure that there are at least n+1 independent function values.

Peckham's method, in common with other direct-search methods, cannot distinguish between a local and global minimum. However, in the conformal transformation application this is not a problem, and the search always converges to the right solution.

Rowlands-Rees[3.2] describes a method for improving the efficiency of Peckham's method when integrals are evaluated. The reader is recommended to read his thesis for details of this method.

3.4 References

3.1 BINNS, K. J. and LAWRENSON, P. J. : 'Analysis and computation of electric and magnetic field problems',(Pergamon, 1973).

3.2 ROWLANDS-REES, G. : 'Analysis of no-load force pulsations and cogging torques in induction machines', Ph.D. thesis, University of Southampton, 1978.

3.3 COHEN, A. M., CUTTS, J. F., FIELDER, R., JONES, D. E., RIBBANS, J. and STUART, E. : 'Numerical analysis', (McGraw Hill, 1973).

3.4 PECKHAM, G. : 'A new method for minimising a sum of squares without calculating gradients', The Computer Journal, 1970, 13, pp.418-420.

3.5 POWELL, M. J. D. : 'A method for minimising a sum of squares of non-linear functions without calculating derivatives', The Computer Journal, 1965, 7, pp.303-307.

3.6 LAWRENSON, P. J. and GUPTA, S. K. : 'Conformal transformation employing direct-search techniques of minimisation', Proc. I.E.E., 1968, 115, (3), pp.427-431.

3.7 BINNS, K. J., ROWLANDS-REES, G. and KAHAN, P. A. : 'The evaluation of improper integrals encountered in the use of conformal transformation,'Journal of Numerical Methods in Engineering,1979, Vol. 14, pp.567-580.

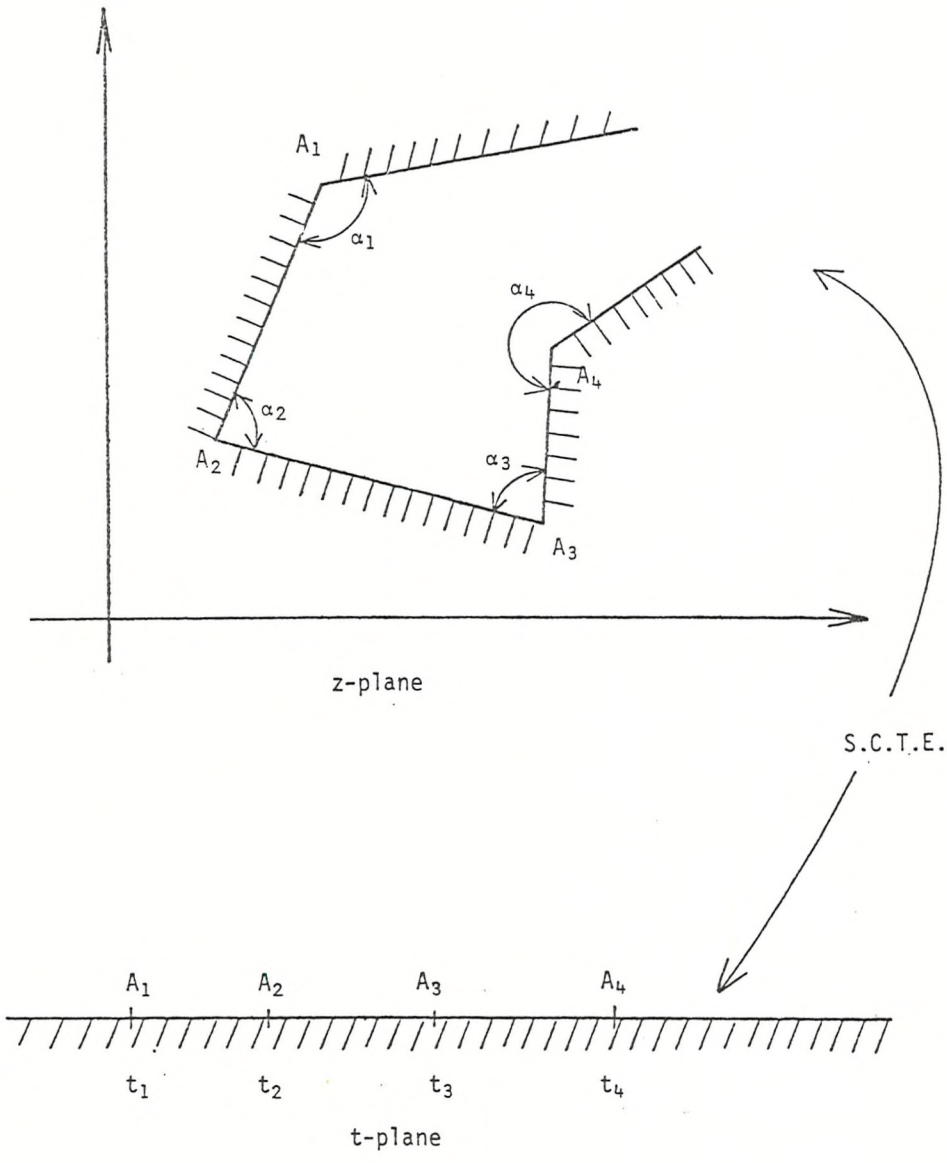

Figure 3.1 The mapping of the general polygonal boundary in the z-plane from the real axis of the t-plane using the Schwarz-Christoffel transformation equation.

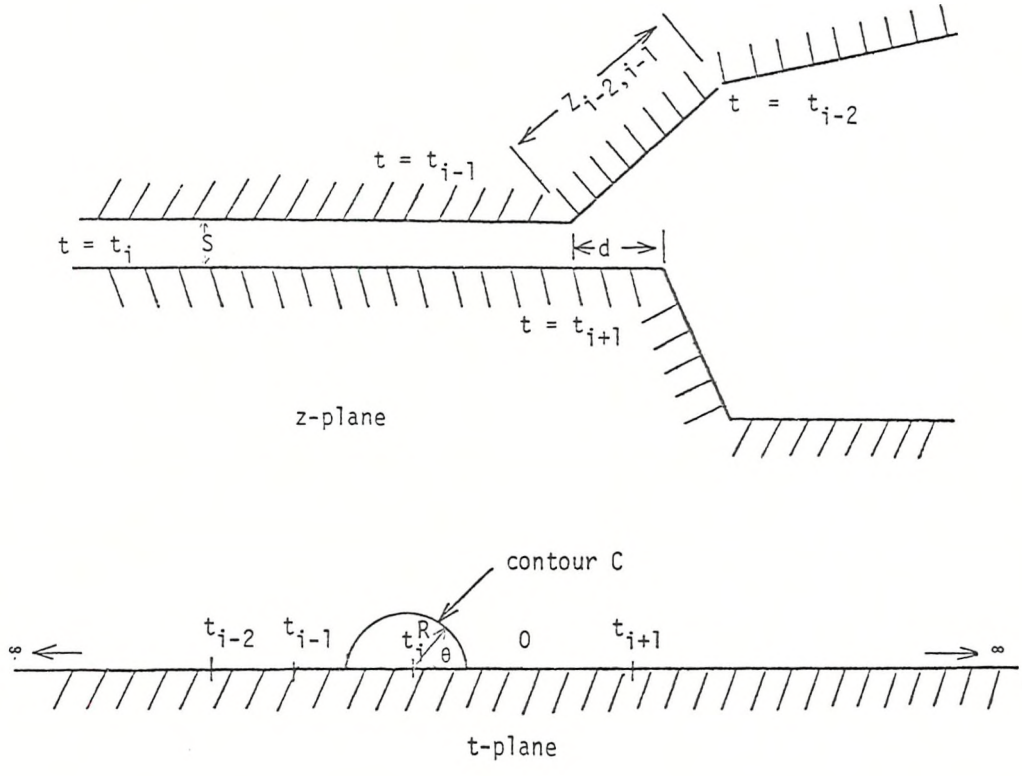

Figure 3.2 General polygonal boundary with parallel sides

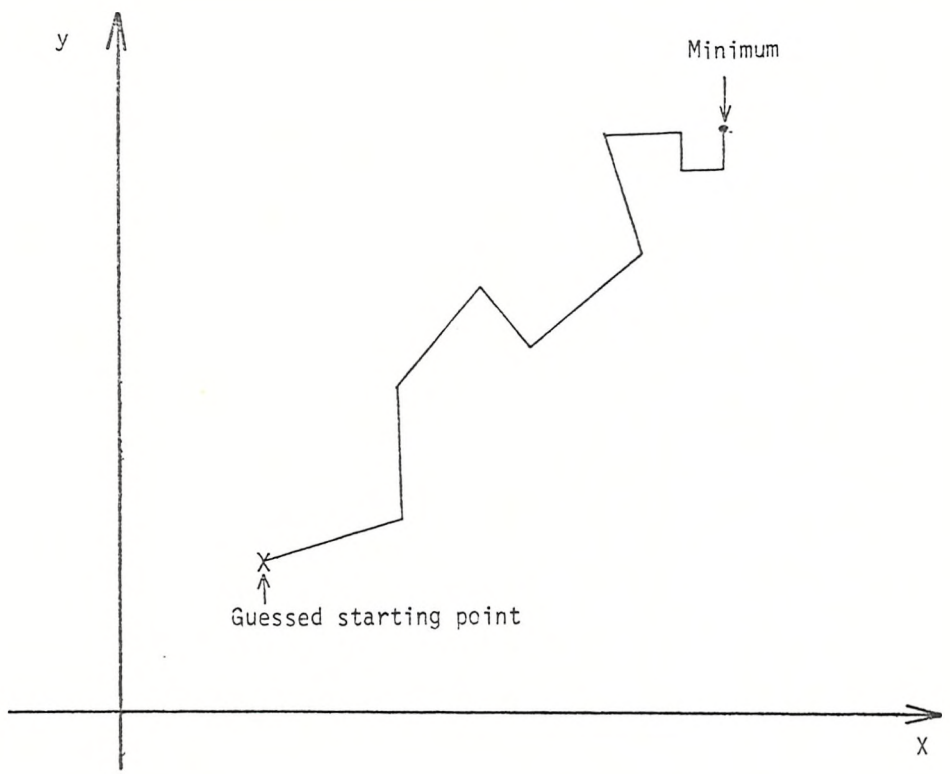

Figure 3.3 An illustration of Powell's method showing a possible path from the guessed starting point to the minimum of the function

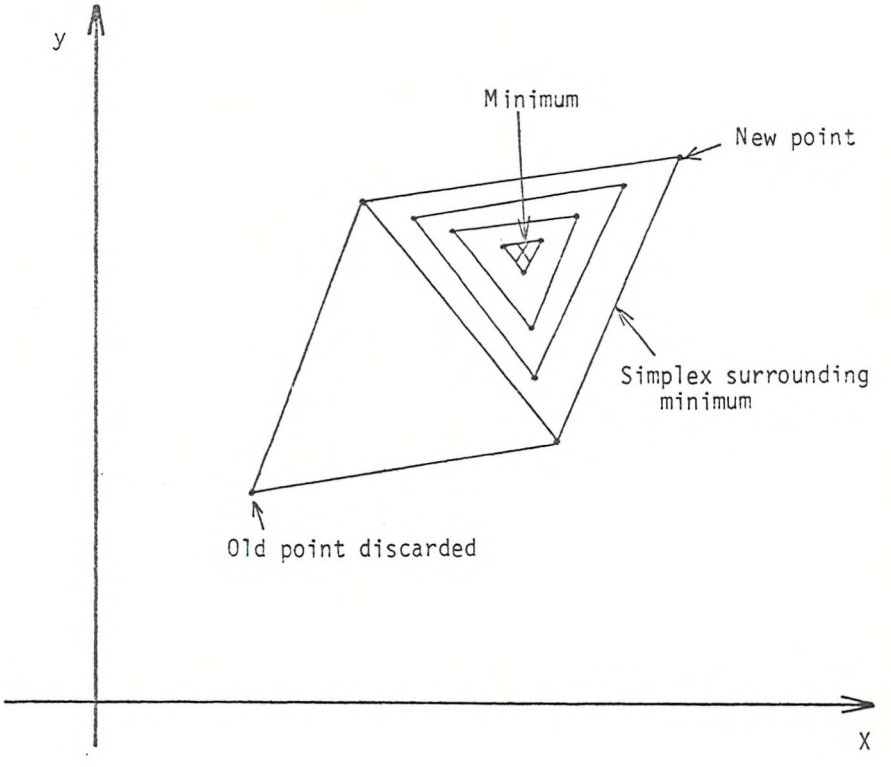

Figure 3.4 The Simplex method in which a simplex first surrounds the minimum and is then shrunk until the solution is obtained to the desired accuracy

CHAPTER 4

THE ANALYTICAL AND NUMERICAL EVALUATION OF INTEGRALS ENCOUNTERED IN CONFORMAL TRANSFORMATION PROBLEMS

4. Introduction

4.1 Limitations of Analytical Methods

4.2 Quadrature Methods

4.3 Methods for the Solution of Integrals with End-Point Singularities

4.3.1 Integrals Associated with Boundaries having Right-Angled Vertices

4.3.2 Integrals Associated with a General Boundary Shape

4.3.3 Displacing the Singularity

4.3.4 The Change of Variable Method

4.3.5 Gauss-Jacobi Method

4.3.6 The Method of Branders and Piessens

4.3.7 A Comparison of the Different Forms of Quadrature

4.4 The Evaluation of Cauchy Principal Values

4.4.1 Evaluation of the Integral using the Chebyshev Series

4.4.2 Evaluation of C_r

4.4.3 Cases where I_0 and I_1 can be Evaluated Analytically

4.4.4 The Evaluation of the Improper Integral by Subtracting Out the Singularity

4.4.5 A Comparison of the Two Methods

4.5 A Further Problem

4.6 Conclusions

4.7 References

4. Introduction

It is essential that the definite and improper integrals, defined in the previous chapter, can be evaluated both accurately and efficiently if the method of conformal transformation is to be applied to problems with complicated boundaries. Therefore, this chapter is mainly concerned with the numerical evaluation of these two types of integral.

The air-gap region of an induction motor has rectangular boundaries (the vertices of the boundary are right-angles) and it is possible to evaluate the integrals that arise with these boundaries analytically. However, these analytical methods have their limitations and it is shown, in Section 4.1, that a numerical approach is more suitable.

Having established this, Section 4.2 deals with the numerical integration of a well-behaved function. This section is included, firstly, to give a brief introduction to numerical integration and, secondly, because some of the methods used to evaluate the definite and improper integrals involve making their integrands well-behaved

This is followed in Section 4.3 by a description and comparison of four methods suitable for the numerical evaluation of the definite integral. In the next section, Section 4.4, two methods are derived which are suitable for the evaluation of the improper integral. A numerical example is then given to compare the accuracy and efficiency of the two methods.

With the numerical methods described in Sections 4.3 and 4.4, it is possible to apply conformal transformation methods to problems with complicated boundaries. To illustrate this, an example is given in Section 4.5 of a region containing a pair of semi-closed slots. The necessary equations required to find the constants of the transformation equation are defined.

The chapter is concluded in Section 4.6 with a brief comparison between the methods used to evaluate both the definite and improper integrals.

4.1 Limitations of Analytical Methods

Although this chapter is mainly concerned with the numerical evaluation of integrals associated with complicated polygonal boundaries, the first integrals to be discussed are those that occur as a result of the application of conformal transformation methods to the air-gap region of an induction machine and can be evaluated analytically. These are of two types and may be expressed in the following forms:

$$K_1 \int \frac{f(t)\,dt}{g(t)\,\sqrt{(t-a)(t-b)}} \tag{4.1}$$

$$K_2 \int \frac{h(t)\,dt}{K(t)\,\sqrt{(t-c)(t-d)(t-e)(t-f)}} \tag{4.2}$$

where K_1 and K_2 are constants and $f(t)$, $g(t)$, $h(t)$ and $K(t)$ are polynomials of t.

The first type of integral is associated with a boundary having two right-angled vertices, which results in two square root terms in the denominator of the integrand. This integral may be evaluated analytically using a transformation equation of the form:

$$p = \frac{t - b}{t - a} \tag{4.3}$$

The solution contains a number of terms which are themselves simple functions of p, such as $\tan^{-1} p$ and $\log_e p$. A boundary involving this type of integral will be considered in the next chapter.

The second type of integral is associated with a boundary having four right-angled vertices and is an elliptic integral. Whilst it is possible to obtain an analytical solution to this type of integral, the manipulation and subsequent numerical evaluation may be extremely

difficult and laborious. To illustrate these difficulties, consider the following example.

Figure 4.1 shows a complicated boundary in the z-plane with four right-angled vertices. It will be shown in the next chapter that this boundary represents a pair of open slots in the slotted air-gap region. The Schwarz-Christoffel transformation equation, which maps the real axis of t-plane into this region, is given by

$$\frac{dz}{dt} = K \frac{\sqrt{(t+t_0)(t+t_1)(t-t_2)(t-t_4)}}{t(t+1)(t-t_3)} \tag{4.4}$$

An expression for z may be obtained by integrating equation (4.4), that is

$$z = K \int \frac{\sqrt{(t+t_0)(t+t_1)(t-t_2)(t-t_4)}}{t(t+1)(t-t_3)}\, dt \tag{4.5}$$

It is shown in Appendix 1 that the analytical solution of this integral is given by

$$Z = K \left[A\, F(x,k') + \sum_{i=1}^{4} B_i\, \Pi\,(x, K_{1i}, K') + \sum_{i=1}^{4} C_i \sinh^{-1} \frac{(v_i - \ell_i)}{S_i} \right] \tag{4.6}$$

where A and all the values of B_i and C_i are constants, $F(x, K')$ is an elliptic function of the first kind and $\Pi(x, K_{1i}, K')$ is an elliptic function of the third kind. Only a brief description of the algebraic manipulation necessary to obtain this solution is given in the appendix. A complete derivation would take many pages. Obviously, such a derivation is time consuming and laborious as each stage must be carefully checked.

There are also a number of difficulties that arise when considering the numerical evaluation of equation (4.6). If the evaluation is carried out by hand, the only practical method of performing this is to use tables. However, the main difficulty in using tables, is that, in some cases, there are large intervals between given values, which makes

interpolation very difficult. The alternative is to use a digital computer to evaluate the functions from a series expansion. Binns and Lawrenson[4.1] list a number of these series in Appendix II of their book. Clearly this is preferable to feeding tables into a computer store. Freeman[4.2] has applied the series developed by King, which are most suitable for the evaluation of elliptic integrals and functions, as they converge more rapidly than other, better-known series. However, the numerical methods described later in this chapter were preferred when evaluating equation (4.5) and other integrals associated with the air-gap geometry. This choice was made because these numerical methods are more convenient to use and give an accurate solution (typical error of the order of 10^{-10}) to all the integrals that occur when calculating the field in the air-gap of an induction machine.

4.2 Quadrature Methods

In this section, a number of numerical methods are described which are suitable for the evaluation of the integral

$$\int_a^b f(x)\, dx \tag{4.7}$$

where $f(x)$ is a well-behaved function. These methods are used later in this chapter when methods for the evaluation of the definite and improper integral, defined in the previous chapter, are considered.

Essentially, all methods of numerical integration consist of approximating the above integral by a weighted sum of function values, that is, by the equation

$$\sum_{i=1}^{n} w_i\, f(x_i) \tag{4.8}$$

where the w_i are the weights and the x_i are the nodes. All the

x_i lie in the interval (a,b) and can include the two end points a and b .

A whole class of formulae, known as Newton-Coles formulae, has been derived using equally spaced nodes. Of these formulae, the most commonly used is Simpson's rule. The n-point form of this rule is obtained by integrating the interpolating polynomial of degree n-1, which is equal to the integrand f(x), at each of the n equally-spaced values in the interval (a,b). In practice, the interval (a,b) is divided into 2 m equally spaced segments. It can be shown[4.3] that the n-point formula is given by

$$\frac{1}{6\,m} \cdot (b-a)\,(f_0 + 4f_1 + 2f_2 + 4f_3 + 2f_4 + \ldots 4f_{2m-1} + f_{2m}) \quad (4.9)$$

where 2 and 4 are the weights of the equation

Comparison of two results is a common method of assessing the accuracy of integrals evaluated on a digital computer by Simpson's rule. However, this check can be unreliable, as is shown by Clenshaw and Curtis[4.3], who considered the following example.

$$f(x) = \frac{23}{25}\cosh x - \cos x\,, \quad a = -1,\ b = 1 \quad (4.10)$$

The values obtained from equation (4.9) are 0.4795546 for m = 1, and 0.4795551 for m = 2, whereas the true value of the integral is 0.4794282.

The possibility of the check failing can be greatly reduced if at least three successive values are taken, although this, of course, increases the amount of computation.

The nodes of equation (4.8) do not have to be equally spaced and a whole class of formulae has been derived, called Gauss formulae, with unequally spaced nodes which are, in general, more accurate than Simpson's rule. The Gauss formula, which can be used to approximate equation

(4.7), is given by

$$(b - a) \sum_{i=1}^{n} H_i \, f(x_i) \qquad (4.11)$$

where $x_i = \frac{1}{2}(b + a) + \frac{1}{2} t_i (b - a)$

$$H_i = \frac{1}{(1 - t_i^2)\{P_n'(t_i)\}^2}$$

and $t_1, t_2, \ldots t_n$ are the zeroes of the Legendre polynomial $P_n(t)$. Equation (4.11) is exact if $f(x)$ is a polynomial of degree not exceeding $2n - 1$. Thus, if $n = 3$, equation (4.11) will be exact for a polynomial up to and including a fifth order term. However, this considerable power is achieved only by introducing a set of irrational values of x_i and H_i, whose values need to be stored.

It is also more difficult to check the Gauss formulae than Simpson's rule. Repetition with a new set of n requires a completely new set of values of x_i and H_i. Unlike Simpson's rule, previously computed co-ordinates cannot be used when n is increased.

Patterson[4.4] has developed a method which overcomes the difficulty of checking the Gauss formulae. This method uses a family of interlacing Gauss formulae in the following way. Beginning with the 3-point Gauss formula, a new 7-point rule is derived, 3 points of which have abscissae that coincide with the original Gauss abscissae. The remaining 4 points are chosen to give the greatest possible increase in polynomial degree. The resulting 7-point formula has a degree of precision 11. The procedure is then repeated, adding 2 new points to the 7-point rule, to give a 15-point formula with degree of precision 23. Continuing, further rules using 31, 63, 127 and 255 points are derived, all with an increasing degree of precision. Thus, two

results can be checked after each new formulae has been derived.

This method has been used extensively when evaluating the integrals that occur as a result of the application of conformal transformation methods to the air-gap region of an induction machine.

Finally in this section, the method developed by Clenshaw and Curtis[4.3] is briefly described. This method consists of expanding the integrand f(x) in a finite Chebyshev series and integrating the terms in the series individually. Smith and Imhof[4.5, 4.6] have derived a quadrature formula of the form of equation (4.8) for this method and Smith and O'Hara[4.7], after tests on various functions, give an expression for a reliable error estimate. The Chebyshev series is chosen in preference to other series, because it is rapidly convergent. This is important both in the reduction of computational time and in the estimation of an accurate upper bound for the error[4.8].

4.3 Methods for the Solution of Integrals with End-Point Singularities

This section discusses the evaluation of the definite integral,

$$\left|Z_{i-2,i-1}\right| = \left|\int_{t_{i-2}}^{t_{i-1}} kf(t)\,dt\right| = \left|k\int_{t_{i-2}}^{t_{i-1}} (t-t_{i-2})^{\alpha}\,(t_{i-1}-t)^{\beta}\,H(t)\,dt\right| \qquad (4.12)$$

defined in the previous chapter. The integration of the function f(t) is not as straightforward as that of a well-behaved function due to the presence of the two terms $(t - t_{i-2})^{\alpha}$ and $(t_{i-1} - t)^{\beta}$. In particular, the powers α and β play an important role in determining the nature of the integrand, f(t), in the vicinity of the end-points. Consider, for example, the influence of the value of α on the function f(t).* If α is greater than minus one but less than zero, the term $(t - t_{i-2})^{\alpha}$ is a pole of the function f(t) and $f(t) = \infty$ at the point $t = t_{i-2}$. If,

*The values of α and β in equation (4.12) always lie in the range $-1 < \alpha$ or $\beta < 1$.

however, α is greater than zero but less than one, the term $(t - t_{i-2})^{\alpha}$ is a zero of the function f(t) and f(t) = 0 at the point $t = t_{i-2}$. In this case f(t) has an infinite first derivative at the point $t = t_{i-2}$.

Exactly the same considerations apply to the other term, $(t_{i-1}-t)^{\beta}$. Therefore, if the two terms are combined, there are four possible cases that can occur, each of which is shown in Figure 4.2. Whichever case occurs, there are difficulties in integrating equation (4.12) numerically.

4.3.1 Integrals Associated with Boundaries having Right-Angled Vertices

Consider first the four combinations where (α, β) equals $(-\frac{1}{2}, -\frac{1}{2})$, $(-\frac{1}{2},+\frac{1}{2})$, $(+\frac{1}{2}, -\frac{1}{2})$ and $(+\frac{1}{2}, +\frac{1}{2})$. These cases are associated with a boundary having at least two right-angled vertices. It is not always recognised that in these cases the integrand f(t) can be made well-behaved by using a simple transformation equation. Consider, for example, the case where (α, β) equals $(-\frac{1}{2}, -\frac{1}{2})$, then equation (4.12) becomes

$$\left| Z_{i-2,i-1} \right| = \left| k \int_{t_{i-2}}^{t_{i-1}} \frac{H_t(t)\, dt}{(t - t_{i-2})^{\frac{1}{2}} (t_{i-1} - t)^{\frac{1}{2}}} \right| \qquad (4.13)$$

The range of integration can be changed to the interval (-1, 1) by using the linear transformation equation

$$t = \tfrac{1}{2} \left(t_{i-2} + t_{i-1} + x\, (t_{i-1} - t_{i-2})\right)$$

so equation (4.13) then becomes

$$\left| Z_{i-2,i-1} \right| = \left| k \int_{-1}^{1} \frac{H_x(x)\, dx}{(1 + x)^{\frac{1}{2}} (1 - x)^{\frac{1}{2}}} \right| \qquad (4.14)$$

Then, if the substitution $x = \cos\theta$ is made, equation (4.14) becomes

$$\left| Z_{i-2,i-1} \right| = \left| k \int_{0}^{\pi} H_{\theta}\, (\cos\theta)\, d\theta \right| \qquad (4.15)$$

The integrand in equation (4.15) is now well-behaved in the interval $(0, \pi)$ and the integral can be evaluated using any of the numerical methods described in the previous section. The remaining three cases can be treated in a similar manner and the results of the transformation are listed below.

$$\left| k \int_{-1}^{1} \frac{(1 - x)^{\frac{1}{2}}}{(1 + x)^{\frac{1}{2}}} H_x(x)\, dx \right| = \left| k \int_{0}^{\pi} (1 - \cos\theta)\, H_\theta(\cos\theta)\, d\theta \right| \quad (4.16)$$

$$\left| k \int_{-1}^{1} \frac{(1 + x)^{\frac{1}{2}}}{(1 - x)^{\frac{1}{2}}} H_x(x)\, dx \right| = \left| k \int_{0}^{\pi} (1 + \cos\theta)\, H_\theta(\cos\theta)\, d\theta \right| \quad (4.17)$$

$$\left| k \int_{-1}^{1} (1 + x)^{\frac{1}{2}} (1 - x)^{\frac{1}{2}} H_x(x)\, dx \right| = \left| k \int_{0}^{\pi} \sin^2\theta\, H_\theta(\cos\theta)\, d\theta \right| \quad (4.18)$$

4.3.2 Integrals Associated with a General Boundary Shape

When dealing with values of (α, β) other than the four just considered, the simple transformation equation can no longer be used. However, a number of methods have been developed to evaluate the general integral and four of these methods are now considered.

4.3.3 Displacing the Singularity

The difficulties caused by the singularities are overcome by Binns[4.9] and Lawrenson and Gupta[4.10] by commencing the integration at a point removed from the singularities by a small amount . Thus, on displacing the singularity, equation (4.12) becomes

$$\left| Z_{i-2,i-1} \right| = \left| k \int_{t_{i-2}+\delta}^{t_{i-1}-\delta} (t - t_{i-2})^{\alpha} (t_{i-1} - t)^{\beta} H(t)\, dt + E(\delta) \right| \quad (4.19)$$

where $E(\delta) = k \int_{t_{i-2}}^{t_{i-2}+\delta} (t - t_{i-2})^{\alpha} (t_{i-1} - t)^{\beta} H(t)\, dt + k \int_{t_{i-1}-\delta}^{t_{i-1}} (t - t_{i-2})^{\alpha} \cdot (t_{i-1} - t)^{\beta} H(t)\, dt \quad (4.20)$

The term $E(\delta)$ is relatively small and Lawrenson and Gupta assume that if a suitably small value of δ is chosen, $E(\delta)$ can be neglected. Binns does not neglect this term but approximates it in the following way. Consider the first term on the right hand side of equation (4.20)

$$k\int_{t_{i-2}}^{t_{i-2}+\delta} (t - t_{i-2})^{\alpha} (t_{i-1} - t)^{\beta} H(t)\, dt \qquad (4.21)$$

This can be written in the following form

$$\int_{t_{i-2}}^{t_{i-2}+\delta} (t - t_{i-2})^{\alpha} F(t)\, dt \qquad (4.22)$$

where $F(t) = k(t_{i-1} - t)^{\beta} H(t)$

In the interval $(t_{i-2},\ t_{i-2} + \delta)$, $F(t)$ is generally monotonic and its range of variation is small. For both these reasons equation (4.22) can be closely approximated by

$$F(t_{i-2} + \tfrac{\delta}{2}) \int_{t_{i-2}}^{t_{i-2}+\delta} (t - t_{i-2})^{\alpha}\, dt = \frac{F(t_{i-2} + \frac{\delta}{2})}{\alpha + 1}\, \delta^{\alpha+1} \qquad (4.23)$$

The second term on the r.h.s. of equation (4.20) can be treated in the same manner and hence $E(\delta)$ can be evaluated.

A suitable choice of δ is very important if the method is to be successful, and the value chosen is essentially a compromise. It must be small enough to ensure that $E(\delta)$ is small, but must not be so small that the integrand of the first term on the r.h.s. of equation (4.19) becomes too large. Binns recommends a value of 0.001 for δ as being the most suitable for most practical problems. Lawrenson and Gupta suggest that a more efficient method is to relate δ to each of the limits of integration. They recommend that for the interval $(t_{i-2},\ t_{i-1})$ that $\delta_{i-2} = 0.001\ |t_{i-2}|$ and $\delta_{i-1} = 0.001\ |t_{i-1}|$. However, Rowlands-Rees[4.11] shows by an example that such a procedure is incorrect and recommends instead that the value of δ should be related to the range

of integration, that is

$$\delta = 0.001 \, |t_{i-1} - t_{i-2}| \tag{4.24}$$

All that remains is to consider the evaluation of

$$\left[k \int_{t_{i-2}+\delta}^{t_{i-1}-\delta} (t - t_{i-2})^{\alpha} \, (t_{i-1} - t)^{\beta} \, H(t) \, dt \right] \tag{4.25}$$

Since the integrand of this equation is well-behaved, any of the numerical methods described in Section 4.2 can be used.

4.3.4 Change of Variable

As mentioned earlier, the integrand of a function can sometimes be made well-behaved by using a suitable transformation equation. This is true in the case of equation (4.12).

To show this, consider the following integral

$$Z_{ab} = \int_{a}^{b} \frac{F(t) \, dt}{(t - a)^{\alpha}} \tag{4.26}$$

where the integrand has a pole at the lower limit of integration. This pole may be removed from the integrand by using the transformation equation

$$y = (t - a)^{1-\alpha} \tag{4.27}$$

Equation (4.26) then becomes

$$Z_{ab} = \int_{0}^{(b-a)^{1-\alpha}} \frac{F(a + y^{\frac{1}{1-\alpha}})}{1 - \alpha} \, dy \tag{4.28}$$

and the integrand is a well-behaved function.

In a similar manner the zero of the integral

$$Z_{ab} = \int_{a}^{b} (t - a)^{\alpha} \, F(t) \, dt \tag{4.29}$$

can be removed by using the transformation equation

$$y = (t - a)^{1+\alpha} \tag{4.30}$$

Equation (4.29) then becomes

$$Z_{ab} = \int_0^{(b-a)^{1+\alpha}} \frac{F(a + y^{\frac{1}{1+\alpha}})}{1 + \alpha} \, dy \qquad (4.31)$$

This procedure can now be applied to an integral having singularities at both limits of integration. Consider, for example, the case where the terms $(t - t_{i-2})^{\alpha}$ and $(t_{i-1} - t)^{\beta}$ are poles of the integrand in equation (4.12). Then this integral can be written in the following form

$$\left|Z_{i-2,i-1}\right| = \left| k \int_{t_{i-2}}^{t_{i-1}} \frac{H(t)\, dt}{(t - t_{i-2})^{\alpha} (t_{i-1} - t)^{\beta}} \right| \qquad (4.32)$$

Furthermore, this integral can be separated into two integrals,

$$\left|Z_{i-2,i-1}\right| = \left| k \int_{t_{i-2}}^{tz} \frac{H(t)\, dt}{(t - t_{i-2})^{\alpha} (t_{i-1} - t)^{\beta}} + k \int_{tz}^{t_{i-1}} \frac{H(t)\, dt}{(t - t_{i-2})^{\alpha} (t_{i-1} - t)^{\beta}} \right| \qquad (4.33)$$

where tz has a value lying somewhere in the interval $\left[t_{i-2}, t_{i-1}\right]$. The integrand of both integrals can be made well-behaved by using equation (4.27), and then they can be evaluated using the numerical methods described previously. Obviously, the remaining three cases shown in Figure 4.2 can be treated in a similar manner. Murthy Vamaraju[4.12] used this technique when applying the method of conformal transformation to the calculation of electromagnetic fields.

4.3.5 Gauss-Jacobi Method

Another approach to the evaluation of equation (4.12) is described by Howe[4.13]. In this method the interval $[t_{i-2}, t_{i-1}]$ is again transformed into the interval $[-1, 1]$ by the linear transformation equation

$$t = \tfrac{1}{2} \left[t_{i-2} + t_{i-1} + x(t_{i-1} - t_{i-2})\right] \qquad (4.34)$$

and equation (4.12) then becomes

$$\left|Z_{i-2,i-1}\right| = \left|k \int_{-1}^{1} (1 + x)^{\alpha} (1 - x)^{\beta} H_x(x)\, dx\right| \qquad (4.35)$$

In this form, the integral can be approximated by using the Gauss Jacobi quadrature formula. This formula is another example of the very powerful Gauss quadrature formulae mentioned previously. An approximation to equation (4.35) is given by

$$\sum_{i=1}^{n} A_i H_x (x_i) \qquad (4.36)$$

where the A_i are the coefficients and the x_i are the nodes of the quadrature formula. These coefficients and nodes can be calculated using the formulae derived by Krylov[4.14] in his book. The highest degree of precision of this quadrature formulae is 2n - 1.

Stroud and Secrest[4.15] have written a computer program to evaluate the nodes and coefficients of equation (4.36) for arbitrary values of α, β and n. They have also tabulated the nodes and coefficients for a range of values of α, β and n.

Consistency of results with different values of n is used to check the accuracy of integration. Once again, new values of the nodes and coefficients have to be calculated for each new value of n and stored in the computer.

4.3.6 The method of Branders and Piessens

This method is an extension of the Clenshaw-Curtis method to include integrands with end-point singularities. A quadrature scheme has been developed to calculate the integral

$$\int_{a}^{b} \omega(t)\, f(t)\, dt \qquad (4.37)$$

where the weighting function $\omega(t)$ is any one of the following five:

$\omega(t) = 1$

$\omega(t) = 1/(t - \alpha)$ $\quad a < \alpha < b$

$\omega(t) = (b - t)^{\alpha} (t - a)^{\beta}$ $\quad \alpha, \beta > -1, a < b$

$\omega(t) = (b - t)^{\alpha} (t - a)^{\beta} \ell n(t - a)$ $\quad \alpha, \beta > -1, a < b$

$\omega(t) = (b - t)^{\alpha} (t - a)^{\beta} \ell n(b - t)$ $\quad \alpha, \beta > -1, a < b$

and $f(t)$ is a well-behaved function. The method of solution involves transforming the range of integration to the interval $\left[-1, 1\right]$, as previously described. This gives equation (4.37) in the form

$$I = \frac{b-a}{2} \int_{-1}^{1} v(x)\, g(x)\, dx \tag{4.38}$$

where $v(x)$ and $g(x)$ are the transformed weighting and continuous functions respectively. The function $g(x)$ is then expanded in a truncated Chebyshev series (following the procedure of the Clenshaw-Curtis method), that is

$$g(x) \simeq \sum_{j=0}^{N}{}'' \; c_j \, T_j \, (x) \tag{4.39}$$

where the double prime indicates that both the first and last terms in the expansion are to be multiplied by a $\frac{1}{2}$. I is then approximately given by

$$I \simeq \frac{b-a}{2} \sum_{j=0}^{N}{}'' \; c_j \, m_j \tag{4.40}$$

where the m_j are the modified moments of the weighting function $v(x)$. Branders and Piessens[4.16] have derived recursive formulae for these moments.

A computer package is now available consisting of a subroutine using the integration scheme. A Fast Fourier Transform algorithm is used to calculate the Chebyshev coefficients, this being applied to the sequence $N = 6, 12, 24, 48, \ldots$. Using this sequence, the integral is

computed until the difference between any two successive computed values satisfies $|\varepsilon| < \max(A, B|J|)$, where A and B are the specified absolute and relative tolerances and J is the last computed approximation of the integral.

4.3.7 A Comparison of the Different Forms of Quadrature

The method of displacing the singularity has been used successfully in several interesting problems[4.10] but cannot be recommended as a generally reliable method of integration.

The technique of changing the variable is attractive, due to its simplicity, but the author has a very limited experience in the use of this method.

The Gauss-Jacobi method in general gives accurate results but is more difficult to program than the previous two methods as the nodes X_k and the coefficients A_k have to be recalculated for each new value of n.

The method of Branders and Piessens is particularly attractive, especially as it is available as a computer package. One feature of this package is that, in common with library routines that integrate well-behaved functions, the user is able to specify the degree of accuracy required.

4.4 The Evaluation of Cauchy Principal Values

This section is concerned with the numerical evaluation of the improper integral.

$$d = P\int_{t_{i-1}}^{t_{i+1}} |k| \frac{(t - t_{i-1})^{\alpha} (t_{i+1} - t)^{\beta}}{t - t_i} G(t)\, dt \qquad (4.41)$$

This integral is more difficult to evaluate than the one in the previous section because in addition to having the end-point singularities, the integrand also has a simple pole. Thus, for the case where the two

terms $(t - t_{i-1})^{\alpha}$ and $(t_{i+1} - t)^{\beta}$ are poles of the integrand, the integrand will be infinite at three points in the interval $[t_{i-1}, t_{i+1}]$. Two methods have been developed for evaluating this integral to a high degree of accuracy and these are now described and compared.

4.4.1 Evaluation of the Integral using the Chebyshev Series

This is a further extension of the Clenshaw-Curtis method to include integrals of the type described by equation (4.41). The interval $[t_{i-1}, t_{i+1}]$ is, as before, transformed into the interval $[-1, 1]$ by the linear transformation

$$t = \tfrac{1}{2}\left[t_{i-1} + t_{i+1} + x\,(t_{i+1} - t_{i-1})\right] \tag{4.42}$$

Equation (4.41) can now be rewritten as

$$d = P\int_{-1}^{1} S \cdot \frac{(1 + x)^{\alpha}\,(1 - x)^{\beta}}{x - A}\,G(x)\,dx \tag{4.43}$$

where $S = \left[K.\left|(t_{i+1} - t_{i-1})/2\right|^{\alpha+\beta}\right]$

and $A = \dfrac{2t_i - t_{i-1} - t_{i+1}}{t_{i+1} - t_{i-1}}$, $|A| < 1$

As G(x) is a well-behaved function in the interval $[-1, 1]$, it can be expanded as a Chebyshev series, following the procedure of Clenshaw-Curtis.

Writing G(x) as a truncated Chebyshev series gives

$$G(x) = \sum_{r=0}^{n}{}' b_r\,T_r(x) + E_n(x) \tag{4.44}$$

where $\sum_{r=0}^{n}{}' q_r = \tfrac{1}{2} q_0 + q_1 + q_2 + \ldots q_n$

Equation (4.43) can now be rewritten

$$d = P\int_{-1}^{1} \frac{S(1 + x)^{\alpha}\,(1 - x)^{\beta}}{x - A}\left(\sum_{r=0}^{n}{}' b_r\,T_r(x) + E_n(x)\right) dx \tag{4.45}$$

or

$$d = \sum_{r=0}^{n}{}' \; b_r . I_r + EPS_n(x) \tag{4.46}$$

where

$$I_r = P \int_{-1}^{1} \frac{S(1 + x)^{\alpha} \; (1 - x)^{\beta}}{x - A} \; T_r(x) \; dx$$

The error term is

$$EPS_n(x) = P \int_{-1}^{1} \frac{S(1 + x)^{\alpha} \; (1 - x)^{\beta}}{x - A} \; E_n(x) \; dx$$

and if an upper limit EPS_n is found for $E_n(x)$ then

$$EPS_n(x) \leq I_o \; EPS_n$$

The Chebyshev polynomials $T_r(x)$ are related by the well known recurrence relation

$$T_{r+1}(x) - 2x \; T_r(x) + T_{r-1}(x) = 0 \; , \quad T_0(x) = 1, \quad T_1(x) = x$$

and by using this, a recursive system can be found which relates the terms I_r.

Since

$$I_{r+1} = P \int_{-1}^{1} \frac{S(1 + x)^{\alpha} \; (1 - x)^{\beta}}{x - A} \; T_{r+1}(x) \; dx$$

$$= P \int_{-1}^{1} \frac{S(1 + x)^{\alpha} \; (1 - x)^{\beta}}{x - A} \left(2x \; T_r(x) - T_{r-1}(x) \right) \; dx$$

$$= 2 \int_{-1}^{1} S \; (1+x)^{\alpha} (1-x)^{\beta} \; T_r(x) \; dx + P \int_{-1}^{1} 2A \cdot \frac{S(1+x)^{\alpha}(1-x)^{\beta}}{x - A} \; T_r(x) \; dx - I_{r-1}$$

this integral may be written as

$$I_{r+1} - 2A \; I_r + I_{r-1} = C_r \tag{4.47}$$

where

$$C_r = 2 \int_{-1}^{1} S \; (1+x)^{\alpha} \; (1-x)^{\beta} \; T_r(x) \; dx \tag{4.48}$$

$$I_o = P \int_{-1}^{1} \frac{S(1+x)^{\alpha} \; (1-x)^{\beta}}{x - A} \; dx \tag{4.49}$$

and

$$I_1 = \int_{-1}^{1} S\,(1+x)^{\alpha}\,(1-x)^{\beta}\,dx + A\,I_o \qquad (4.50)$$

The recurrence system defined by equation (4.47) has a general solution which is trignometric, since $|A| < 1$, and so the system is well conditioned when recurred in the forward direction to find I_2, I_3 ... I_n. This is discussed further by Fox and Mayer[4.17].

4.4.2 Evaluation of C_r

The values of C_r are found by evaluating equation (4.48) and, if this equation cannot be evaluated analytically, it can readily be approximated by either the Gauss-Jacobi quadrature formula or by using the method of Branders and Piessens[4.16]. It is important to note that the constants C_r have to be calculated only once, which is a great advantage if the integration is to be performed many times.

4.4.3 Cases where I_0 and I_1 can be Evaluated Analytically

The four cases where (α, β) equals $(-\frac{1}{2}, -\frac{1}{2})$, $(-\frac{1}{2}, +\frac{1}{2})$, $(+\frac{1}{2}, -\frac{1}{2})$ and $(+\frac{1}{2}, +\frac{1}{2})$ are the only ones for which I_0 can be evaluated analytically. Only the case $(\alpha, \beta) = (-\frac{1}{2}, -\frac{1}{2})$ is considered as the value of I_0 for the remaining three cases can be derived from this case.

Substituting the values $\alpha = -\frac{1}{2}$ and $\beta = -\frac{1}{2}$ into equation (4.49) gives

$$I_0 = P\int_{-1}^{1} \frac{S(1+x)^{-\frac{1}{2}}\,(1-x)^{-\frac{1}{2}}}{x - A}\,dx = P\int_{-1}^{1} \frac{S\,dx}{(1-x^2)^{\frac{1}{2}}\,(x-A)} \qquad (4.51)$$

Making the substitution, $x = \cos\theta$

$$I_0 = P\int_{0}^{\pi} S\,\frac{d\theta}{\cos\theta - A}, \quad |A| < 1 \qquad (4.52)$$

and taking the limit involved in the Cauchy Principal Value it is found that $I_0 = 0$.

The method above can be adapted to deal with the other three cases. All values of I_0, I_1 and C_r that can be found analytically have been collected together and are presented in Table 4.1.

α	β	I_0	I_1	C_r
$-\frac{1}{2}$	$-\frac{1}{2}$	0	$S\pi$	$C_r = 0,\ r = 1, \infty$
$-\frac{1}{2}$	$+\frac{1}{2}$	$-S\pi$	$S\pi(1 - A)$	$C_1 = -S\pi,\ C_r = 0,\ r = 2, \infty$
$+\frac{1}{2}$	$-\frac{1}{2}$	$S\pi$	$S\pi(1 + A)$	$C_1 = S\pi,\ C_r = 0,\ r = 2, \infty$
$+\frac{1}{2}$	$+\frac{1}{2}$	$-S\ A\ \pi$	$S\pi(\frac{1}{2} - A^2)$	$C_1 = 0,\ C_2 = -S\pi/2,\ C_r = 0,\ r = 3, \infty$

Table 4.1

a) $\underline{\alpha + \beta = 0}$

In this, and the following case, it is helpful to consider the transformation equation

$$\frac{dw}{dt} = S\,\frac{(t+1)^{\alpha}\,(t-1)^{\beta}}{t - A} \tag{4.53}$$

The relationship between I_0 and equation (4.53) is shown in Figure 4.3. The case represented in Figure 4.3 is $\alpha > 0$, and the I_0 shown is a positive number. It is important to realise that I_0 is not a modulus but can have negative as well as positive values.

By evaluating the residues at $t = A$ and at infinity, the following values of u and v are obtained.

$$u = |S\pi(A + 1)^{\alpha}\,(1 - A)^{\beta}| \tag{4.54}$$

$$v = |S\pi| \tag{4.55}$$

It is then a simple trigometric exercise to show that

$$I_0 = \left(v - u\cos(\alpha\pi)\right)\sin(\alpha\pi) \tag{4.56}$$

Using equation (4.56) and substituting it in equation (4.50),

$$I_1 = S \int_{-1}^{1} \frac{(1 + x)^{\alpha}}{(1 - x)^{\alpha}} dx + A\left[v - u \cos(\alpha\pi)\right] \sin(\alpha\pi) \qquad (4.57)$$

which can be integrated by the calculus of residues to give

$$I_1 = \frac{2 S \pi \alpha}{\sin(\alpha\pi)} + A \left[v - u \cos(\alpha\pi)\right] \sin(\alpha\pi) \qquad (4.58)$$

b) $\underline{\alpha + \beta < 0}$

When $\alpha + \beta$ is negative the configuration is as shown in Figure 4.4, where the lines meet at the point B, corresponding to $t = \infty$.

By evaluating the residue at $t = A$, the value of u is obtained as

$$u = |S\pi (A + 1)^{\alpha} (A - 1)^{\beta}|$$

Making the substitution

$$x = \frac{1}{t}$$

$$v = \left| S \int_{-1}^{0} \frac{(1 + x)^{\alpha} (1 - x)^{\beta} x^{-(\alpha+\beta+1)}}{(1 - Ax)} dx \right| \qquad (4.59)$$

and

$$y = \left| S \int_{0}^{1} \frac{(1 + x)^{\alpha} (1 - x)^{\beta} x^{-(\alpha+\beta+1)}}{(1 - Ax)} dx \right| \qquad (4.60)$$

Equations (4.59) and (4.60) can be evaluated numerically using either the Gauss-Jacobi quadrature or the method used by Branders and Piessens.

With the application of simple trigonometry to Figure 4.4, the following equations are obtained

$$u = -v \sin(\alpha\pi) - y \sin(\beta\pi) \qquad (4.61)$$

$$I_0 = v \cos(\alpha\pi) - y \cos(\beta\pi) \qquad (4.62)$$

It is not necessary to evaluate both v and y, as they are related to u by equation (4.61).

c) $\alpha + \beta > 0$

Under these conditions, I_0 can be conveniently found by reducing the improper integral to a form that has already been considered.

$$I_0 = P\int_{-1}^{1} \frac{S(1+x)^{\alpha}\,(1-x)^{\beta}}{x - A}\,dx$$

$$= S\int_{-1}^{1} (1+x)^{\gamma}\,(1-x)^{\beta}\,dx + P\int_{-1}^{1} \frac{S(1+A)(1+x)^{\gamma}(1-x)^{\beta}}{x - A}\,dx \qquad (4.63)$$

where $\gamma = \alpha - 1$.

The first term on the r.h.s. of equation (4.63) can be integrated in terms of the beta function

$$S\int_{-1}^{1} (1+x)^{\gamma}\,(1-x)^{\beta}\,dx = S.2^{\gamma+\beta+1}\,\beta(1+\gamma,\ 1+\beta) \qquad (4.64)$$

The integration of the second term on the r.h.s. of equation (4.63) depends on the value of $\gamma + \beta$. If $\gamma + \beta \leq 0$ then it can be integrated by the methods already described ; if $\gamma + \beta > 0$, then the procedure is repeated until the integral is in a suitable form.

4.4.4 The Evaluation of the Improper Integral by Subtracting Out the Singularity

This technique of evaluating Cauchy Principal Values is based on the method of 'subtracting' or 'weakening' the singularity[4.18]. Consider again equation (4.43)

$$d = P\int_{-1}^{1} S\,\frac{(1+x)^{\alpha}\,(1-x)^{\beta}}{x - A}\,G(x)\,dx$$

Since G(x) is a well-behaved function in the interval [-1, 1], it can be expanded as a Taylor series about the point x = A to give

$$G(x) = G(A) + G'(A)\,(x-A) + \frac{G''(A)\,(x-A)^2}{2!} + \ldots \qquad (4.65)$$

If a function H(x) is now defined as

$$H(x) = \frac{G(x) - G(A)}{x - A} \tag{4.66}$$

it can be seen that

$$H(x) = G'(A) + \frac{G''(A)\ (x-A)}{2\ !} + \ldots \tag{4.67}$$

which is also a well-behaved function in the interval $[-1, 1]$.

Returning to equation (4.43), it is evident that this can be rearranged into the following form

$$d = P \int_{-1}^{1} S\ G(A)\ \frac{(1+x)^{\alpha}\ (1-x)^{\beta}}{x - A}\ dx + \int_{-1}^{1} S\ H(x)\ (1+x)^{\alpha}\ (1-x)^{\beta}\ dx \tag{4.68}$$

The first term on the r.h.s of equation (4.68) is a principal value and can be evaluated by the techniques described earlier. The second term is, of course, a definite integral and can be evaluated by the methods described in the previous section.

4.4.5 A Comparison of the Two Methods

To compare the accuracy and efficiency of the two methods, it is useful to consider the one finite value of d' in Figure 4.1 for which the constants of equation (4.4) can be found analytically. This occurs when the slot centres are aligned, so that

$$d' = (S_B - S_A)/2 \tag{4.69}$$

Rowlands-Rees[4.11] has shown that the constants, in this case, are given by the following equations

$$S = \frac{1}{\pi} \tag{4.70}$$

$$t_0 = \frac{x + \sqrt{x^2 - 4}}{2} \tag{4.71}$$

$$t_0 = \frac{1}{t_1} \tag{4.72}$$

$$t_4 = \frac{y + \sqrt{y^2 - 4}}{2} \tag{4.73}$$

$$t_2 = \frac{1}{t_4} \tag{4.74}$$

$$t_3 = 1 \tag{4.75}$$

where $$x = \frac{S_A^2 - S_B^2 + \sqrt{(S_A^2 - S_B^2 + 4)^2 + 16S_B^2}}{2} \tag{4.76}$$

and $$y = x + S_B^2 - S_A^2 \tag{4.77}$$

The comparison is made by evaluating the following two integrals

$$\left| P \int_{-t_1}^{-t_0} \frac{S\sqrt{(t+t_0)(t+t_1)(t-t_2)(t-t_4)}}{t(t+1)(t-t_3)}\, dt \right| = 0 \tag{4.78}$$

and

$$d' = P \int_{-t_1}^{t_2} \frac{S\sqrt{(t+t_0)(t+t_1)(t-t_2)(t-t_4)}}{t(t+1)(t-t_3)}\, dt \tag{4.79}$$

The first integral shows the condition that the two surfaces on either side of the slot are collinear, whilst the second integral relates the slot displacement, d', to the constants of the transformation equation.

Three typical sets of values of S_A and S_B were chosen and the constants were calculated using equations (4.69) - (4.77). Equations (4.78) and (4.79) were then evaluated using the Chebyshev method (called method 1 for short) and the method of weakening the singularity (called method 2). The results of the calculations are presented in Table 4.2. In this table, n is the number of Chebyshev coefficients used in method 1 and H is the result obtained from evaluating equation (4.78). The error term, E_{nT}, was taken as the sum of the absolute values of the last three terms in the Chebyshev series multiplied by I_0, that is

$$E_{nT} = (|b_n| + |b_{n-1}| + |b_{n-2}|)\, I_0 \tag{4.80}$$

In method 2, the second integral of equation (4.68) was evaluated using

$S_A = 1.0 \qquad S_B = 1.25$

$t_0 = 0.23218932 \times 10^{+1}$		$t_1 = 0.43068303 \times 10^{0}$
$t_2 = 0.33563320 \times 10^{0}$	$t_3 = 1$	$t_4 = 0.29794430 \times 10^{+1}$
Method 1		
n = 15	$d' = -0.12500000$	$E_{nT} = 0.20 \times 10^{-9}$
n = 25	$H = 0.00000000$	$E_{nT} = 0.19 \times 10^{-8}$
Method 2		
	$d' = -0.12500000$	
	$H = 0.18189894 \times 10^{-10}$	

$S_A = 2.0 \qquad S_B = 2.5$

$t_0 = 0.36791859 \times 10^{+1}$		$t_1 = 0.27179926 \times 10^{0}$
$t_2 = 0.16569204 \times 10^{0}$	$t_3 = 1$	$t_4 = 0.60352931 \times 10^{2}$
Method 1		
n = 12	$d' = -0.25000000$	$E_{nT} = 0.81 \times 10^{-9}$
n = 33	$H = 0.00000000$	$E_{nT} = 0.12 \times 10^{-7}$
Method 2		
	$d' = -0.25000000$	
	$H = 0.29103830 \times 10^{-6}$	

$S_A = 5.0 \qquad S_B = 7.5$

$t_0 = 0.44126434 \times 10^{+1}$		$t_1 = 0.22662127 \times 10^{0}$
$t_2 = 0.27885148 \times 10^{-1}$	$t_3 = 1$	$t_4 = 0.35861385 \times 10^{+2}$
Method 1		
n = 10	$d' = -1.25000000$	$E_{nT} = 0.94 \times 10^{-8}$
n = 44	$H = 0.00000001$	$E_{nT} = 0.34 \times 10^{-7}$
Method 2		
	$d' = -1.25000000$	
	$H = 0.00000000$	

Table 4.2

the Gauss four and six point formulae to a specified accuracy of 10^{-6}.

The integrals have been evaluated to a higher degree of accuracy than would normally be required in a direct-search process. However, the results illustrate the high accuracy that can be obtained using either method.

A number of integrals have been evaluated using both methods and it has been found that method 2 is more efficient, in terms of both computer storage and time. For example, when finding the constants for the slot combination $S_A = 1.0$, $S_B = 1.25$, with slot centres displaced at intervals of 0.1 units from 0.0 to 2.0 units, a program using the first method required 23,433 words of store and took 2,479 seconds, whilst a program using the second method required only 13,134 words of store and took 1,047 seconds. Both programs were run on the London University C.D.C. 7600 computer.

In general, the second method of integration is more efficient than the first because fewer integrals have to be evaluated. For this reason it has been preferred when evaluating the integrals that occur when applying conformal transformation methods to the air-gap region of an induction machine.

4.5 A Further Problem

The methods described in this and the previous chapter can be used to find the constants of a boundary whose complexity approaches that of a boundary normally treated by the finite element method. To illustrate this, consider the boundary shown in Figure 4.5. This shows a region of the air-gap containing a pair of semi-closed slots.

The Schwarz-Christoffel transformation equation, which maps the real axis of the t-plane on to the boundary in Figure 4.5, is given by

$$\frac{dz}{dt} = \frac{S'(t+t_0)^{\alpha_1}(t+t_1)^{\alpha_2}(t+t_2)^{\alpha_3}(t+t_3)^{\alpha_4}(t-t_4)^{\alpha_5}(t-t_5)^{\alpha_6}(t-t_7)^{\alpha_7}(t-t_8)^{\alpha_8}}{t\ (t+1)\ (t-t_6)} \qquad (4.81)$$

where

$$\alpha_1 = \frac{\gamma_1}{\pi} - 1 \ , \quad \alpha_2 = \frac{\gamma_2}{\pi} - 1 \ , \ \ldots \ \alpha_8 = \frac{\gamma_8}{\pi} - 1$$

There are ten constants and ten equations are required for the direct-search process.

Four of the ten equations can be obtained by evaluating the residues at the poles of dz/dt. Another four equations can be defined by relating the transformation equation to the four dimensions z_1, z_2, z_3 and z_4. For example,

$$|Z_1| = \left| \int_{-t_0}^{-t_1} \frac{S'(t+t_0)^{\alpha_1}(t+t_1)^{\alpha_2}(t+t_2)^{\alpha_3}(t+t_3)^{\alpha_4}(t-t_4)^{\alpha_5}(t-t_5)^{\alpha_6}(t-t_7)^{\alpha_7}(t-t_8)^{\alpha_8}}{t\,(t+1)(t-t_6)} \right| \tag{4.82}$$

A ninth equation can be found by using the condition that the surfaces on either side of a slot are collinear and the tenth equation can be obtained by relating the transformation equation to the slot displacement, d'. Thus, ten equations have been defined and can be used in a direct-search process to find the constants.

A computer program, incorporating Peckham's direct-search method has been written to find the constants of the transformation equation for various values of S_A, S_A', S_B, S_B' and d'. The values of the α are, at present, fixed. It is, however, a relatively simple matter to change these values. Unfortunately, convergence is not very rapid because of the large number of equations involved and because of the complexity of these equations. It is also noticeable that the rate of convergence decreases as S_A' and S_B' become smaller.

The reason for examining this slot shape is to find the slot widths of an equivalent open slot configuration. A possible equivalent open slot configuration is shown in dotted lines in Figure 4.6. It is proposed to obtain these equivalent slot openings by calculating the flux entering the slots of the boundary shown in Figure 4.6 using a

conformal transformation field solution. These flux values are then compared with those obtained by calculating the flux entering the slots of a number of open slot profiles, until equivalent open slot widths are found. This would give the required values of S_A and S_B, the equivalent open slot widths.

It is hoped that this technique may be extended to include other slot shapes. Thus it may be possible to replace a particular slot shape with an equivalent open slot configuration. This is clearly an advantage because of the relative simplicity of the transformation equation associated with the open slot shape (see equation 4.4). Furthermore, in the following chapter it will be shown that the constants of the open slot shape can be found very rapidly, given values of S_A, S_B and slot displacement.

4.6 Conclusions

Methods have been described and compared for evaluating the definite and improper integrals that arise in conformal transformation problems.

For evaluating the definite integrals, the Gauss-Jacobi method and the method of Branders and Piessens are particularly suitable. However, good results have also been obtained in some problems by displacing the limits of integration from the singularities and using Simpson's quadrature. A simple change of variable method may also be used to remove the singularities.

Cauchy Principal Values often arise in practical problems and two methods have been developed to evaluate this type of integral. Both methods evaluate the integral to a high degree of accuracy. One method involves the use of a recursive formula based on a Chebyshev series and the other is based on the method of weakening the singularity. A numerical example shows the latter method to be the more efficient.

4.7 References

4.1 BINNS, K. J. and LAWRENSON, P. J. : 'Analysis and computation of electric and magnetic field problems',(Pergamon, 1973).

4.2 FREEMAN, E. M. : 'The calculation of harmonics due to slotting in the flux-density waveform of a dynamo-electric machine', Proc. I.E.E., 1962, 109c, p.581.

4.3 CLENSHAW, C. W. and CURTIS, A. R. : 'A method for numerical integration on an automatic computer', Num. Maths., 1962, 2, pp.197-205.

4.4 PATTERSON, T. N. L. : 'The optimum addition of points to quadrature formulae', Maths. Comp., 1968, 22, pp.847-856.

4.5 SMITH, F. J. : 'Quadrature methods based on the Euler-Maclaurin formula and on the Clenshaw-Curtis method of integration', Num. Math., 1965, 7, pp.406-411.

4.6 IMHOF, J. P. : 'On the method for numerical integration of Clenshaw and Curtis, Num. Math.,1963, 5, p.138.

4.7 O'HARA, H. and SMITH, F. J. : 'Error estimation in the Clenshaw-Curtis quadrature formula', Comp. Journal, 1968, 11, pp.213-219.

4.8 FOX, L. and PARKER, I. B. : 'Chebyshev Polynomials in Numerical Analysis', (Oxford University Press, London, 1968).

4.9 BINNS, K. J. : 'Numerical methods of conformal transformation', Proc. I.E.E., 1971, 118, (7), pp.909-910.

4.10 LAWRENSON, P. J. and GUPTA, S. K. : 'Conformal transformation employing direct-search techniques of minimisation', Proc. I.E.E., 1968, 115, (3), pp.427-431.

4.11 ROWLANDS-REES, G. : 'Analysis of no-load force pulsations and cogging torques in induction machines', Ph.D. Thesis, University of Southampton, 1978.

4.12 MURTHY VAMARAJU, S. R. : 'Improvements in numerical techniques for conformal transformation with particular reference to electromagnetic fields', I.E.E.E. Transaction on Magnetics, 1978, 14, (4), pp.233-240.

4.13 HOWE, D. : 'The application of numerical methods to the conformal transformation of polygonal boundaries', J. Inst. Maths. Applics., 1973, 12, pp.125-136.

4.14 KRYLOV, V. I. : 'Approximate calculation of integrals', (London and New York, Macmillan, 1962).

4.15 STROUD, A. H. and SECREST, D. : 'Gaussian quadrature formulae' (New Jersey, Prentice Hall, 1966).

4.16 BRANDERS, M.and PIESSENS, R. : 'An extension of Clenshaw Curtis Quadrature', J. Comp. and Appl. Maths. 1, 1975, pp.55-57.

4.17 FOX, L. and MAYER, D. G. : 'Computing Methods for Scientists and Engineers' (Clarendon Press, Oxford, 1968).

4.18 DAVIS, P. J. and RABINOWITZ, P. : 'Methods of Numerical Integration' (Academic Press, 1975).

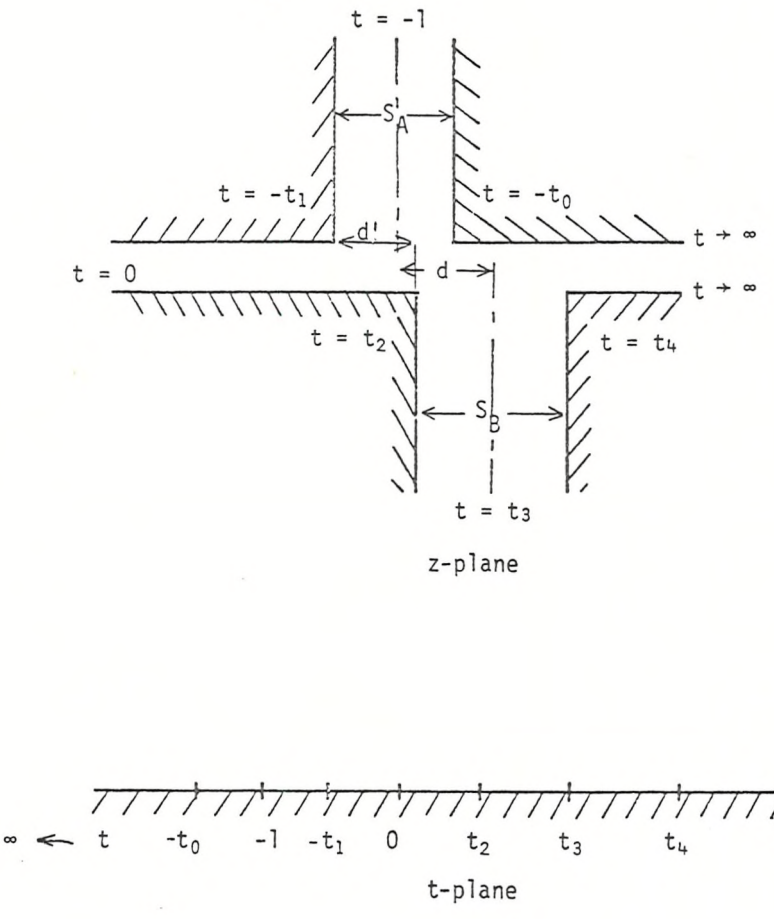

Figure 4.1 A complicated boundary with four right-angled vertices.

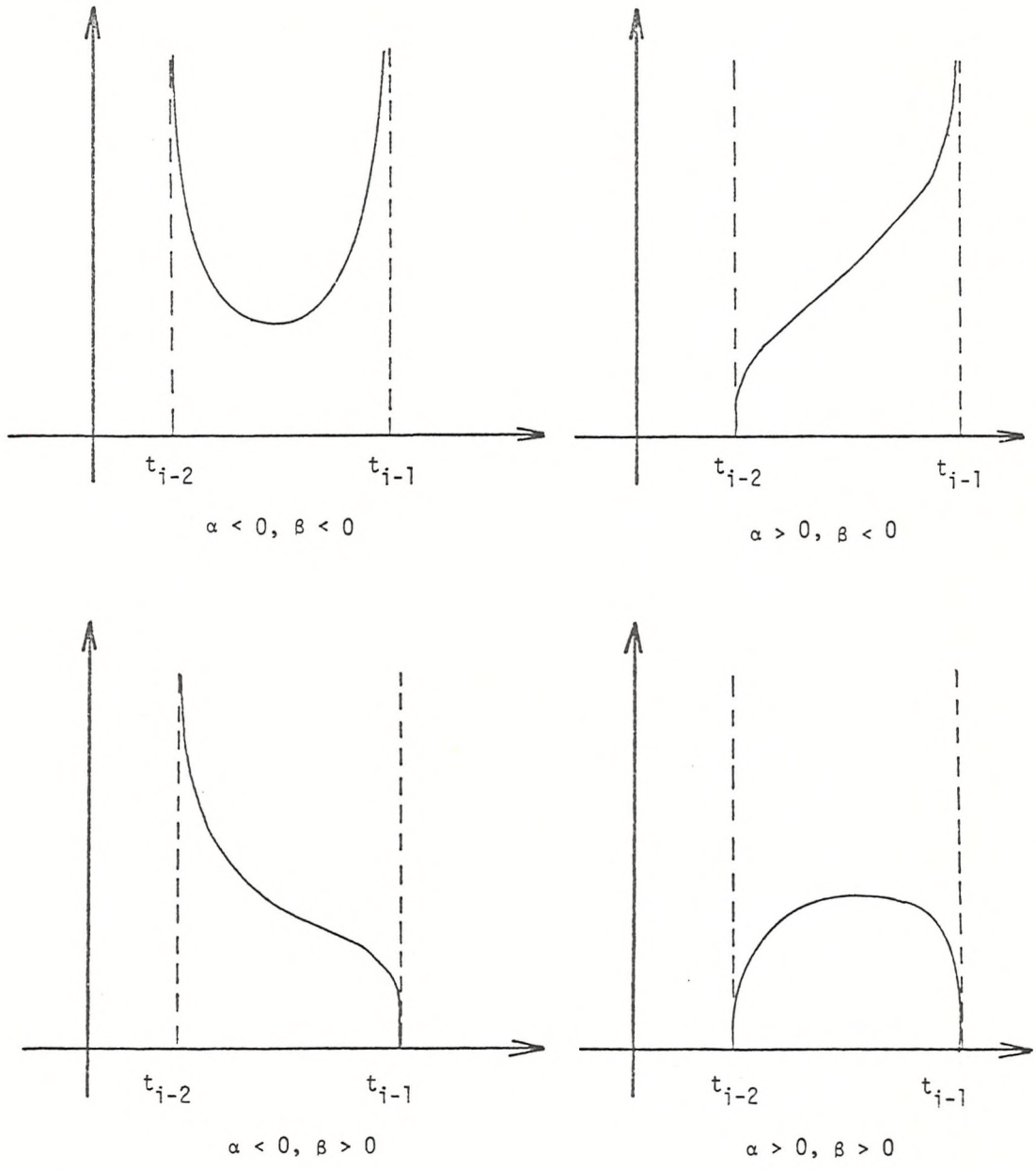

Figure 4.2 The four types of integrand associated with the definite integral evaluated in Chapter 4.

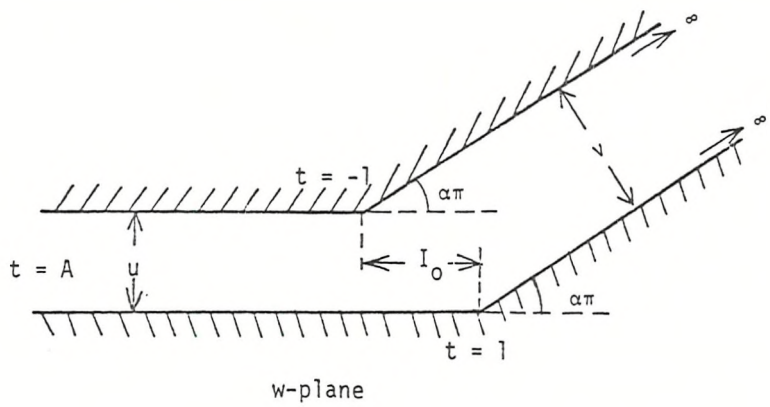

Figure 4.3 Configuration in w-plane used to evaluate I_o when $\alpha + \beta = 0$

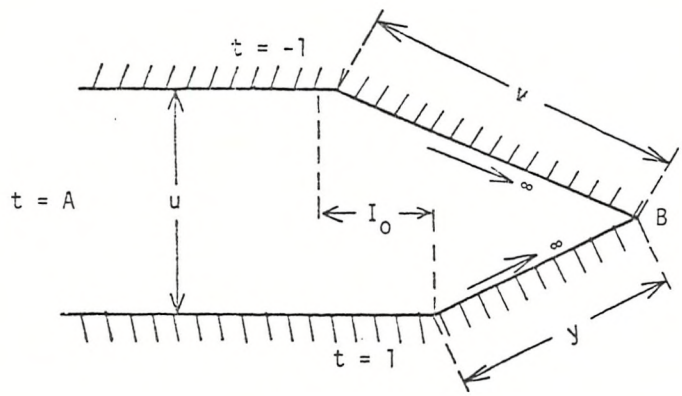

Figure 4.4 Configuration in w-plane used to evaluate I_o when $\alpha + \beta < 0$

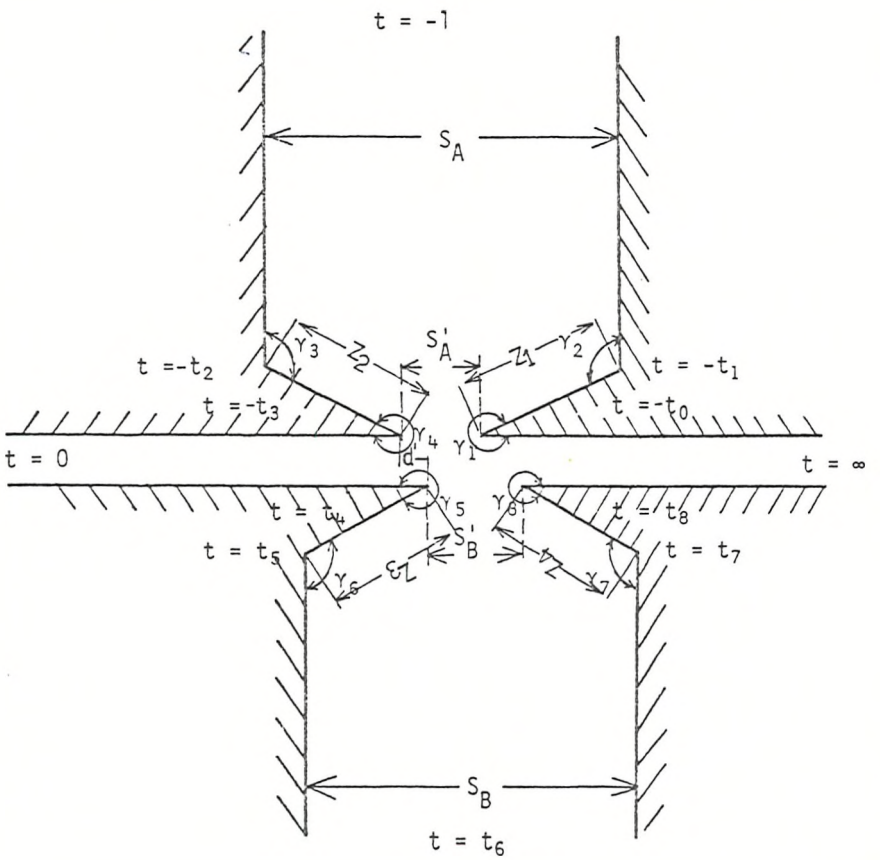

Figure 4.5 A pair of semi-closed slots shown in the z-plane.

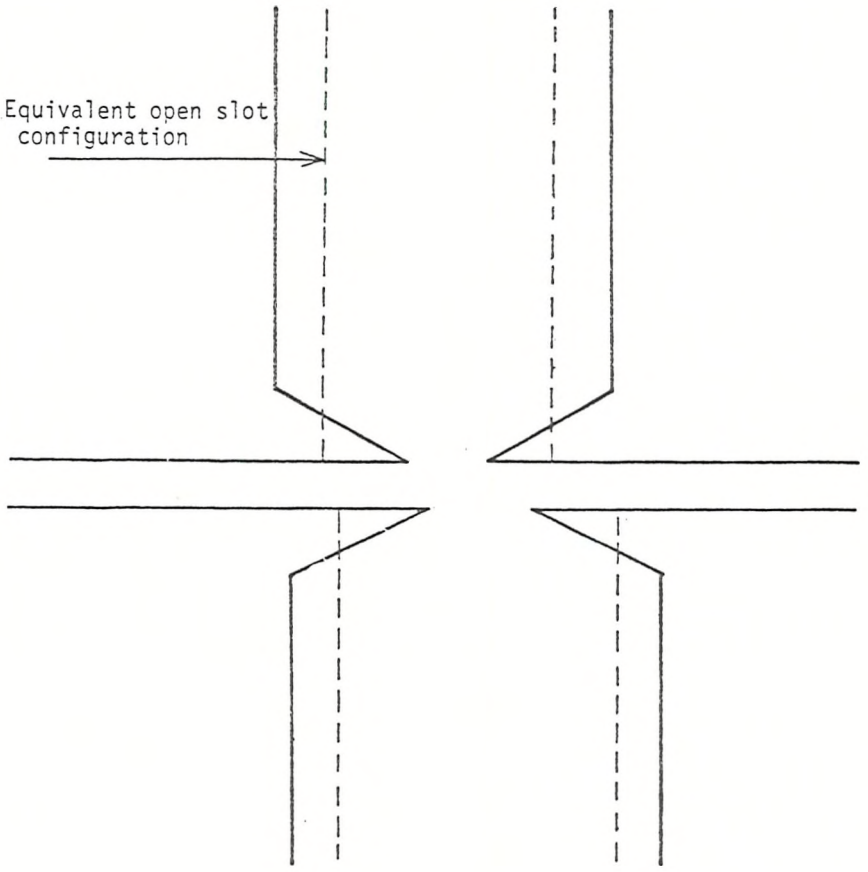

Figure 4.6 A pair of semi-closed slots and a possible equivalent open slot configuration.

CHAPTER 5

THE CALCULATION OF THE TOTAL FLUX ENTERING ANY TOOTH AND THE TANGENTIAL AND NORMAL FORCES ACTING ON IT

5. Introduction

5.1 List of Assumptions

5.2 Division of Air-gap into Regions

5.3 The Transformation Equations of the Singly and Doubly-Slotted Boundaries

5.3.1 Singly-Slotted Boundary

5.3.2 Doubly-Slotted Boundary

5.4 The Calculation of Flux in a Tooth

5.4.1 The Calculation of the Flux Components in the Singly-Slotted Region

5.4.2 The Calculation of the Flux Components in the Doubly-Slotted Region

5.5 The Relationship between Field and Force Distributions

5.6 The Tangential Force Acting on a Tooth

5.7 The Normal Force Acting on a Tooth

5.8 The Computer Program

5.9 References

5. Introduction

This chapter is concerned with the application of the conformal transformation method to the solution of the field in the slotted air-gap boundary of an induction machine. The numerical methods described in the previous two chapters are used extensively here.

The main object of this chapter is to describe the analysis used to calculate the flux in a tooth and the tangential and normal components of force. This analysis has been incorporated into a computer program. This program can be used to obtain the instantaneous flux and force quantities associated with all the stator and rotor teeth and, thus, gives the instantaneous distribution of these quantities over a double pole pitch of the machine. The flux and force pulsations in the teeth of the machine can be obtained by calculating these distributions at a number of different positions of the rotor relative to the stator. This process is described in greater detail in the following chapters. Clearly, therefore, the calculation of the flux and force quantities forms the basis of the later work and is to be explained in detail in this chapter. The assumptions used in applying the conformal transformation method to calculating the field in the slotted air-gap region are stated and discussed in Section 5.1.

The flux distribution around a tooth, and the components of force acting on it, can be obtained from a combination of the solution of the field in three regions. These regions are identified in Section 5.2 as a region containing two displaced slots (doubly-slotted boundary), a region containing a single slot (singly-slotted boundary) and a region having no slots in which the gap density is assumed uniform. The Schwarz-Christoffel transformation equations of the singly and doubly-slotted boundaries are derived in Section 5.3.

In Section 5.4, it is shown how the total flux in a tooth can be obtained from the solution of the field in these three regions.

The force acting on any part of the slotted-boundary can be obtained using the Maxwell stress method described in Chapter 2. In Section 5.5, the integral of the Maxwell stress function is expressed in a more convenient form as a function of t (the complex variable in the t-plane) rather than z (the complex variable in the z-plane). This form of the integral is then used to obtain the tangential and normal forces acting on a tooth by integrating over the appropriate surfaces. This is explained in detail in Sections 5.6 and 5.7.

Finally, it is shown how the analysis in Sections 5.3 to 5.7 has been incorporated into a computer program. A simplified block diagram of this program is shown.

5.1 List of Assumptions

This section lists the assumptions made in the analysis of the tooth flux and force pulsations under load conditions. These are:

(i) The air-gap field in an unskewed machine can be analysed using a two-dimensional cross-section of the machine. In a skewed machine, the field can be taken as axially uniform over a small element of the bore length dl, and the field may be analysed using a two-dimensional cross-section of the machine.

(ii) The curvature of the air-gap is neglected.

(iii) The relative permeability of the iron is high ($\mu \to \infty$).

(iv) Any slot shape can be represented by an equivalent open slot shape.

(v) The slots are infinitely deep.

(vi) Since the slots in a machine only perturb the field over a limited region, it is assumed that, at any instant, at no part of the air-gap boundary is the field affected by more than one pair

of slots situated on the opposite side of the air-gap.

(vii) The field at any point on the boundary can be calculated using the boundary conditions defined for the load case in Section 2.3.1 of Chapter 2.

Assumptions (i), (iii) and (vii) are discussed in Sections 2.1, and 2.3.1 of Chapter 2.

Assumption (ii) involves a negligible error since the air-gap width is small compared with the radius of curvature.

In practice, induction machines have a variety of slot shapes; some typical examples are shown in Figure 5.1. Assumption (iv) is commonly made when treating problems of this kind. It is reasonable because the main aim of the present analysis is to derive a set of equations relating the flux and force pulsations to the stator and rotor slot pitches, rather than to calculate these pulsations in a machine having a particular slot shape. If the teeth are highly saturated, a value between that of the actual slot opening and slot width may be taken.

Figure 5.2 shows an open slot containing one or more rectangular conductors. When the conductors carry current, they set up a slot leakage flux pattern of complex shape. Typical flux patterns have been obtained for the steady state condition by Carter[5.1]. If there is an appreciable space below the bottom conductor, and the width of the conductor is substantially less than that of the slot, the flux pattern is that shown in Figure 5.2a. However, apart from those cases of machines having high voltage windings with thick insulation, the proportions of the conductor are usually more like those of Figure 5.2b and the flux pattern is approximately in the form of straight lines crossing the slot. Robertson and Terry[5.2] have used this assumption

when calculating slot leakage inductance. Thus, it is reasonable to assume that the flux crossing the slot becomes uniform at a point remote from the slot opening. This assumption is necessary if the boundary conditions defined for the load case in Section 2.3.1 of Chapter 2 are to be satisfied. Furthermore, if the slot depth is much greater than the width, as is usually the case, the depth can be assumed to be infinite and this gives a simpler transformation equation.

Assumption (vi) only ceases to be valid when the teeth on one side of the air-gap are less than about 1.5 times the width of the slots on the opposite side. This rarely, if ever, occurs in practice.

5.2 Division of the Air-Gap into Regions

The flux distribution around a tooth and the components of force acting on it can be obtained from a combination of the solutions of the fields in the three regions shown in Figure 5.3. Region 1 contains two displaced slots. It is important to note that the flux in the air-gap is almost uniform at points AA' and BB', which are remote from the slot openings, so that the separate solutions can be combined. Region 2 contains one slot. Again the flux in the air-gap is almost uniform at points AA' and BB'. Region 3 contains no slots and the air-gap field is uniform everywhere.

5.3 The Transformation Equations of the Singly and Doubly-Slotted Boundaries

5.3.1 Singly-Slotted Boundary

The singly-slotted boundary is shown in Figure 5.4, located in the z-plane with corresponding points in the t-plane. The slot has a width S/g. It is convenient in the following analysis to take the gap width, g, as unity. The equation which transforms the real axis of the t-plane into the singly-slotted boundary is given by

$$\frac{dz}{dt} = \frac{K\sqrt{(t + t_0)(t + t_1)}}{t\,(t + 1)} \tag{5.1}$$

A set of equations relating the constants of the transformation equation to the slot width, S/g, can be obtained by evaluating the residues at the poles of dz/dt. The equations are as follows:

$$K = \frac{1}{\pi} \tag{5.2}$$

$$t_0\, t_1 = 1 \tag{5.3}$$

$$t_0 = \frac{\left((S/g)^2 + 2\right)}{2} + S/g.\frac{\sqrt{(S/g)^2 + 4}}{2} \tag{5.4}$$

The transformation equation can be integrated to give z ;

$$z = \frac{1}{\pi}\int \frac{\sqrt{(t+t_0)(t+t_1)}}{t(t+1)}\,dt \tag{5.5}$$

This integral can be solved analytically. In the interval $(-t_0, -t_1)$ the integrand in equation (5.5) is complex and has to be rearranged as follows:

$$z = \frac{j}{\pi}\int \frac{\sqrt{(-t-t_1)(t+t_0)}}{t(t+1)}\,dt \tag{5.6}$$

This integral can be integrated formally as a function of t , but a simpler solution can be obtained by using the transformation equation

$$p^2 = -\frac{(t + t_1)}{(t + t_0)} \tag{5.7}$$

After substitution for t and suitable algebraic manipulation, the solution becomes

$$Z = \frac{2j}{\pi}\left[\tan^{-1}p - \tan^{-1}\frac{p}{t_1} + \frac{S/g}{2}\,.\,\log\left(\frac{\sqrt{t_1} + p}{\sqrt{t_1} - p}\right)\right] + \text{constant} \tag{5.8}$$

for the interval $(-t_1, -1)$ in Figure 5.4 and

$$z = \frac{2j}{\pi}\left[\tan^{-1} p - \tan^{-1}\frac{p}{t_1} - \frac{S/g}{2}.\log\left(\frac{p-\sqrt{t_1}}{p+\sqrt{t_1}}\right)\right] + \text{constant} \qquad (5.9)$$

for the interval $(-1, -t_0)$.

In the other intervals of t, the integrand of equation (5.5) is real, and the integral can be integrated using the transformation equation

$$p^2 = \frac{t + t_0}{t + t_1} \qquad (5.10)$$

which gives the following solution

$$z = \frac{1}{\pi}\left[\log\left|\frac{1+p}{1-p}\right| - \log\left|\frac{t_0+p}{t_0-p}\right| - 2.S/g\ \tan^{-1}\frac{p}{\sqrt{t_0}}\right] + \text{constant} \qquad (5.11)$$

In addition to giving a simpler solution, the p transformation has another advantage. This can be illustrated by considering the calculation of the distance between a point on the tooth surface and a tooth corner. This involves finding a point t' corresponding to a particular point z'. The point t' could be located in either of the two intervals $(0, -t_1)$ or $(-t_0, \infty)$. Numerical problems can arise when finding t' in either interval. In the first interval t' is very small (for example, if $S/g = 5.0$, $t_1 = -0.037$) whilst in the second interval t' is unbounded. However, under the p transformation the interval $(-t_0, \infty)$ is mapped into the interval $(0, 1)$ in the p-plane and the corresponding values of p' and z' can be found with comparative ease.

5.3.2 Doubly-Slotted Boundary

The doubly-slotted boundary is shown in Figure 5.5 located in the z-plane with corresponding points on the real axis of the t-plane. The upper slot has a width S_A/g, the lower slot a width S_B/g and $S_B/g > S_A/g$. The gap width is again taken as unity. The Schwarz-

Christoffel transformation can be used to give the mapping function[5.3]

$$\frac{dz}{dt} = \frac{k\sqrt{(t+t_0)(t+t_1)(t-t_2)(t-t_4)}}{t(t+1)(t-t_3)} \tag{5.12}$$

It is necessary to establish six equations to find the constants. Four of the equations can be found by evaluating the residues at the poles of dz/dt, and this leads to

$$K = \frac{1}{\pi} \tag{5.13}$$

$$t_3^2 = t_0 \,.\, t_1 \,.\, t_2 \,.\, t_4 \tag{5.14}$$

$$(S_A/g)^2(1+t_3)^2 = (t_1-1)(1-t_0)(1+t_2)(1+t_4) \tag{5.15}$$

and $$(S_B/g)^2 (1+t_3)^2 \,.\, t_3^2 = (t_3+t_0)(t_3+t_1)(t_3-t_2)(t_4-t_3) \tag{5.16}$$

The remaining two equations can be obtained by relating the transformation equation to the dimensions of the z-plane boundary. The first equation implies the condition that the two surfaces on either side of a slot are collinear. For the upper slot in Figure 5.5, this involves evaluating the integral

$$P \left| \frac{1}{\pi} \int_{-t_0}^{-t_1} \frac{\sqrt{(t+t_0)(t+t_1)(t-t_2)(t-t_4)}}{t\,(t+1)(t-t_3)} dt \right| = 0 \tag{5.17}$$

The second equation can be obtained by relating the transformation equation to the slot centre displacement, d. This leads to the equation

$$d = P \frac{1}{\pi} \int_{-t_1}^{t_2} \frac{\sqrt{(t+t_0)(t+t_1)(t-t_2)(t-t_4)}}{t\,(t+1)(t-t_3)} dt - \left(\frac{S_A - S_B}{2g} \right) \tag{5.18}$$

It is, of course, possible to rearrange equations (5.14) - (5.18) to form the elements of a function which involves a sum of squares suitable for use with Peckham's direct-search method. However, by making t_0, t_1 and t_2 functions of t_3, t_4, S_A/g and S_B/g the number of

constants to be found in the direct-search program can be reduced from five to two. These functional relationships may be obtained in the following way. Let a function f(t) be defined such that

$$f(t) = (t+t_0)(t+t_1)(t-t_2) = a_0 + a_1\, t + a_2\, t^2 + t^3 \qquad (5.19)$$

Substituting the values t = 0, -1 and t_3 into equation (5.19) gives

$$f(0) = -\, t_0 \,.\, t_1 \,.\, t_2 = \frac{-t_3^{\,2}}{t_4} \qquad (5.20)$$

$$f(-1) = (t_1-1)(1-t_0)(1+t_2) = (S_A/g)^2 \,.\, \frac{(1+t_3)^2}{t_4+1} \qquad (5.21)$$

$$f(t_3) = (t_3+t_0)(t_3+t_1)(t_3-t_2) = \frac{(S_B/g)^2 \,.\, (1+t_3)^2 \,.\, t_3^{\,2}}{(t_4-t_3)} \qquad (5.22)$$

or in terms of the coefficients a_0, a_1 and a_2

$$f(0) = a_0 \qquad (5.23)$$

$$f(-1) = a_0 - a_1 + a_2 - 1 \qquad (5.24)$$

$$f(t_3) = a_0 + a_1\, t_3 + a_2\, t_3^{\,2} + t_3^{\,2} \qquad (5.25)$$

Equations (5.23) - (5.25) can be rearranged to give

$$f(-1) - f(0) + 1 = -a_1 + a_2 \qquad (5.26)$$

$$f(t_3) - f(0) - t_3^{\,2} = t_3\, a_1 + t_3^{\,2}\, a_2 \qquad (5.27)$$

Accordingly, equations (5.26) and (5.27) can be solved to give a_1 and a_2 in terms of t_3, t_4, S_A/g and S_B/g. This leads to the following two equations,

$$a_1 = t_3\left[\frac{-(t_3-1)}{t_4} + (1 + t_3) \,.\, \left(\frac{(S_B/g)^2}{(t_4-t_3)} \quad \frac{-(S_A/g)^2}{(t_4+1)}\right) - 1\right] \qquad (5.28)$$

$$a_2 = (S_A/g)^2 \,.\, \frac{(1+t_3)}{(1+t_4)} + \frac{t_3}{t_4} + (S_B/g)^2 \,.\, \frac{(1+t_3)}{(t_4-t_3)} \,.\, t_3 + (1-t_3) \qquad (5.29)$$

Also, from equations (5.20) and (5.23)

$$a_0 = \frac{-t_3^2}{t_4} \tag{5.30}$$

Thus, for any values of t_3 and t_4, the remaining three constants can be found by solving equation (5.19). A method suitable for finding the roots of a cubic equation is given by Selby[5.4].

The above method has been incorporated into a computer program designed to find the constant of the doubly-slotted boundary for specified values of S_A/g, S_B/g and d. The program also includes a subroutine package based on Peckham's direct-search method (see Chapter 3). The elements of the sum of squares function are obtained by rearranging equations (5.17) and (5.18). Both integrals are evaluated using the method of weakening the singularity. Since only two variables have to be found in the direct-search program, the constants can be found very efficiently, as is confirmed by the results shown in Section 4.4.5 of Chapter 4.

The doubly-slotted boundary also exhibits a form of symmetry. This may be shown by considering the two boundaries in Figure 5.6. It should be noted that the two boundaries have slot displacements equal in magnitude but opposite in sign.

The transformation equation of the boundary in Figure 5.6a was defined earlier and is given by

$$\frac{dz}{dt} = \frac{1}{\pi} \frac{\sqrt{(t+t_0)(t+t_1)(t-t_2)(t-t_4)}}{t(t+1)(t-t_3)} \tag{5.31}$$

The transformation equation of the boundary in Figure 5.6b is given by

$$\frac{dz}{du} = \frac{1}{\pi} \frac{\sqrt{(u+t_0')(u+t_1')(u-t_2')(u-t_4')}}{u(u+1)\ (u-t_3')} \tag{5.32}$$

Let

$$t = \frac{1}{u}$$

then

$$\frac{dz}{du} = \frac{dz}{dt} \cdot \frac{dt}{du}$$

where

$$\frac{dt}{du} = \frac{-1}{u^2}$$

Therefore

$$\frac{dz}{du} = \frac{-1}{u^2\pi} \frac{\sqrt{(\frac{1}{u} + t_0)(\frac{1}{u} + t_1)(\frac{1}{u} - t_2)(\frac{1}{u} - t_4)}}{\frac{1}{u}(\frac{1}{u} + 1)(\frac{1}{u} - t_3)}$$

or

$$\frac{dz}{du} = \frac{1}{\pi} \frac{\sqrt{t_0 \cdot t_1 \cdot t_2 \cdot t_4}}{t_3} \frac{\sqrt{(u + \frac{1}{t_0})(u + \frac{1}{t_1})(u - \frac{1}{t_2})(u - \frac{1}{t_4})}}{u(u + 1)(u - \frac{1}{t_3})}$$

However, from equation (5.14)

$$\frac{\sqrt{t_0 \cdot t_1 \cdot t_2 \cdot t_4}}{t_3} = 1$$

so that

$$\frac{dz}{du} = \frac{1}{\pi} \frac{\sqrt{(u + \frac{1}{t_1})(u + \frac{1}{t_0})(u - \frac{1}{t_2})(u - \frac{1}{t_4})}}{u(u + 1)(u - \frac{1}{t_3})} \qquad (5.33)$$

By comparison with equation (5.32), the following relationships are obtained

$$t_0' = \frac{1}{t_1}, \quad t_1' = \frac{1}{t_0}, \quad t_2' = \frac{1}{t_4}, \quad t_4' = \frac{1}{t_2} \text{ and } \quad t_3' = \frac{1}{t_3} \qquad (5.34)$$

This set of relationships is of particular importance because the constants have only to be found for positive values of displacement in the direct-search program. Furthermore, the symmetry exhibited by the boundary is of great value when calculating the flux and normal components of force in the region of the doubly-slotted boundary

corresponding to the intervals $(-t_0, \infty)$ and (t_4, ∞) in the t-plane.

5.4 The Calculation of Flux in a Tooth

This section is concerned with the calculation of flux in any tooth of an induction motor. The solutions of the field in the three regions, defined in Section 5.2, are used to calculate this flux.

The section of the slotted-boundary shown in Figure 5.7 is the most complicated region of the air-gap in which the flux in a tooth has been calculated. Thus, the calculation of flux in tooth B involves solving the field in two doubly-slotted regions, a singly-slotted region and two regions containing no slots. The calculation of flux in tooth A is much simpler, involving the solution of the field in one doubly-slotted region, one singly-slotted region and one region containing no slots. A number of other cases can occur but the calculation of flux in the tooth is similar to the cases shown here.

It is important when calculating the tooth flux to define the direction of flux across any part of the iron. The definition used here is that if the flux crossing any part of the tooth is entering the iron it is given a positive value, if it is leaving the iron it is given a negative value.

Figure 5.7 also shows the notation used to identify the various components of flux which, when summed together, give the total flux in a tooth. Each component represents the amount of flux crossing the boundary between the two points on the tooth associated with that component. The field at these points is, of course, almost uniform. Thus, the flux in tooth A is given by

$$\phi_A = \phi_{d1} + \phi_{n1} + \phi_{s2} \tag{5.35}$$

and the flux in tooth B is given by

$$\phi_B = \phi_{d4} + \phi_{n1} + \phi_{s3} + \phi_{n2} + \phi_{d3} \tag{5.36}$$

An equation for the component of flux, ϕ_n, in the region containing no slots can now be derived. The flux crossing a segment of the boundary, z, in the region shown in Figure 5.8 can be calculated by evaluating the integral

$$\phi_n = \iint_S \underline{B} \cdot ds \tag{5.37}$$

which becomes

$$\phi_n = \int Bdz \tag{5.38}$$

for unit axial length. If the potential difference across the air-gap is M and the gap width is g, then

$$\int_0^g H \cdot d\ell = M \tag{5.39}$$

However, H is constant, so that

$$Hg = M$$

or

$$B = \frac{\mu_0 M}{g} \tag{5.40}$$

Thus, an expression for ϕ_n can be obtained in terms of the potential difference, M, by substituting equation (5.40) into equation (5.38) and integrating. This leads to the following equation

$$\phi_n = \frac{\mu_0 Mz}{g} \tag{5.41}$$

The remaining components of flux can be found by solving the field in the singly and doubly slotted regions. To obtain the correct field in either region it is necessary to find a complex potential function

$$w = \phi + j\psi \tag{5.42}$$

which satisfies the boundary conditions defined in Section 2.3.1 of Chapter 2. As in the previous section, the two boundaries are treated separately.

5.4.1 The Calculation of the Flux Components in the Singly-Slotted Region

The complex potential function for this region is obtained by satisfying the boundary conditions shown in Figure 5.9. The terms $I_1 + I_3$, I_3 and zero denote the values of the potential on the different parts of the iron. The corresponding intervals in the t-plane have the same values of potential. A function which satisfies these boundary conditions in the t-plane is given by

$$w = \frac{I_3}{\pi} \log t + \frac{I_1}{\pi} \log(t+1) \qquad (5.43)$$

I_1 is the instantaneous value of the current flowing in the conductor in the slot and I_3 is the instantaneous value of the air-gap m.m.f. in the region of the machine where the slot is located. Both I_1 and I_3 are represented in the t-plane by point current sources, I_1 being located at the point $t = -1$ which corresponds to a distance infinitely far down the slot in the z-plane and I_3 is located at the point $t = 0$ which corresponds to a distance infinitely far down the air-gap.

From equation (5.43), the potential can be obtained directly in S.I. units by calculating the imaginary part of the function. The flux can be found in units of webers by multiplying the real part of the function by μ_0.

The flux crossing any segment of the singly-slotted boundary has not been obtained by direct application of equation (5.43) because it is very difficult to determine the direction of flux. Instead, the boundary conditions associated with the two terms in equation (5.43) were applied separately as shown in Figure 5.10. Clearly, the direction of flux in the two figures on the r.h.s. of Figure 5.10 is dependent upon the values of I_1 and I_3. Thus, the flux crossing any segment of the boundary can be found by calculating the two terms in

equation (5.43) separately, assigning each term a positive or negative value depending on the direction of flux, and then summing the two terms together.

The components of flux are given by

$$\phi_{s1} = \mu_0 \left\{ \pm \left| \frac{I_3}{\pi} \log \left(\frac{t_b}{t_a} \right) \right| \pm \left| \frac{I_1}{\pi} \log \frac{(t_b-1)}{(t_a-1)} \right| \right\} \qquad (5.44)$$

$$\phi_{s2} = \mu_0 \left\{ \pm \left| \frac{I_3}{\pi} \log \left(\frac{t_d}{t_c} \right) \right| \pm \left| \frac{I_1}{\pi} \log \frac{(1-t_d)}{(1-t_c)} \right| \right\} \qquad (5.45)$$

and

$$\phi_{s3} = \mu_0 \left\{ \pm \left| \frac{I_3}{\pi} \log \left(\frac{t_f}{t_e} \right) \right| \pm \left| \frac{I_1}{\pi} \log \frac{(t_f+1)}{(t_e+1)} \right| \right\} \qquad (5.46)$$

where t_a, t_b, t_c, etc. are all positive values. The gap density at the points corresponding to $t = -t_a$ and $-t_d$ is almost uniform. The values of t_a, t_b, t_c, t_d, t_e and t_f are found by solving the equation

$$|z| - |f(p)| = 0 \qquad (5.47)$$

where z is the distance from the appropriate tooth corner to the point on the slotted-boundary corresponding to any one of the six point $t = t_a$, t_b, etc. The function f(p) is one of the three functions on the r.h.s. of equations (5.8), (5.9) or (5.11) depending, of course, on the interval in which the point corresponding to p lies. Equation (5.47) has been solved using the bisection method[5.5].

5.4.2 The Calculation of the Flux Components in the Doubly-Slotted Region

The complex potential function for this region can be obtained by satisfying the boundary conditions shown in Figure 5.11. A function which satisfies these conditions is given by

$$w = \frac{I_3}{\pi} \log t + \frac{I_1}{\pi} \log (t+1) + \frac{I_2}{\pi} \log (t-t_3) \qquad (5.48)$$

where I_1 and I_2 are the values of the current flowing in the conductors and I_3 is the value of the air-gap m.m.f. in the region of the machine in which the slots are located. In the t-plane there are point current sources of values I_2 and I_3 at the points $t = -1$, t_3 corresponding to points infinitely far down both slots and a current source of value I_3 at $t = 0$, corresponding to a point infinitely far down the air-gap.

The components of flux ϕ_{d1}, ϕ_{d2}, ϕ_{d3} and ϕ_{d4} are given by the following equations

$$\phi_{d1} = \mu_0 \left(\pm \left| \frac{I_3}{\pi} \log \left(\frac{t_b}{t_a} \right) \right| \pm \left| \frac{I_1}{\pi} \log \frac{(t_b-1)}{(t_a-1)} \right| \pm \left| \frac{I_2}{\pi} \log \frac{(t_b+t_3)}{(t_a+t_3)} \right| \right) \tag{5.49}$$

$$\phi_{d2} = \mu_0 \left(\pm \left| \frac{I_3}{\pi} \log \left(\frac{t_d}{t_c} \right) \right| \pm \left| \frac{I_1}{\pi} \log \frac{(1-t_d)}{(1-t_c)} \right| \pm \left| \frac{I_2}{\pi} \log \frac{(t_d+t_3)}{(t_c+t_3)} \right| \right) \tag{5.50}$$

$$\phi_{d3} = \mu_0 \left(\pm \left| \frac{I_3}{\pi} \log \left(\frac{t_f}{t_e} \right) \right| \pm \left| \frac{I_1}{\pi} \log \frac{(1+t_f)}{(1+t_e)} \right| \pm \left| \frac{I_2}{\pi} \log \frac{(t_3-t_f)}{(t_3-t_e)} \right| \right) \tag{5.51}$$

and

$$\phi_{d4} = \mu_0 \left(\pm \left| \frac{I_3}{\pi} \log \left(\frac{t_h}{t_g} \right) \right| \pm \left| \frac{I_1}{\pi} \log \frac{(1+t_h)}{(1+t_g)} \right| \pm \left| \frac{I_2}{\pi} \log \frac{(t_h-t_3)}{(t_g-t_3)} \right| \right) \tag{5.52}$$

where t_a, t_b, t_c... etc. are all positive values. The gap density at the points in the z-plane corresponding to $t = -t_a$ and $-t_d$ is almost uniform. The values of these eight t-plane variables can be found by solving an equation of the form

$$|z| - \left| \frac{1}{\pi} \int_{ty}^{tx} \frac{\sqrt{(t+t_0)(t+t_1)(t-t_2)(t-t_4)}}{t\,(t+1)(t-t_3)}\, dt \right| = 0 \tag{5.53}$$

where z is the distance from the appropriate tooth corner (at which

the value of the constant is t_y) to the point on the slotted-boundary corresponding to t_x (where t_x is any one of the eight t-plane variables). As in the case of the singly-slotted region, equation (5.53) can be solved by the bisection method.

The same numerical difficulties have been encountered in finding the values of t_a, t_b, t_c... etc. as reported by Rowlands-Rees in his thesis[5.6]. Consider, for example, the equation

$$|z_1| - \left| \frac{1}{\pi} \int_{-t_1}^{-t_d} \frac{\sqrt{(t+t_0)(t+t_1)(t-t_2)(t-t_4)}}{t\,(t+1)(t-t_3)}\, dt \right| = 0 \qquad (5.54)$$

which relates the distance z_1, in Figure 5.11, to the constants of the transformation equation. It is often found necessary to make the distance z_1 large (for example, $S_A/g = 5.0$, $S_B/g = 7.50$, displacement = 5.0, $z_1 = 12.75/g$) to ensure that a point has been found sufficiently remote from the slot openings for the flux density to have become uniform. However, if z_1 is too large, the value of $|t_d|$ becomes very small. The integrand of equation (5.54) then has a very large value due to the pole of order 1 at $t = 0$. This gives rise to numerical difficulties when trying to find $|t_d|$. It has, therefore, been found necessary to limit the value of z_1. However, for all slot combinations considered in this thesis, it was found possible to make z_1 large enough to ensure that a point had been found where the flux density was sufficiently uniform.

Consider now the equation

$$|z_2| - \left| \frac{1}{\pi} \int_{-t_0}^{-t_a} \frac{\sqrt{(t+t_0)(t+t_1)(t+t_2)(t-t_4)}}{t\,(t+1)(t-t_3)}\, dt \right| = 0 \qquad (5.55)$$

In this case, if z_2 is too large, then $|t_a|$ becomes very large and difficulties are encountered in producing consistently accurate

results. To overcome these difficulties the doubly-slotted boundary with opposite slot centre displacement is used, the problem being reformulated on the left hand side of the top slot. The limits of integration are then $-t_1'$ and $-t_a'$, where $0 > -t_a' > -t_1'$. In this way it is possible to obtain an accurate value for t_a' and hence t_a. This formulation has the added advantage that the search is carried out in a finite interval $(0, -t_1')$ rather than an infinite interval $(-t_0, \infty)$. In fact, the same search program can be used to find both t_a and t_d. Exactly the same considerations apply to the variables t_e and t_h.

To find the values of t_b, t_c, t_f and t_g, a point is found sufficiently remote from the slot opening for the flux to have become uniform. If a greater slot depth is required, the slot leakage flux for the additional depth can simply be calculated and added to the value of the flux obtained by the conformal transformation field solution.

5.5 The Relationship between Field and Force Distributions

The force acting on any part of the slotted-boundary can be calculated using the Maxwell stress method described in Chapter 2. It will be recalled that this method involves the evaluation of the integral

$$\frac{1}{2}\int_{C_\sigma} \underline{B} \cdot \underline{H}\, d\sigma \qquad (5.56)$$

over a suitable contour. This equation becomes

$$\frac{1}{2\mu_0}\int_{C_z} B^2\, dz \qquad (5.57)$$

per unit axial length. It is more convenient to solve this integral as a function of t rather than z, and since $B = \left|\frac{dw}{dz}\right|$, (5.3)

$$\frac{1}{2\mu_0}\int_{C_z} B^2 \,.\, dz = \frac{1}{2\mu_0}\int_{C_z} \left(\frac{dw}{dz}\right)^2 \,.\, dz \qquad (5.58)$$

which after a change of variable becomes

$$\frac{1}{2\mu_0}\int_{C_t} \left(\frac{dw}{dt}\right)^2 \left(\frac{dt}{dz}\right) \,.\, dt \qquad (5.59)$$

The force acting on any part of the singly-slotted boundary, under load conditions, can be obtained as a function of t by substituting equations (5.1) and (5.43) into equation (5.59) to give

$$\frac{1}{2\mu_0\,\pi}\int \frac{(I_3.\,(t+1) + I_1\,.\,t)^2}{t(t+1)\,\sqrt{(t+t_0)(t+t_1)}}\,dt \qquad (5.60)$$

The analytical solution of this integral is described in the following two sections.

In a similar manner, the force acting on any part of the doubly-slotted boundary can be obtained as a function of t by substituting equations (5.12) and (5.48) into equation (5.59) to give

$$\frac{1}{2\mu_0\,\pi}\int \frac{(I_3\,.\,(t+1)\,(t-t_3) + I_1\,.\,t\,(t-t_3) + I_2\,.\,t(t+1)\,)^2}{t\,(t+1)(t-t_3)\,\sqrt{(t+t_0)(t+t_1)(t-t_2)(t-t_4)}}\,dt \qquad (5.61)$$

This integral can be solved by the analytical techniques described in Chapter 4, but it is more convenient to solve it by the numerical quadrature methods described in the same chapter.

In the following two sections, equations (5.60) and (5.61) will be used to obtain the tangential and normal components of force acting on any tooth of an induction machine.

5.6 The Tangential Force Acting on a Tooth

It was shown, in Section 2.5.1 of Chapter 2, that the tangential force acting on any tooth can be obtained by evaluating the integral of the Maxwell stress function over the two slot sides that enclose the tooth. Accordingly, the tangential force on tooth A, in Figure 5.12,

is the difference between the forces associated with the slot sides of the two doubly-slotted regions. The force on tooth B is the difference between the force on the slot side of the singly-slotted region and the force on the slot side of the doubly-slotted region. The solution of equation (5.60), the integral of the Maxwell stress function associated with the singly-slotted region, is considered first.

Equation (5.60) can be integrated formally as a function of t, but, as in the case of the transformation equation of the singly-slotted region, a simpler solution can be obtained by using the transformation equation

$$p^2 = \frac{-(t+t_1)}{(t+t_0)} \tag{5.62}$$

This leads to two solutions. In the interval $(-t_1, -1)$, the solution is given by

$$\frac{j}{\mu_0 \pi}\left((I_1 + I_3)^2 \tan^{-1} p - I_3^2 \tan^{-1} \frac{p}{t_1} - \frac{I_1^2}{2.S/g} \cdot \log \frac{\sqrt{t_1}+p}{\sqrt{t_1}-p} \right) \tag{5.63}$$

and in the interval $(-1, -t_0)$

$$\frac{j}{\mu_0 \pi}\left((I_1 + I_3)^2 \tan^{-1} p - I_3^2 \tan^{-1} \frac{p}{t_1} + \frac{I_1^2}{2S/g} \log \frac{p - \sqrt{t_1}}{p + \sqrt{t_1}} \right) \tag{5.64}$$

In the interval $(-t_1, -1)$, the limits of integration are $-t_1$, $-t_c$ (see Figure 5.9) and in the interval $(-1, -t_0)$ the limits of integration are $-t_b$, $-t_0$. Thus, the forces associated with the two slot surfaces are calculated to a slot depth at which the flux has become almost uniform. The additional force contribution associated with the slot leakage flux can simply be calculated and added to the value of the force obtained by the conformal transformation field solution.

As mentioned in the previous section, the integral of the Maxwell

stress function associated with the doubly-slotted region, equation (5.61), is evaluated numerically. The method of weakening the singularity is used to make the integral proper, and Patterson's method is then used in the numerical integration. In this way, equation (5.61) can be integrated to a high degree of accuracy. For example, when using a routine based on Patterson's method, the absolute error was specified to 10^{-10} and this value was always obtained.

For the upper slot, in Figure 5.11, the limits of integration are $-t_1$, $-t_c$ on one side and $-t_b$, $-t_o$ on the other. For the lower slot, the limits of integration are t_f, t_2 on one side, and t_4, t_g on the other. Thus, the force associated with the four slot sides is again calculated to a slot depth at which the flux has become almost uniform.

5.7 The Normal Force Acting on a Tooth

In Section 2.5.1 of Chapter 2, it was shown that the normal force on a tooth can be evaluated by integrating the Maxwell stress function over the air-gap surface of the tooth. To determine the total normal force on a tooth, using a conformal transformation field solution, the section of the slotted-boundary associated with the tooth is again separated into connected regions (see Figure 5.7). The normal force component on each region is then calculated by integrating the Maxwell stress function over that part of the air-gap surface of the tooth which lies within the region. The total normal force on a tooth is obtained from the summation of these components. To illustrate this, consider Figure 5.13, which shows a section of the slotted air-gap boundary containing a tooth on which the normal force is to be calculated. The total normal force on tooth A, F_{NA}, is given by

$$F_{NA} = F_{N1} + F_{N2} + F_{N3} \tag{5.65}$$

where

F_{N1} = the integral of the Maxwell stress function over the surface between the tooth corner and point A,

F_{N2} = the integral of the Maxwell stress function over the surface between points A and B,

F_{N3} = the integral of the Maxwell stress function over the surface between point B and the tooth corner.

It is important to remember that at points A and B the gap density is almost uniform.

In the singly-slotted region, shown in Figure 5.9, the normal components of force are found by integrating equation (5.60) over the surfaces corresponding to the t-plane intervals $(-t_0, -t_a)$, $(-t_d, -t_1)$ and (t_f, t_e). In these three ranges of integration, equation (5.60) has an analytical solution given by

$$\frac{1}{2\mu_0 \pi}\left\{(I_1+I_3)^2 \log\left|\frac{1+p}{1+p}\right| - I_3^2 \log\left|\frac{t_o+p}{t_o-p}\right| + \frac{2.I_1^2}{(S/g)} \tan^{-1}\frac{p}{\sqrt{t_o}}\right\} \tag{5.66}$$

Similarly, in the doubly-slotted region, shown in Figure 5.11, the normal force components are found by integrating equation (5.61) over the surfaces corresponding to the t-plane intervals $(-t_0, -t_a)$, $(-t_d, -t_1)$, (t_2, t_e) and (t_h, t_4). Equation (5.61) has again been integrated to a high degree of accuracy (an absolute error less than 10^{-10}) in all four ranges of integration for relative displacements of stator and rotor slot centres.

Of course, it is possible in another part of the slotted air-gap boundary to have a region with no slots in which the flux is assumed uniform. Such a region is shown in Figure 5.8. The magnetic pull exerted on the segment, z, is given by

$$\frac{B^2}{2\mu_0} z \tag{5.67}$$

Substituting for B using equation (5.40) gives

$$\frac{\mu_0}{2} \left(\frac{M}{g} \right)^2 z \qquad (5.68)$$

Thus, the normal force component in this region can be expressed in terms of the potential difference across the gap.

5.8 The Computer Program

The analysis described in the previous sections has been incorporated into a computer program which calculates the total flux in any tooth and the tangential and normal forces. A simplified block diagram of this program is shown in Figure 5.14. This program has been used to obtain the distribution of flux and forces on the stator and rotor teeth over a double pole pitch of an induction machine. Furthermore, by displacing the stator and rotor surfaces it was possible to obtain a number of distributions and, thus, to determine the flux and force pulsations into the teeth. This investigation has been carried out for a number of slot combinations and the results and conclusions are presented in the following chapters.

The program can obtain both flux and force distributions very rapidly. For example, for a machine with 36 stator slots and 32 rotor bars, the program takes 4 seconds(execution time) on a C.D.C. 7600 computer to calculate the flux, tangential and normal force distributions for eight relative displacements of stator and rotor surfaces. This involves the calculation of flux and force on 64 teeth. It is believed that this program is presently one of the fastest available for calculating flux and force distributions using a two-dimensional field solution. In fact, such is its speed that it is proposed to use the program to generate the time history of the flux and forces on a tooth. This may be achieved by calculating the flux and force on a tooth for very many

positions of stator and rotor surfaces and for varying currents in the windings. One can envisage this as taking hundreds of 'snap shots' of the field and then combining them to produce a film of the complete time history.

The main limitation of the program at present is that a large amount of data processing is required. The constants of the doubly-slotted boundary are calculated in a separate program. The stator and rotor current distributions are calculated separately(see Chapter 6) and the currents flowing in the conductors in the region where the tooth flux and forces are being calculated are read into the program. This also applies to the air-gap m.m.f. values. The slotted air-gap boundary has to be drawn out in full for every position of the stator and rotor surfaces so that it can be separated into the connected sections used in the program. This involves, in particular, finding a number of points at which the gap density is uniform. The later two processes involve a large amount of laborious data processing.

It would, of course, be possible to do some of the data processing by computer. For example, a small computer program has already been written to find the constants of the doubly-slotted boundary. This program can be incorporated into the main program without greatly increasing computing time as it is a very efficient routine. A sub-routine could be written to generate the stator and rotor currents and the values of the air-gap m.m.f. Such a routine could be based on the method described in Chapter 6. This method involves only simple calculations and would not, therefore, greatly increase computing time. The development of a routine which separates the slotted air-gap boundary into sections is more difficult but not impossible. These additional modifications have not been incorporated into this program mainly because of time. It was believed more important to obtain

results of engineering importance rather than develop a highly efficient computer program. Nevertheless, it is hoped to include these refinements in the program so that eventually it will only be necessary to specify the overall design parameters (i.e. slot widthsand slot pitches).

5.9 References

5.1 CARTER, F. W. : 'The magnetic field of the dynamo-electric machine', J. Inst. Elect. Engrs., 1926, 359, pp.1115-1138.

5.2 ROBERTSON, B. L. and TERRY, J. A. : 'Analytical determination of magnetic fields', Trans. Am. Instn. Elect. Engrs., 1929, 48, pp.1242-1269.

5.3 BINNS, K. J. and LAWRENSON, P. J. : 'Analysis and computation of electric and magnetic field problems' (Pergamon, 1973).

5.4 SELBY, S. M. : 'Standard Mathematical Tables' (C.R.C., 1973).

5.5 PHILLIPS, G. M. and TAYLOR, P. J. : 'Theory and Application of Numerical Analysis' (Academic Press, 1973).

5.6 ROWLANDS-REES, G. : 'Analysis of no-load force pulsations and cogging torques in induction machines', Ph.D. thesis, University of Southampton, 1978.

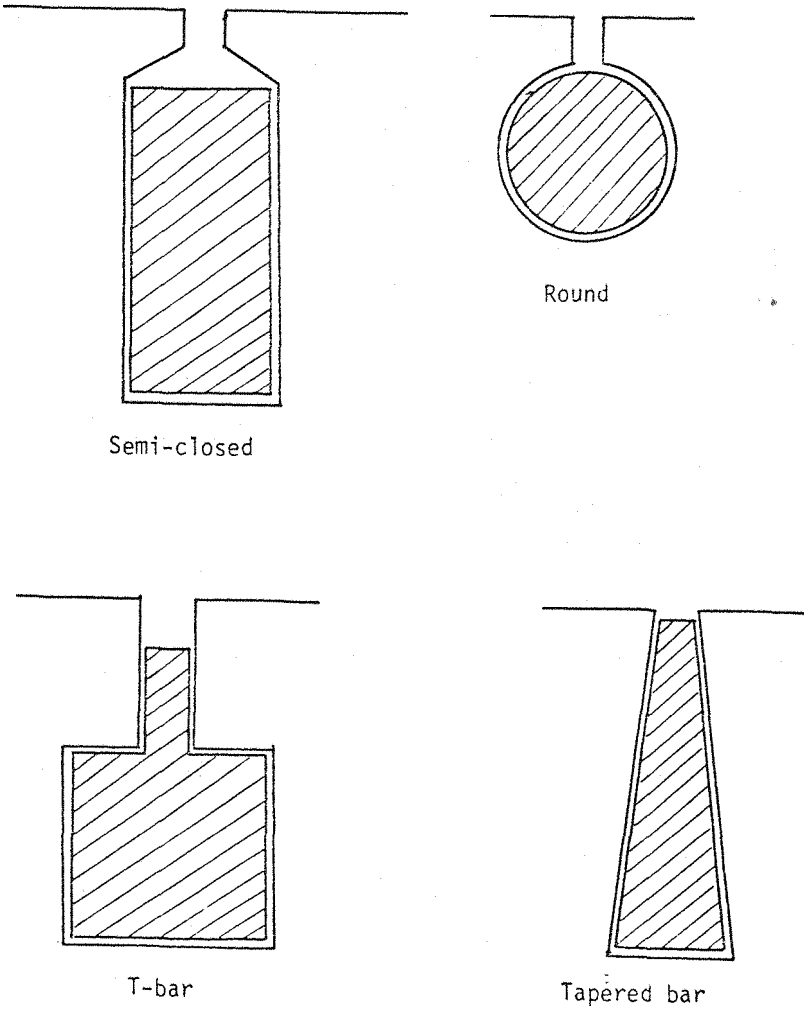

Figure 5.1 Some typical induction motor slot profiles

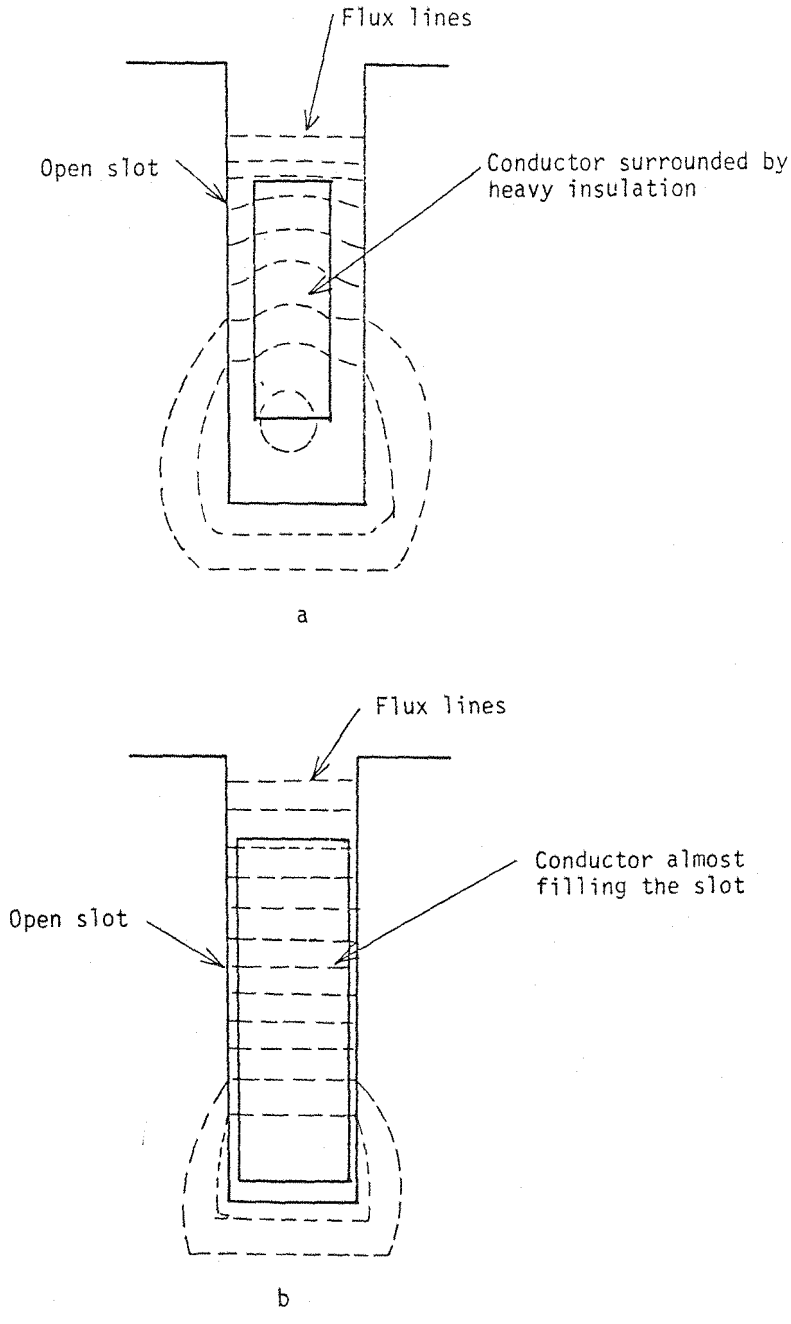

Figure 5.2 The slot leakage flux pattern of a high voltage and normal induction machine

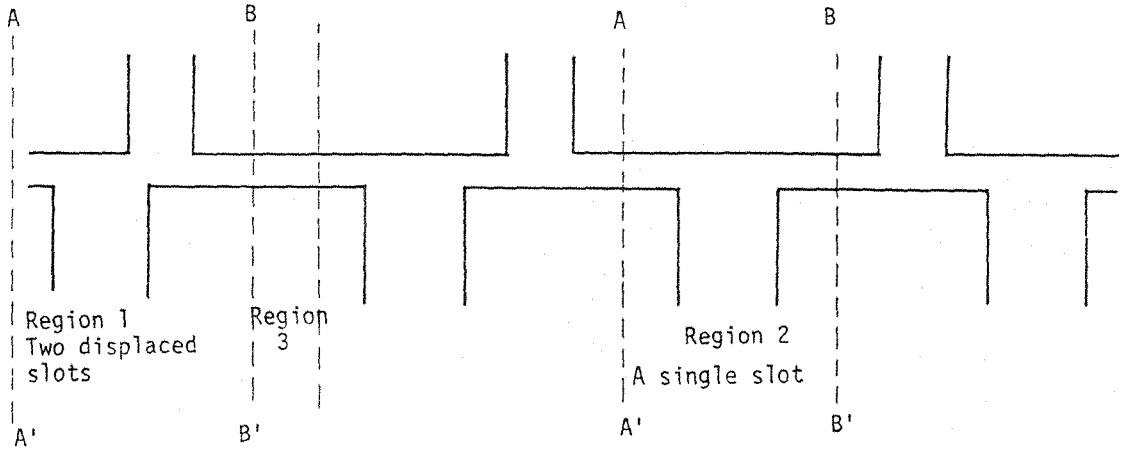

Figure 5.3 A representation of the slotted-boundary of an induction machine

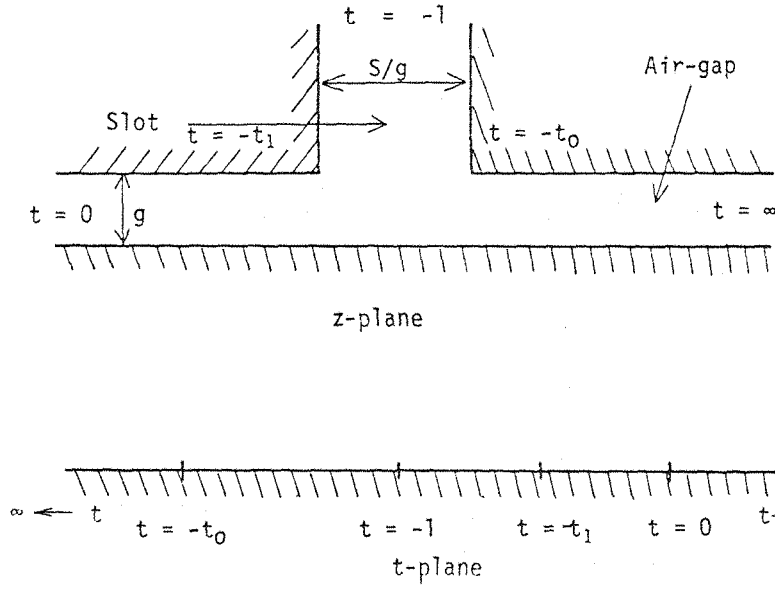

Figure 5.4 Representation of the singly-slotted boundary in the z-plane and its relationship with the complex t-plane

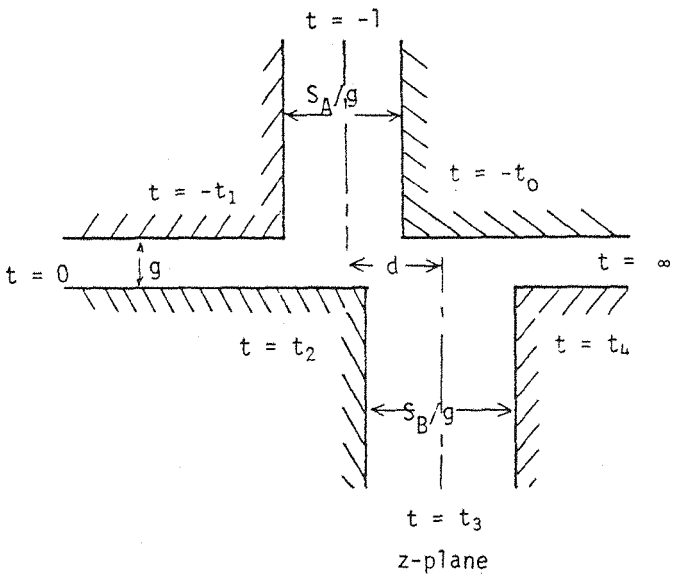

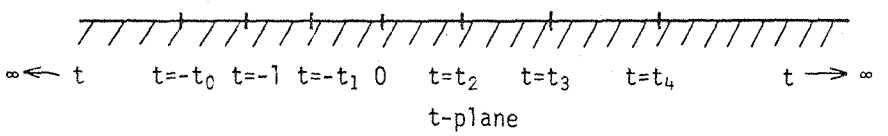

Figure 5.5 Representation of the doubly-slotted boundary in the complex z-plane and its relationship with the complex t-plane

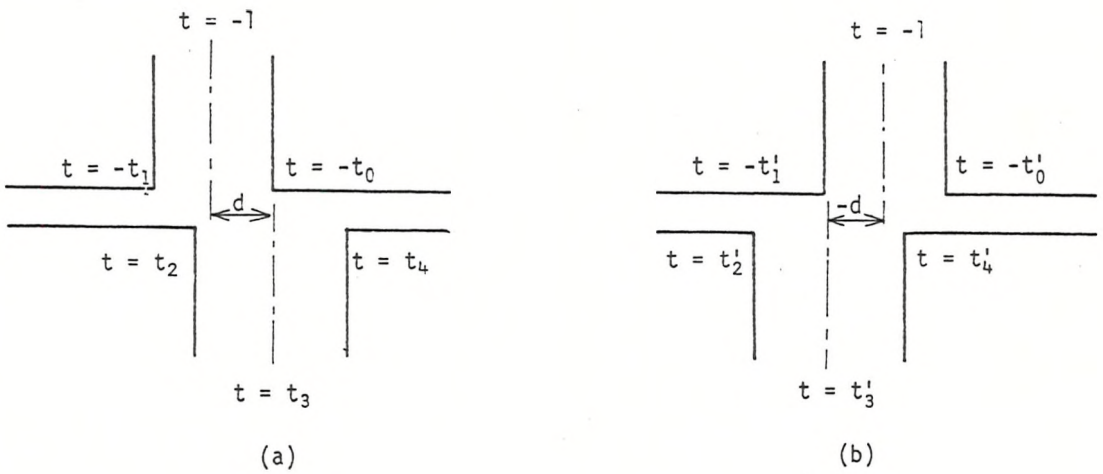

Figure 5.6 Two doubly-slotted boundaries having a positive and negative displacement, d. A simple relationship exists between these two sets of transformation constants.

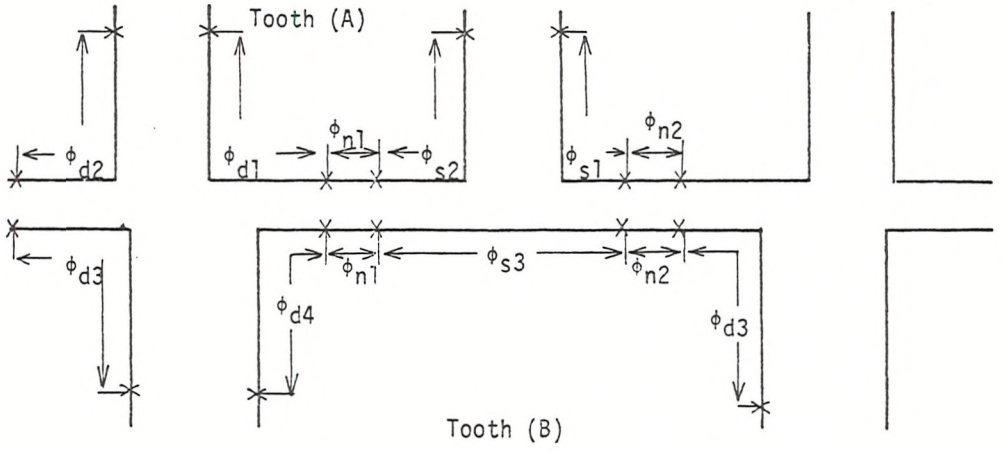

Figure 5.7 The most complicated section of the slotted air-gap boundary in which the flux in a tooth has been calculated

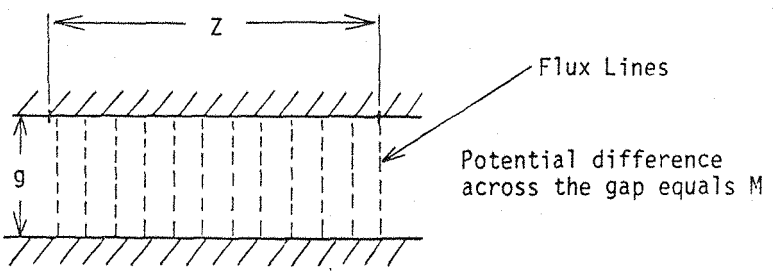

Figure 5.8 A region containing no slots

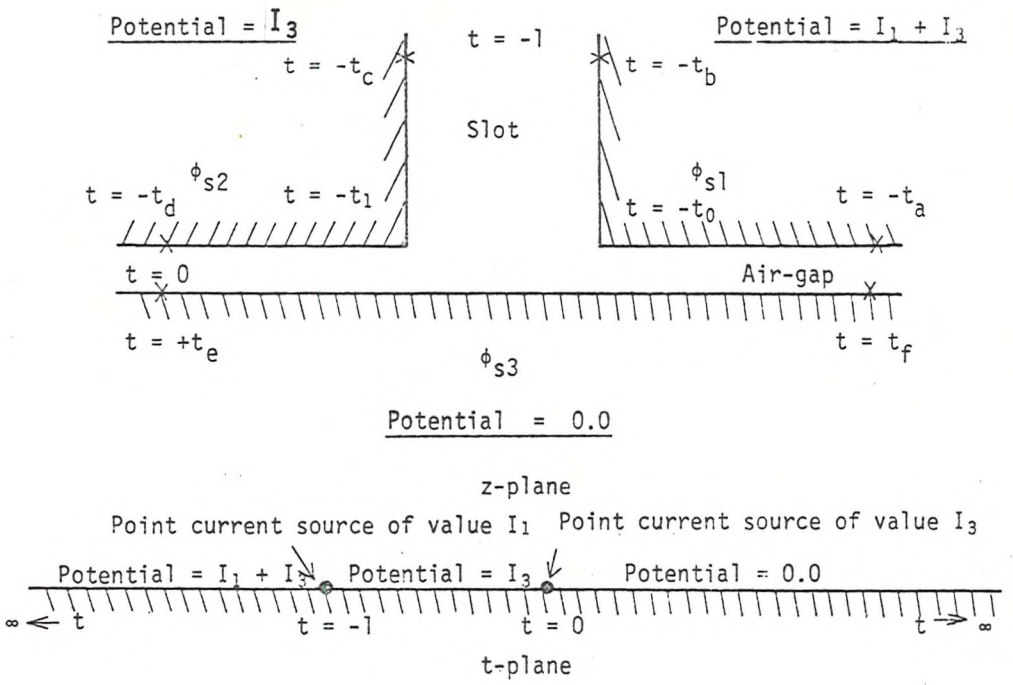

Figure 5.9 The singly-slotted region showing the correct boundary conditions

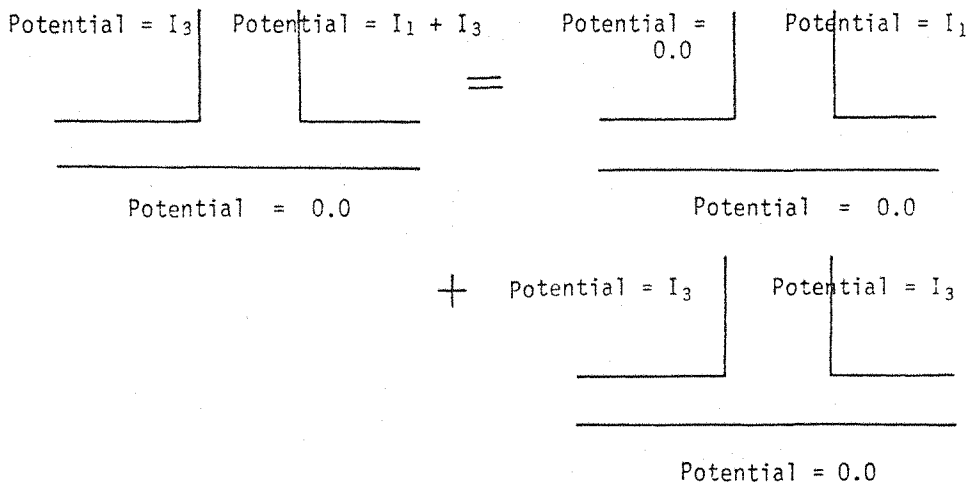

Figure 5.10 The separate boundary conditions on the singly-slotted boundary used to determine the direction of flux

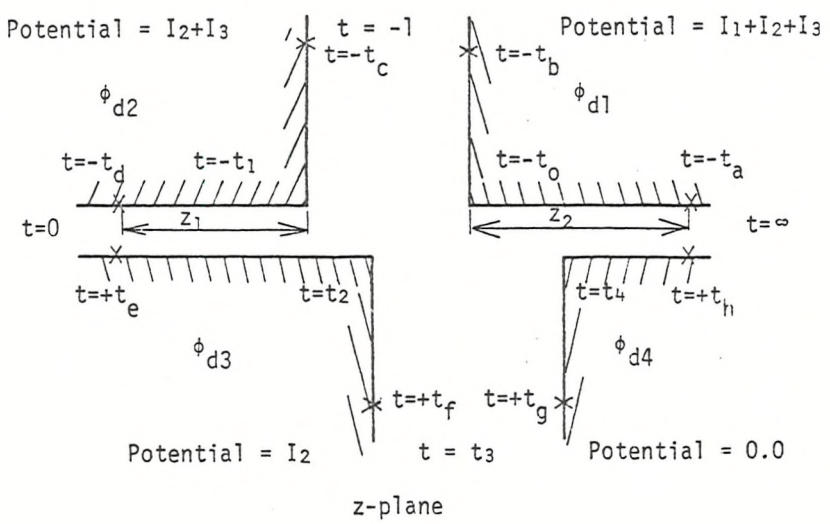

Figure 5.11 The doubly-slotted region showing the correct boundary conditions

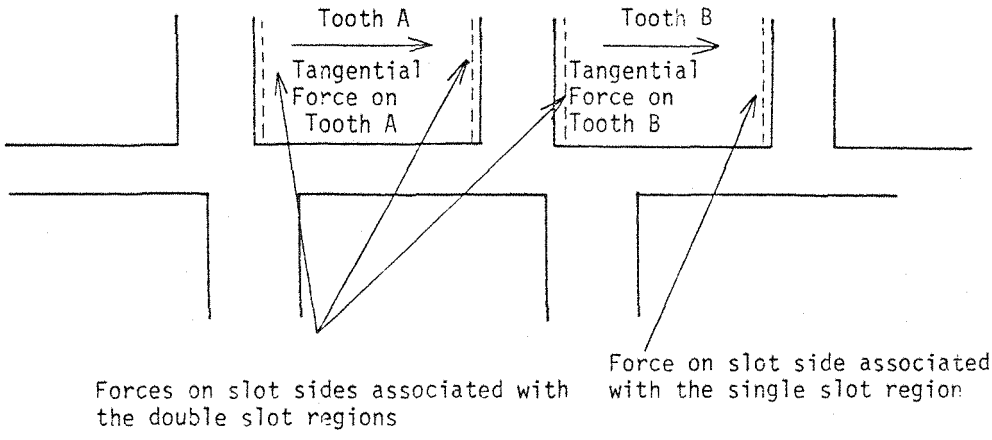

Figure 5.12 The tangential force on two consecutive teeth

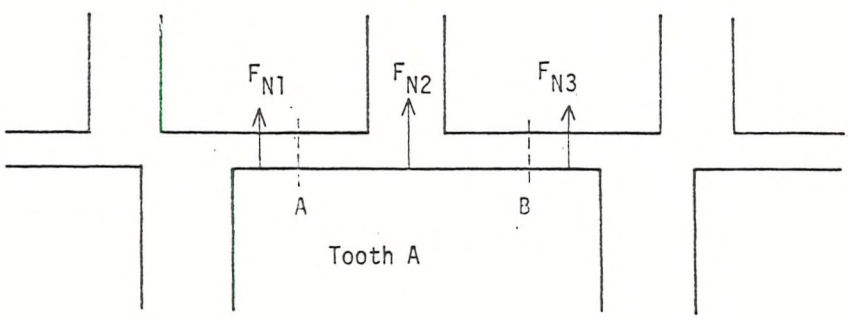

Figure 5.13 The section of slotted air-gap boundary used to illustrate the calculation of the total normal force on a tooth

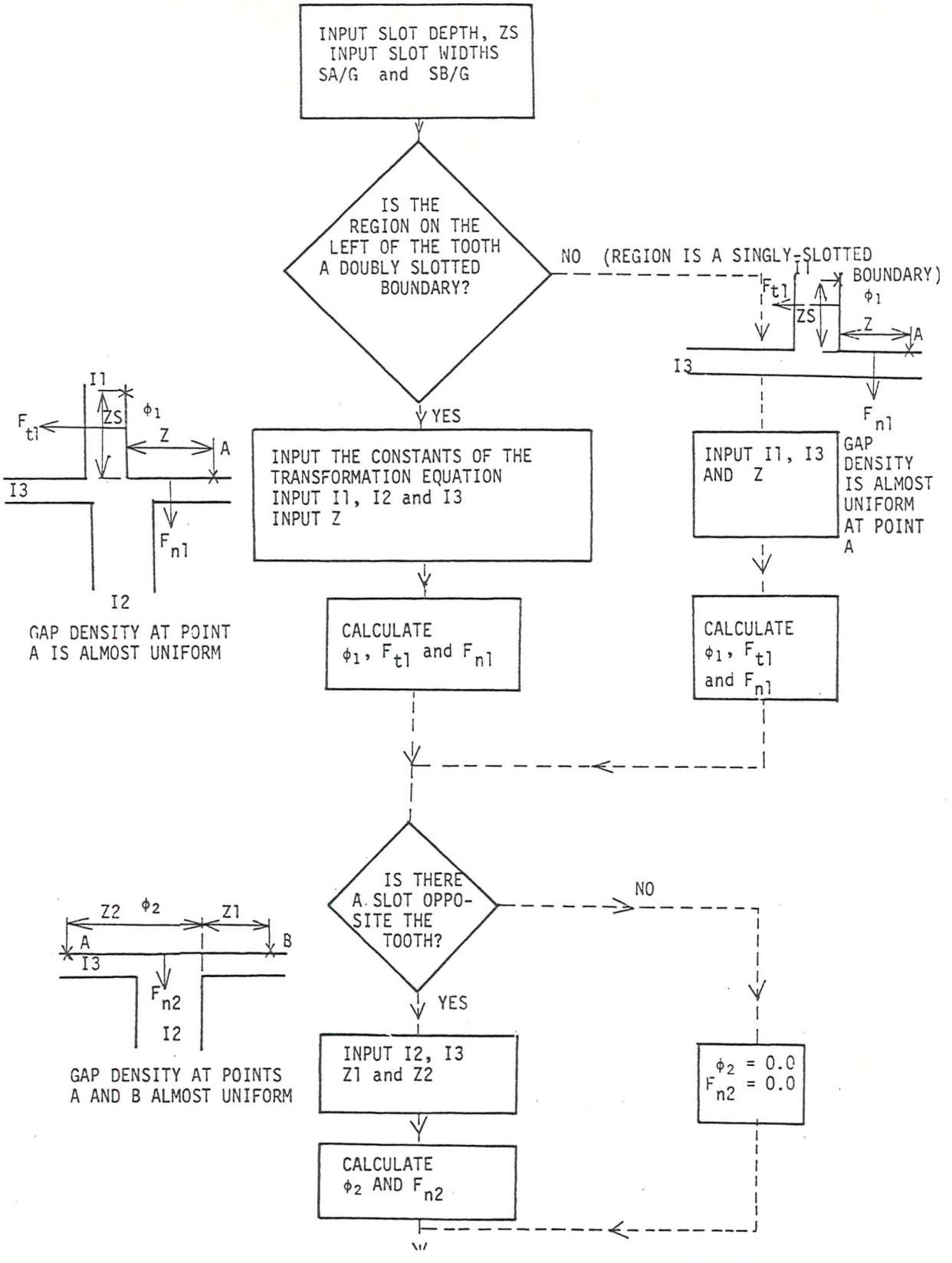
INPUT SLOT DEPTH, ZS
INPUT SLOT WIDTHS
SA/G and SB/G
IS THE REGION ON THE LEFT OF THE TOOTH A DOUBLY SLOTTED BOUNDARY?
NO (REGION IS A SINGLY-SLOTTED BOUNDARY)
YES
INPUT THE CONSTANTS OF THE TRANSFORMATION EQUATION
INPUT I1, I2 and I3
INPUT Z
INPUT I1, I3 AND Z
GAP DENSITY IS ALMOST UNIFORM AT POINT A
CALCULATE ϕ_1, F_{t1} and F_{n1}
CALCULATE ϕ_1, F_{t1} and F_{n1}
GAP DENSITY AT POINT A IS ALMOST UNIFORM
IS THERE A SLOT OPPOSITE THE TOOTH?
NO
YES
INPUT I2, I3
Z1 and Z2
CALCULATE ϕ_2 AND F_{n2}
$\phi_2 = 0.0$
$F_{n2} = 0.0$
GAP DENSITY AT POINTS A AND B ALMOST UNIFORM

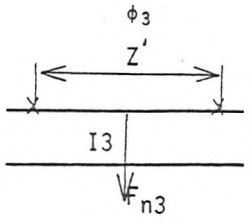

IS THERE A REGION WITH NO SLOTS IN WHICH THE GAP DENSITY IS ASSUMED UNIFORM?

NO

YES

$\phi_3 = 0.0$
$F_{n3} = 0.0$

INPUT I3 (THE AIR-GAP M.M.F. IN THE REGION) AND Z'

CALCULATE F_{n3} AND ϕ_3

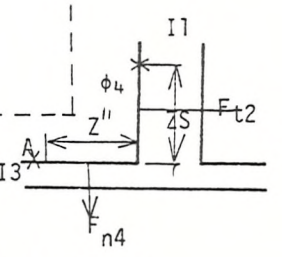

IS THE REGION TO THE RIGHT OF THE TOOTH A DOUBLY SLOTTED BOUNDARY?

NO (REGION IS A SINGLY-SLOTTED BOUNDARY)

YES

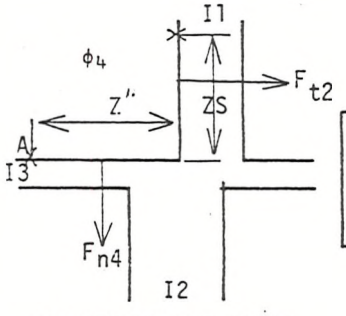

GAP DENSITY AT POINT A IS ALMOST UNIFORM

INPUT I1, I3, AND Z''

INPUT CONSTANTS OF THE TRANSFORMATION EQUATION
INPUT I1, I2 and I3
INPUT Z''

CALCULATE ϕ_4, F_{t2} and F_{n4}

CALCULATE ϕ_4, F_{t2} and F_{n4}

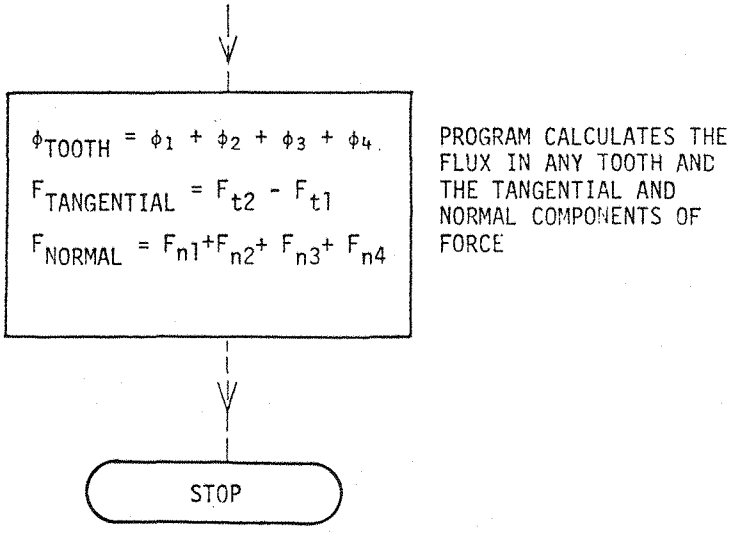

Figure 5.14 A simplified block diagram of the computer program which calculates the total flux in any tooth and the total tangential and normal forces

CHAPTER 6

A METHOD FOR CALCULATING THE APPROXIMATE ROTOR CURRENT AND AIR-GAP M.M.F. DISTRIBUTIONS

6. Introduction.

6.1 The Concept of a Distributed M.M.F.

6.2 Assumptions.

6.3 The Calculation of the Peak Value of the Fundamental No-Load Air-Gap M.M.F.

6.4 The Calculation of an Approximate Rotor Current Distribution on Load.

6.5 The Calculation of the Air-gap M.M.F. in the Conformal Transformation Model.

6.6 References.

6. Introduction

It is a requirement of the present analysis that the flux, tangential and normal force components associated with all the teeth over a double pole pitch be calculated and for this it is necessary to calculate the stator and rotor currents and the air-gap m.m.f. distributions. In order to do this, the concept of m.m.f. as a distributed quantity is used and a brief introduction to this subject is given in Section 6.1.

It is not practical to consider all types of stator winding and only one winding is considered in the analysis. This analysis is not primarily concerned with the modulation of the tooth-ripple carrier by the m.m.f. harmonics, but rather, with the influence of the rotor slot number on the carrier. This subject is discussed in detail in Section 6.2.

In Section 6.3 the peak value of the fundamental no-load air-gap m.m.f., associated with the stator winding used in the analysis, is calculated. In large machines it is reasonable to assume that the air-gap m.m.f. remains constant and sinusoidal when a load is applied to the machine.

An approximate rotor m.m.f. distribution is obtained for a set of imposed stator currents in Section 6.4. This distribution is found by subtracting the fundamental air-gap m.m.f. distribution from the m.m.f. distribution associated with the stator current on load. From this rotor m.m.f. distribution, a rotor current distribution can be obtained.

Finally, in Section 6.5, it is shown how the air-gap m.m.f. distribution associated with the point current sources and slotted-boundary used in conformal transformation is calculated.

6.1 The Concept of a Distributed M.M.F.

The concept of a distributed m.m.f. is used extensively throughout this chapter and a brief introduction to this subject is now presented.

The basis of the concept of m.m.f. is Maxwell's equation:

$$\text{curl } \underline{H} = \underline{J} + \frac{d\underline{D}}{dt} \tag{6.1}$$

At power frequencies the displacement current is negligible and the m.m.f. can be written in the more familiar form of Ampere's circuital law:

$$\oint \underline{H} \cdot d\underline{\ell} = I \tag{6.2}$$

This equation is commonly used in the calculation of flux in magnetic circuits. In such circuits, the m.m.f. is a lumped quantity analogous to e.m.f. in electrical circuits. In a similar way, flux and reluctance are analogous to current and resistance respectively. In most applications, part of the magnetic circuit is in iron and part in air, and it is assumed that equation (6.2) can be written as

$$I = H_I \cdot \ell_I + H_A \cdot \ell_A \tag{6.3}$$

where ℓ_i and ℓ_A are the mean lengths of the magnetic circuit in iron and air respectively and H_I and H_A are the moduli of the magnetic field in the iron and air respectively. Since the normal component of flux density is continuous at a boundary, the following equation can be obtained:

$$\mu_0 H_A = \mu_0 \mu_r H_I \tag{6.4}$$

The magnetic circuit quantities are related through the equation

$$\text{m.m.f.} = \text{Flux} \times \text{Reluctance} \tag{6.5}$$

The reluctance of the circuit, R, can be found by solving equations (6.3) and (6.4).

It is quite common to discuss the properties of the air-gap field in an induction machine in terms of a magnetic circuit. Such an approach presents, essentially, a one-dimensional view of the magnetic phenomena. The magnetic circuit quantities described in the previous paragraph are all 'lumped' parameters, but in the analysis of the air-gap field, many quantities of interest, such as losses, forces and torque, depend not upon 'lumped' parameters, but on distributed quantities such as flux and current densities. To overcome this problem, the concepts of distributed m.m.f. and permeance were introduced. These have been clearly defined by Binns and Schmid[6.1] and only the concept of a distributed m.m.f. will be discussed here.

The idea of an m.m.f. distributed circumferentially around the air-gap is a one-dimensional view of current driving flux across the gap. To realise how an m.m.f. distribution can be obtained, consider Figure 6.1. To obtain the m.m.f. associated with current I_1, flowing in the point current source in Slot 1, the magnetic field strength, H, is integrated around the closed path shown by a dotted line. On the line AA', the m.m.f. is arbitrarily chosen to be zero and this line acts as the origin of the m.m.f. distribution. In using the distributed m.m.f. approach, it is generally assumed that the permeability of the iron is high or even ∞. This assumption is also made, of course, when using a conformal transformation field solution. Thus, the magnetic field strength in the iron is zero and the path of integration reduces to the two line segments AA' and BB' crossing the gap. However, the m.m.f. at AA' is zero, so that the m.m.f. at BB' is simply equal to I_1. If the path is now enlarged to include Slot 2, the m.m.f. at CC' is given by $I_1 + I_2$. In this way a complete m.m.f. distribution can be obtained as shown in Figure 6.2. This distribution is periodic in a double pole pitch.

6.2 Assumptions

For the purpose of assessing the influence of slot combination, a 4-pole, 36 slot stator with a double-layer winding of 8/9 pitch is chosen. The stator has a slot pitch, P_s/g, of 25.0. It is not necessary or appropriate to consider all hypothetical stator winding distributions since the object of this investigation is to consider the influence of stator-rotor slot combinations, and it is not reasonable or necessary to consider every possible stator winding. The object of this analysis is to examine the conditions which give rise to large flux or force pulsations at the stator and rotor teeth. Each m.m.f. harmonic will modulate the fundamental and harmonic tooth-ripple frequencies[6.1], but if the fundamental carrier is small the resultant effect will be small. The modulation by m.m.f. harmonics is well known and there are limits to the practical reduction of such modulations. The tooth-ripple carrier, however, critically dependson the slot dimensions and the rotor slot number is clearly a parameter which can be chosen by the designer.

It should be emphasised that the damping effect of the cage on the harmonics is ignored. To include this effect it would be necessary to specify the type of cage used and its appropriate resistance and reactance values which are frequency dependent. From a practical point of view, only a few cage configurations can be considered but it is known that the relative merits of different slot combinations are not critically dependent on cage design. Hence, the applied electromagnetic field pulsations are computed and the possibility of making these small is considered. The damping influence of the cage is further beneficial but does not influence critically the choice of slot combination. In short, a bad choice of slot combination can only be

slightly improved by cage design, its relative merits compared to other choices remains largely the same.

It should be emphasised that in this thesis only squirrel-cage rotors are considered. This type of winding reacts with all the harmonics produced by the stator. The cage tends to drastically reduce the amplitude of those components of the air-gap leakage field associated with the wavelength of a phase belt (these components will be referred to as the phase belt harmonics). The reason for this reduction is that there is a large difference between the angular velocities of the cage and these harmonics. For example, if the cage has a velocity of 1450 r.p.m., the 5th m.m.f. harmonic travels in the opposite direction to the cage at one-fifth its velocity, that is, at 290 r.p.m. Therefore, the relative angular velocity is 1740 r.p.m.. This large difference in velocity results in the 5th harmonic of the air-gap field inducing a large e.m.f. in the cage. The cage offers a very low impedance to the phase belt harmonics so that very large damping currents flow. In fact, the cage acts as a virtual short-circuit. The result of this heavy damping action is that the phase belt harmonics of the air-gap field are greatly reduced and the air-gap m.m.f. waveform is remarkably sinusoidal. It should, however, be noted that the tooth-ripple harmonics of the air-gap field are still present, just as in a wound rotor machine.

In the analysis, therefore, attention has been focussed on the process by which the fundamental air-gap m.m.f reacts with the currents in the slots which, of course, give rise to the tooth-ripple fluxes and forces. Therefore, the analysis proceeds by imposing currents on the stator, considering the fundamental gap m.m.f. alone and examining the effects which occur when the rotor moves relative to the stator for the same imposed stator currents. If the rotor is displaced by a rotor

slot pitch the field distribution is unaltered since all rotor bars are assumed to be the same.

In the investigation, a range of rotor slot numbers is taken (see Table 6.1) for a given stator slot number and the flux and force pulsations are calculated under certain heteropolar field conditions. It is then possible to determine not only the flux and force pulsations, but their dependence on slot combination.

It should be mentioned that the equivalent slot openings of both stator and rotor are kept constant throughout the analysis. Thus, the effect on the flux and force pulsations of varying these two parameters has not been investigated. It is worth noting that in practice a designer has only a limited choice of slot openings. For example, the stator slot openings must be large enough to allow the machine to be wound. They cannot, however, be too large as this results in excessive tooth losses[6.2] in the rotor. Likewise, large rotor slot openings produce large stator flux pulsations.[6.2] Rotor tooth flux pulsations can be reduced by inserting magnetic wedges into the stator slot openings and stator tooth flux pulsations can be minimised by having closed rotor slots. In practice, the optimal slot combination is not critically affected by the choice of slot opening.

Rotor slot number	Rotor tooth pitch P_R/g
24	37.50
28	32.14
30	30.00
32	28.13
36	25.00
40	22.50
42	21.43
44	20.45
48	18.75
60	15.00

TABLE 6.1

6.3 The Calculation of the Peak Value of the Fundamental No-Load Air-gap M.M.F.

The stator winding used in the present analysis is shown in Figure 6.3. The conductors in the stator slots are represented by point current sources which is, of course, a requirement of the conformal transformation method. Before an approximate rotor current distribution on load can be obtained, it is necessary to calculate the value of the fundamental component of the air-gap m.m.f. on no-load.

The fundamental air-gap m.m.f. is obtained as follows. Let the stator current distribution be frozen at an instant in time. It is assumed that the rotor currents are negligible as discussed in Chapter 2. For convenience, let the stator current distribution be frozen at the instant when the no-load current in phase A is zero. The current in phase B is $-0.866\ \hat{I}_{NL}$ and in phase C is $0.866\ \hat{I}_{NL}$, where $\hat{I}_{NL}$ is the peak no-load current per phase. Figure 6.3 shows the stator current distribution at this instant. The quantity, I, is equal to $n_c\ \hat{I}_{NL}$, where n_c is the number of turns per coil side. The exact value of this quantity will be obtained shortly.

The m.m.f. distribution associated with the current distribution can be obtained, as explained in Section 6.1, by summation of the current distribution from the arbitrary reference shown in Figure 6.3. This m.m.f. distribution is shown in Figure6.4,and it can be seen that its peak value is 5.196 I. The peak value of the fundamental air-gap m.m.f. can be found by using Fourier analysis. This value will be the same regardless of the instant at which the stator current distribution is frozen. The peak value of the fundamental is 5.4154 I. This value coincides with the peak value of the flux density wave. Thus

$$\oint \underline{\hat{H}}.\underline{d\ell} = 5.4154\ I \qquad (6.6)$$

or

$$\hat{H} \int_0^g d\ell = 5.4154\ I$$

$$\hat{H}_g = 5.4154\ I$$

$$\frac{\hat{B}_g}{\mu_0} = 5.4154\ I$$

It is convenient to normalise all quantities to a gap width of 1 m and a peak fundamental flux density of 1 Tesla. Thus

$$I = \frac{1}{5.4154 \times \mu_0}$$

$$= 1.4695 \times 10^5$$

This gives a peak value of the fundamental air-gap m.m.f. of 7.96×10^5 Amps/m.

Whilst normalising I in this way results in large values of slot current under both no-load and load conditions, it has the advantage that it is not necessary to specify, N_{ph}, the number of turns in series per phase. One consequence of the large slot currents is that the values of the tooth fluxes and forces are unrealistically large.

6.4 The Calcualtion of an Approximate Rotor Current Distribution on Load

The steady state operation of an inducton machine on load was described in Chapter 2. In all but small machines (output < 100 W) the magnetising flux is virtually constant, for a given terminal voltage, and consequently the resultant air-gap m.m.f. is also constant as the load changes. The fundamental rotor m.m.f. distribution when subtracted from the fundamental stator m.m.f. distribution at any load results in the m.m.f. across the air-gap driving the magnetising flux. The currents passing in the rotor bars for a given stator current can

then be obtained from the rotor m.m.f. distribution. However, before discussing this further, it is necessary to consider the choice of an appropriate load current level.

The load current level can be expressed in terms of the stator magnetising current. Depending on the size of the machine, this ratio will vary, being close to unity for a very small machine and being quite large for machines of megawatt ratings. Undesirable effects of flux pulsations due to load begin to be revealed gradually and in comparing designs as regards, for example, rotor slot number, the exact load level is not vital. This is important since it means that different sizes of machine do not have to be considered in isolation except for the very small machines which are stator winding resistance dominated. It was decided to take the ratio 5 : 1 for the stator current on load relative to the magnetising current.

To show how flux pulsations increase with load current level, the flux pulsations in a rotor tooth where computed for the slot combination N_S = 36, N_R = 40 at two load current levels. Figures 6.5 and 6.6 show the rotor tooth-ripple flux pulsations for stator currents 2.5 and 5 times as large as the magnetising current, at the same power factor of 0.866. These types of curves will be discussed in greater detail in the next chapter. The shape of the waveforms are similar, but the amplitude of the pulsations at the load current level of 5 : 1 are larger than at 2.5 : 1. In a similar manner, the normal force pulsations are greater at the load level of 5 : 1 than at 2.5 : 1. These two curves confirm, therefore, that the amplitude of the flux and force pulsations steadily increase with increasing load current level.

The stator current distribution on load is shown in Figure 6.7. The currents shown there represent the values of the imposed stator

currents discussed in Section 6.2. It should be noted that the stator current distribution on load has been frozen at the same instant of time as the no-load current distribution shown in Figure 6.3. The m.m.f. distribution associated with the current distribution on load is obtained, as before, by summation of the current distribution from the reference point shown in Figure 6.7. This distribution is shown in Figure 6.8 along with the fundamental air-gap m.m.f. The fundamental of this m.m.f. waveform is, of course, five times as large as the fundamental of the no-load air-gap m.m.f.

It is not possible to obtain a perfect balance of the stator and rotor m.m.f.s using the stepped waveform shown in Figure 6.8. The reason for this is that the stepped waveform represents a piecewise continuous function where the m.m.f. is constant between the current sources, whereas the air-gap m.m.f. is a continuous function in which both phase belt and tooth-ripple harmonic components have been neglected. The rotor m.m.f. waveform which results from the subtraction of the air-gap m.m.f. from the stepped waveform does not correctly represent the rotor m.m.f. distribution. To overcome this difficulty, only the points at the centres of the steps corresponding to the centres of the stator teeth are taken. This amounts to sampling the waveform at these points. To ensure that a rotor m.m.f. distribution can be obtained for any rotor position, these points are joined by straight lines as shown in Figure 6.9. In doing this, one is neglecting the effect that the slotting has on the m.m.f. waveform. A balance is obtained using a more continuous waveform in which only the fundamental and lower order m.m.f. harmonics are present. Interestingly, as shown in Table 6,2, there is scarcely any change in the values of the fundamental and lower order harmonics when

the stepped waveform is smoothed.

	Fund	5th	7th
Smoothed Waveform	39.56×10^5	-1.02×10^5	0.29×10^5
Stepped Waveform	39.76×10^5	-1.19×10^5	0.36×10^5

Table 6.2

Of course, the value of the higher order harmonics are quite different.

An approximate rotor m.m.f. distribution can be obtained, for a given rotor displacement, by subtracting the fundamental of the air-gap m.m.f. from the m.m.f. waveform shown in Figure 6.9 at points corresponding to the centres of the rotor teeth. This will now be illustrated by considering a slot combination in which $N_S = 36$, $N_R = 32$. The rotor displacement is zero, that is, the centre of rotor slot 1 aligns with an arbitrary reference on the stator, namely the centre of the slot containing the coil side $A\text{-}\overline{B}$. The values of the rotor m.m.f.s at the centres of the teeth are shown in Figure 6.10.

The value of current flowing in any rotor conductor can be obtained simply be subtracting the values of m.m.f.s on the adjacent teeth. In this way, a complete rotor current distribution can be found. The values of these currents represent, of course, the values of the point current sources in the conformal transformation model. When the rotor is moved to a new position, the rotor m.m.f.s at the centres of the teeth are calculated and a new current distribution determined.

6.5 The Calculation of the Air-gap M.M.F. in the Conformal Transformation Model

In the conformal transformation model, the air-gap m.m.f. distribution cannot be represented simply by a continuous function, as the teeth are present. Instead, this distribution has a constant value

between current sources and only changes when a current source is encountered. This stepped air-gap m.m.f. can be obtained by integration of both stator and rotor current distributions from an arbitrary reference.

When calculating the air-gap m.m.f. distribution in the slotted air-gap region used in conformal transformation, two conditions must be applied. The first condition is that, in any region where the field is to be computed, the sum of the currents must be zero. Accordingly, in Figure 6.11 there is a current of value $-(I_1 + I_2 + I_3)$ in the air-gap to the right of the two slots to balance the three currents $\underline{+}I_1$, I_2 and I_3. The second condition is that when the field is calculated in the next slotted region, the current $-(I_1 + I_2 + I_3)$ becomes $(I_1 + I_2 + I_3)$, this current representing the air-gap m.m.f. to the left of the slots in the new region. To explain this, consider an observer at the point X, in Figure 6.11. If he is looking to the left, the gap flux is rotating anticlockwise. If he is looking to the right, the gap flux is rotating clockwise. To account for this change in flux rotation, the sign of the m.m.f. is changed.

The air-gap m.m.f. distribution can be found by integration of both stator and rotor currents from an arbitrary reference. In the case of those slot combinations where

$$\frac{N_S - N_R}{N_p} = \text{integer}$$

the value of the air-gap m.m.f. at $\theta + \pi$ (where θ is the angle subtended at the centre of the machine expressed in electrical degrees) is equal in magnitude but opposite in sign to the value of the m.m.f. at θ. The air-gap m.m.f. is, therefore, an odd function of θ and it is only necessary to calculate this distribution in one pole pitch of the machine. It is convenient, for a given rotor displacement, to draw

a diagram of the part of the slotted air-gap boundary which represents one pole pitch of the machine. To start the distribution, the stator and rotor currents are summed together. The value that results from this summation is divided by two, its sign changed, and it is then inserted into the part of the air-gap at the extreme left-hand end of the diagram (that is before the first slot or slots). Then using the conditions discussed previously, a complete air-gap m.m.f. distribution is calculated. In this form, the part of the slotted air-gap boundary representing the pole can be divided into connected sections and the flux and force distributions computed.

In the case of those slot combinations where

$$\frac{N_S - N_R}{N_P} \neq \text{integer}$$

the air-gap m.m.f. distribution has to be calculated over the full double pole pitch. In this case the part of the slotted-boundary corresponding to a double pole pitch is drawn and the values of the point current sources are inserted in the slots. A value of m.m.f., x, is inserted in the air-gap at the extreme left hand end of the diagram. A new value of m.m.f. is then calculated each time a current source is encountered (each value will, of course, be a function of x the unknown m.m.f.). This new value of the m.m.f. is multiplied by the distance between the last current source and the next one that will be encountered. The values of all the m.m.f.s multiplied by the distances are then summed together and equated to zero. The reason for this is that the area under the air-gap m.m.f. distribution must, of course, equal zero over a double pole pitch. It should be noted that the distance between current sources can either be expressed in terms

of a ratio of g, where g = unity, or in electrical degrees. Thus, a value of x can be obtained and the air-gap m.m.f. distribution can be calculated.

An example of a complete stator and rotor current and air-gap m.m.f. distribution is shown in Figure 6.12. This case is the same as the one considered previously in which N_S = 36, N_R = 32 and the rotor displacement, d, equals zero. It is interesting to note that large changes occur in the air-gap m.m.f. distribution when a slot containing a large current is directly under a tooth. This is not surprising since the air-gap leakage flux is large in such regions, giving rise to a significant change in air-gap m.m.f.

6.6 References

6.1 BINNS, K. J. and SCHMID, E. : 'Some concepts involved in the analysis of the magnetic field in cage induction machines', Proc. I.E.E., 1975, 122, (2), pp.169-175.

6.2 BINNS, K. J. and ROWLANDS-REES, G. : 'Main-flux pulsations and tangential tooth-ripple forces in induction motors', Proc. I.E.E., 1975, 122, (3), pp.273-277.

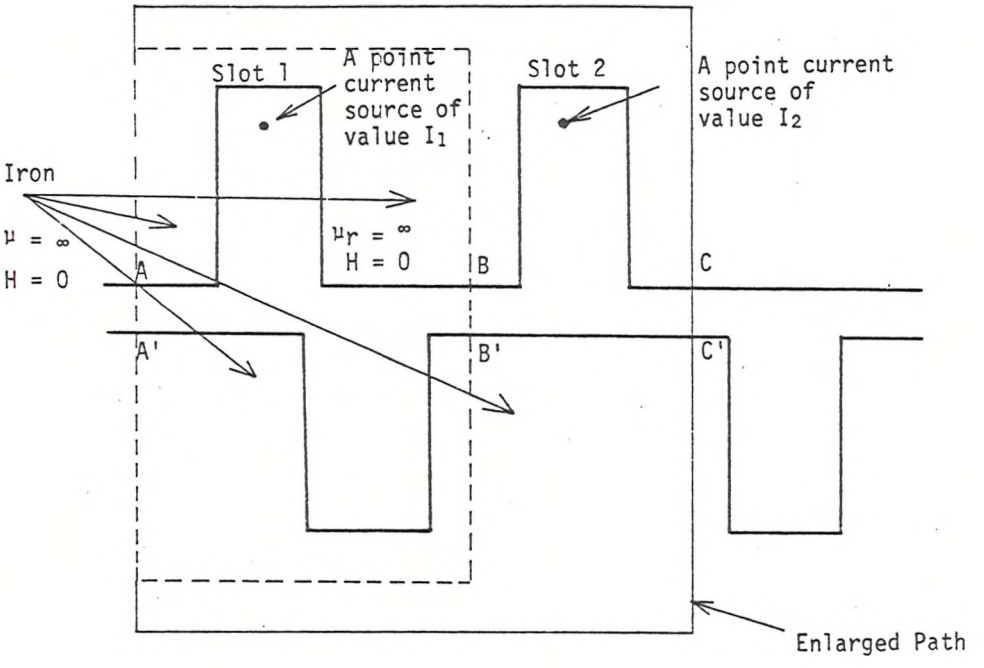

Figure 6.1 A section of the slotted air-gap boundary showing the path of integration taken to obtain part of the m.m.f. distribution

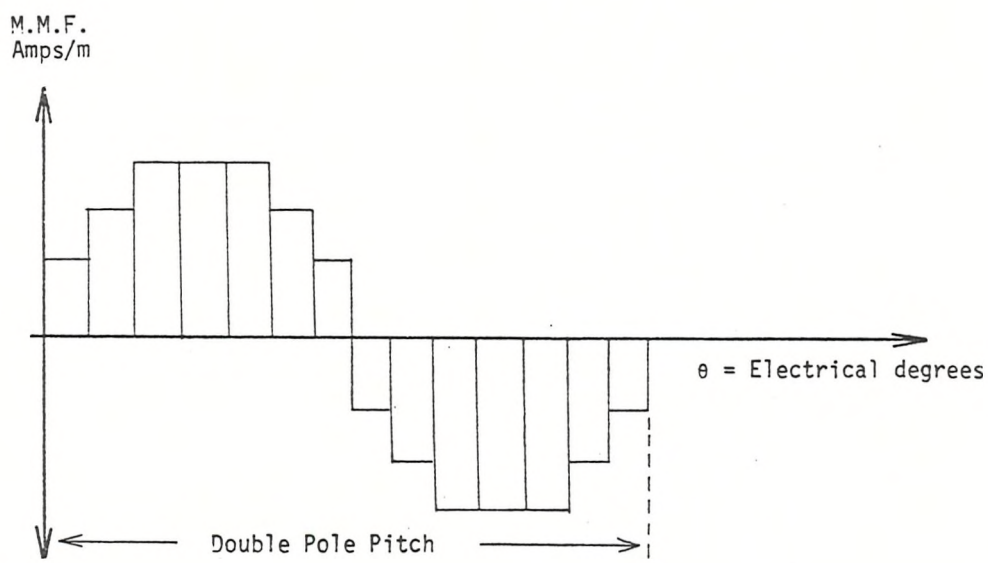

Figure 6.2 A typical m.m.f. distribution, the current carrying conductors in the slots have been replaced by point current sources as is the case in conformal transformation.

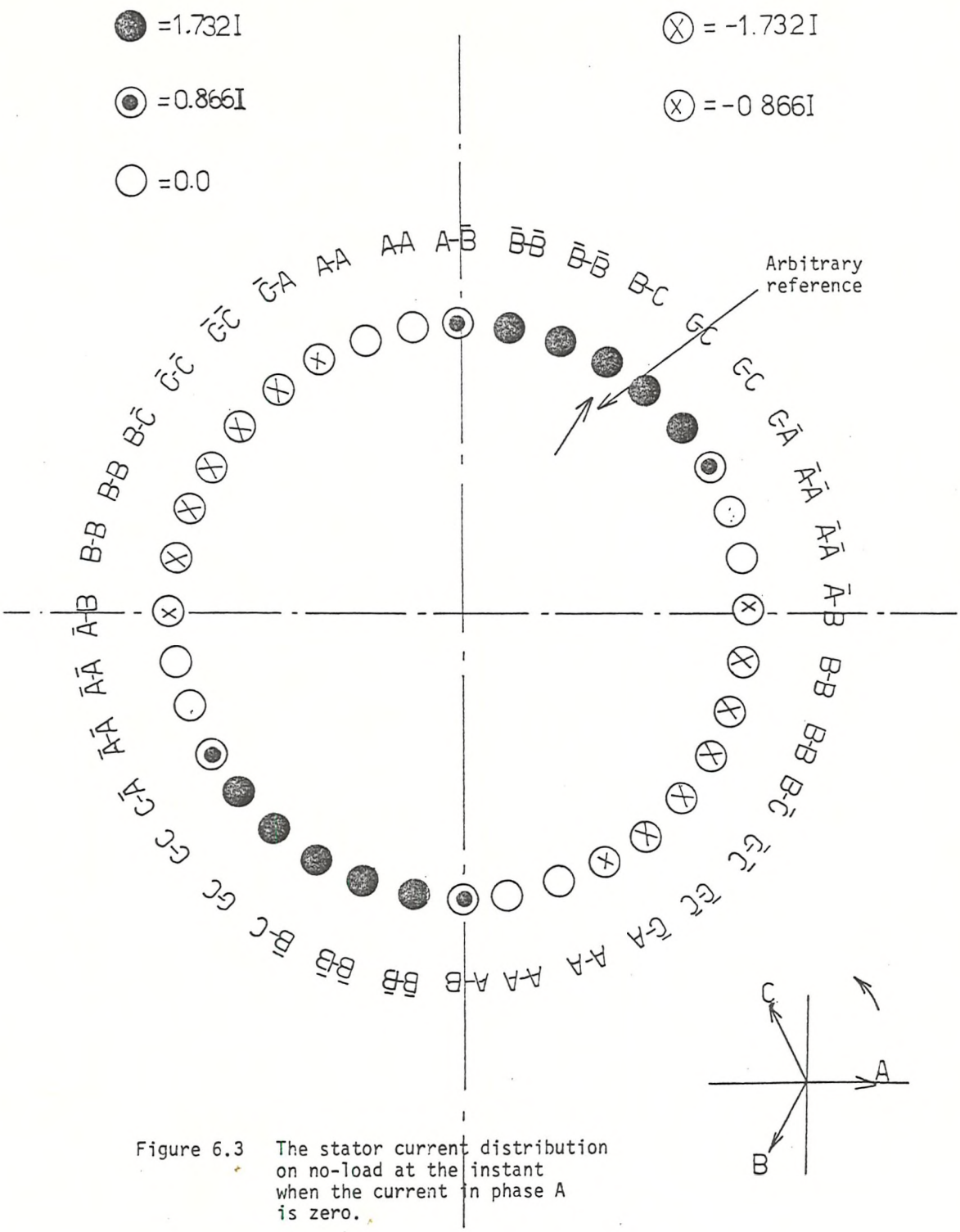

Figure 6.3 The stator current distribution on no-load at the instant when the current in phase A is zero.

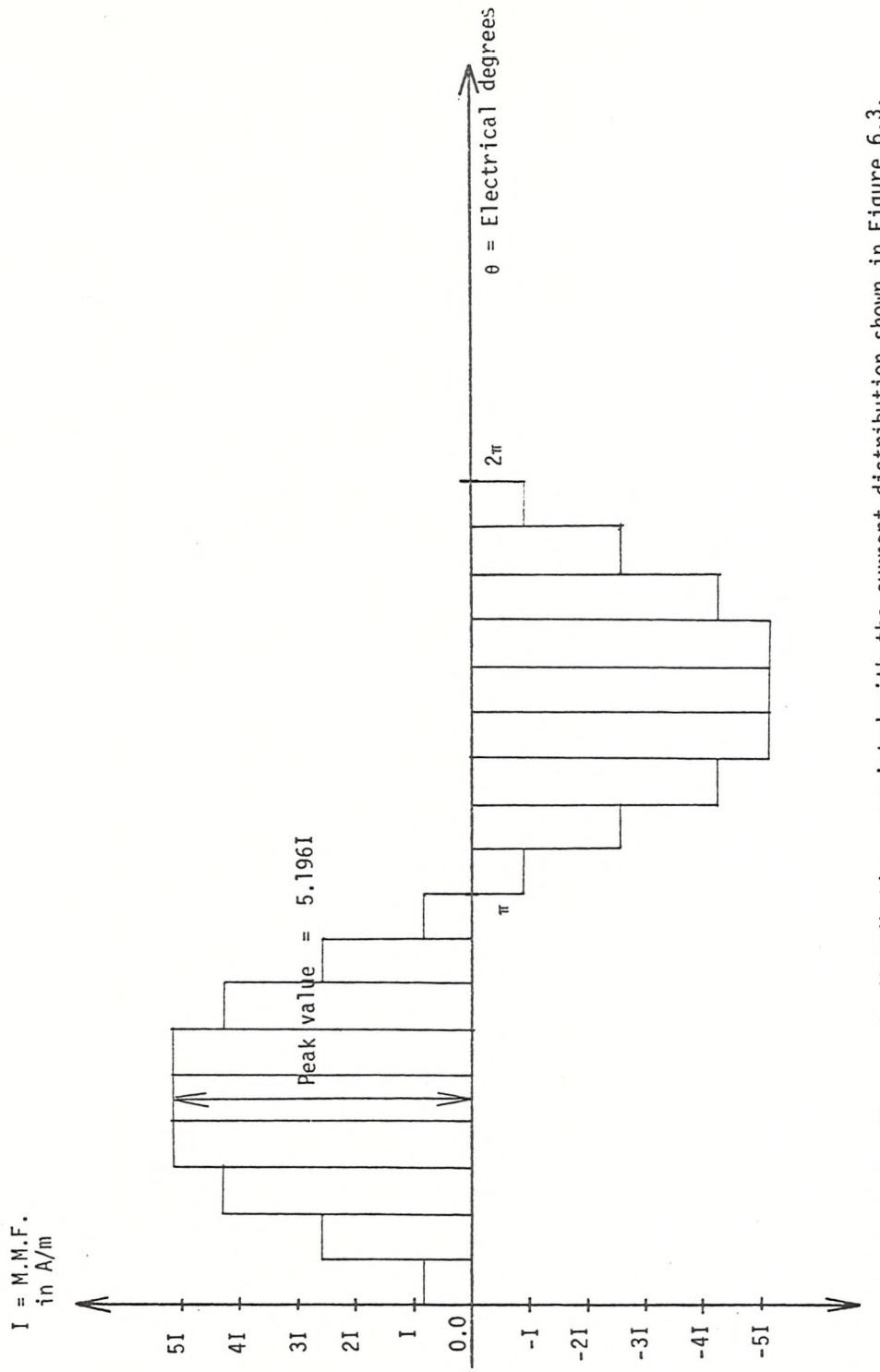

Figure 6.4 The m.m.f. distribution associated with the current distribution shown in Figure 6.3.

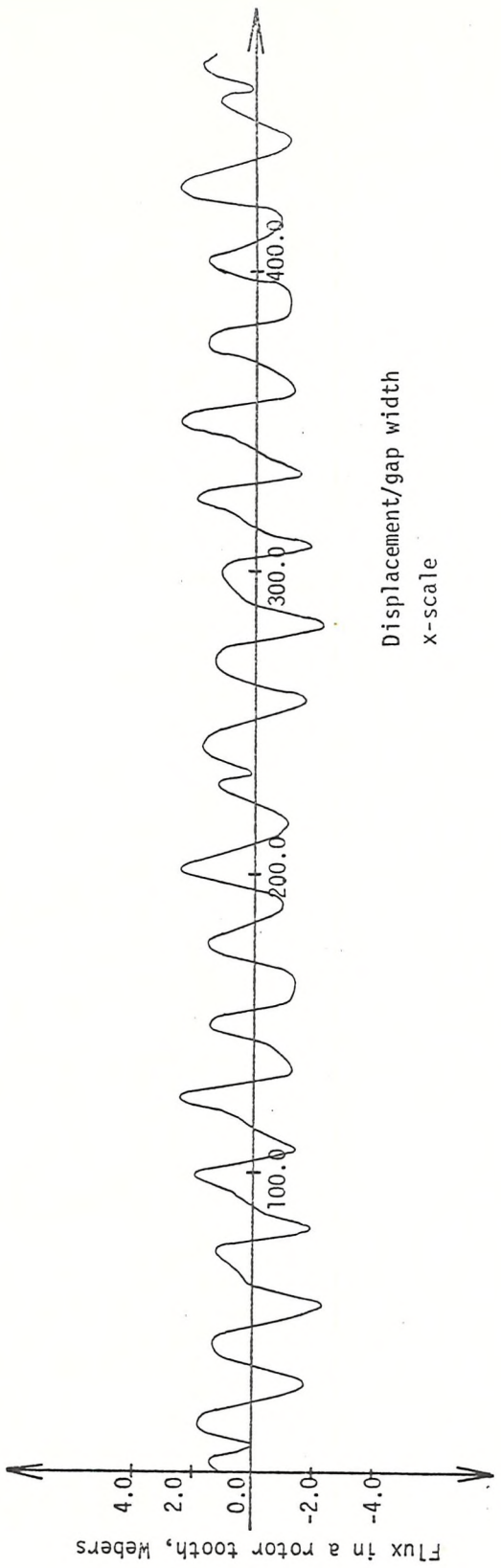

Figure 6.5 The tooth-ripple flux pulsations in a rotor tooth at a load level of 2.5 : 1

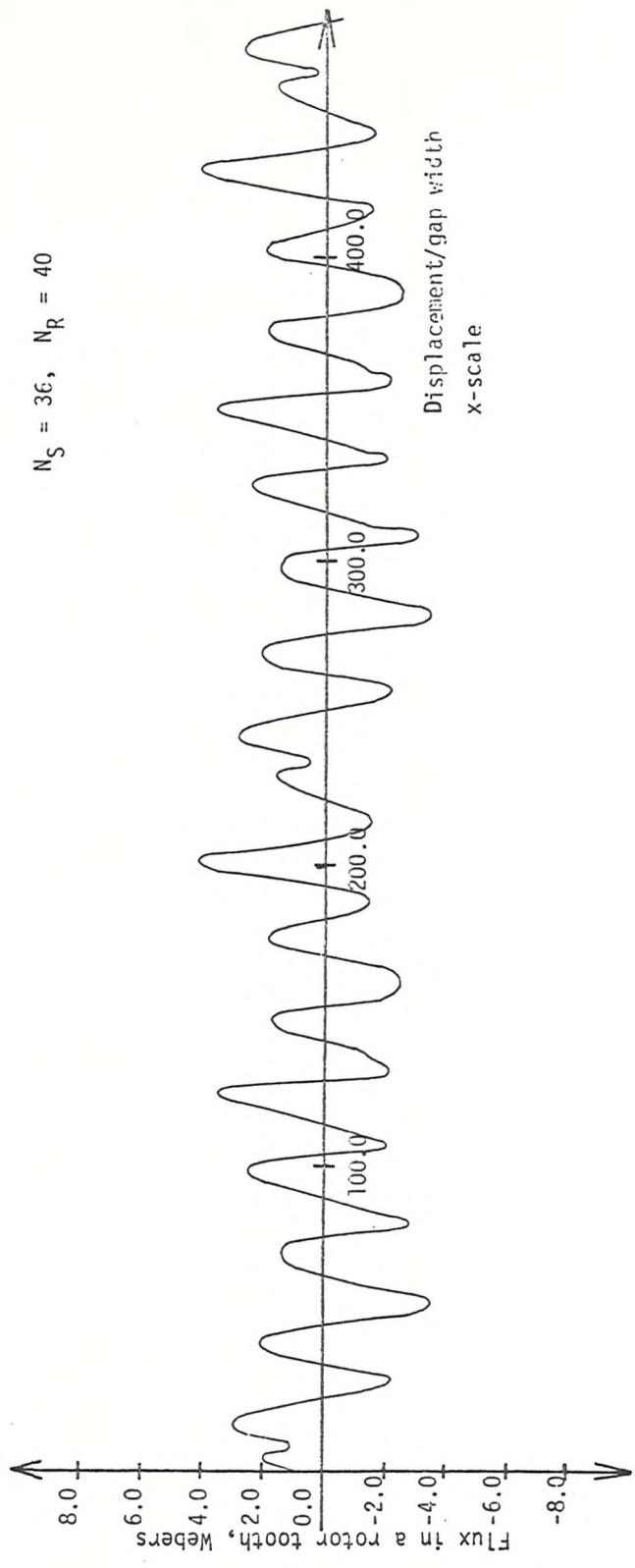

Figure 6.6 The tooth-ripple flux pulsations in a rotor tooth at a load level of 5 : 1

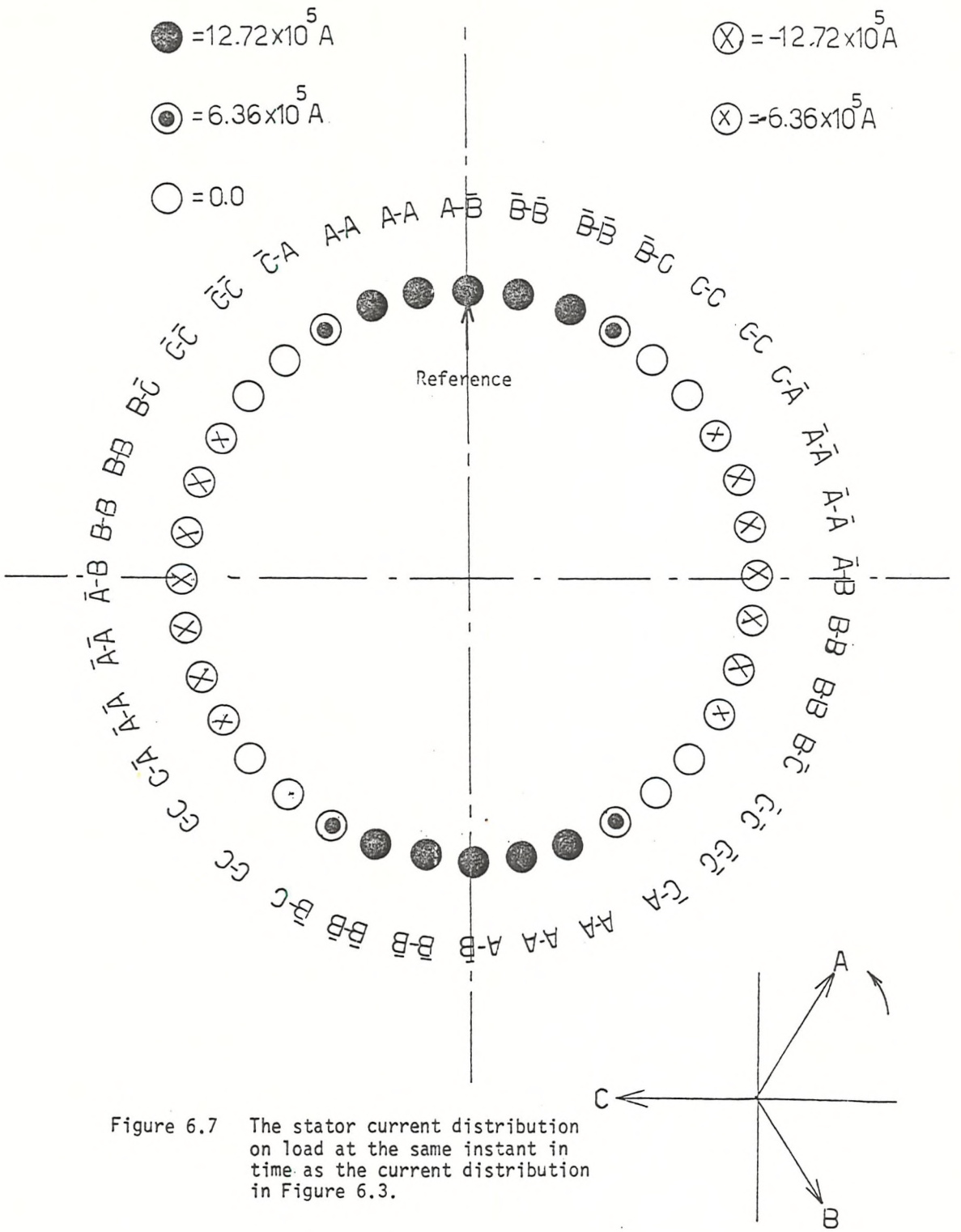

Figure 6.7 The stator current distribution on load at the same instant in time as the current distribution in Figure 6.3.

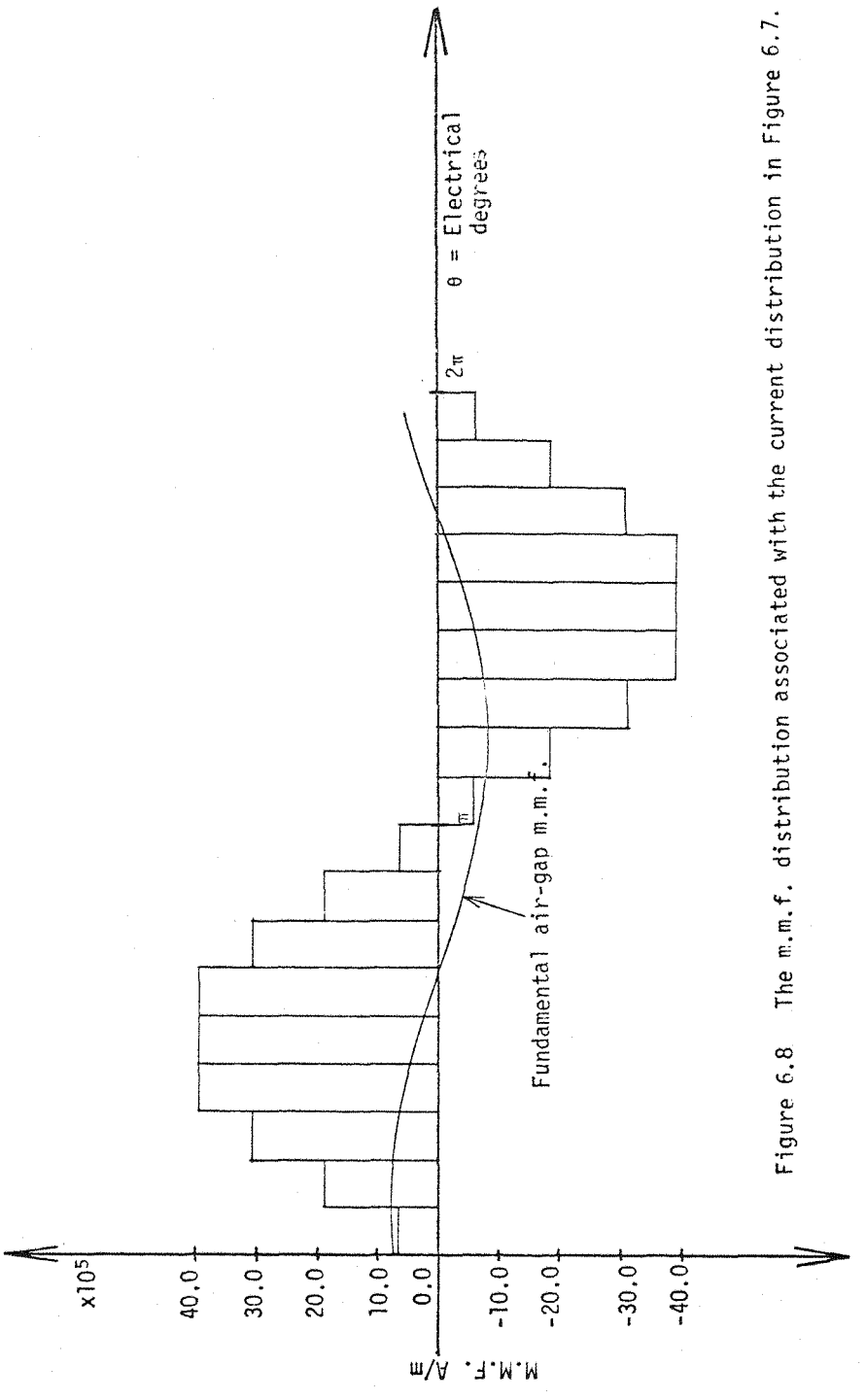

Figure 6.8 The m.m.f. distribution associated with the current distribution in Figure 6.7.

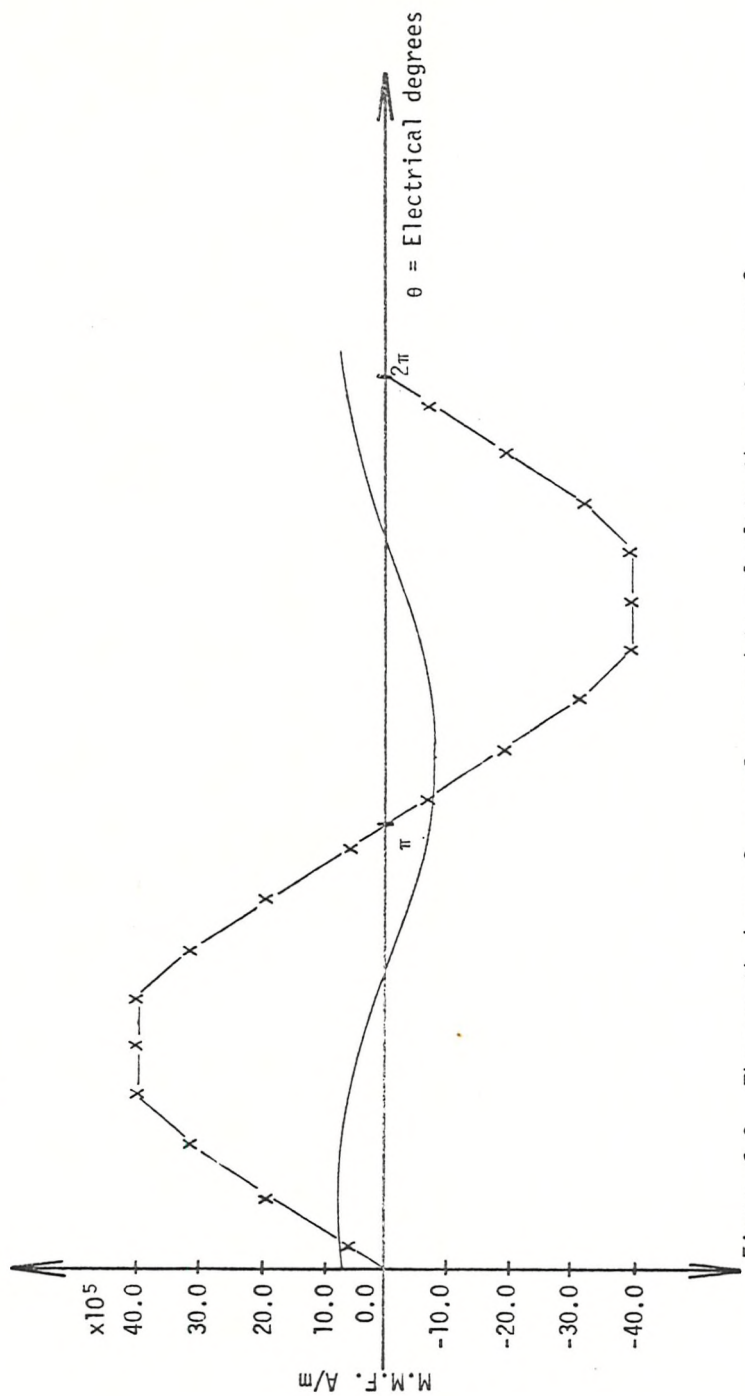

Figure 6.9 The smoothed m.m.f. waveform used to calculate the rotor m.m.f.

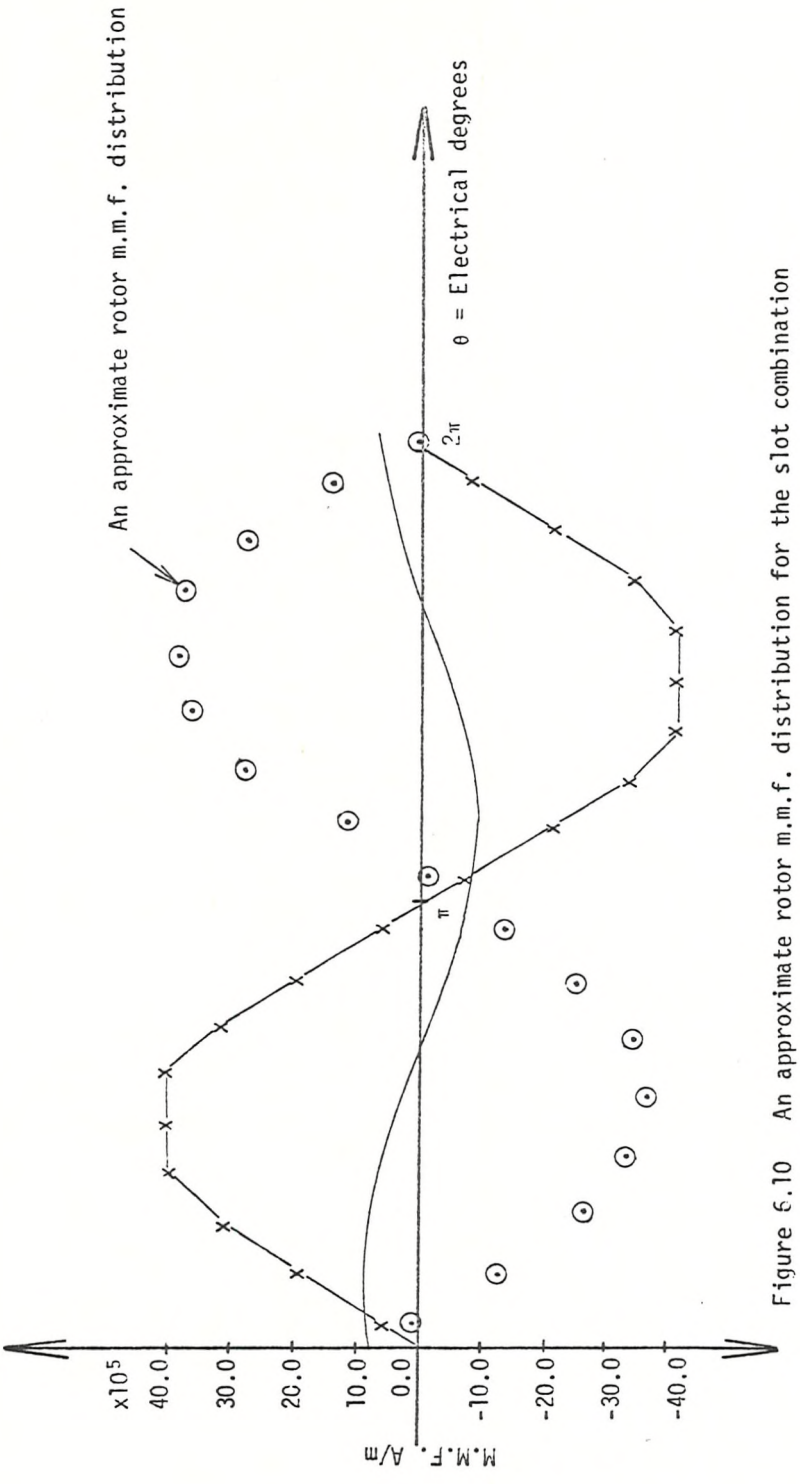

Figure 6.10 An approximate rotor m.m.f. distribution for the slot combination $N_S = 36$, $N_R = 32$, rotor displacement, d = 0.0

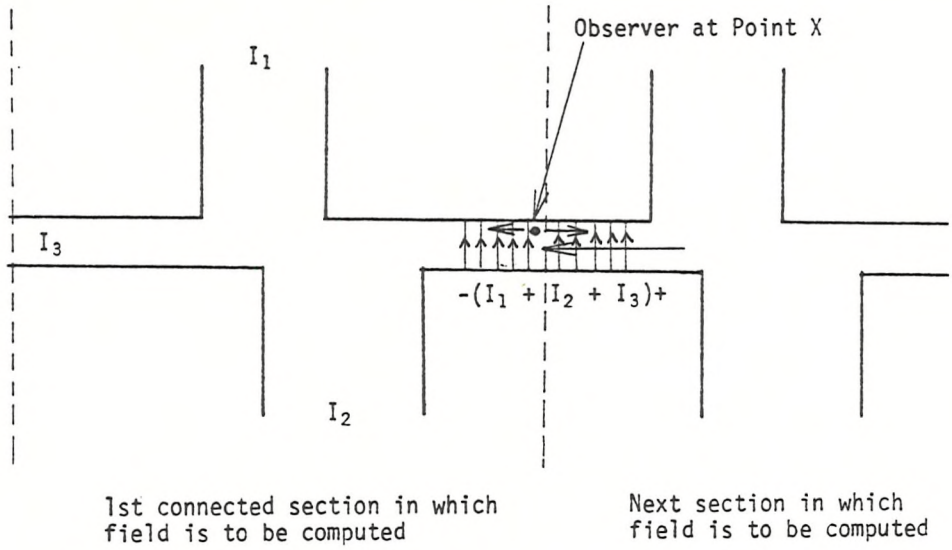

Figure 6.11 A section of the slotted air-gap boundary illustrating the two conditions discussed in Section 6.5.

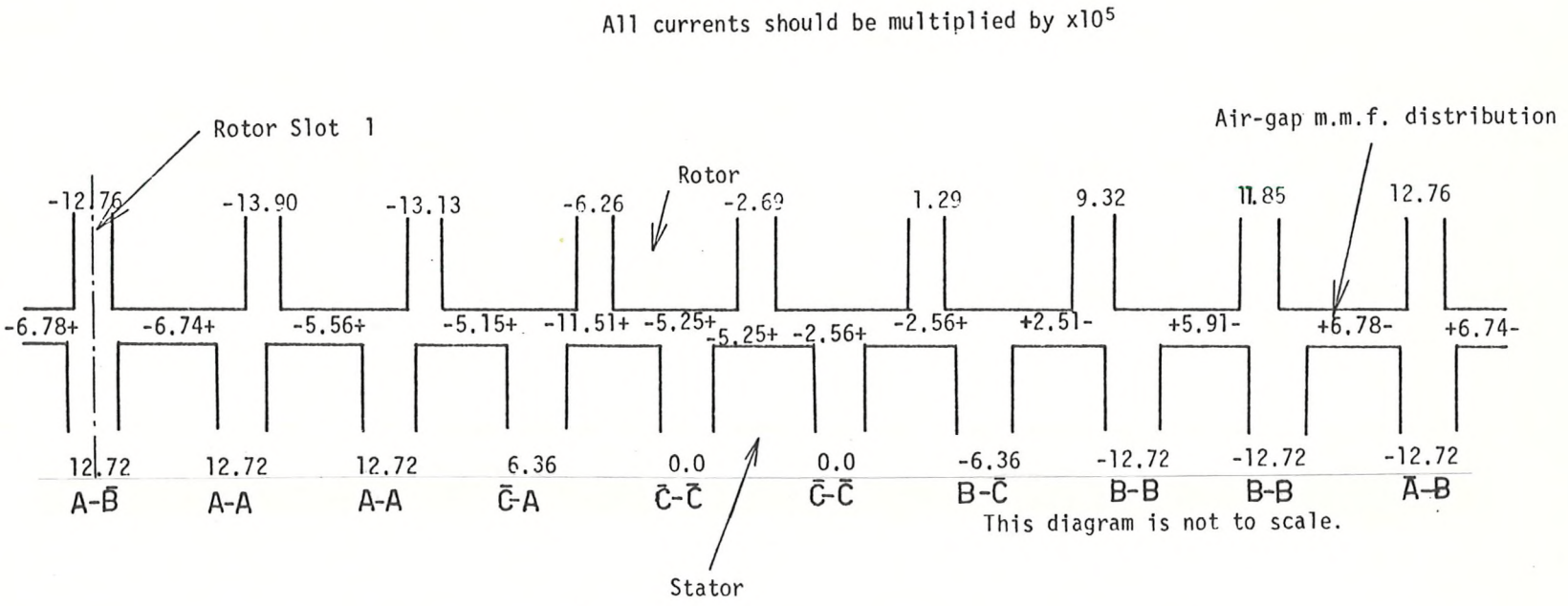

Figure 6.12 The complete stator and rotor current and air-gap m.m.f. distributions for the slot combination $N_S = 36$, $N_R = 32$, rotor displacement, d = 0.0

CHAPTER 7

AN EXAMINATION OF THE TOOTH-RIPPLE FLUX PULSATIONS ON LOAD

7. Introduction

7.1 Flux Distributions

7.2 The Tooth-Ripple Flux Pulsations in a Rotor Tooth

7.3 The Tooth-Ripple Flux Pulsations in Two Stator Teeth, One Contained Within and One at the End of a Phase Belt

7.4 Conclusions

7.5 References

7. Introduction

This is the first of three chapters which are concerned with the results obtained from the computation of the flux and force quantities, under load, with the ten slot combinations defined in the previous chapter. This chapter deals specifically with the tooth-ripple flux pulsations in the stator and rotor teeth.

In Section 7.1, it is shown that the instantaneous values of flux entering the stator and rotor teeth can be represented as a distribution of stator fluxes and a distribution of rotor fluxes. It is shown in Section 7.2 how the time history of the tooth-ripple flux in a rotor tooth can be obtained by computing the rotor flux distributions at a number of positions of the rotor within a rotor slot pitch. In the same section, the important defining quantity is shown to be the peak to peak value of the largest flux pulsation expressed as a fraction of the peak value of the fundamental flux wave. A simple equation is obtained relating this quantity to the slot pitch difference.

In a similar manner, it is shown in Section 7.3 how the time history of the tooth-ripple flux in a stator tooth can be obtained by computing the stator flux distributionsat a number of positions of the rotor within a rotor slot pitch. The position of the tooth relative to its phase belt is taken into account. The important defining quantity is again the peak to peak value of the largest flux pulsation as a fraction of the peak value of the fundamental flux wave. As before, this quantity is related to the slot pitch difference by a simple equation. The two equations defined in Sections 7.2 and 7.3 are compared and conditions are found under which the flux pulsations in a rotor and a stator tooth are minimal.

The important conclusions from the work on tooth-ripple flux pulsations are summarised in Section 7.4.

7.1 Flux Distributions

The analysis described in the previous two chapters has been used to calculate the instantaneous values of flux in the stator and rotor teeth for the ten slot cominations shown in Table 6.1. It is convenient, at any instant, to represent the fluxes in the stator and rotor teeth in the form of a distribution of stator fluxes and a distribution of rotor fluxes. To do this, the flux in any tooth is represented as a point value located at the centre of that tooth. The stator and rotor flux distributions are, therefore, a plot of the fluxes in the teeth against the position of the teeth centres relative to some arbitrary origin. Clearly, these two distributions are periodic in a double pole pitch. The origin is normally taken to be the centre of the tooth on the opposite side of the air-gap which lies closest to the beginning of the pole. Typical stator and rotor flux distributions are shown in Figure 7.1.

In this form, the flux distributions can be used to obtain the rotor and stator tooth-ripple flux pulsations, as is described shortly. The peak value of the fundamental flux wave associated with any flux distribution can be found to a close approximation by joining the flux points by straight lines and using Fourier analysis.

7.2 The Tooth-Ripple Flux Pulsations in a Rotor Tooth

To obtain the flux pulsations in a rotor tooth, it is necessary to compute the rotor flux distributions at a number of positions within a displacement of one rotor slot pitch. In each position, the peak value of the fundamental flux wave associated with the flux distribution is calculated. Since a squirrel-cage rotor has negligible phase belt harmonics[7.1], the value of the tooth-ripple flux in a tooth, in any position, can be obtained by subtracting the value of the fundamental

flux wave at the point corresponding to the tooth centre from the computed flux value. The overall shape of the flux pulsations in each of the rotor teeth, over a displacement of a rotor slot pitch, can be obtained by computing the tooth-ripple fluxes in all the teeth in each rotor position. However, under quasistatic field conditions, the field distribution at any point in the air-gap region is the same after a displacement of exactly one rotor slot pitch. Consider the flux and force pulsations in rotor tooth 1 after an initial displacement of one rotor slot pitch from an arbitrary origin. This origin is normally taken as the centre of the stator slot containing the coil side A-$\overline{B}$. If the rotor is displaced through another rotor slot pitch, rotor tooth 1 will experience the same field distributions and, therfore, the same flux and force pulsations as rotor tooth 2 for the previous rotor displacement. The same argument can be applied to the remaining rotor teeth. Therefore, it is possible by computing the flux pulsations in all the rotor teeth over a displacement of a rotor slot pitch to obtain the time history of the tooth-ripple flux in a rotor tooth as the rotor is displaced through a double pole pitch. Furthermore, as the fundamental air-gap flux wave is stationary, the rotor tooth experiences every part of this field as it is displaced through a double pole pitch. This is an important concept because it allows one to use the information gained from a few rotor flux distributions or 'snapshots' of the air-gap field to obtain the complete time history of the tooth-ripple flux pulsations in a tooth under quasistatic field conditions.

The time histories of the flux pulsations in a rotor tooth are shown in Figures 7.2 - 7.11 for each of the ten slot combinations. The origin of each of these graphs corresponds with the stator tooth centre which lies closest to the centre of the pole. Any point on

the horizontal axis of the ten graphs represents the displacement of the rotor tooth centre from this origin expressed as a ratio of the gap width. The large flux values are due, of course, to the large slot currents and air-gap m.m.f. values. It can be seen that the rotor tooth fluxes follow similar trends, and when the rotor tooth - ripple flux is significantly large the waveform is particularly clear. At any instant, the tooth-ripple fluxes lie on a near sine-wave, periodic in a stator slot pitch and modulated by the fundamental gap m.m.f.

The tooth-ripple flux can, of course, be harmonically analysed although this involves a considerable amount of laborious processing. In practice, however, it is the total flux and force pulsations, and particularly their amplitudes, that are of importance. Therefore, only the peak to peak values of the flux pulsations are considered here. In treating the problem in this manner one is not neglecting the harmonic content of the tooth-ripple flux, for this is included in the peak to peak value.

The important defining quantity for the flux amplitude is the ratio of the peak to peak value of the largest of the flux pulsations relative to the peak value of the fundamental flux entering a tooth. The peak to peak value of the largest flux pulsation is taken because at this point the associated losses are greatest. The peak value of the fundamental flux is, in fact, an average of all the peak values of the fundamental flux obtained at each position in which the rotor flux distribution is computed. This quantity is included to remove the obvious effect that a wider tooth receives more flux.

This flux ratio is plotted in Figure 7.12 against the difference in slot pitches. The computed points show a very clear trend as $(P_R/g - P_S/g)$ varies. When P_R/g is less than P_S/g, that is, the rotor slot number is greater than thirty-six (rotor overslotted), the rotor

tooth flux pulsations steadily increase with an increase in slot pitch difference. When P_R/g is greater than P_S/g, that is, the rotor slot number is less than thirty-six (rotor underslotted), the flux pulsations into the rotor teeth are small and hardly vary when viewed as a fraction of the fundamental.

The case where $(P_R/g - P_S/g) = 12.5$, or $N_S = 36$, $N_R = 24$, is interesting because it suggests that the flux pulsations are again increasing (see Figure 7.12). This trend reveals a limitation in the conformal transformation model, for in this case there is insufficient overlap of the stator and rotor teeth in some sections for the gap flux to be almost uniform. The flux ratio associated with this slot combination, therefore, can only be regarded as approximately correct. The slot combination $N_S = 36$, $N_R = 24$ would not be used in practice because of cogging problems[7.2]. This slot combination serves as a limiting case when $(P_R/g - P_S/g)$ has a large positive value.

Simple functions have been fitted to the graph of the amplitude of the tooth flux pulsation as a fraction of the peak value of the fundamental flux against the difference in slot pitches. It is seen (see Figure 7.12) that the functions are a good fit to the computed values and are as follows:

$$\frac{\hat{\Phi}_{TP}}{\hat{\Phi}_{FP}} = -0.068 \cdot (P_R/g - P_S/g) + 0.21 \qquad \text{if } P_S/g > P_R/g$$

and

$$\frac{\hat{\Phi}_{TP}}{\hat{\Phi}_{FP}} = 0.21 \qquad \text{if } P_R/g \geq P_S/g \qquad (7.1)$$

7.3 The Tooth-Ripple Flux Pulsations in Two Stator Teeth, One Contained Within and One at the End of a Phase Belt

To obtain the tooth-ripple flux pulsations in a stator tooth, it is necessary to compute the stator flux distributions at a number of positions within a rotor slot pitch. In each position, the peak value of the fundamental flux wave associated with the flux distribution is calculated. Unlike a squirrel cage, a stator winding has phase belt m.m.f. and flux harmonics. However, these phase belt flux harmonics cannot be directly calculated from the flux distributions because there is an insufficient number of flux values in the distribution to obtain them to a sufficiently high accuracy. It is assumed, therefore, that the phase belt flux harmonics (which have wavelengths that are simple fractions of a phase belt length) are proportional to the phase belt m.m.f. harmonics[7.3], that is,

$$\hat{\Phi}_n = \frac{K_{dn}\, K_{pn}}{n\, K_d\, K_p}\, \hat{\Phi}_{Fund} \qquad (7.2)$$

where n is the harmonic order, K_{dn} and K_{pn} are the distribution and pitch factors associated with the n^{th} m.m.f. harmonic and K_d and K_p are the distribution and pitch factors associated with the fundamental. For the stator winding shown in Figure 6.3, the 5^{th}, 7^{th}, 11^{th} and 13^{th} m.m.f. harmonics are approximately 3%, 1%, 0.6% and 1% of the fundamental respectively. These harmonic flux waves are added to the fundamental flux wave to give the flux waveform associated with the fundamental m.m.f. wave and the phase belt m.m.f. harmonics. In each rotor position, the value of the tooth-ripple flux is obtained by subtracting the value of the combined stator flux waveform, at the point corresponding to the tooth centre, from the computed flux value. The flux pulsations in the stator, over a displacement of a rotor slot pitch,

are obtained by calculating the tooth-ripple flux in all the teeth in each position. In practice, it was found that as each additional harmonic flux wave was added to the fundamental flux wave the values of the tooth-ripple fluxes tends to constant values. It was only necessary, therefore, to add the flux waves associated with the 5^{th} and 7^{th} m.m.f. harmonics to obtain an accurate value of the tooth-ripple fluxes.

Unlike the rotor, the pulsations in the stator teeth cannot be combined to give the time history of the tooth-ripple flux in a single tooth. The reason for this is explained by Binns and Schmid[7.4] in their paper on harmonic fields in induction motors. In discussing air-gap field harmonics, it is often assumed that the same travelling field is experienced by all the stator teeth regardless of their position relative to the phase belts. Leakage fluxes produce addition effects dependent on the position in the phase belt and are superimposed on the travelling field. The result is that the sidebands (defined in Chapter 1) have different amplitudes for certain teeth. It should be noted that the leakage flux has pulsating components and that these are indistinguishable in frequency from the travelling field components. The authors show experimentally the difference between the amplitudes of the sidebands associated with a tooth at the end of a phase belt (this tooth will be called T_{end}) and one contained within a phase belt (this tooth will be called T_{middle}). On the stator frame, shown in Figure 6.3, both types of teeth are present. Therefore, the information obtained from computing the tooth-ripple flux pulsations, within a rotor slot pitch, can only be used to obtain the partial time histories of the flux in the two types of teeth. On the stator frame, in Figure 6.3, there are twelve teeth at the end of the phase belts and six contained within the phase belts over a double pole pitch. The twelve pulsations associated with the teeth T_{end} can be

viewed as the flux pulsations in a single tooth at the end of a phase belt at different times as the tooth experiences different parts of the travelling field. Similarly, the six flux pulsations associated with the teeth T_{middle} can be viewed as the flux pulsations in a single tooth contained within a phase belt at different times as it experiences different parts of the travelling field. Whilst it is not possible to obtain a complete time history of the flux in both types of teeth, there is sufficient information to obtain the relationships between the amplitude of the flux pulsations relative to the peak value of the fundamental flux and the slot pitch difference.

The flux pulsations in a tooth at the end of a phase belt are shown in Figures 7.13 to 7.19 for the rotor slot numbers 24, 28, 30, 32, 36, 42 and 48. Similarly, the flux pulsations in a tooth contained within a phase belt are shown in Figures 7.20 to 7.26 for the same rotor slot numbers. The origin of these graphs corresponds with the centre of the rotor tooth which lies closest to the centre of the pole. Both sets of stator tooth-ripple fluxes lie on a near sine wave modulated by the fundamental gap m.m.f.

As in the case of the rotor, the important defining quantity is the ratio of the peak to peak value of the largest flux pulsation relative to the peak value of the fundamental flux. For each slot combination, this ratio is obtained separately for the two types of teeth, and plotted against the difference in slot pitches (see Figure 7.27). From this figure it is clear that the position of a stator tooth relative to its phase belt is of only slight significance. The two flux ratios reveal the same trend, that when the stator slot pitch is smaller than the rotor slot pitch (rotor underslotted) the stator flux pulsations steadily increase with an increase in the difference in slot pitches.

When the stator slot pitch is greater than the rotor slot pitch (rotor overslotted), the flux pulsations into the stator are small and hardly vary when viewed as a fraction of the fundamental flux. This is, of course, the exact opposite of what occurs on the rotor.

Functions have been fitted to the computed values in Figure 7.27 and are given by

$$\frac{\Phi_{TP}}{\Phi_{FP}} = -0.068.(P_S/g - P_R/g) + 0.10 \qquad \text{if } P_R/g > P_S/g$$

and

$$\frac{\Phi_{TP}}{\Phi_{FP}} = 0.10 \qquad \text{if } P_R/g \geq P_S/g \quad (7.3)$$

It is apparent from equations (7.1) and (7.3) that the stator and rotor flux pulsations cannot be entirely eliminated. It is also apparent that the rotor and stator tooth flux pulsations obey equations of similar form except that the constant terms differ. It is clear that the applied flux pulsations for a rotor tooth, particularly when $P_S/g > P_R/g$, are greater than that for a stator tooth having the same slot pitch ratio (when $P_R/g > P_S/g$). It is also evident that the condition for minimising stator tooth flux pulsations ($P_S/g > P_R/g$) are incompatible with those for minimising rotor flux pulsations ($P_R/g > P_S/g$). The pulsations in one of the two members inevitably become large if the difference in slot numbersbecomes too great.

7.4 Conclusions

The relationship between slot combination and the peak to peak amplitude of the flux pulsations into the stator and rotor teeth on load have been examined. The following conclusions emerge:

(i) Stator and rotor tooth flux pulsations obey equations of similar form.

(ii) The criteria for minimising stator and rotor flux pulsations on load are incompatible.

(iii) Tooth losses inevitably become large, but in one member only, if the slot number difference is very large.

(iv) Under no-load conditions, Binns and Rowlands-Rees[7.5] determined that the tooth flux pulsations can be minimised by avoiding an excessive difference in slot pitches. The authors suggest that the ratio of pitch should typically lie in the range 10-30% of the smaller. Therefore, the criterion for minimising tooth flux pulsations on load is similar to that for no-load operation.

7.5 References

7.1 ALGER, P. L. : 'The nature of induction machines', (Gordon and Breach, 1965).

7.2 HELLER, B and HAMATA, V. : 'Harmonic Field Effects in Induction Machines' (Elsevier Scientific Pulbishing Company, 1977).

7.3 LIWSCHITZ, M. M. : 'Field harmonics in induction motors', Trans. Am. Inst. Elec. Eng., 1942, 61, pp.797-803.

7.4 BINNS, K. J. and SCHMID, E. : 'Some concepts involved in the analysis of the magnetic field in cage induction machines', Proc. I.E.E., 1975, 122, (2), pp.169-175.

7.5 BINNS, K. J. and ROWLANDS-REES, G. : 'Main-flux pulsations and tangential tooth-ripple forces in induction motors', Proc. I.E.E., 1975, 122, (3), pp.273-277.

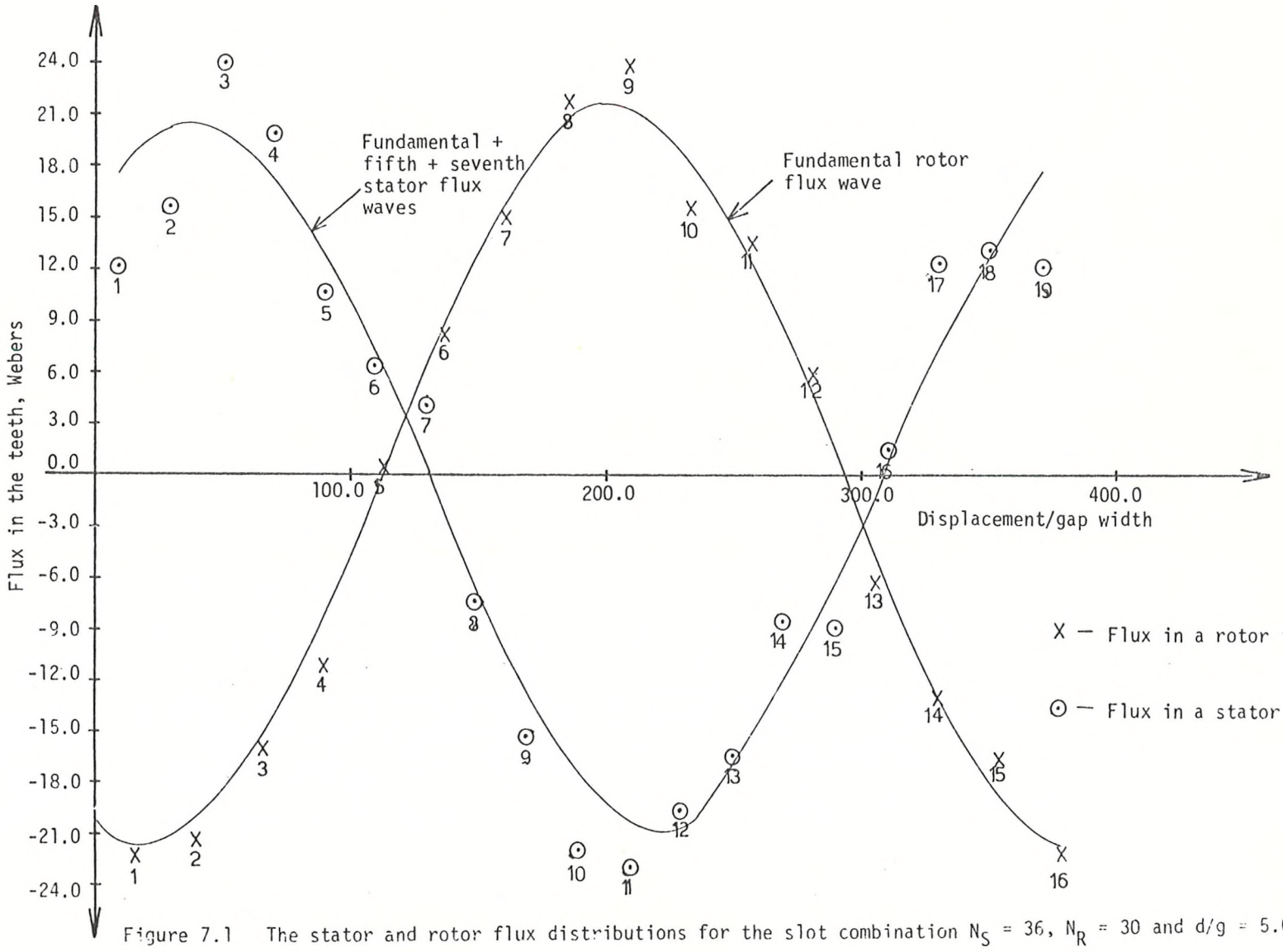

Figure 7.1 The stator and rotor flux distributions for the slot combination N_S = 36, N_R = 30 and d/g = 5.0

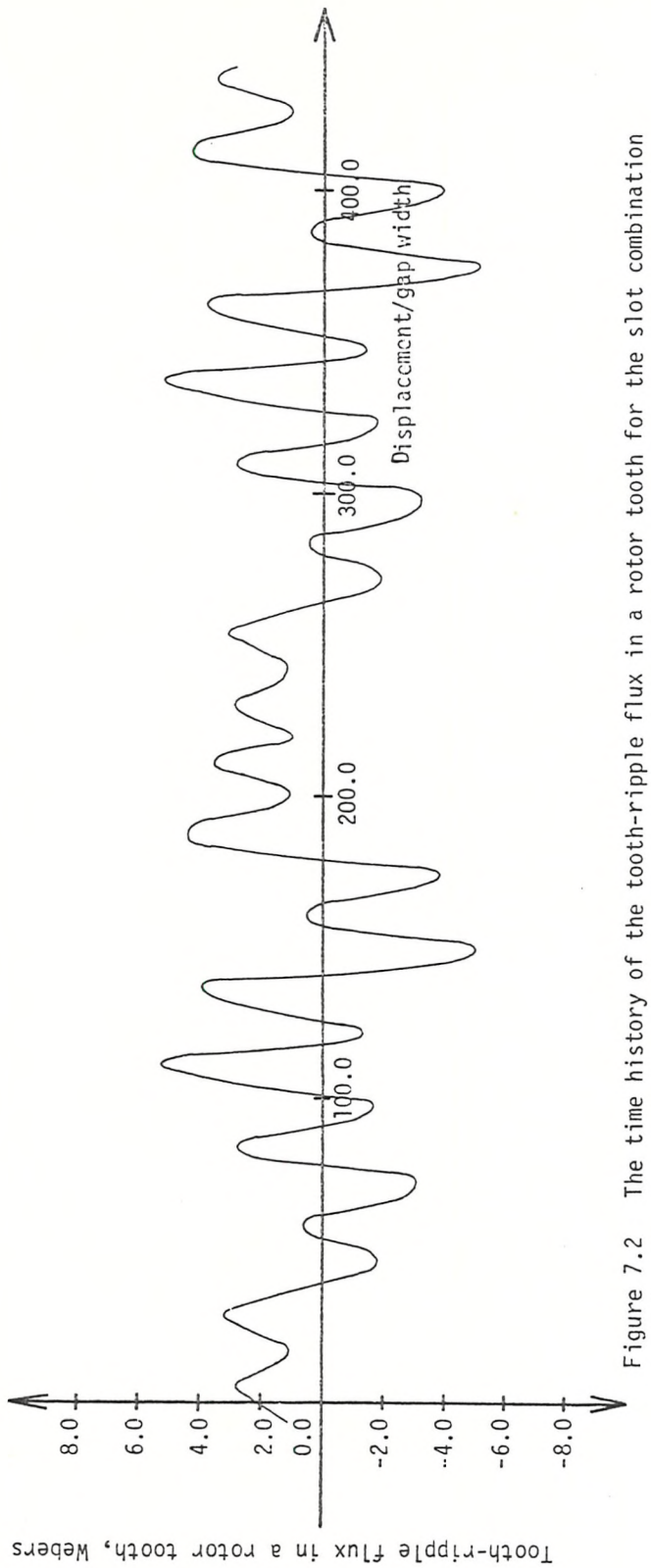

Figure 7.2 The time history of the tooth-ripple flux in a rotor tooth for the slot combination $N_S = 36$, $N_R = 24$

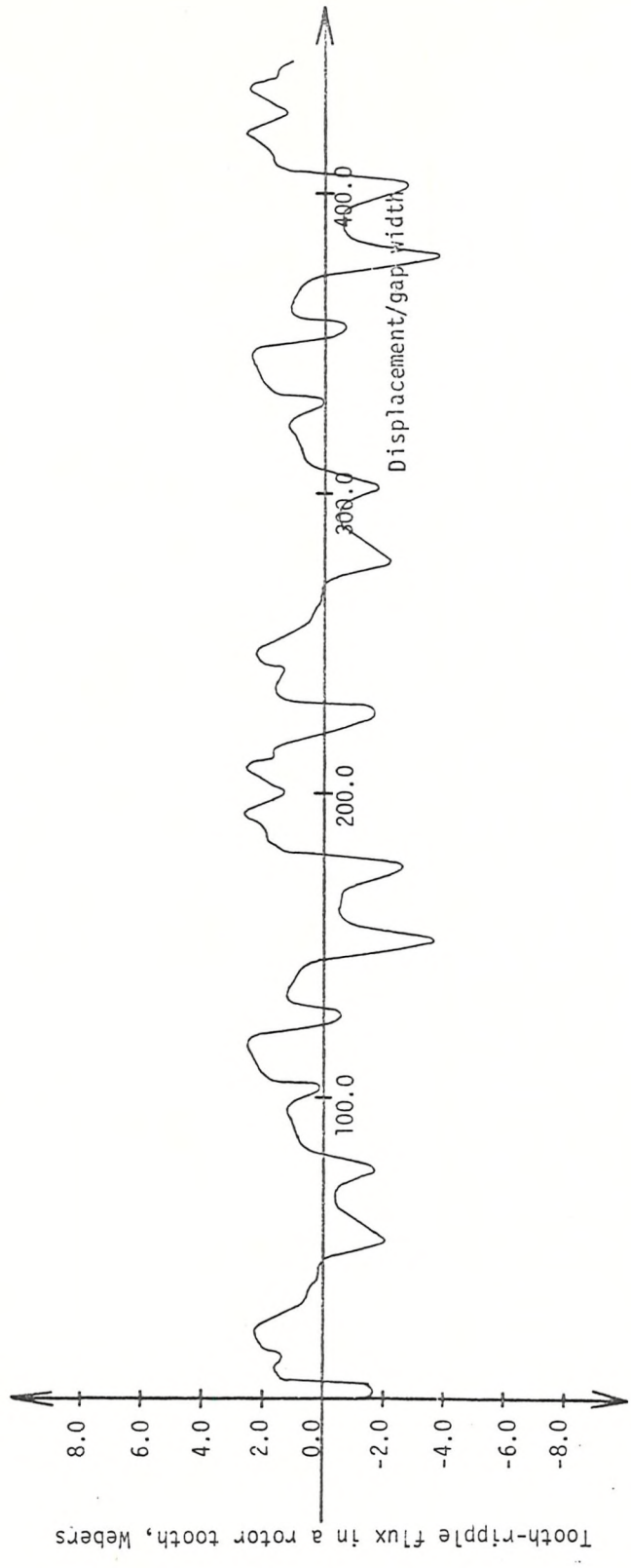

Figure 7.3 The time history of the tooth-ripple flux in a rotor tooth for the slot combination $N_S = 36$, $N_R = 28$

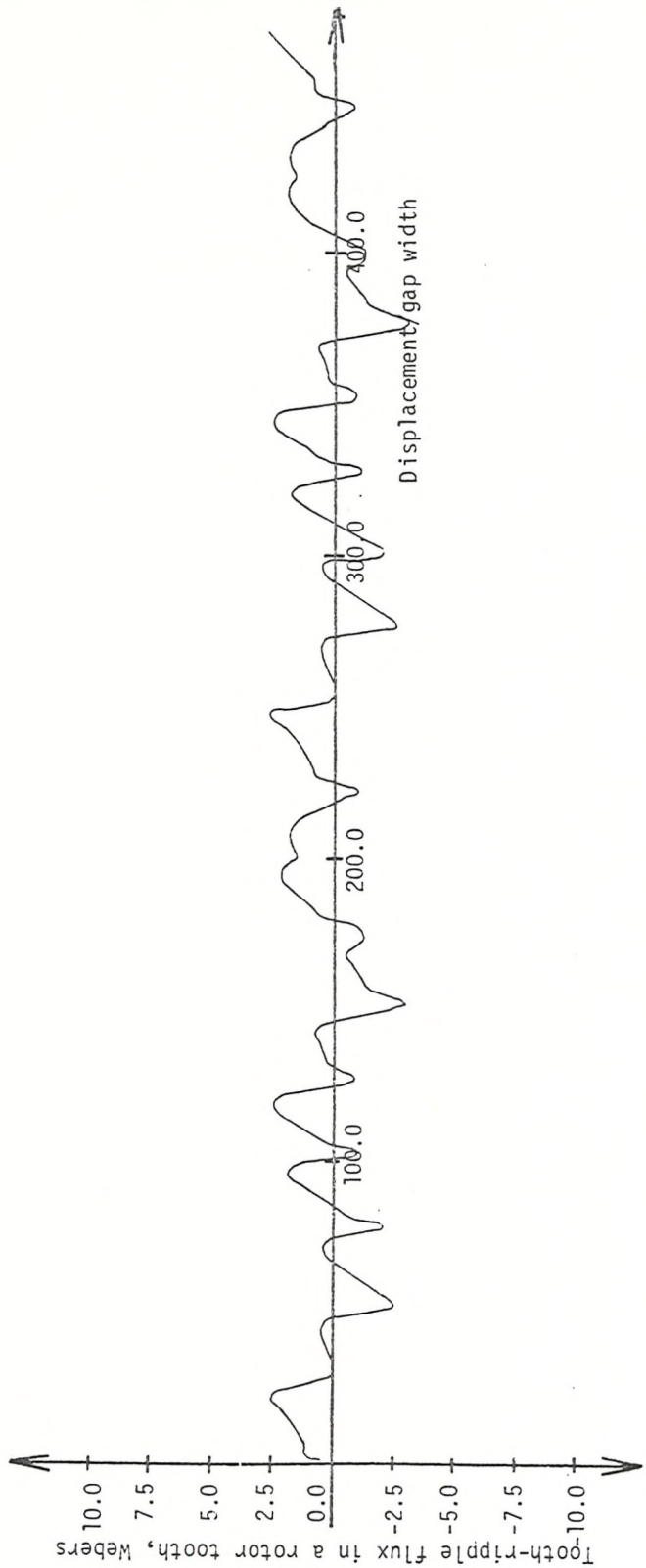

Figure 7.4 The time history of the tooth-ripple flux in a rotor tooth for the slot combination $N_S = 36$, $N_R = 30$

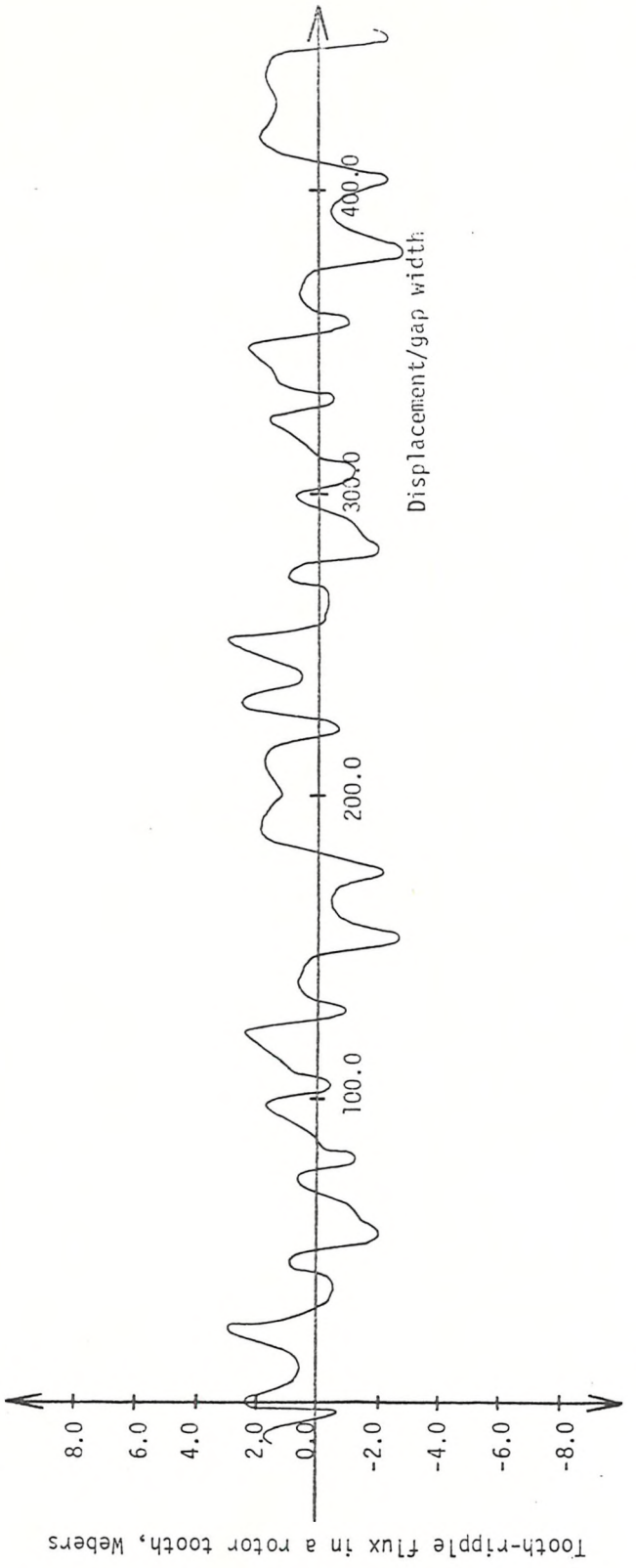

Figure 7.5 The time history of the tooth-ripple flux in a rotor tooth for the slot combination $N_S = 36$, $N_R = 32$

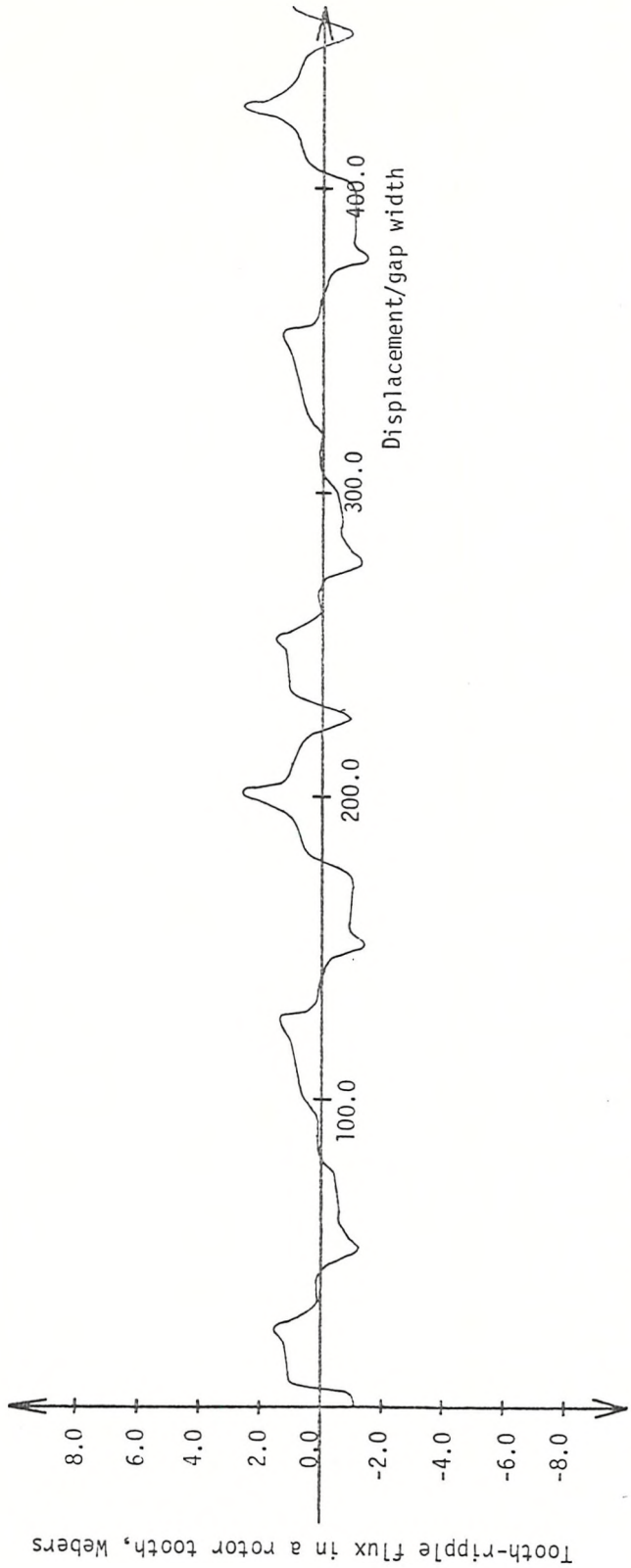

Figure 7.6 The time history of the tooth-ripple flux in a rotor tooth for the slot combination $N_S = 36$, $N_R = 36$

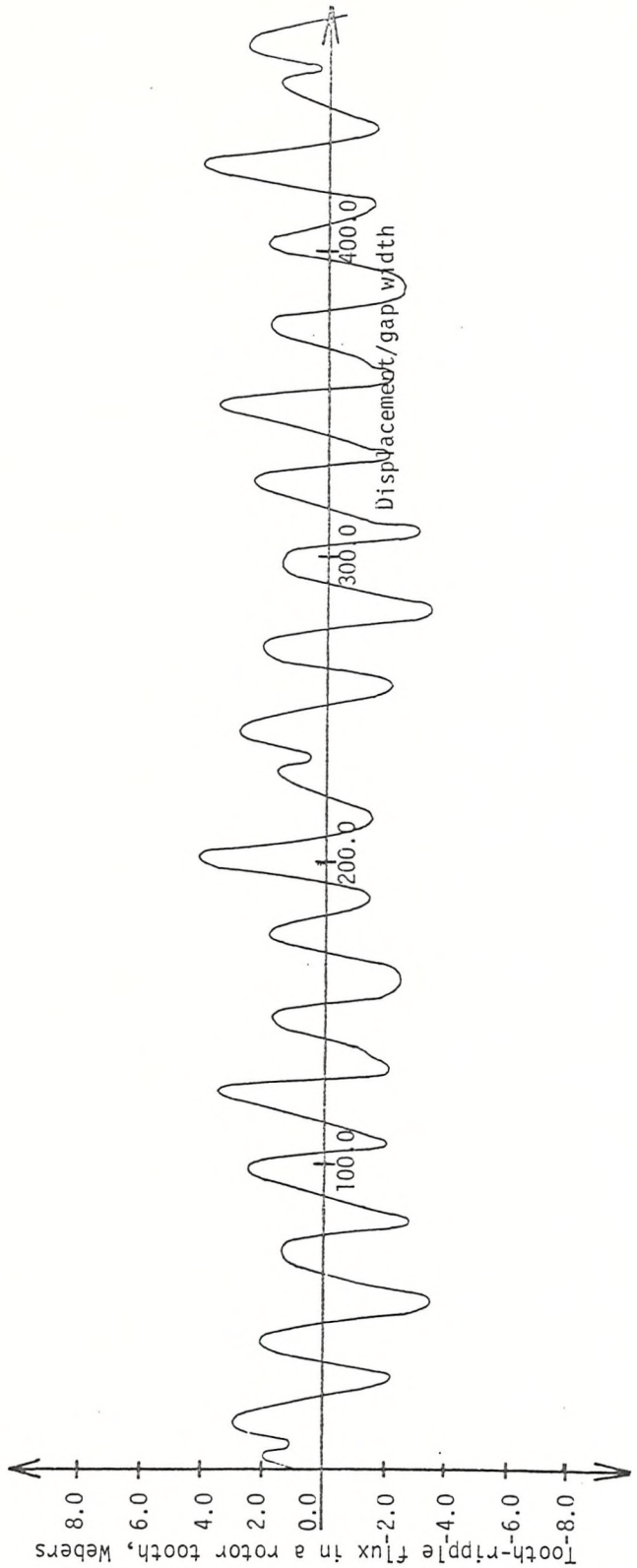

Figure 7.7 The time history of the tooth-ripple flux in a rotor tooth for the slot combination $N_S = 36$, $N_R = 40$

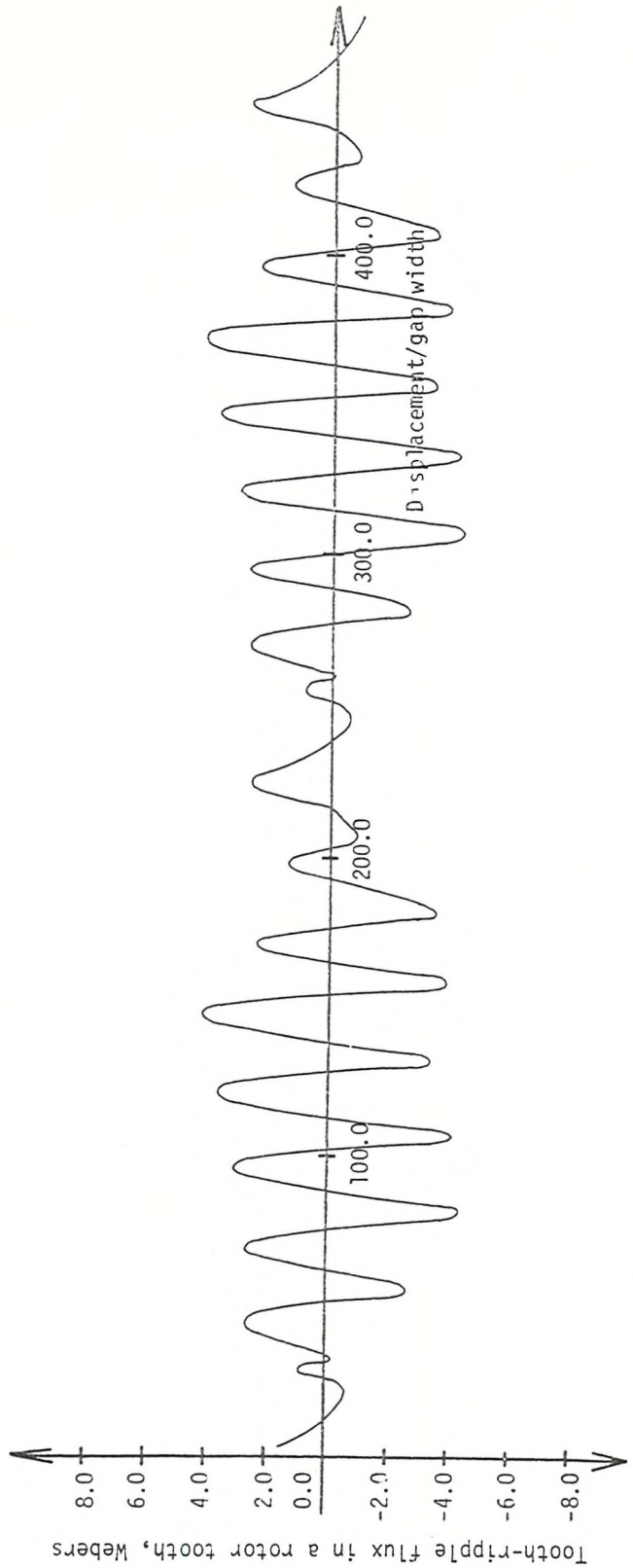

Figure 7.8 The time history of the tooth-ripple flux in a rotor tooth for the slot combination $N_S = 36$, $N_R = 42$

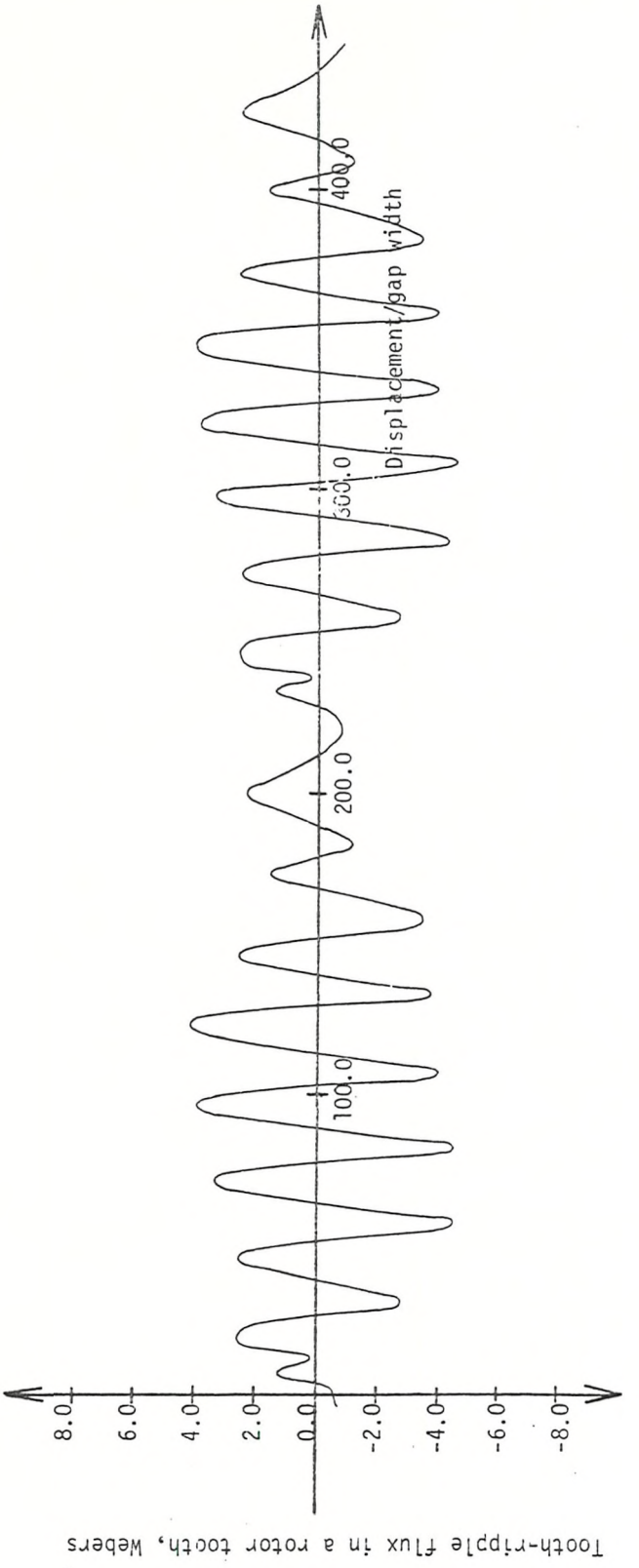

Figure 7.9 The time history of the tooth-ripple flux in a rotor tooth for the slot combination $N_S = 36$, $N_R = 44$

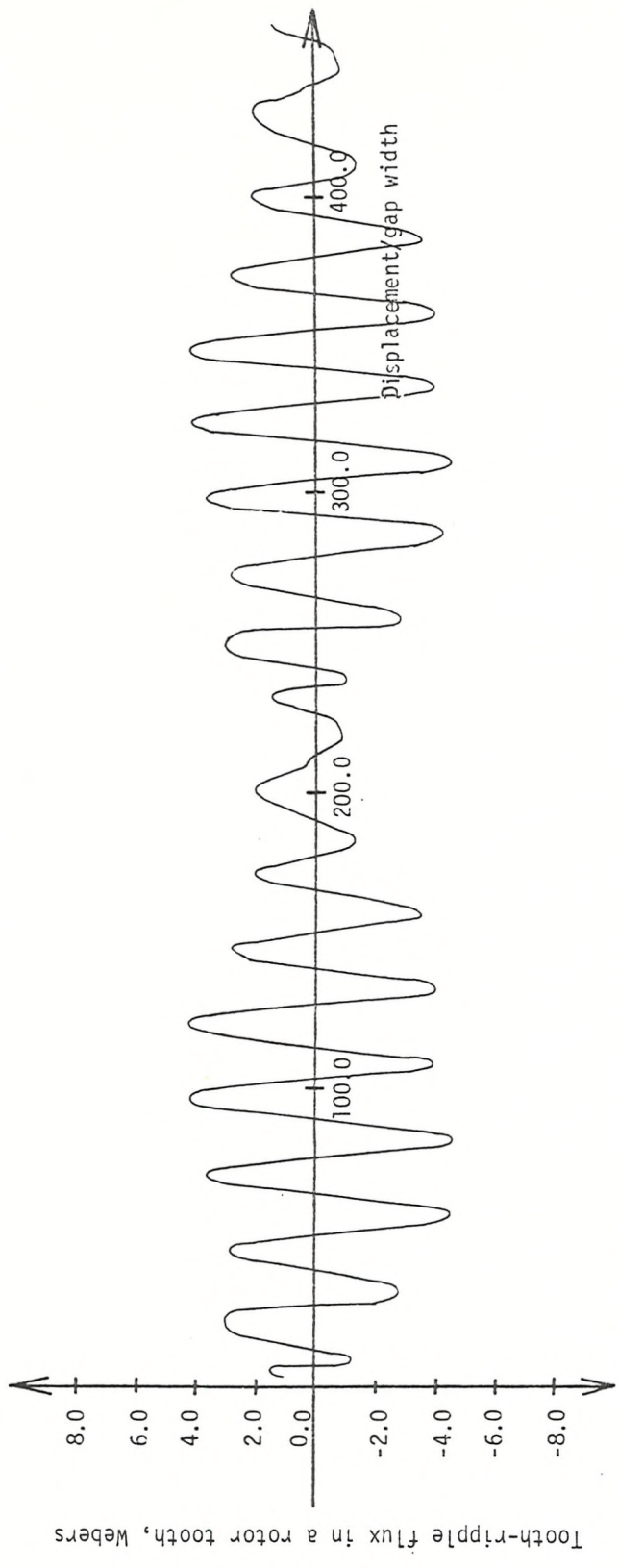

Figure 7.10 The time history of the tooth-ripple flux in a rotor tooth for the slot combination $N_S = 36$, $N_R = 48$

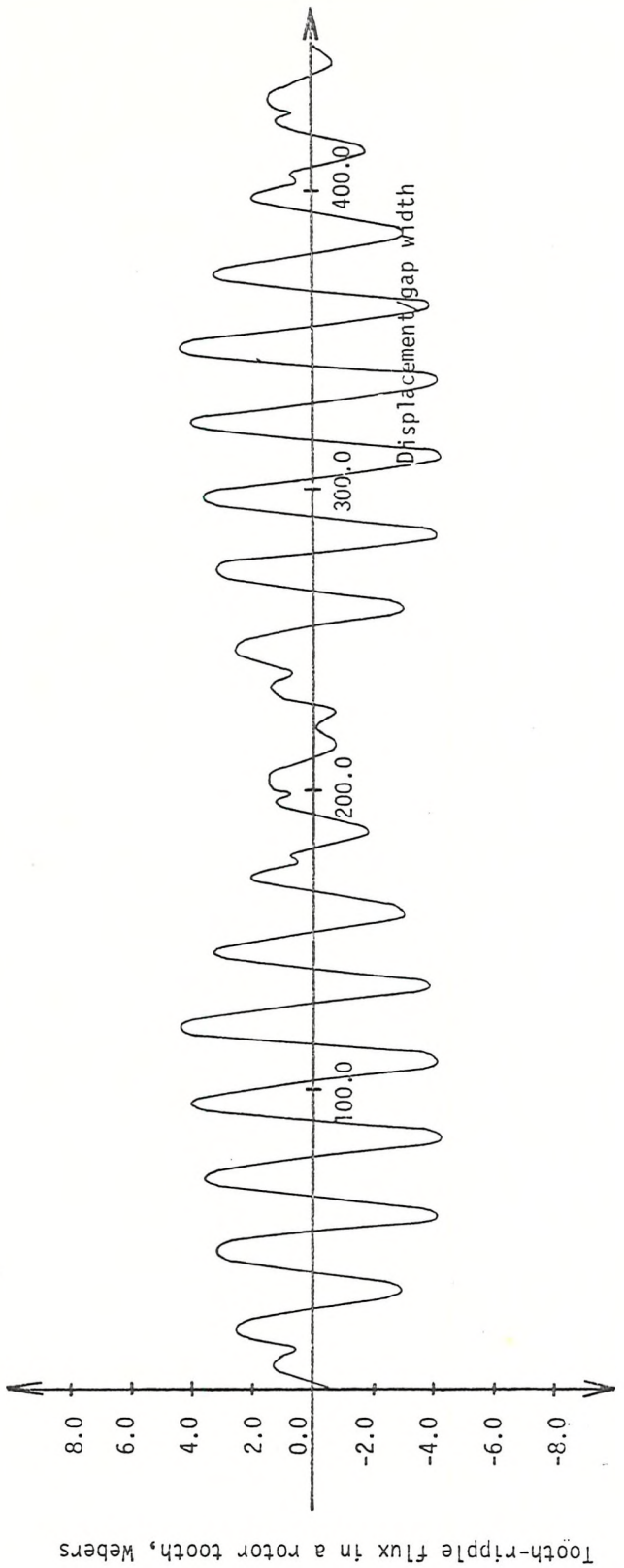

Figure 7.11 The time history of the tooth-ripple flux in a rotor tooth for the slot combination $N_S = 36$, $N_R = 60$

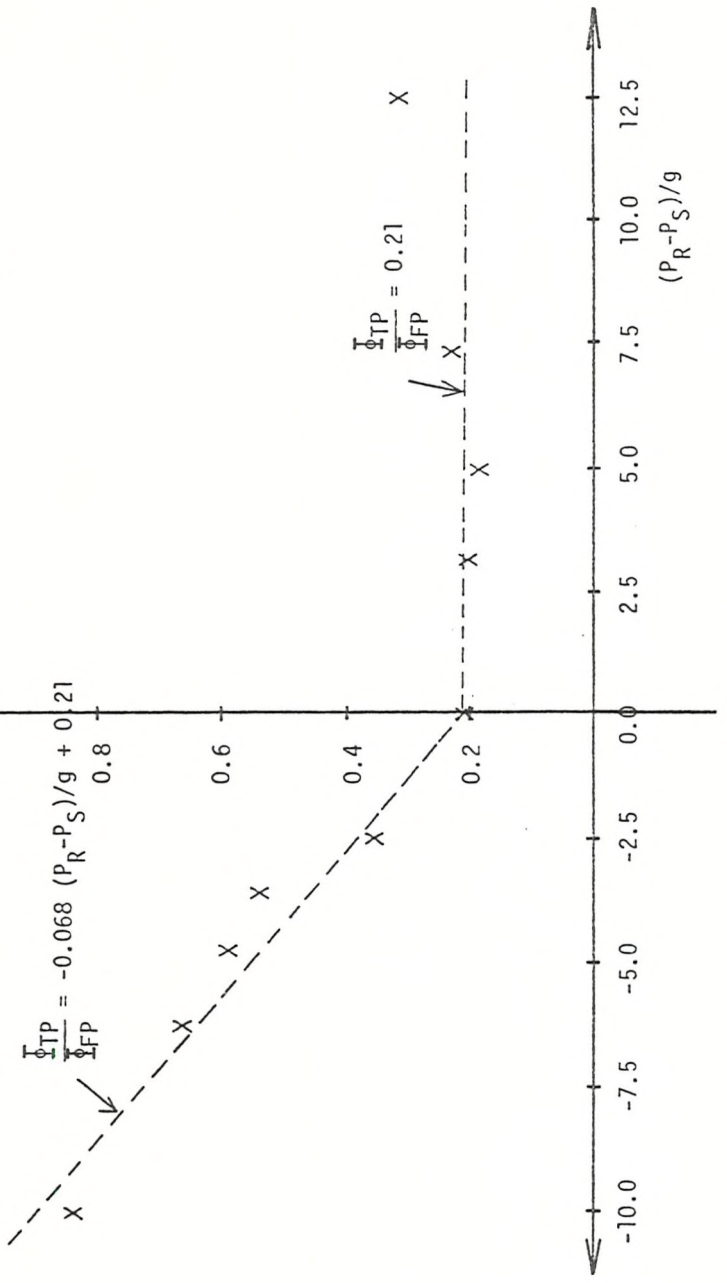

Figure 7.12 The variation in the peak to peak value of the largest flux pulsation as a fraction of the fundamental flux with the difference in slot pitches for the rotor.

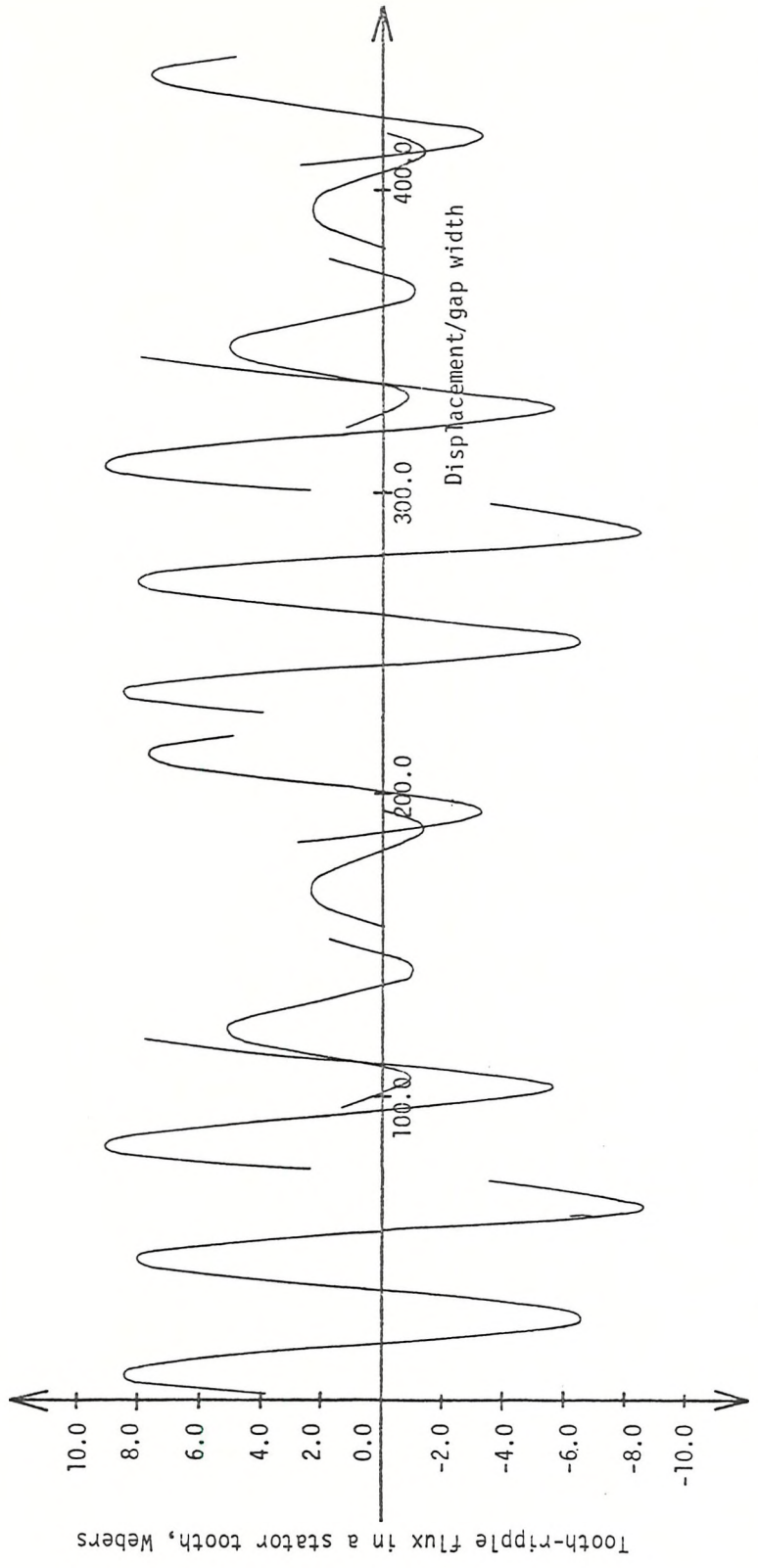

Figure 7.13 The time history of the tooth-ripple flux in a stator tooth (T_{end}) for the slot combination $N_S = 36$, $N_R = 24$

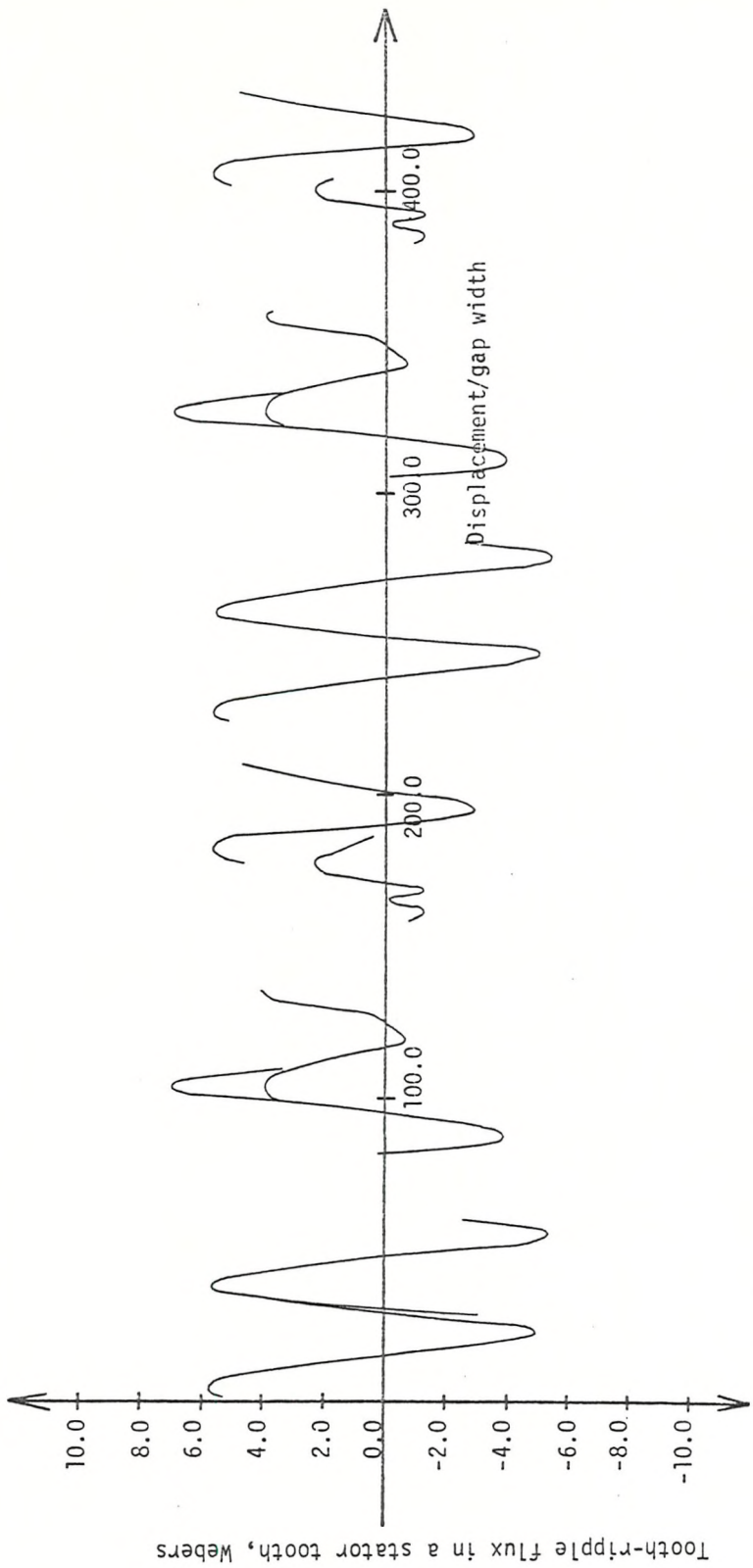

Figure 7.14 The time history of the tooth-ripple flux in a stator tooth (T_{end}) for the slot combination $N_S = 36$, $N_R = 28$

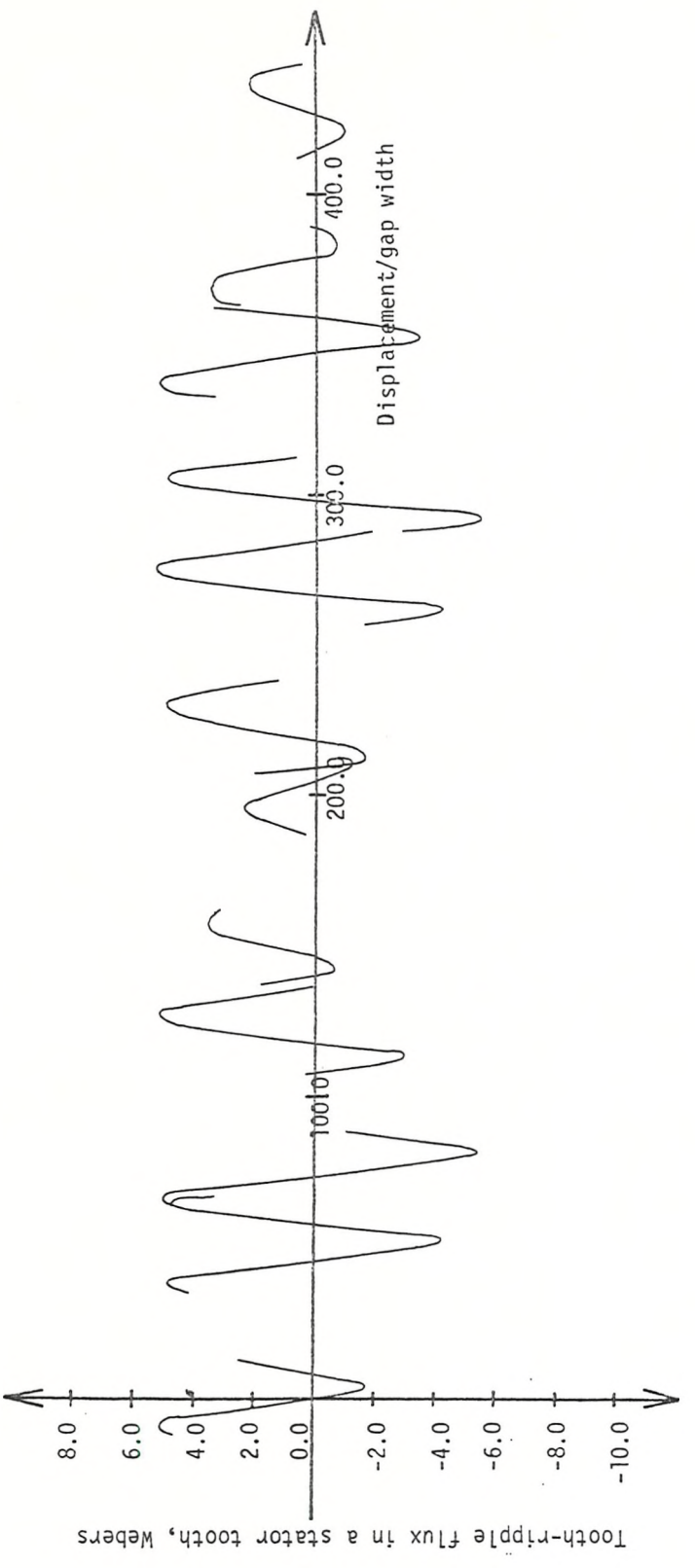

Figure 7.15 The time history of the tooth-ripple flux in a stator tooth (T_{end}) for the slot combination $N_S = 36$, $N_R = 30$

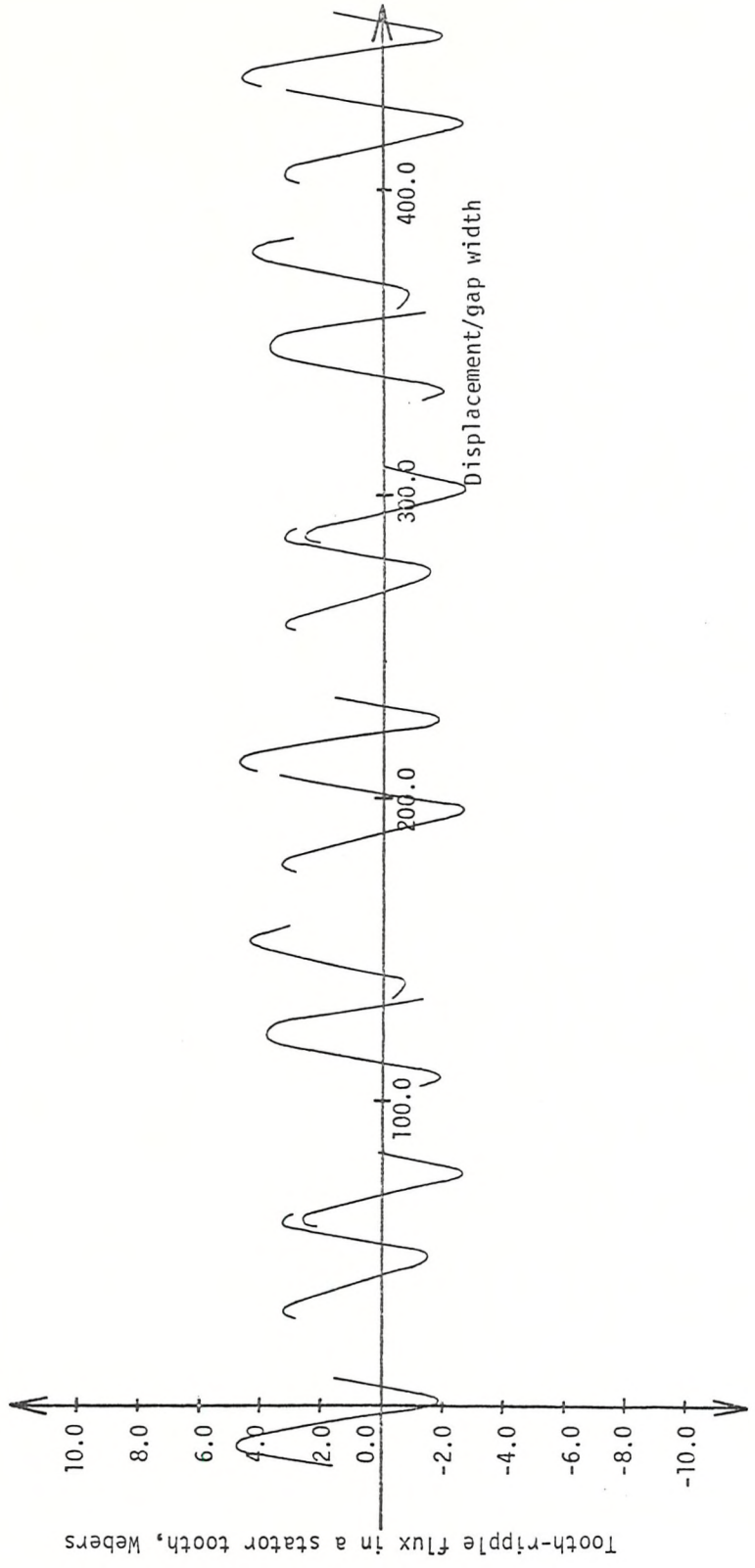

Figure 7.16 The time history of the tooth-ripple flux in a stator tooth (T_{end}) for the slot combinations $N_S = 36$, $N_R = 32$

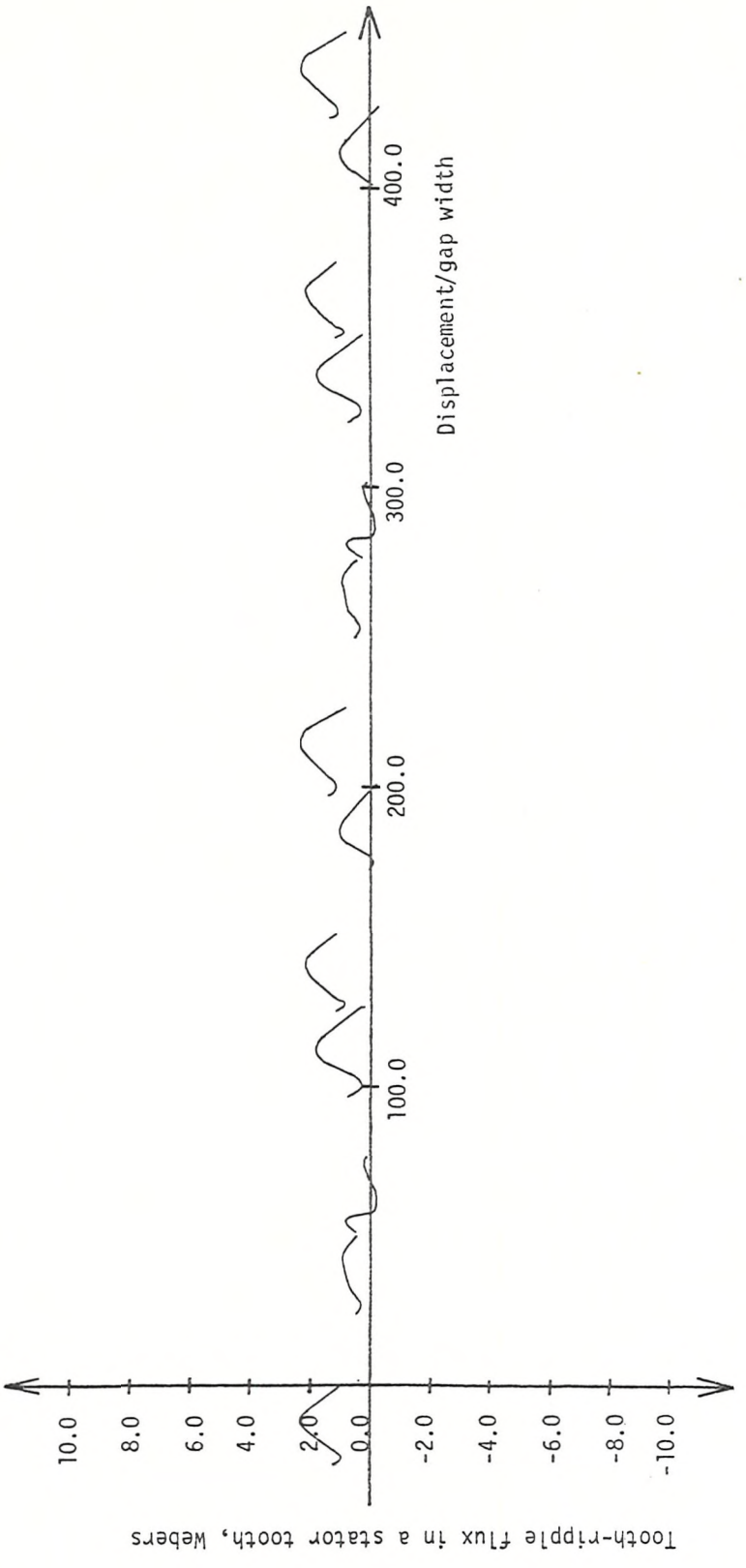

Figure 7.17 The time history of the tooth-ripple flux in a stator tooth (T_{end}) for the slot combination $N_S = 36$, $N_R = 36$

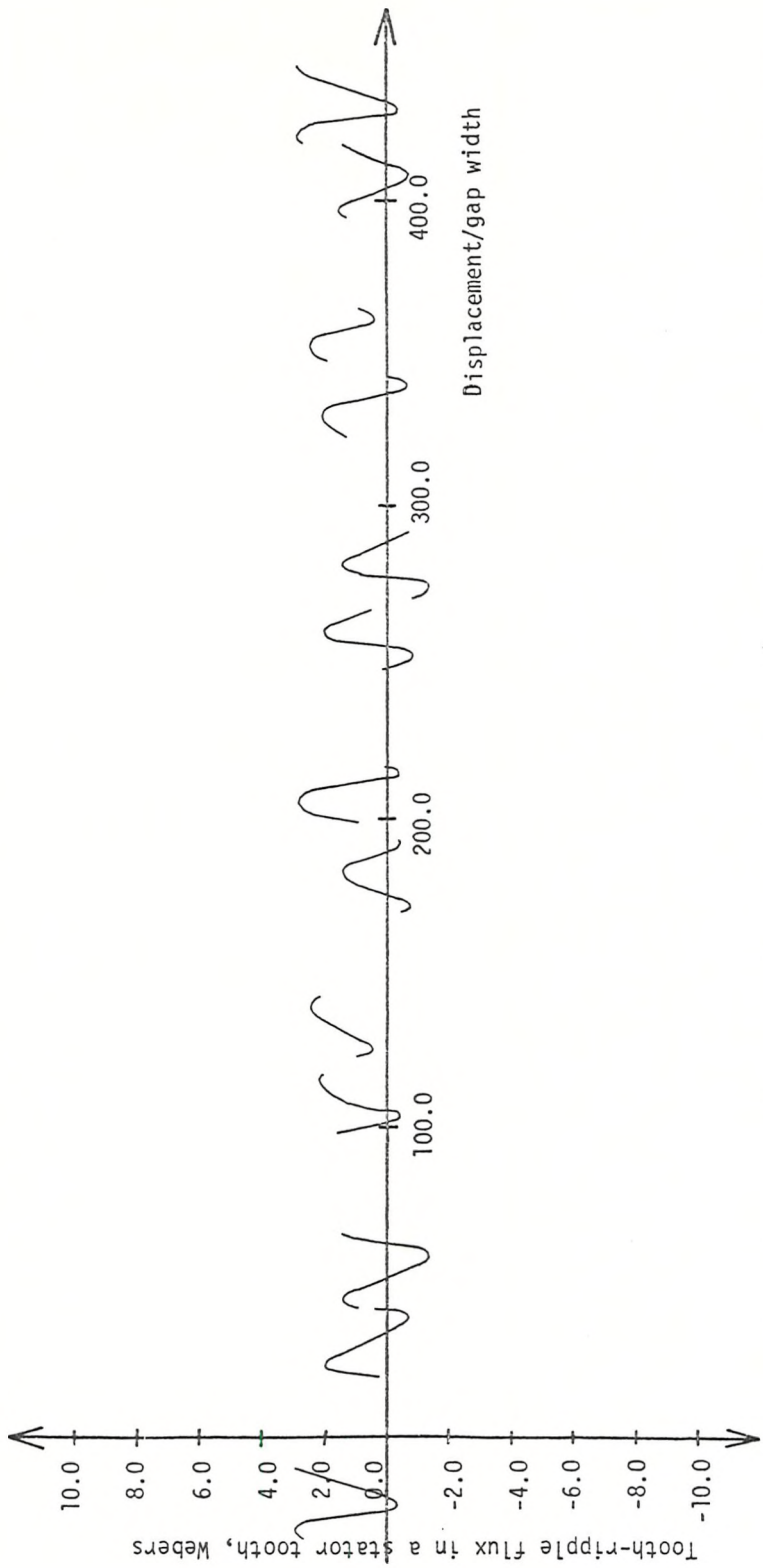

Figure 7.18 The time history of the tooth-ripple flux in a stator tooth (T_{end}) for the slot combination $N_S = 36$, $N_R = 42$

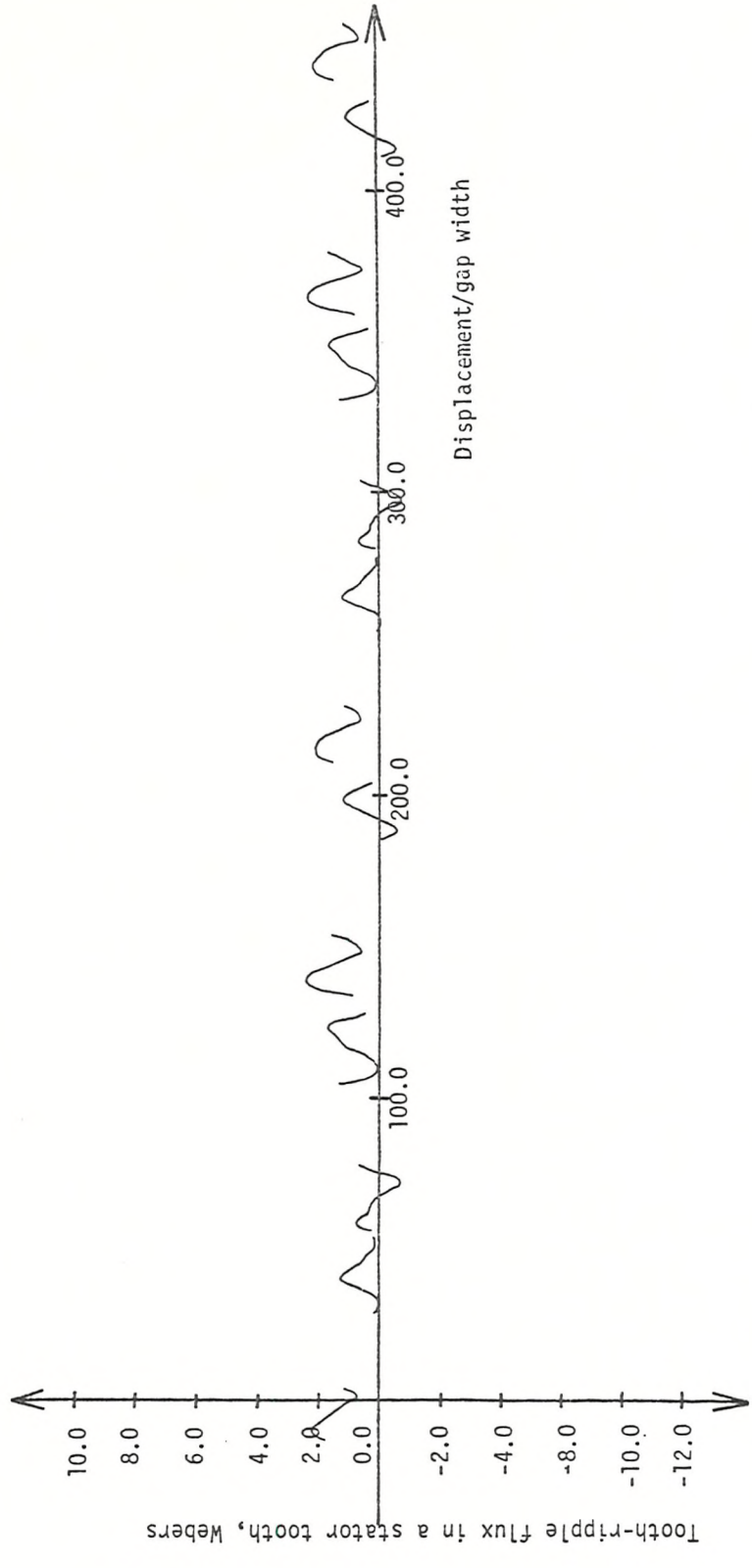

Figure 7.19 The time history of the tooth-ripple flux in a stator tooth (T_{end}) for the slot combination $N_S = 36$, $N_R = 48$

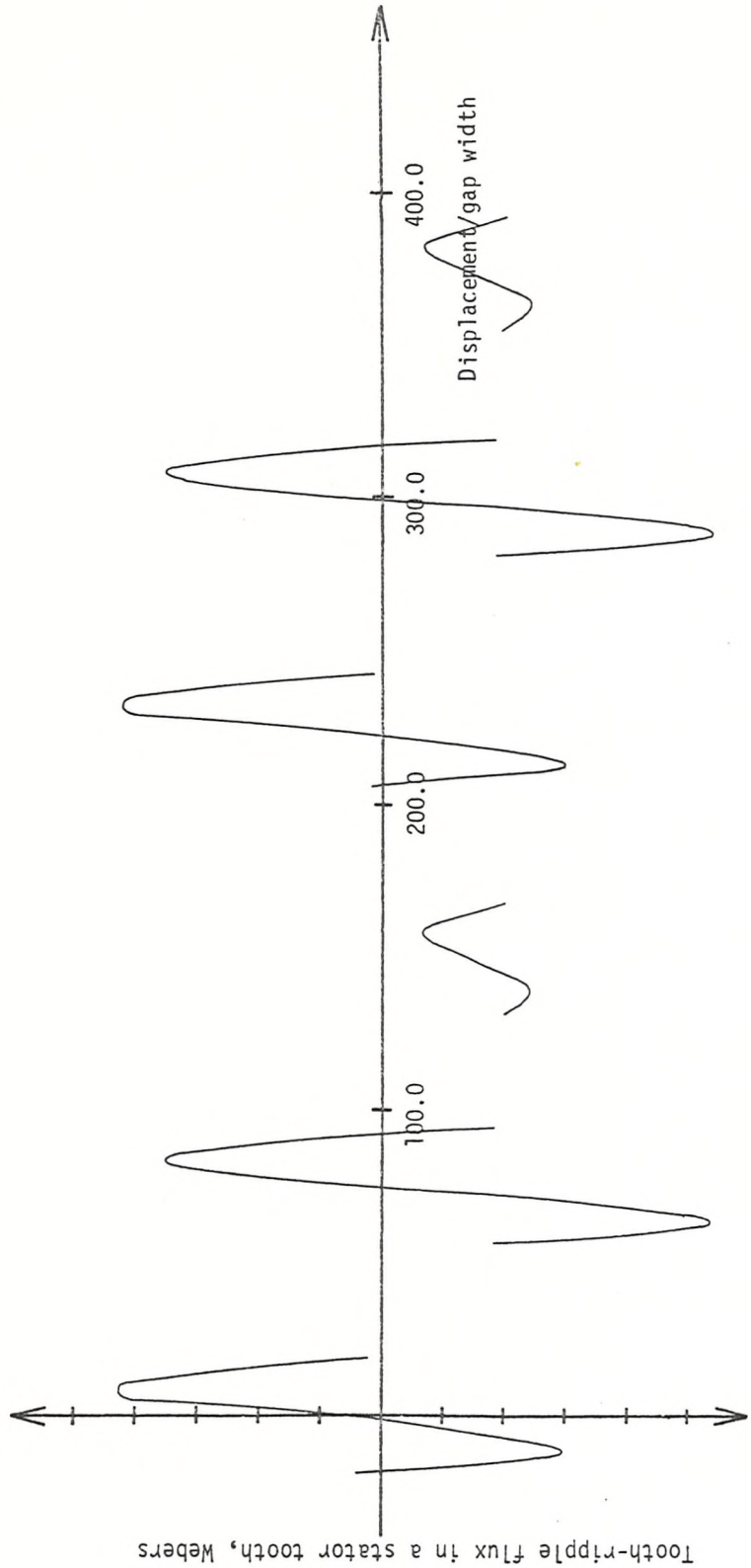

Figure 7.20 The time history of the tooth-ripple flux in a stator tooth (T_{middle}) for the slot combination $N_S = 36$, $N_R = 24$

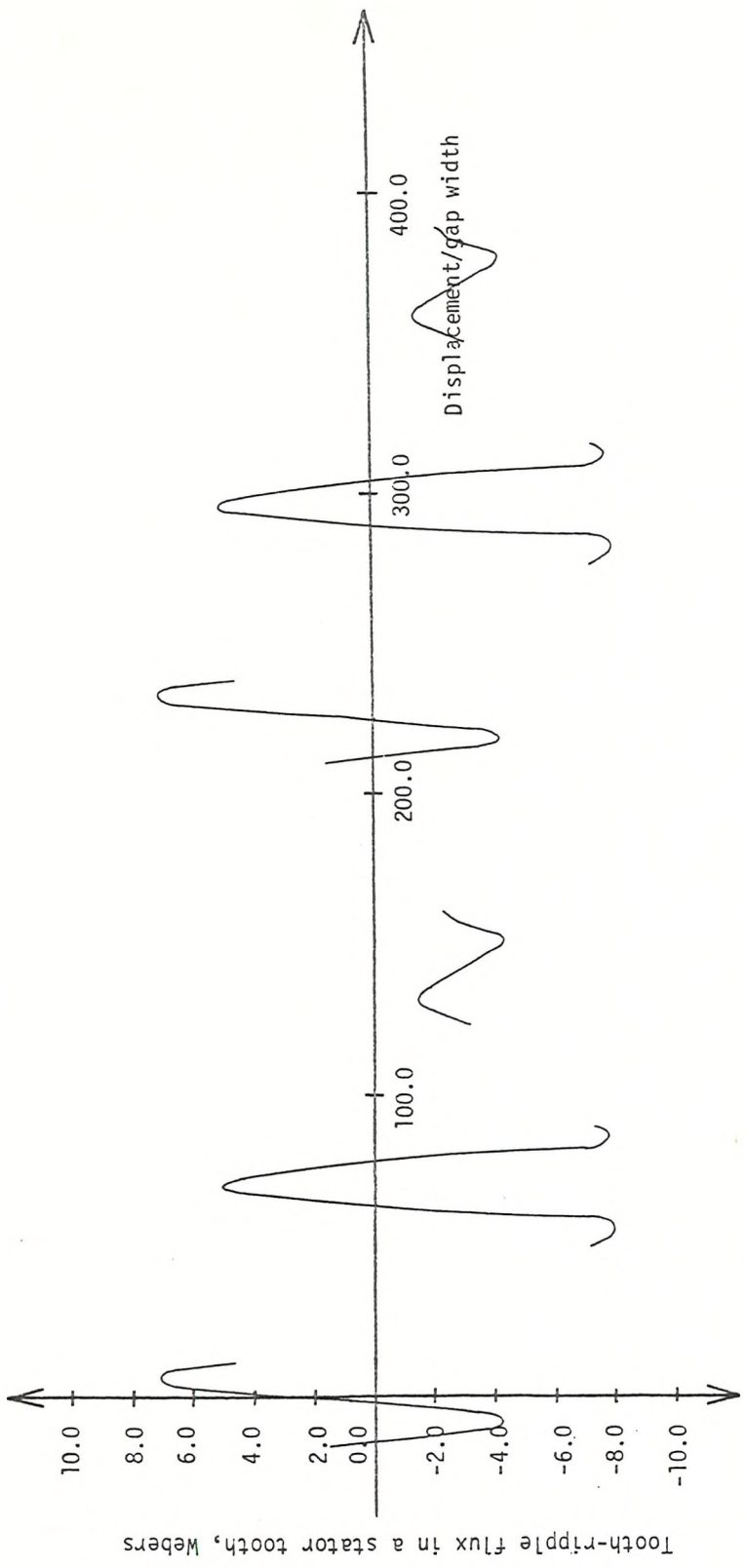

Figure 7.21 The time history of the tooth-ripple flux in a stator tooth (T_{middle}) for the slot combination $N_S = 36$, $N_R = 28$

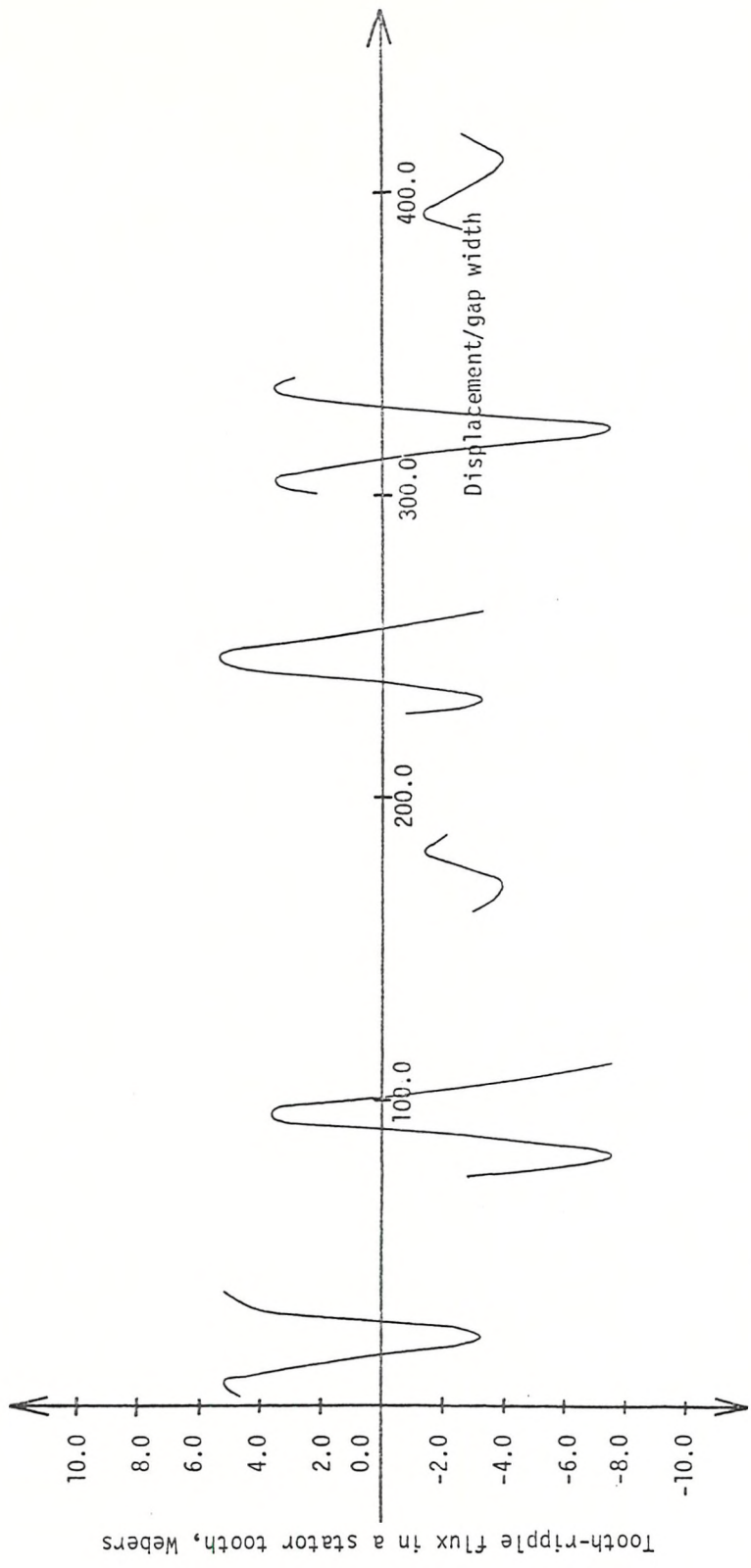

Figure 7.22 The time history of the tooth-ripple flux in a stator tooth (T_{middle}) for the slot combination $N_S = 36$, $N_R = 30$

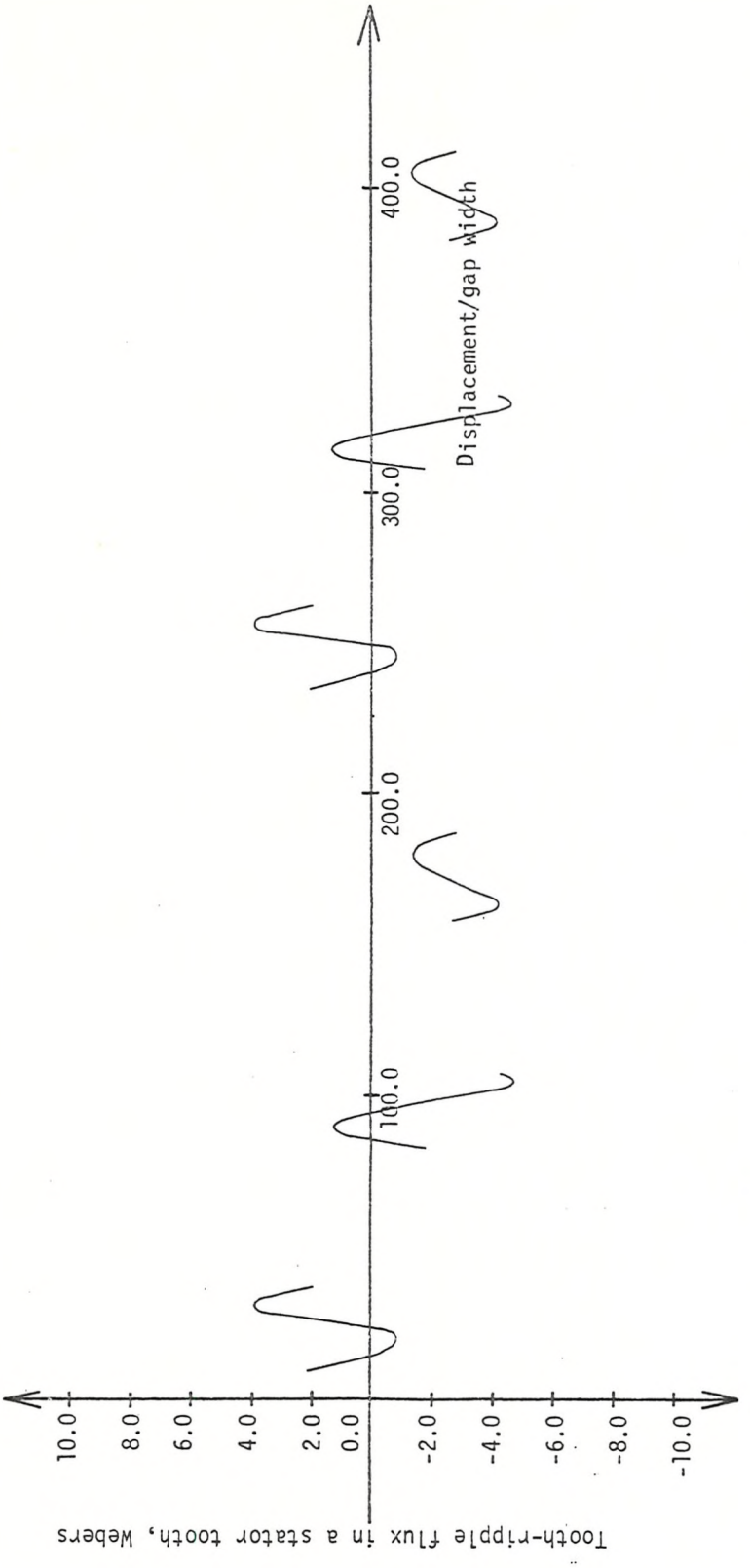

Figure 7.23 The time history of the tooth-ripple flux in a stator tooth (T_{middle}) for the slot combination $N_S = 36$, $N_R = 32$

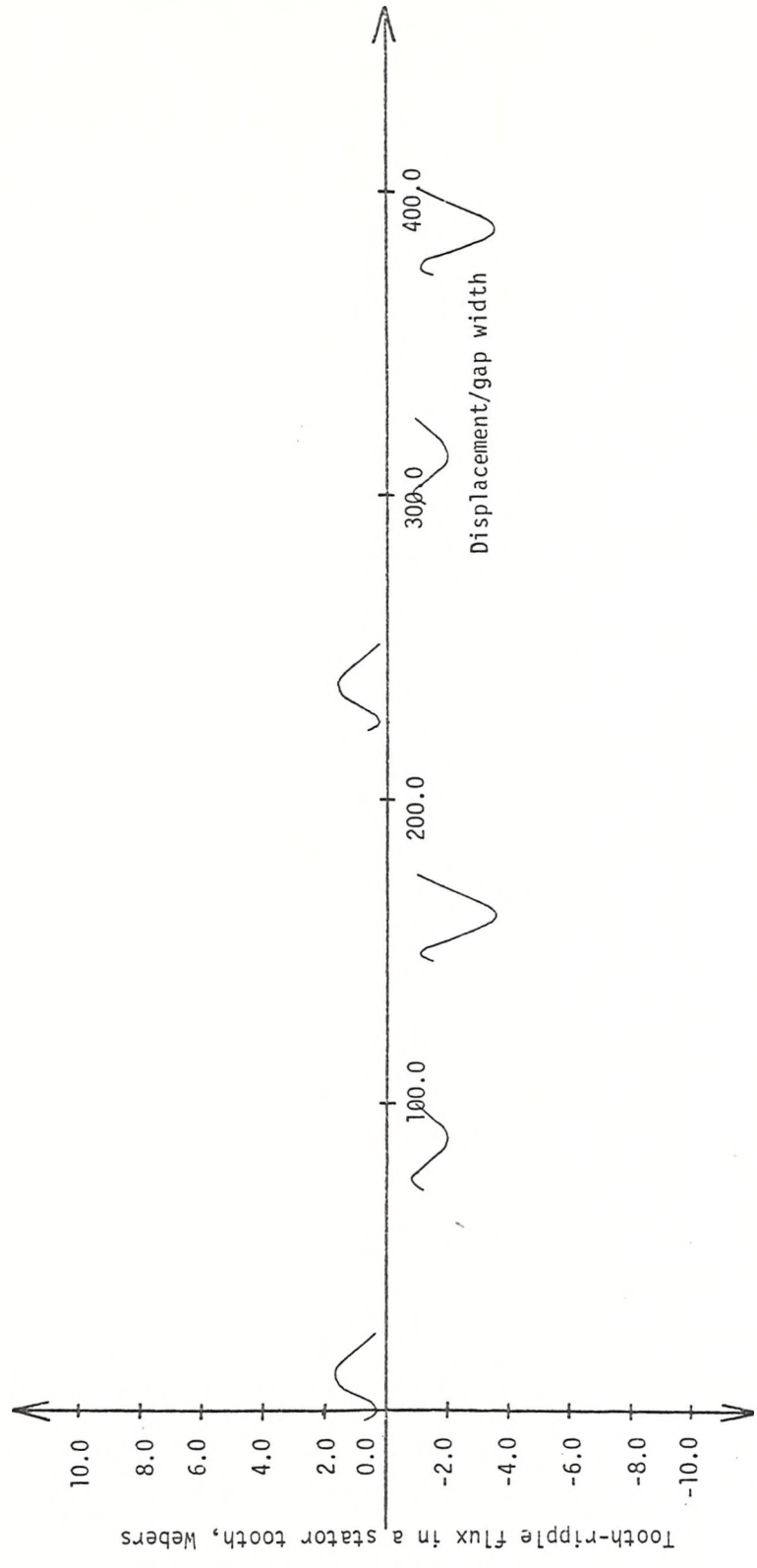

Figure 7.24 The time history of the tooth-ripple flux in a stator tooth (T_{middle}) for the slot combination $N_S = 36$, $N_R = 36$

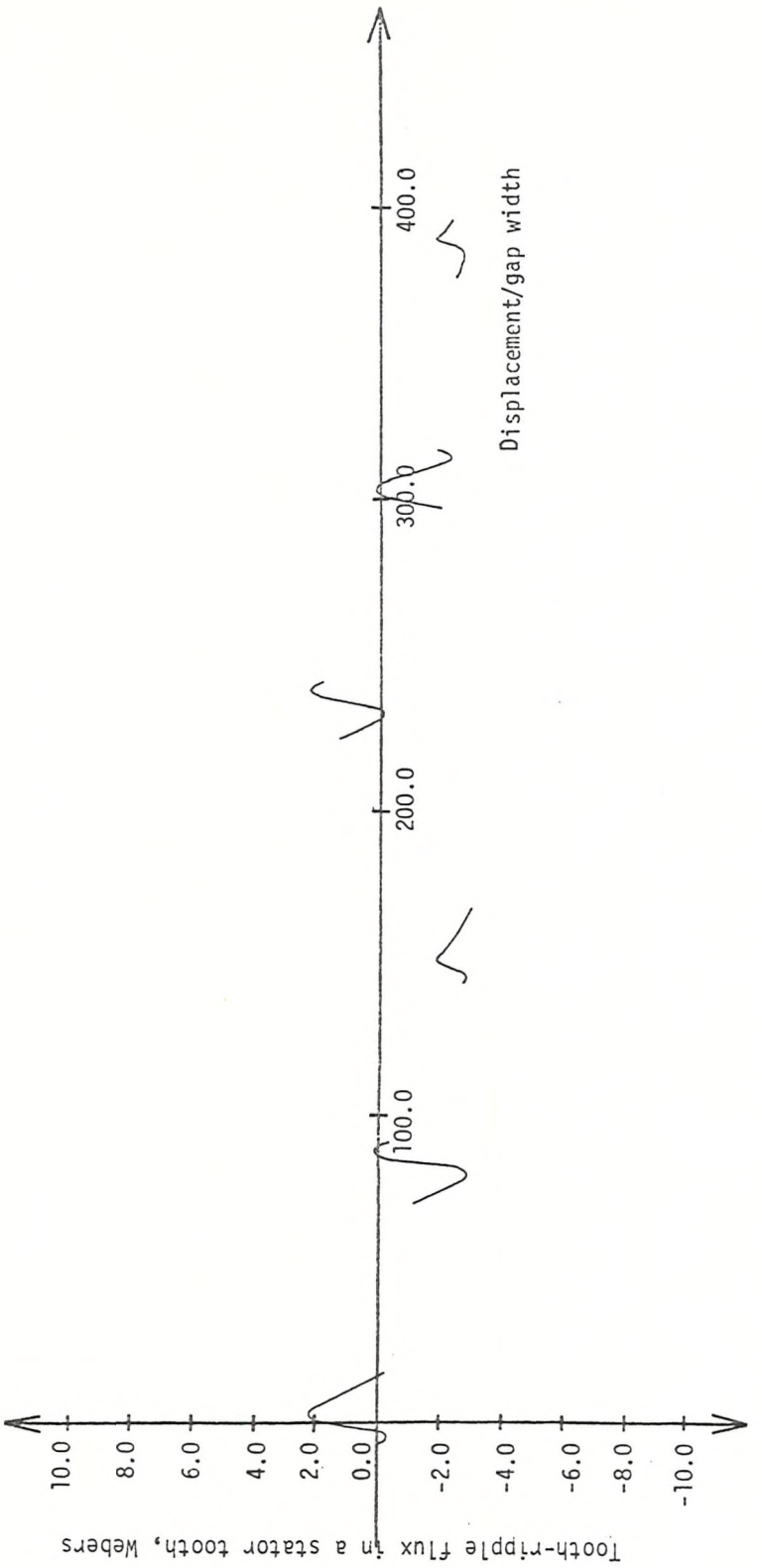

Figure 7.25 The time history of the tooth-ripple flux in a stator tooth (T_{middle}) for the slot combination $N_S = 36$, $N_R = 42$

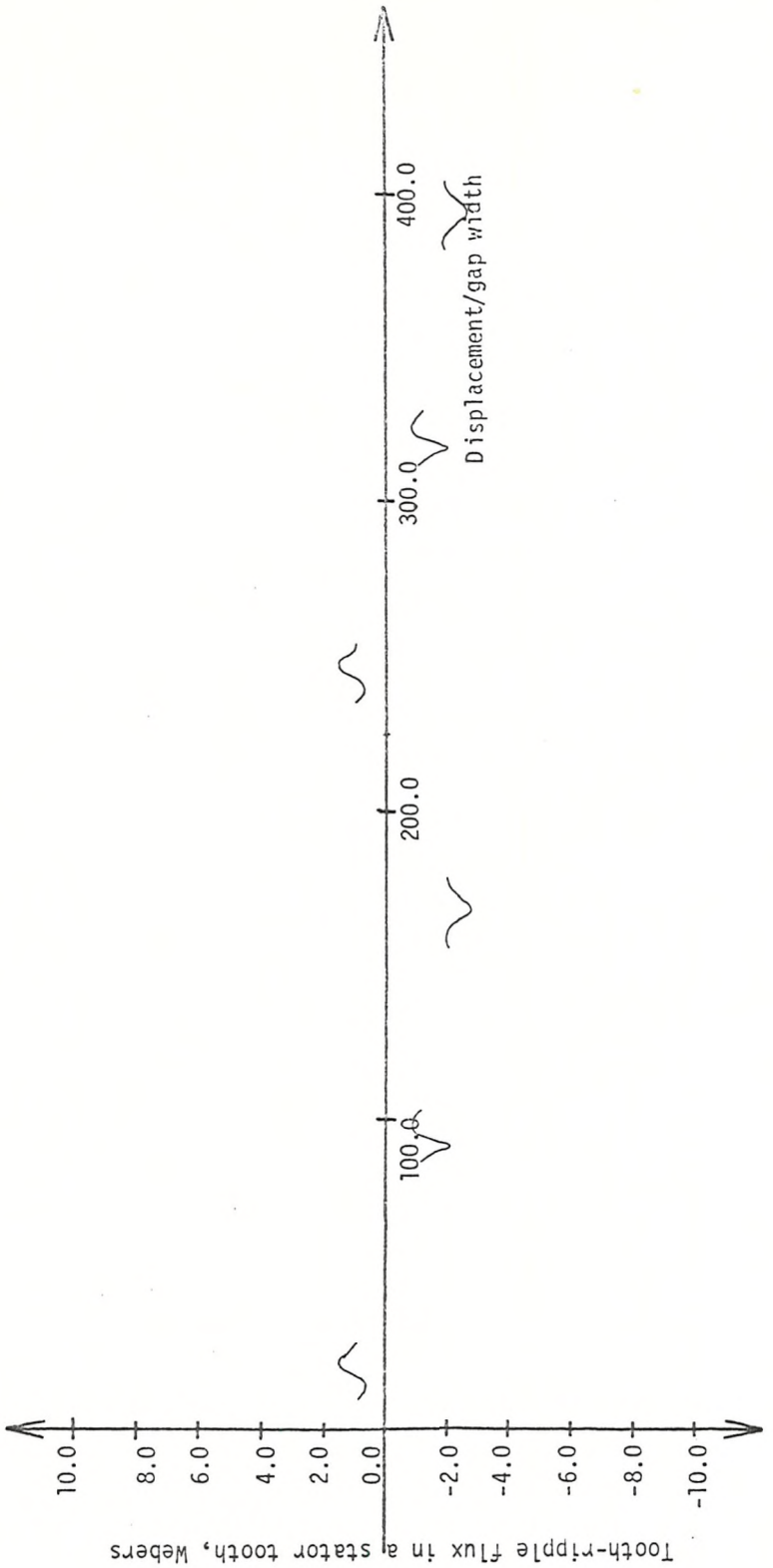

Figure 7.26 The time history of the tooth-ripple flux in a stator tooth (T_{middle}) for the slot combination $N_S = 36$, $N_R = 48$

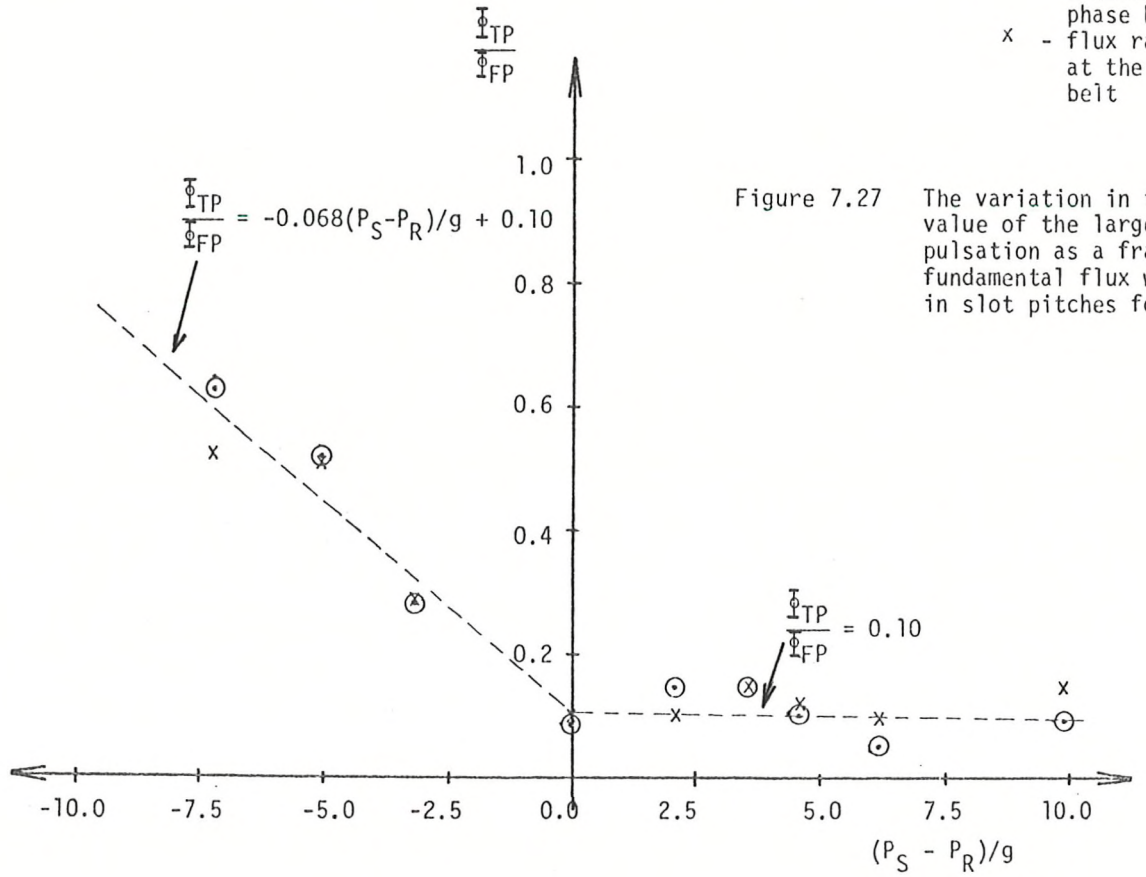

Figure 7.27 The variation in the peak to peak value of the largest tooth flux pulsation as a fraction of the fundamental flux with the difference in slot pitches for the stator.

CHAPTER 8

AN EXAMINATION OF THE NORMAL AND TANGENTIAL TOOTH-RIPPLE FORCE PULSATIONS UNDER LOAD

8. Introduction

8.1 The Normal Force Pulsations acting on a Rotor Tooth

8.2 The Normal Force Pulsations acting on a Stator Tooth

8.3 The Tangential Force Pulsations acting on a Rotor Tooth

8.4 The Tangential Force Pulsations acting on a Stator Tooth

8.5 Conclusions

8.5.1 Normal Force Pulsations

8.5.2 Tangential Force Pulsations

8.5.3 General Conclusions

8.6 References

8. Introduction

In this chapter the normal and tangential force pulsations associated with the ten slot combinations are examined. The normal and tangential forces acting on the stator and rotor teeth are represented, for any rotor position, as four sets of discrete parameters distributed in space. These normal and tangential force distributions are used to obtain the variations of the normal and tangential forces acting on a rotor tooth and on the two stator teeth (a tooth at the end of a phase belt and a tooth contained within a phase belt). The variations in the normal force acting on the rotor and stator teeth are presented in Sections8.1 and 8.2 and the variations in the tangential force acting on the rotor and stator teeth are presented in Sections 8.3 and 8.4.

In order to assess the influence of slot combination on the normal and tangential force pulsations it is most realistic to take the peak to peak values of the largest normal and tangential force pulsations as the defining quantities. Therefore, in Sections 8.1 and 8.2, the peak to peak values of the largest normal force pulsations acting on a rotor or stator tooth are related to the difference in slot pitches by two simple equations. In a similar manner, in Sections 8.3 and 8.4, the peak to peak values of the largest tangential force pulsations acting on a rotor or stator tooth are related to the difference in slot pitches by two simple equations. These four equations are used to determine conditions under which the force pulsations (or tooth-ripple force carriers) are minimal. Finally, in Section 8.5, the main conclusions from the examination of the normal and tangential force pulsations are summarised.

8.1 The Normal Force Pulsations acting on a Rotor Tooth

For the purpose of representing the normal forces acting on the stator or rotor teeth as a set of discrete parameters distributed in space, it is reasonable to assume that the normal force associated with a tooth acts at a point located at the centre of the tooth. The distribution of the normal forces on the teeth is, therefore, a plot of the normal forces acting on the teeth against the position of the teeth centres relative to some arbitrary origin. This origin is the same as that of the corresponding flux distribution. The distribution of tangential forces acting on the stator or rotor teeth may be represented in a similar manner. Typical distributions of normal and tangential forces acting on the rotor teeth of a slot combination having 36 stator slots and 48 rotor slots are shown in Figures 8.1 and 8.2. The normal and tangential force distributions associated with the ten slot combinations have been computed at the same rotor positions relative to the stator as the flux distributions. These distributions have been used in a way similar to the flux distributions to obtain the variations in the normal and tangential forces acting on a rotor tooth.

Figures 8.3 to 8.12 show the variation in the normal force acting on a rotor tooth for each of the ten slot combinations. The origin of these curves are the same as the corresponding tooth-ripple flux curves. The variation in the normal force follows similar trends for all slot combinations. These force variations are nearly sinusoidal, periodic in a stator slot pitch and modulated by the fundamental gap m.m.f.

In determining an appropriate defining quantity, it is important to emphasise that it is not only the amplitude of a force that is important in producing noise, but also its frequency[8.1]. A relatively large force may cause little noise and vibration if the response of the structure at the frequency of a particular mode of vibration is small.

On the other hand, a relatively small force, exciting a particular mode of vibration of some part of the machine structure at or near its resonant frequency may cause considerable noise and vibration. Furthermore, a force wave having a short wavelength,spanning only a few teeth, is unlikely to cause significant core vibration. Whereas a force wave having a long wavelength,spanning many teeth, will probably produce considerable core vibration. Clearly, it is important to be able to predict the response of the machine structure to all force harmonics. However, if part of the machine structure is excited by the normal force pulsations, it is obviously important to minimise the amplitude of these pulsations.

The defining quantity chosen, therefore, is the peak to peak value of the largest normal force pulsation acting on the tooth. This is plotted in Figure 8.13 against the difference in slot pitches and it is apparent that the relationship is almost linear and can be expressed to a close approximation by

$$F_{NP} = (69 + (P_R - P_S)/g) \times 10^5 B^2 L g \qquad (8.1)$$

8.2 The Normal Force Pulsations acting on a Stator Tooth

The normal force distributions on the stator teeth have been used to obtain the variation in the normal force on the two stator teeth (a tooth at the end of a phase belt and a tooth contained within a phase belt). These variations are presented in Figures 8.14 to 8.23 for each of the ten slot combinations. To reduce the number of figures required to present the results, the normal force pulsations associated with the two teeth are shown on the same figure. The pulsations associated with a tooth at the end of a phase belt are shown in full lines and the pulsations associated with a tooth contained within a phase belt are shown in dotted lines. The variations in the normal

force are nearly sinusoidal, periodic in a rotor slot pitch and modulated by the gap m.m.f.

As in the case of the rotor, the important defining quantity is the peak to peak value of the largest force pulsation. This is plotted for the two stator teeth against the difference in slot pitches in Figure 8.24. It is clear from this figure that the position of a stator tooth relative to its phase belt has only a slight influence on the magnitude of the defining quantity. Again the variation of the peak to peak value of the largest force pulsation against the difference in slot pitches is nearly linear. This variation for the stator is given very closely by the equation

$$F_{NP} = [69 - 6\ (P_S - P_R)/g] \times 10^5\ B^2\ L\ g \qquad (8.2)$$

The normal force pulsations for $P_S/g = P_R/g$ are vitaually the same for the stator and rotor, as expected. However, the slopes of the curves are widely different and both stator and rotor force pulsations are minimal when $P_S/g > P_R/g$ (rotor overslotted). An important difference, however, is that the stator force pulsations are much more sensitive to a change in slot pitch ratio. Also, as stator core vibrations are the major cause of magnetic noise, the variation shown in Figure 8.24 is most important.

8.3 The Tangential Force Pulsations acting on a Rotor Tooth

The variations in the tangential force acting on a rotor tooth are shown in Figures 8.25 to 8.29 for the rotor slot numbers 28, 30, 36, 42 and 48. These variations follow similar trends for all the slot combinations; they are nearly sinusoidal and periodic in a stator slot pitch and modulated by the fundamental gap m.m.f.

A plot of the peak to peak value of the largest tangential force pulsation against the difference in slot pitches is shown in Figure 8.30.

It is clear that the relationship is nearly linear and can be expressed to a close approximation by

$$F_{TP} = [13 + 0.37\ (P_R - P_S)/g] \times 10^5\ B^2\ L g \qquad (8.3)$$

8.4 The Tangential Force Pulsations acting on a Stator Tooth

The variations in the tangential force acting on the two stator teeth are shown in Figures 8.31 to 8.35 for the rotor slot number 28, 30, 36, 42 and 48. As in the case of the stator normal force pulsations, the tangential force pulsations associated with a tooth at the end of a phase belt are shown in full lines and the tangential force pulsations associated with a tooth contained within a phase belt are shown in dotted lines. The variations in the tangential force acting on the two teeth show a similar trend for all the slot combinations. These force variations are nearly sinusoidal and periodic in a rotor slot pitch. They are modulated by the fundamental gap m.m.f.

A plot of the peak to peak value of the largest tangential force pulsation (for the two stator teeth) against the difference in slot pitches is shown in Figure 8.36. It is clear from this figure that the position of a tooth relative to its phase belt is of only slight significance. As in the case of the rotor, the peak to peak value of the largest force pulsation varies almost linearly with the difference in slot pitches. This variation for the stator is given very closely by the equation

$$F_{TP} = [12.4 - 0.7\ (P_S - P_R)/g] \times 10^5\ B^2\ L g \qquad (8.4)$$

As in the case of the normal force pulsations, the tangential force pulsations are almost equal when $P_S/g = P_R/g$. Also, like the normal force pulsations, the tangential force pulsations acting on the stator and rotor teeth are minimal when $P_S/g > P_R/g$ (rotor overslotted). However, the slope of the stator graph is almost twice as large as the

rotor graph. Therefore, the stator tangential force pulsations, like the stator normal force pulsations, are more sensitive to a change in slot pitch ratio. A comparison of equations (8.1) with (8.3) and (8.2) with (8.4) reveals that over the range of slot pitch difference considered, the largest tangential force pulsation is of the order of 20% of the largest normal force pulsation for both rotor and stator.

It is unlikely that the tangential force pulsations make a significant contribution to stator core vibration because they act transversely to the core and are small in amplitude in comparison with the normal force pulsations. However, these pulsations can cause the teeth in large machines to vibrate because the resonant frequencies of these teeth lie within the tooth-ripple frequency range. These teeth vibrations have been observed in some large machines, although to some extent they are damped down by the core and the insulation in the slots. However, it is very difficult to determine this damping effect and the subject of tooth vibration lies outside the scope of this thesis.

8.5 Conclusions

8.5.1 Normal Force Pulsations

(i) Normal force pulsations acting on the stator or rotor teeth increase on load with an increase in $(P_R - P_S)$ but the relationship is more sensitive for the stator teeth.

(ii) As regards the stator, the criterion for low stator force pulsations is similar to the no-load case $(P_S > P_R)$[8.2].

(iii) In the case of the rotor, the effect of slot combination on the normal force pulsations is not very significant and the effect of load (leakage flux) is to change the relative amplitudes for load and no-load.

8.5.2 Tangential Force Pulsations

(i) As in the case of the normal force pulsations, the tangential force pulsations acting on the stator and rotor teeth increase with $(P_R - P_S)$. This relationship is more sensitive for the stator teeth.

(ii) The tangential force pulsations acting on the teeth are normally small compared with the normal force pulsations. This conclusion is the same as for the no-load case[8.2].

(iii) As regards the stator, the criterion for low tangential force pulsations on load ($P_S > P_R$) differs from that for the no-load case[8.3]. However, the effect of a change in slot combination on the tangential force pulsations is not very significant when compared with the effect on the normal force pulsations.

(iv) In the case of the rotor, the effect of slot combination on the tangential force pulsations is not very significant.

8.5.3 General Conclusions

(i) Since stator normal force pulsations are a basic cause of 'magnetic noise', attention should be concentrated on the reduction of this cause of core vibration and the choice of rotor slotting is seen to be more critical.

(ii) It is unlikely that the tangential force pulsations make a major contribution to stator core vibration because they act transversely to the core and are small in amplitude in comparison with the normal force pulsations. However, they can cause the teeth in large machines to vibrate because the resonant frequency of these teeth lie within the tooth-ripple frequency range.

(iii) There is no optimum slot combination since specific criteria are incompatible. However, where a choice of rotor slotting is available, the balance between excessive stray loss and vibration producing forces can be guided by these criteria.

8.6 References

8.1 ELLISON, A. J. and MOORE, C. J. : 'Acoustic noise and vibration of rotating electrical machines', Proc. I.E.E., 1968, 115, (11), pp.1633-1640.

8.2 BINNS, K. J. and ROWLANDS-REES, G. : 'Radial tooth-ripple forces in induction motors due to the main flux', Proc. I.E.E., 1978, 125, (11), pp.1227-1231.

8.3 BINNS, K. J. and ROWLANDS-REES, G. : 'Main-flux pulsations and tangential tooth-ripple forces in induction motors', Proc. I.E.E., 1975, 122, (3), pp.273-277.

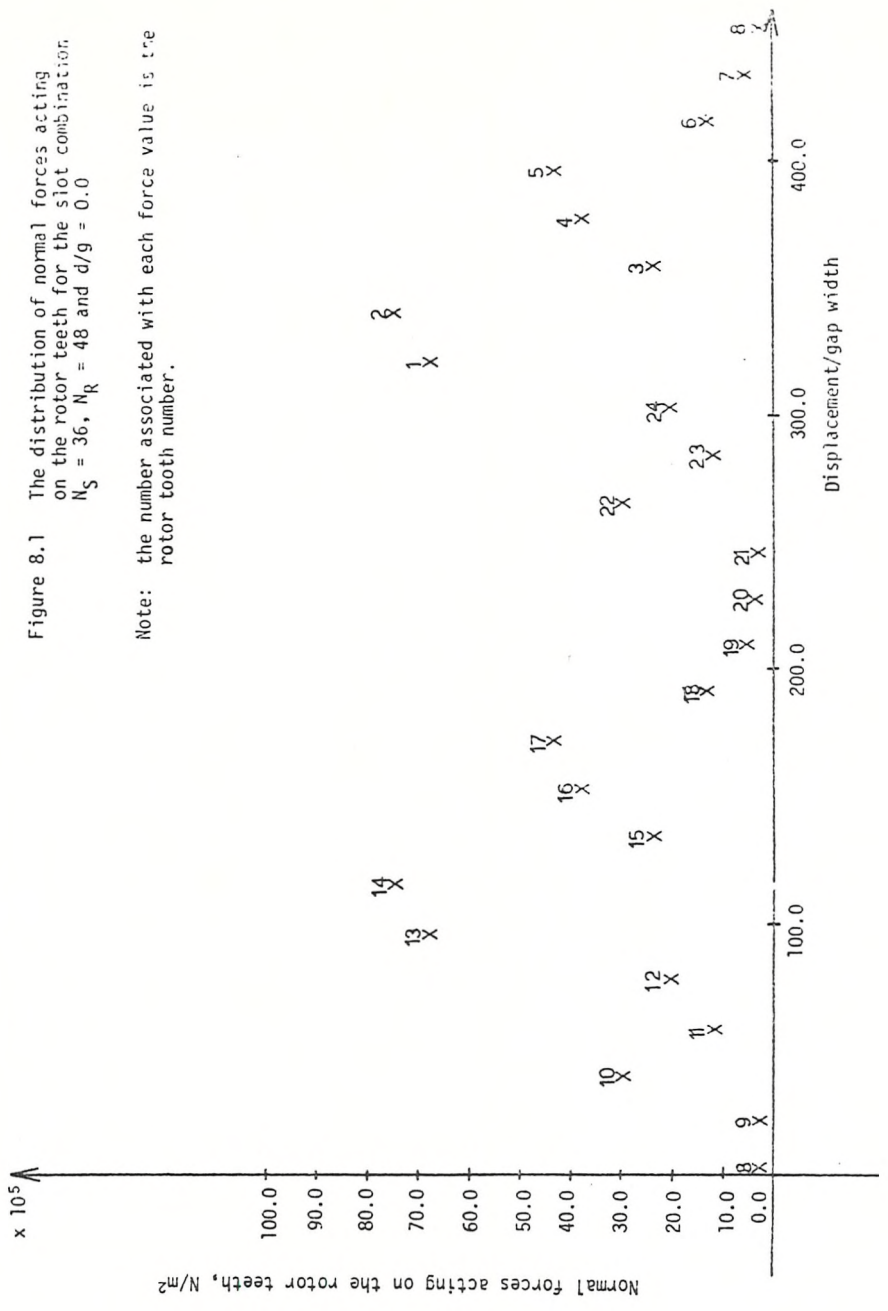

Figure 8.1 The distribution of normal forces acting on the rotor teeth for the slot combination $N_S = 36$, $N_R = 48$ and $d/g = 0.0$

Note: the number associated with each force value is the rotor tooth number.

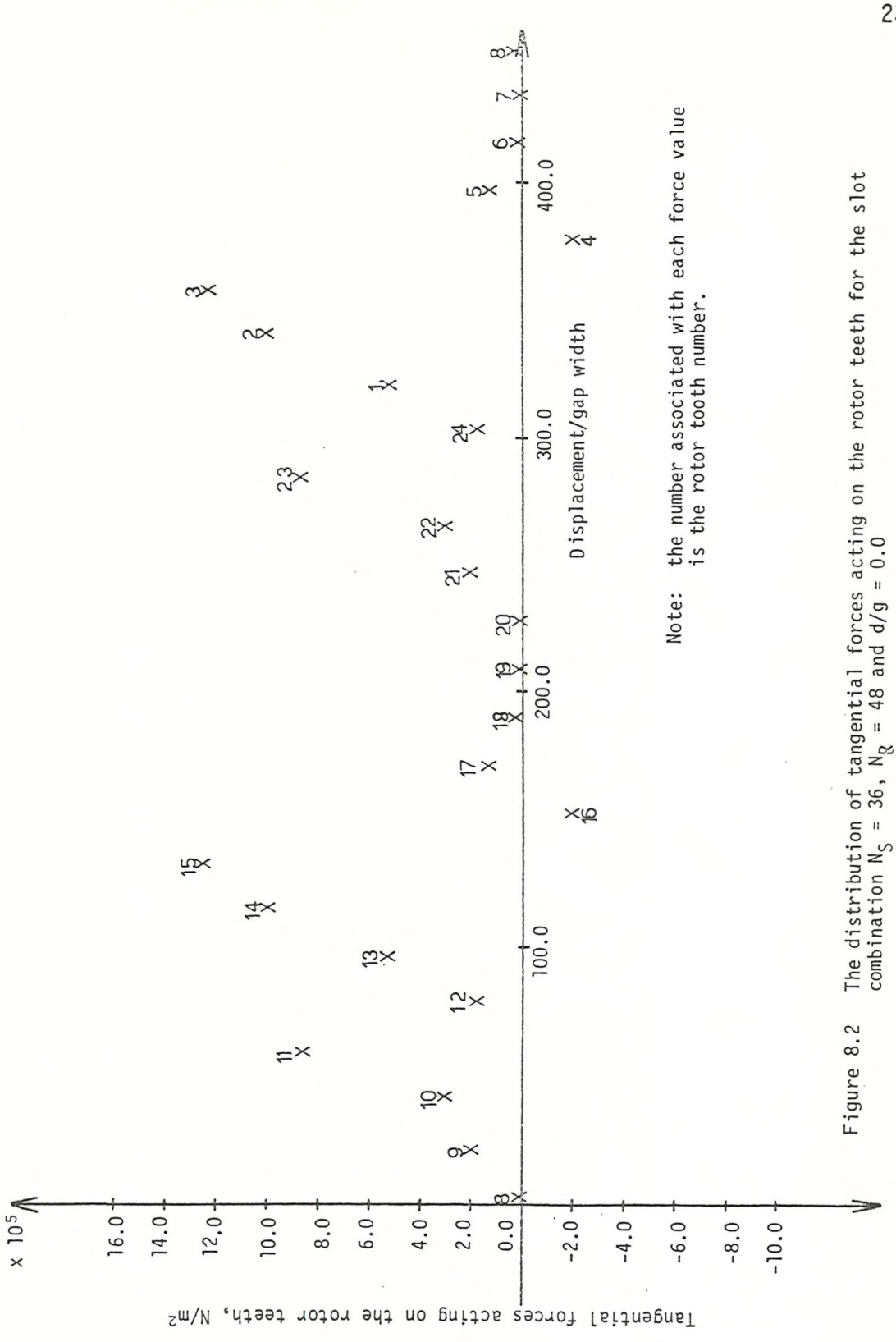

Figure 8.2 The distribution of tangential forces acting on the rotor teeth for the slot combination $N_S = 36$, $N_R = 48$ and $d/g = 0.0$

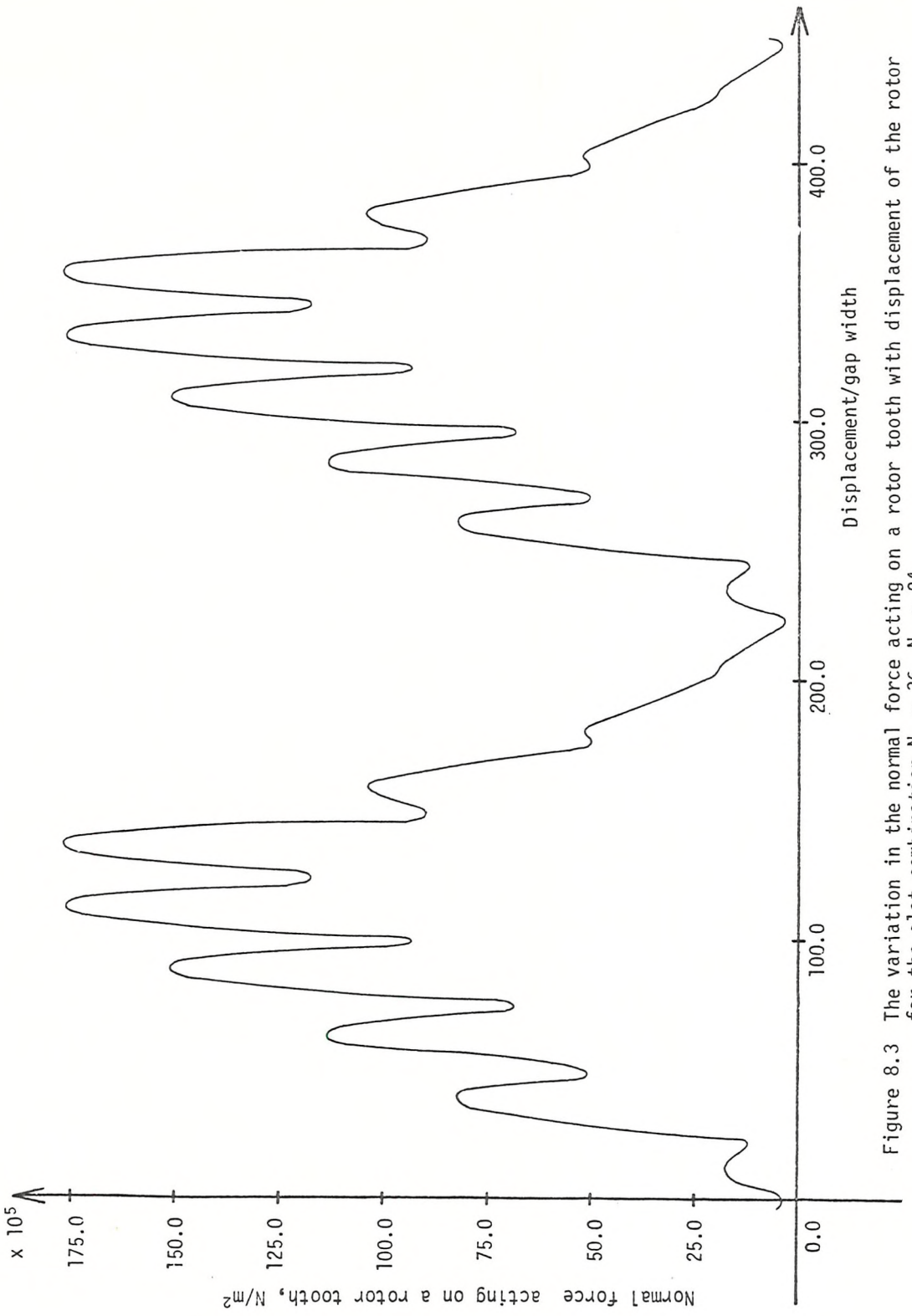

Figure 8.3 The variation in the normal force acting on a rotor tooth with displacement of the rotor for the slot combination $N_S = 36$, $N_R = 24$

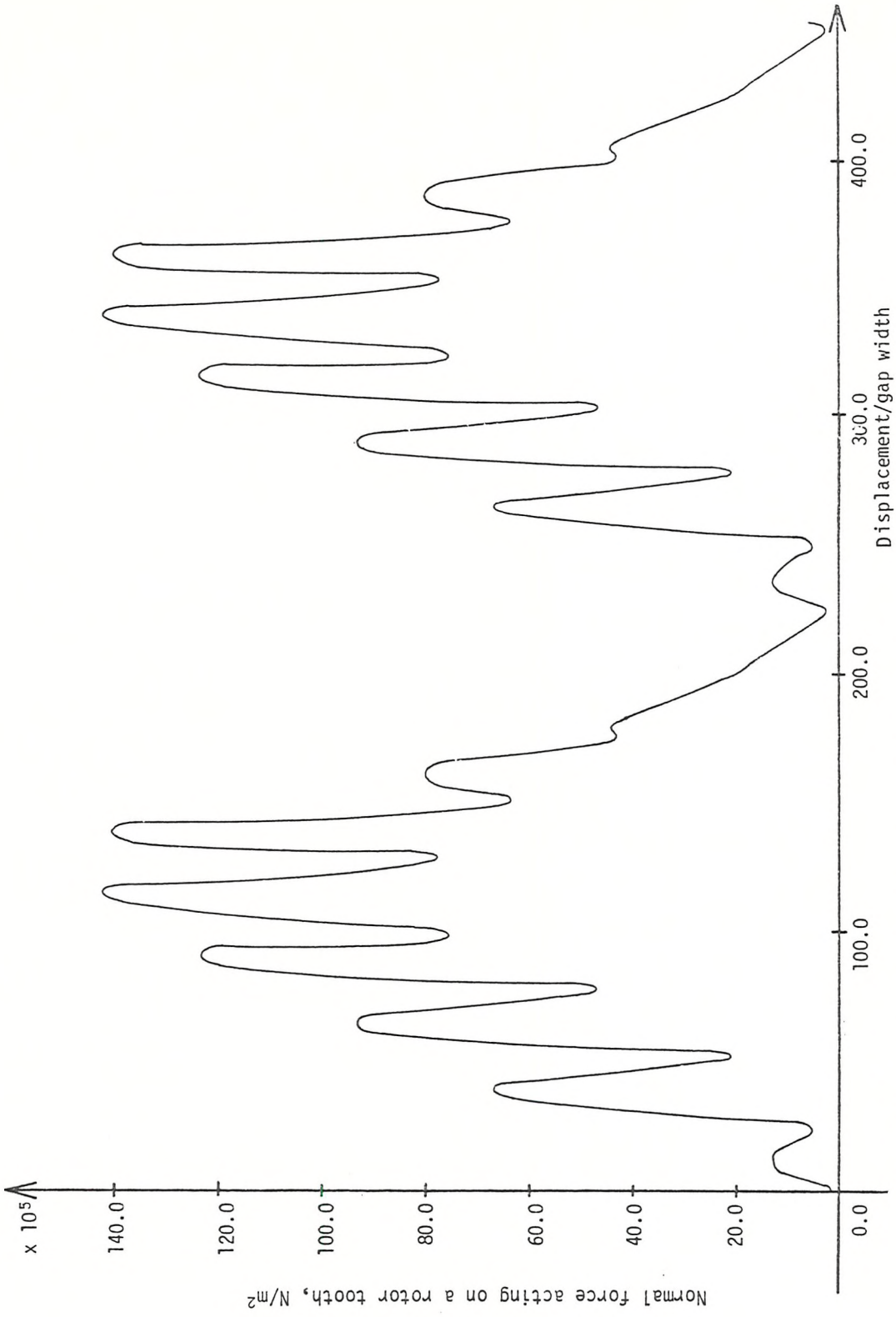

Figure 8.4 The variation in the normal force acting on a rotor tooth with displacement of the rotor for the slot combination $N_S = 36$, $N_R = 28$.

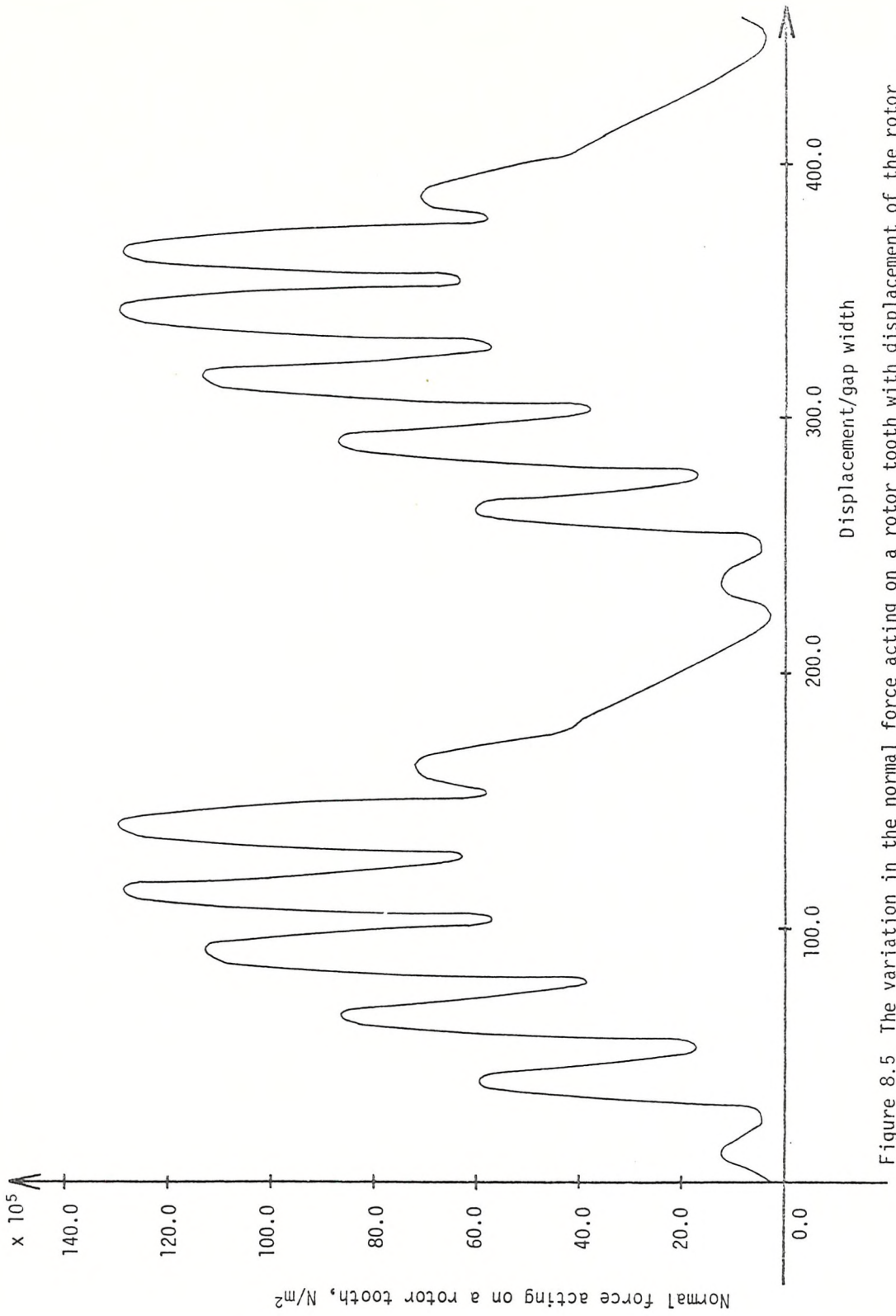

Figure 8.5 The variation in the normal force acting on a rotor tooth with displacement of the rotor for the slot combination $N_S = 36$, $N_R = 30$

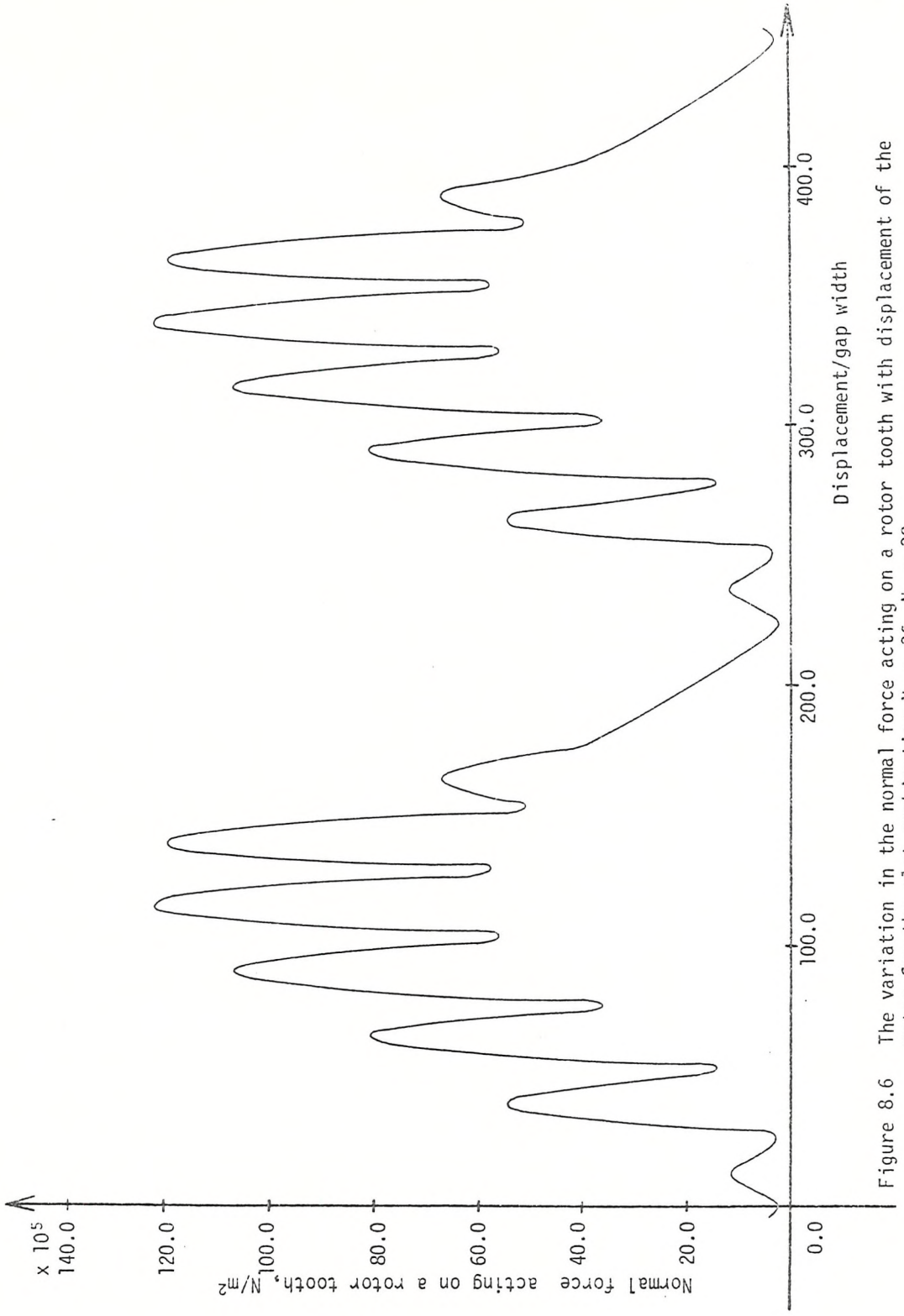

Figure 8.6 The variation in the normal force acting on a rotor tooth with displacement of the rotor for the slot combination $N_S = 36$, $N_R = 32$

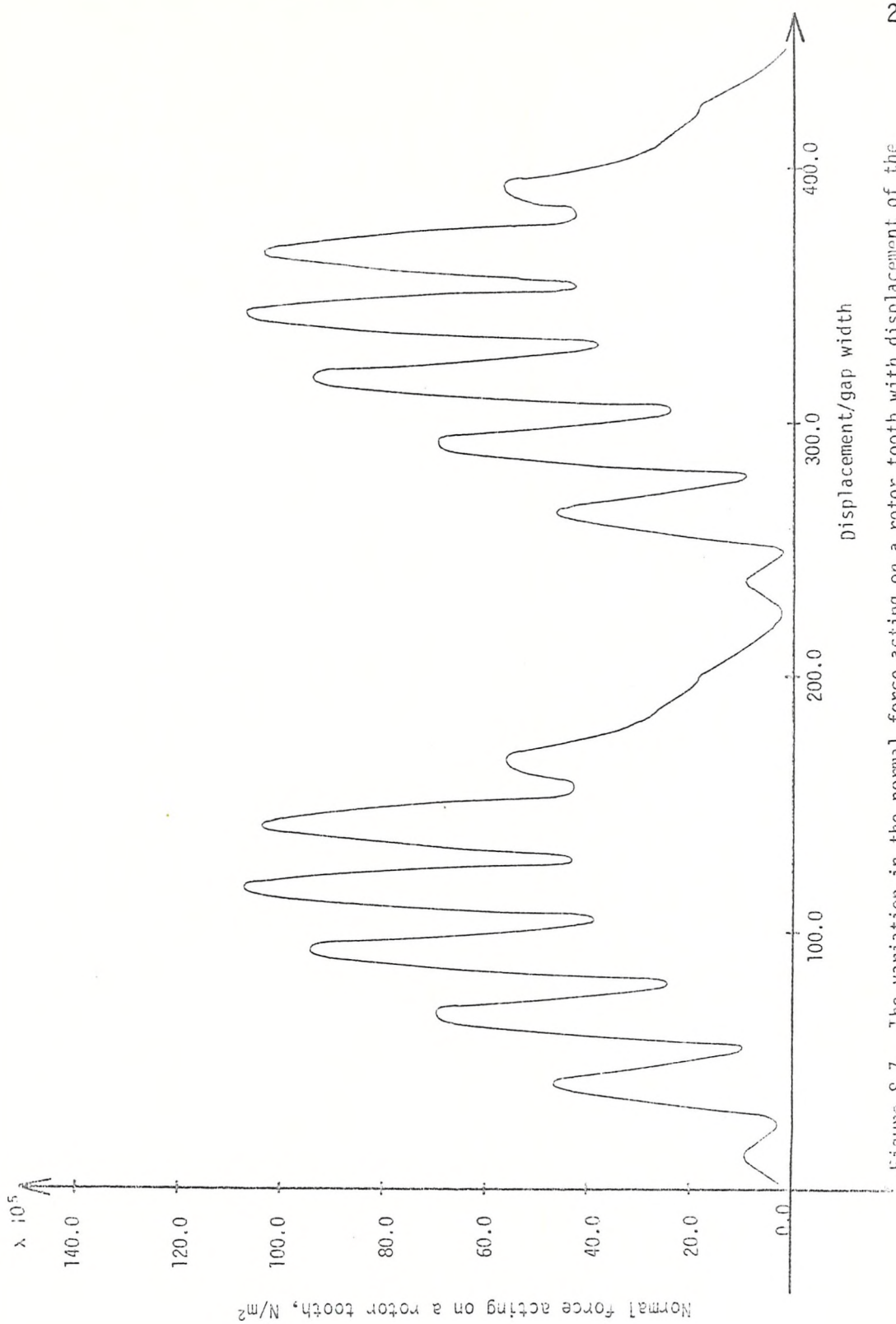

Figure 8.7 The variation in the normal force acting on a rotor tooth with displacement of the rotor for the slot combination $N_S = 36$, $N_R = 36$

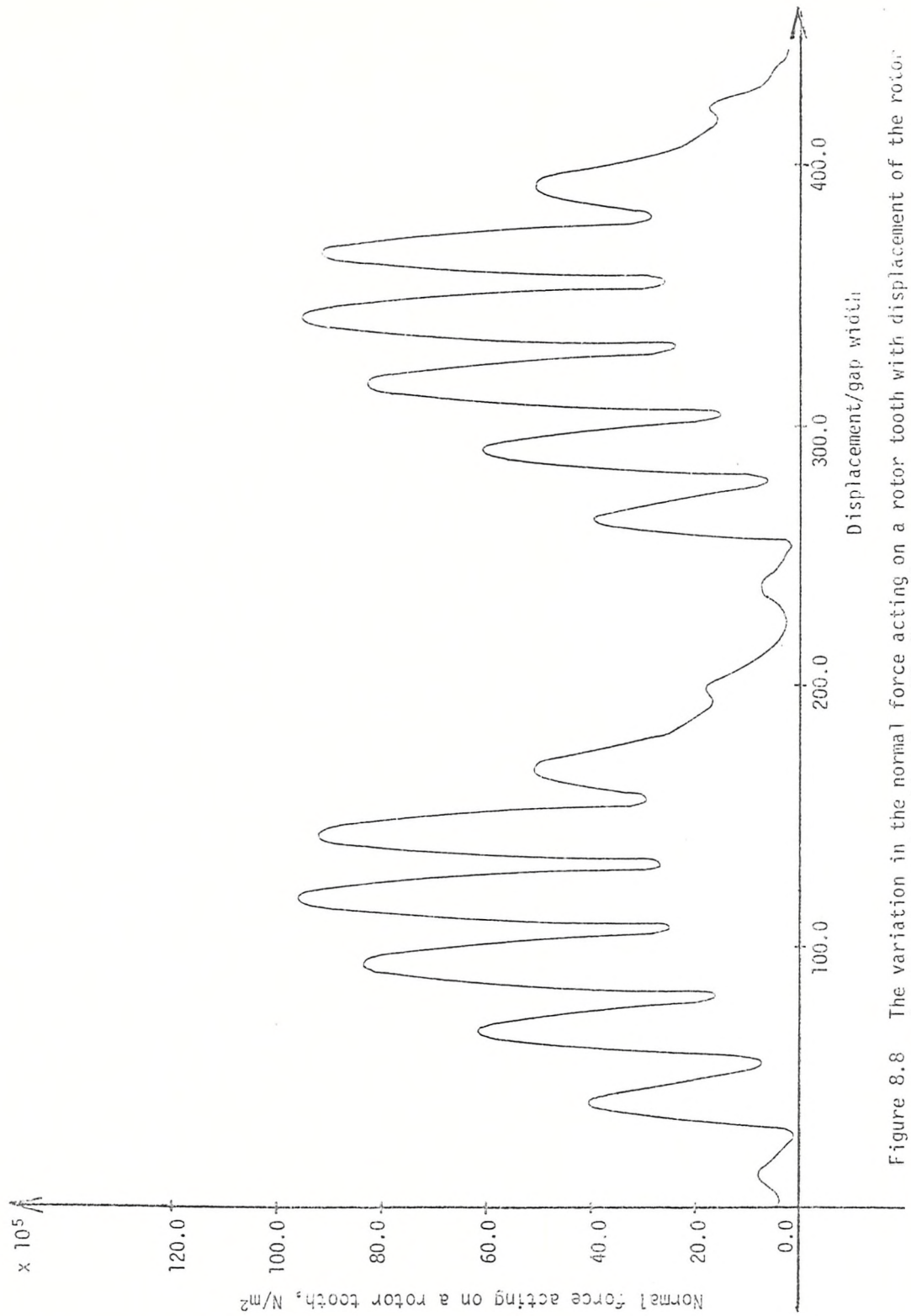

Figure 8.8 The variation in the normal force acting on a rotor tooth with displacement of the rotor for the slot combination $N_S = 36$, $N_R = 40$

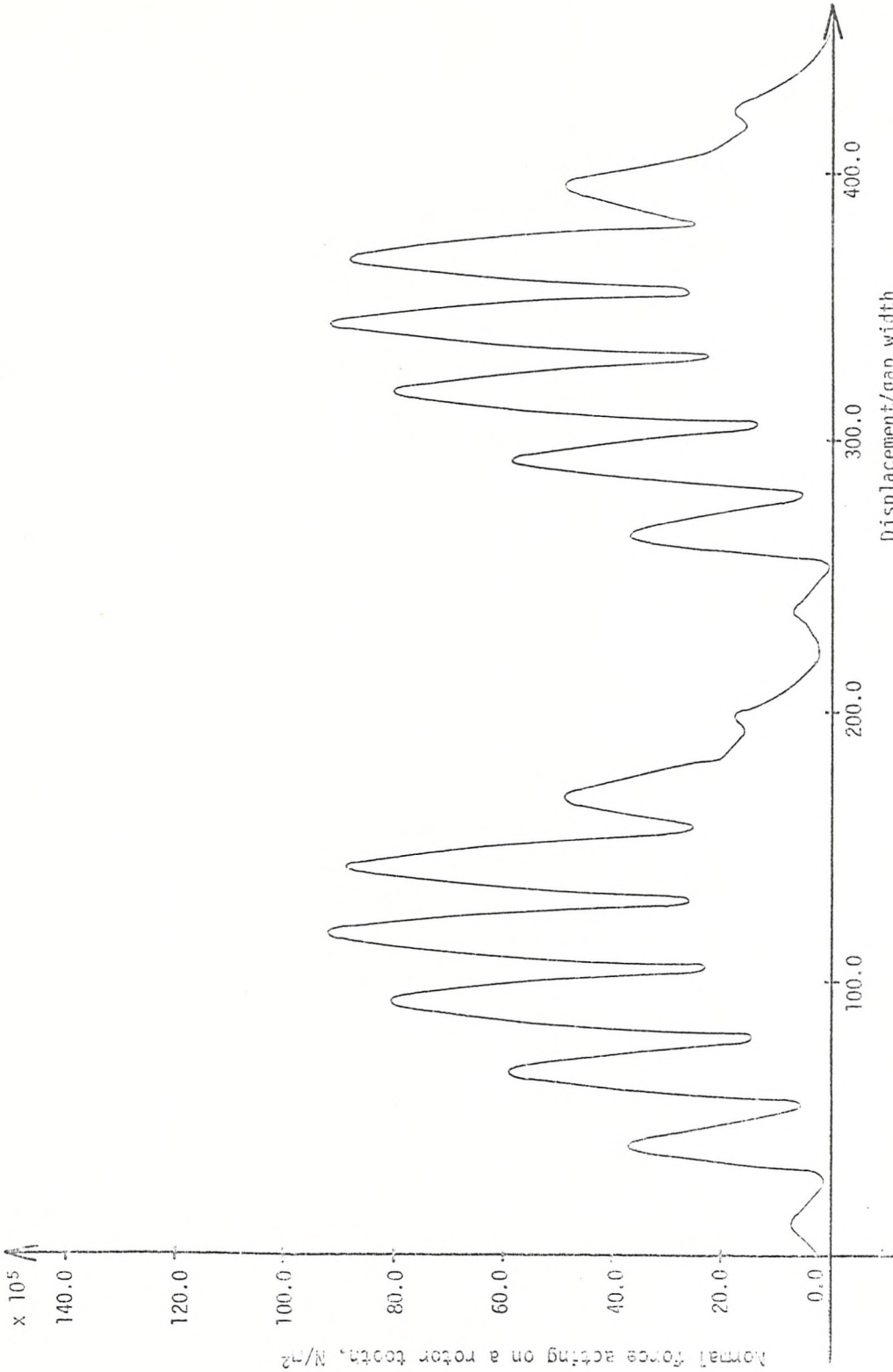

Figure 8.9 The variation in the normal force acting on a rotor tooth with the displacement of the rotor for the slot combination $N_S = 36$, $N_R = 42$

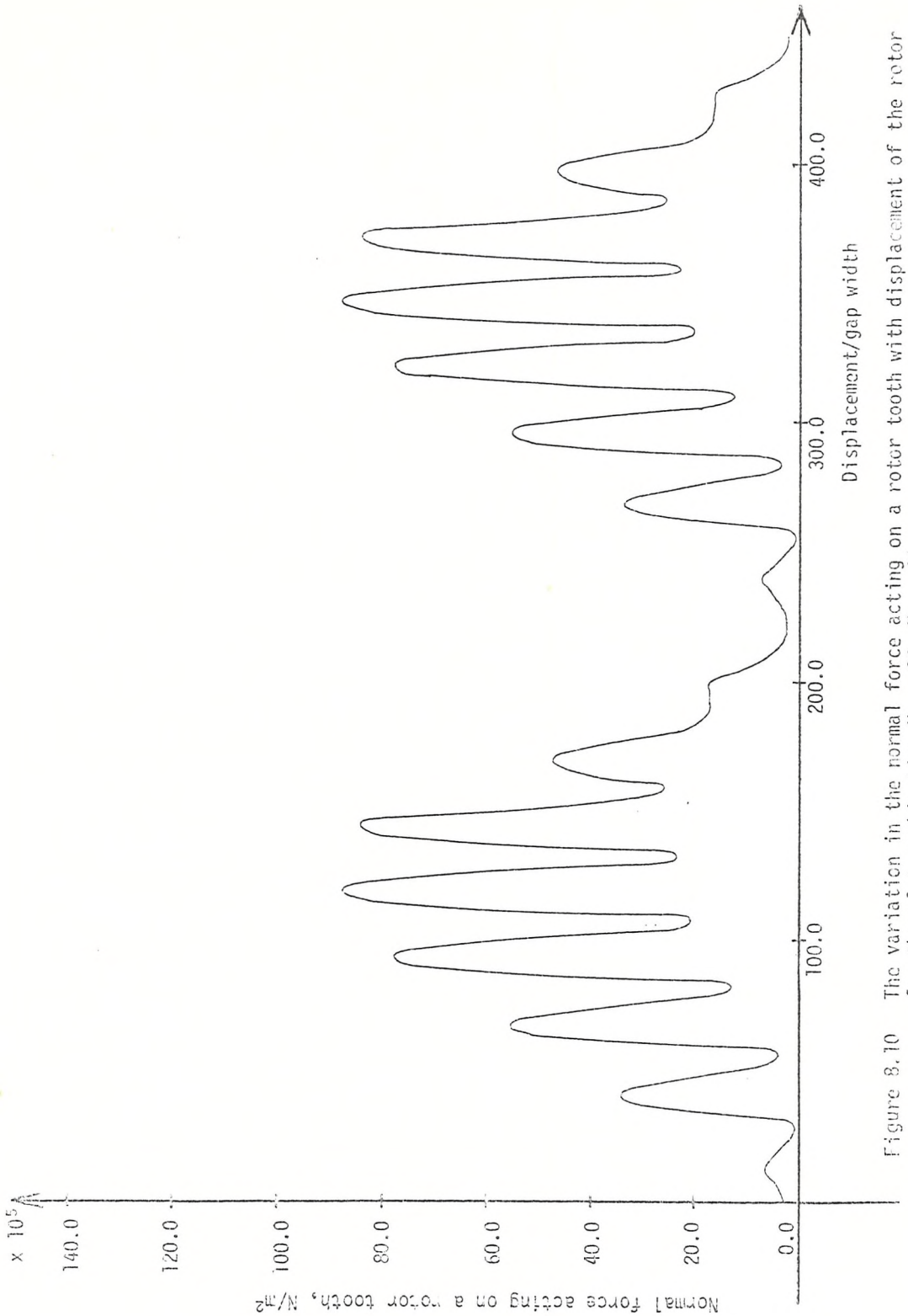

Figure 8.10 The variation in the normal force acting on a rotor tooth with displacement of the rotor for the slot combination $N_S = 36$, $N_R = 44$

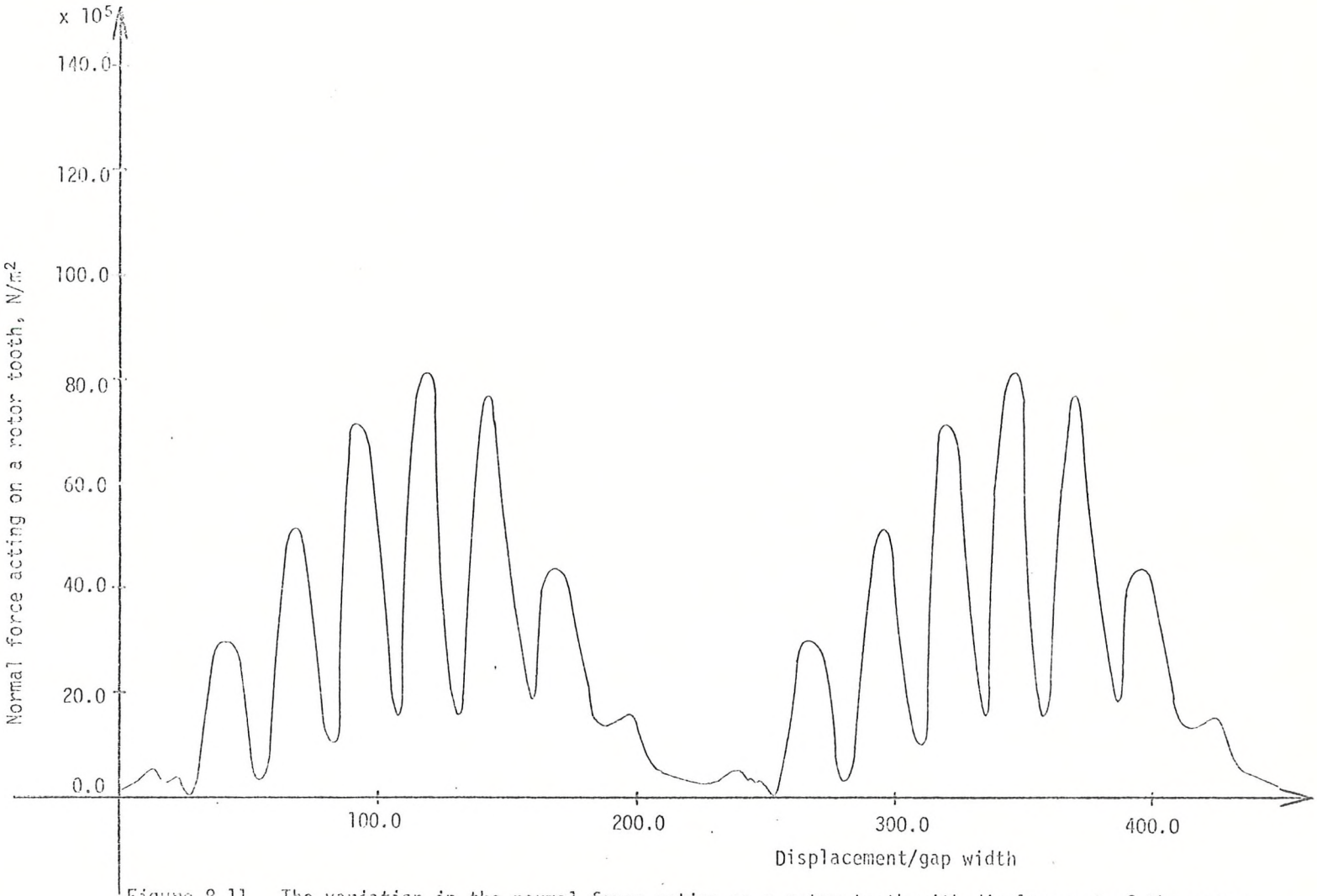

Figure 8.11 The variation in the normal force acting on a rotor tooth with displacement of the rotor for the slot combination $N_S = 36$, $N_R = 48$

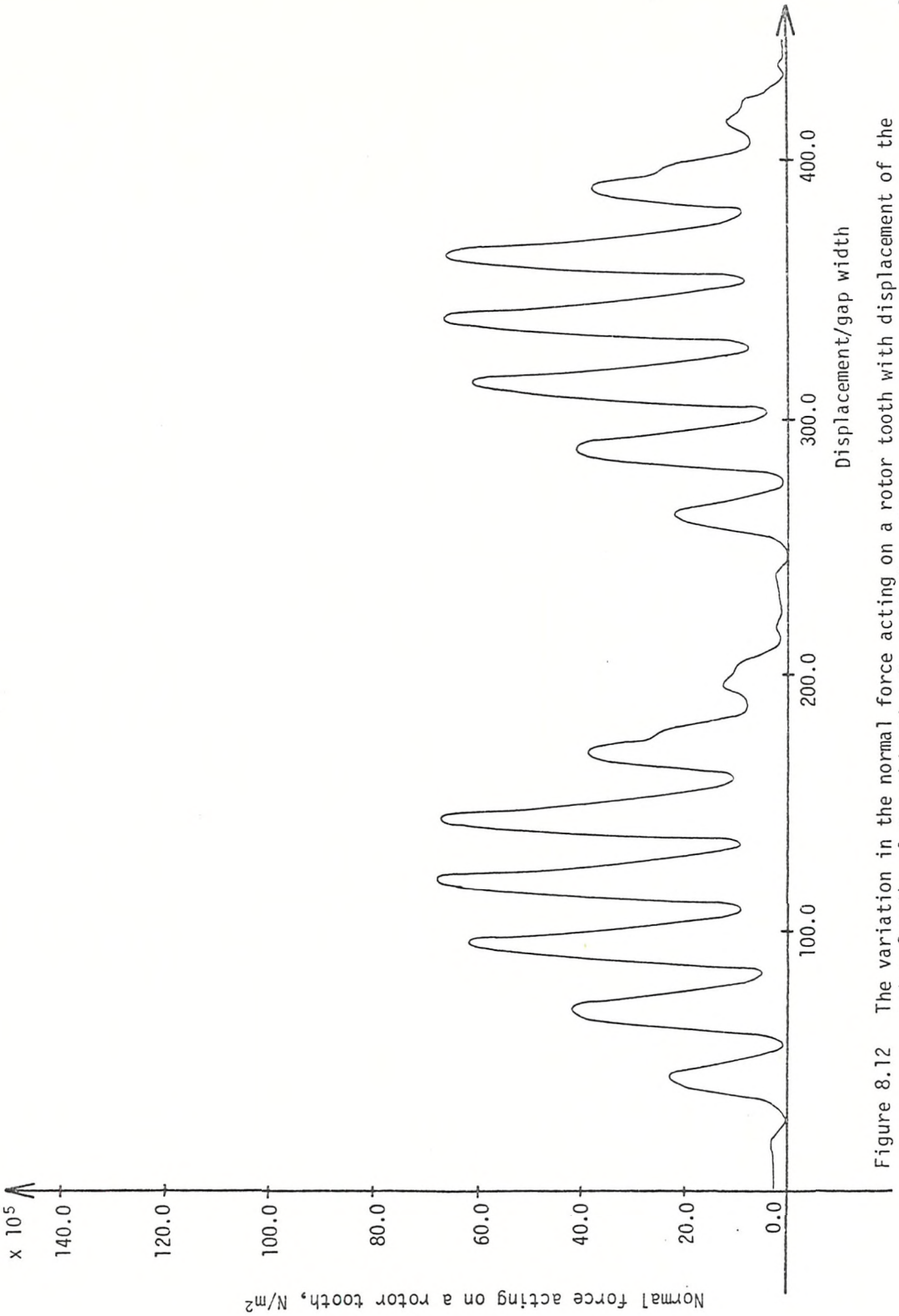

Figure 8.12 The variation in the normal force acting on a rotor tooth with displacement of the rotor for the slot combination $N_S = 36$, $N_R = 60$

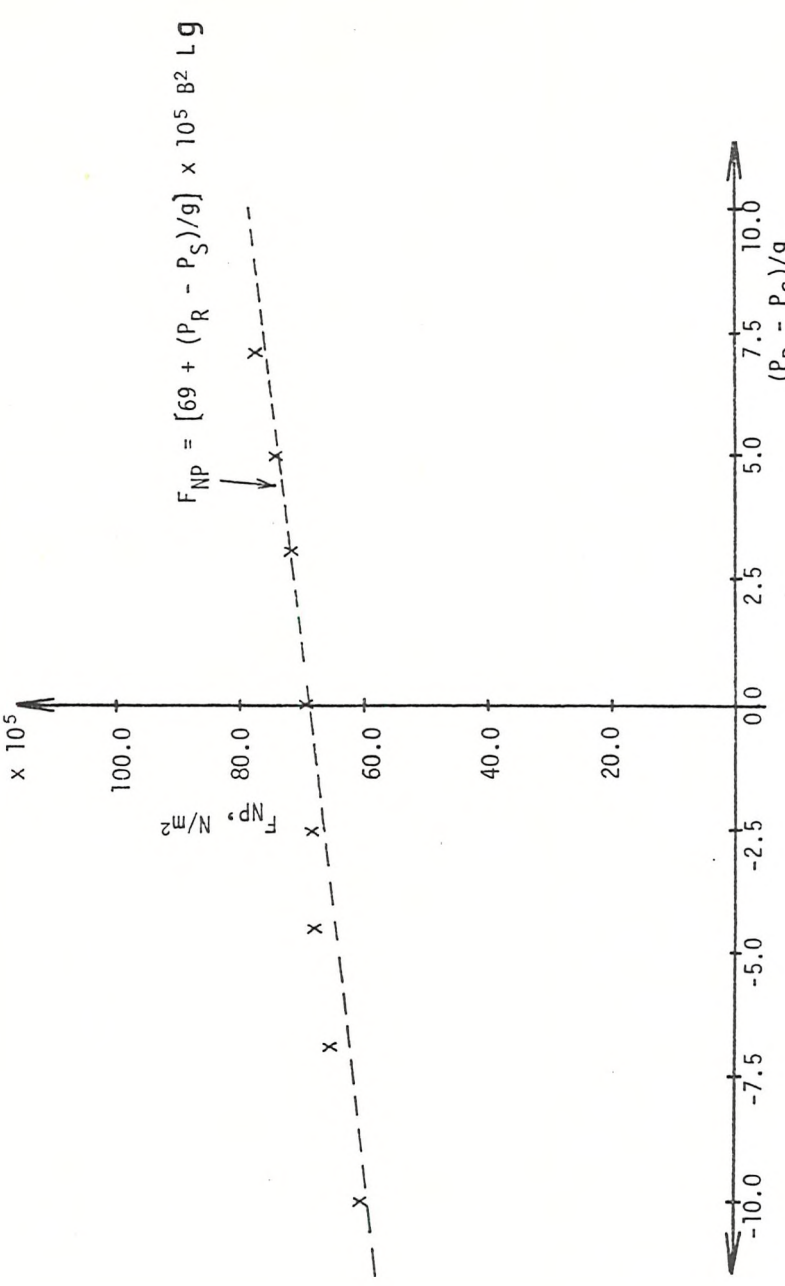

Figure 8.13 The variation in the peak to peak value of the largest normal force pulsation acting on a rotor tooth with difference in slot pitches

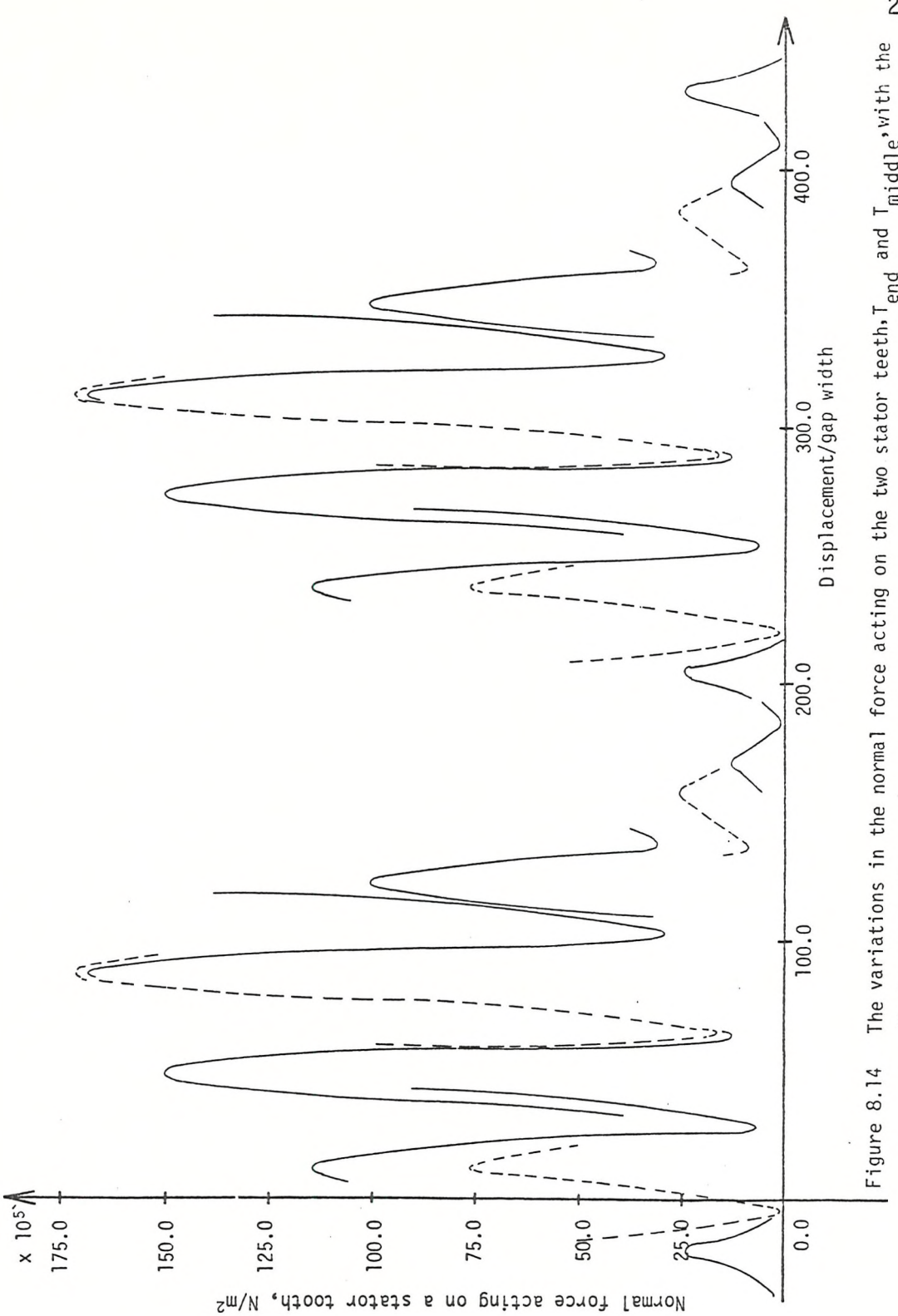

Figure 8.14 The variations in the normal force acting on the two stator teeth, T_{end} and T_{middle}, with the displacement of the rotor for the slot combination $N_S = 36$, $N_R = 24$

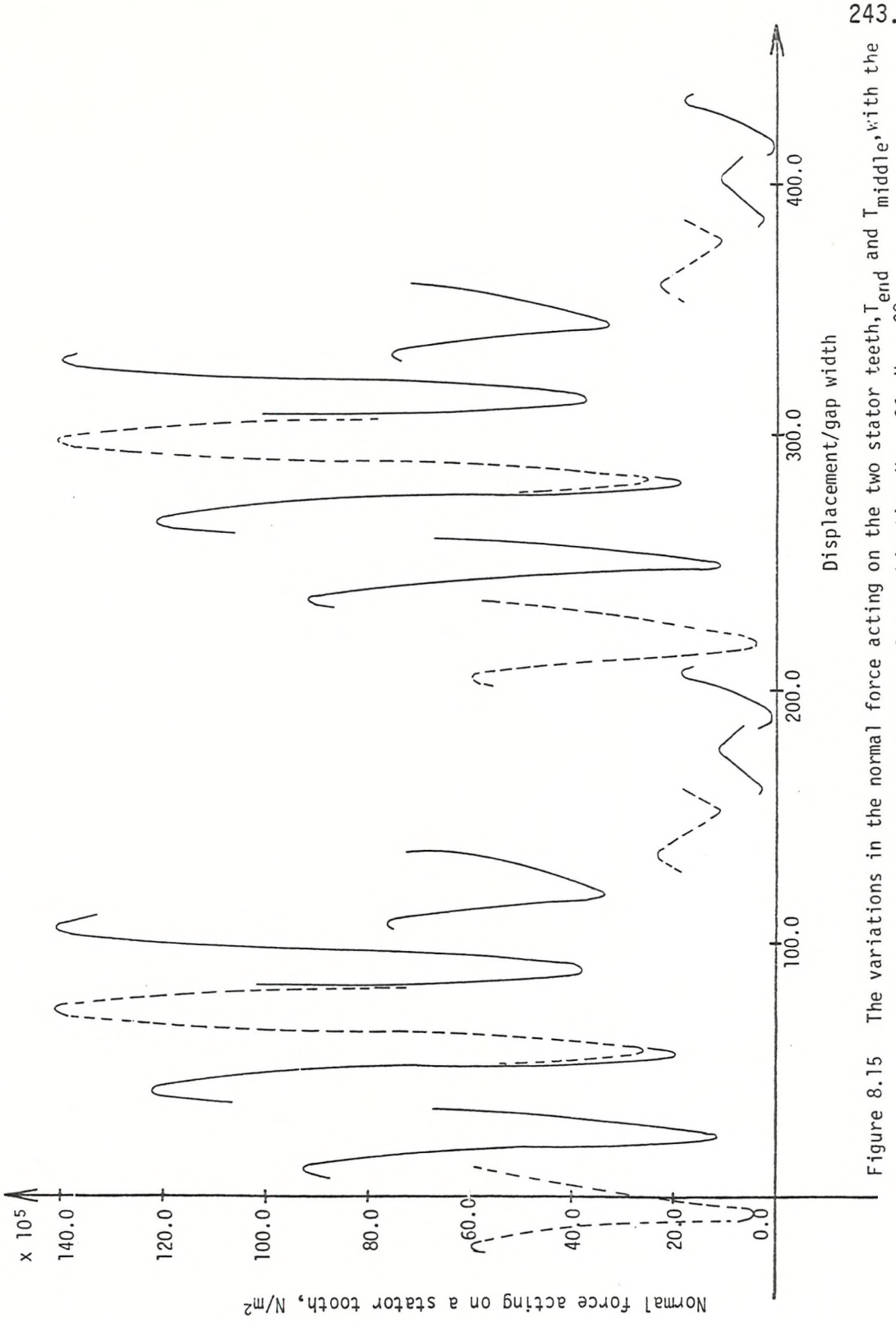

Figure 8.15 The variations in the normal force acting on the two stator teeth, T_{end} and T_{middle}, with the displacement of the rotor for the slot combination $N_S = 36$, $N_R = 28$

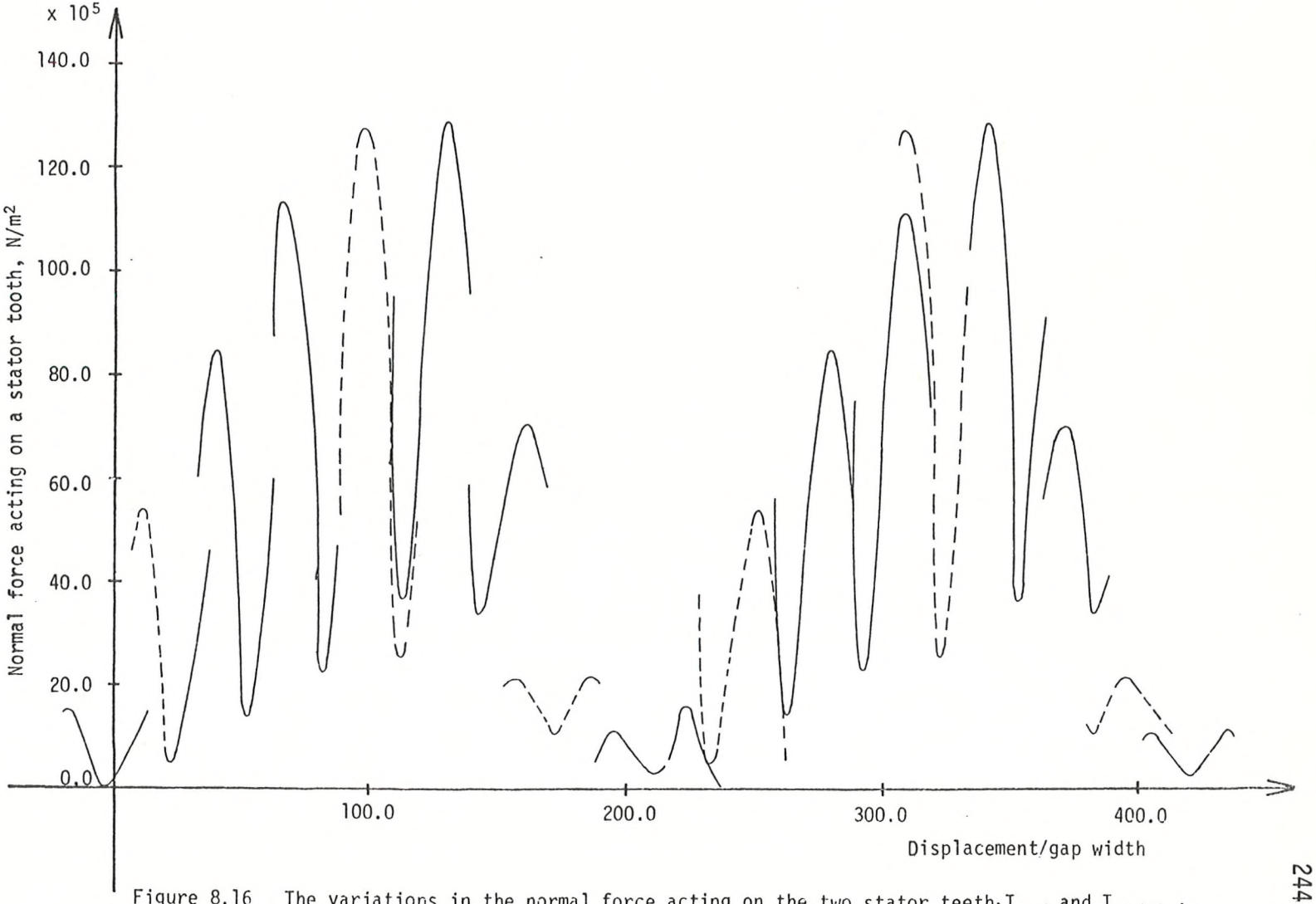

Figure 8.16 The variations in the normal force acting on the two stator teeth, T_{end} and T_{middle}, with the displacement of the rotor for the slot combination $N_S = 36$, $N_R = 30$

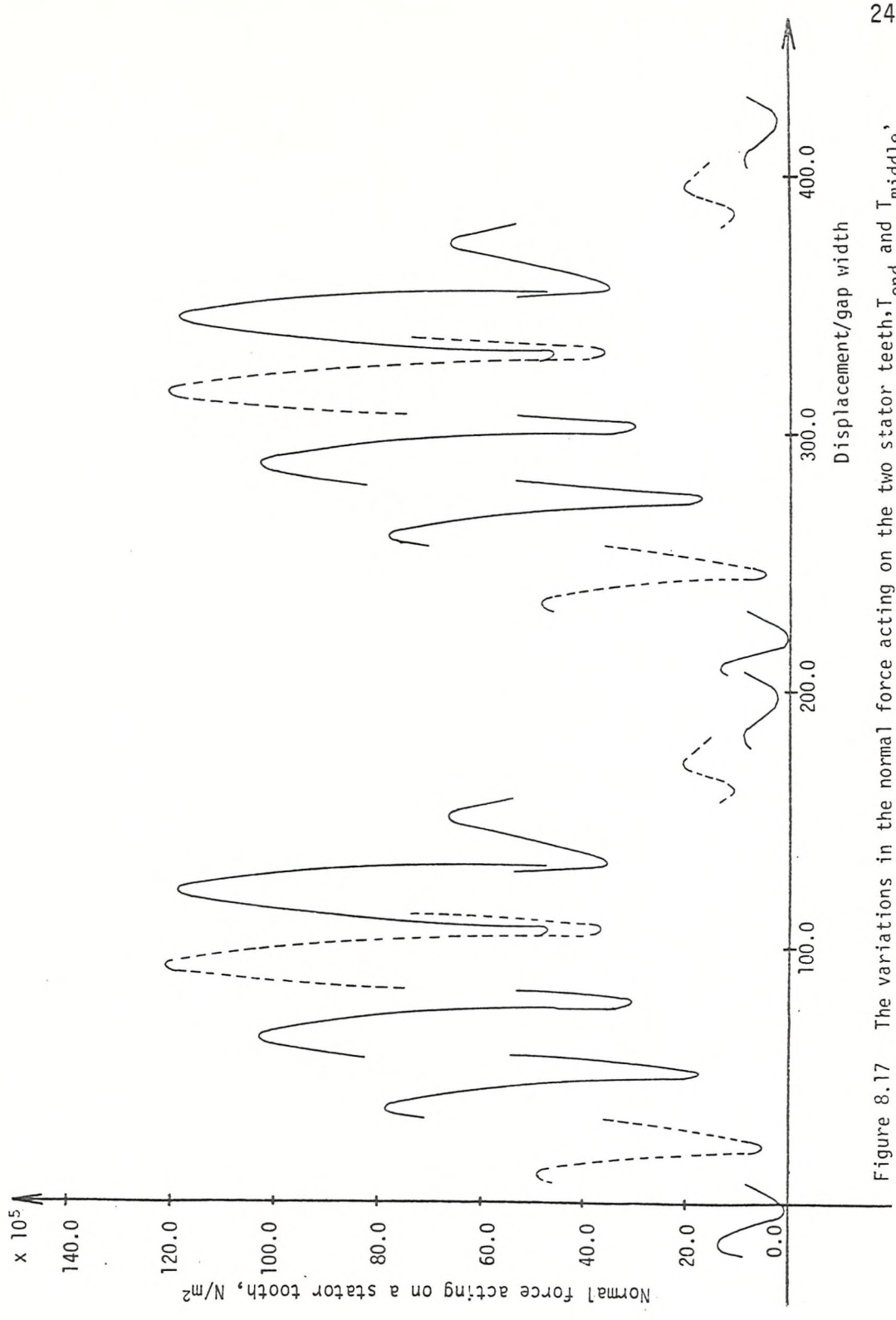

Figure 8.17 The variations in the normal force acting on the two stator teeth, T_{end} and T_{middle}, with the displacement of the rotor for the slot combination $N_S = 36$, $N_R = 32$

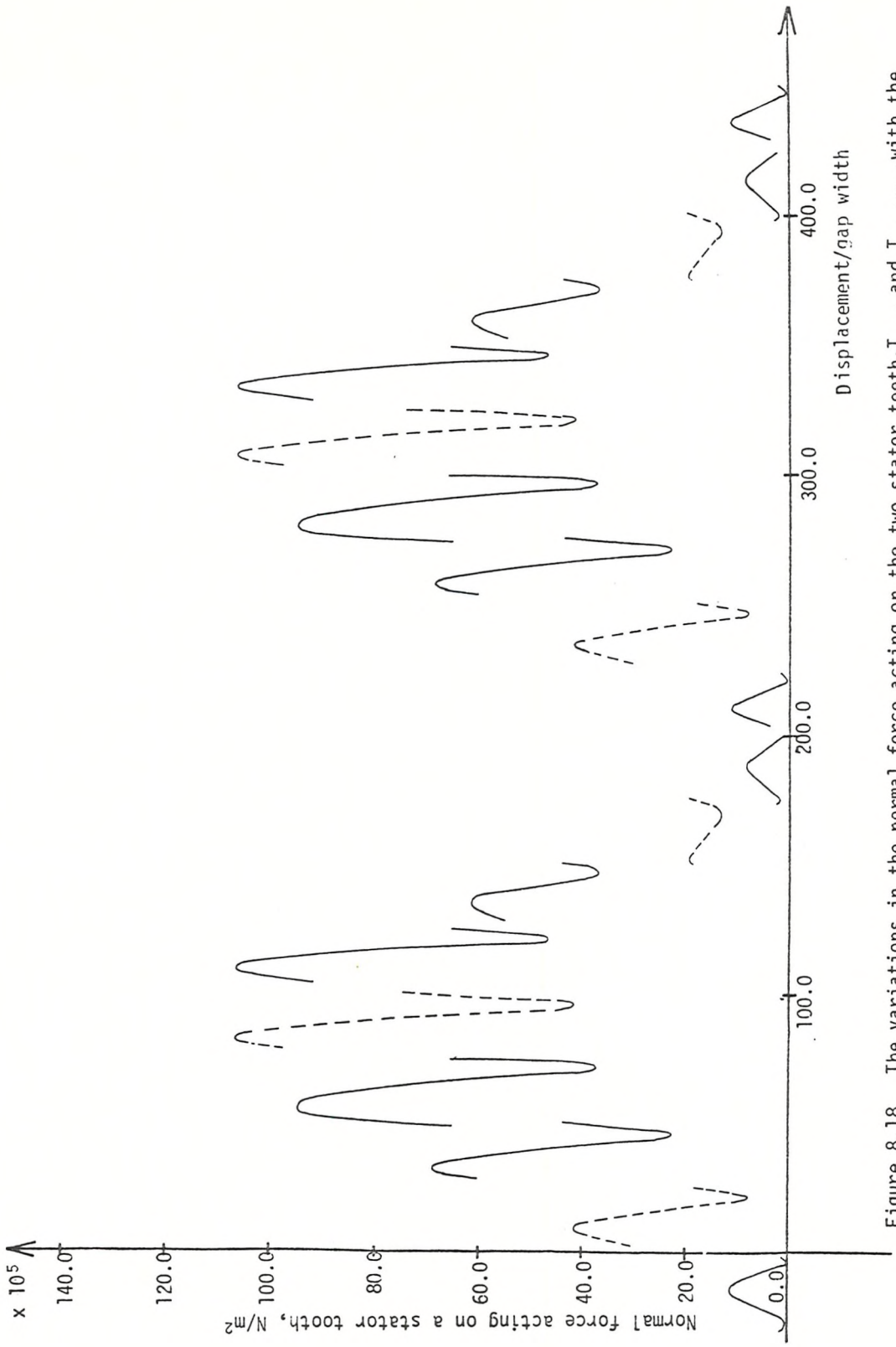

Figure 8.18 The variations in the normal force acting on the two stator teeth, T_{end} and T_{middle}, with the displacement of the rotor for the slot combination $N_S = 36$, $N_R = 36$

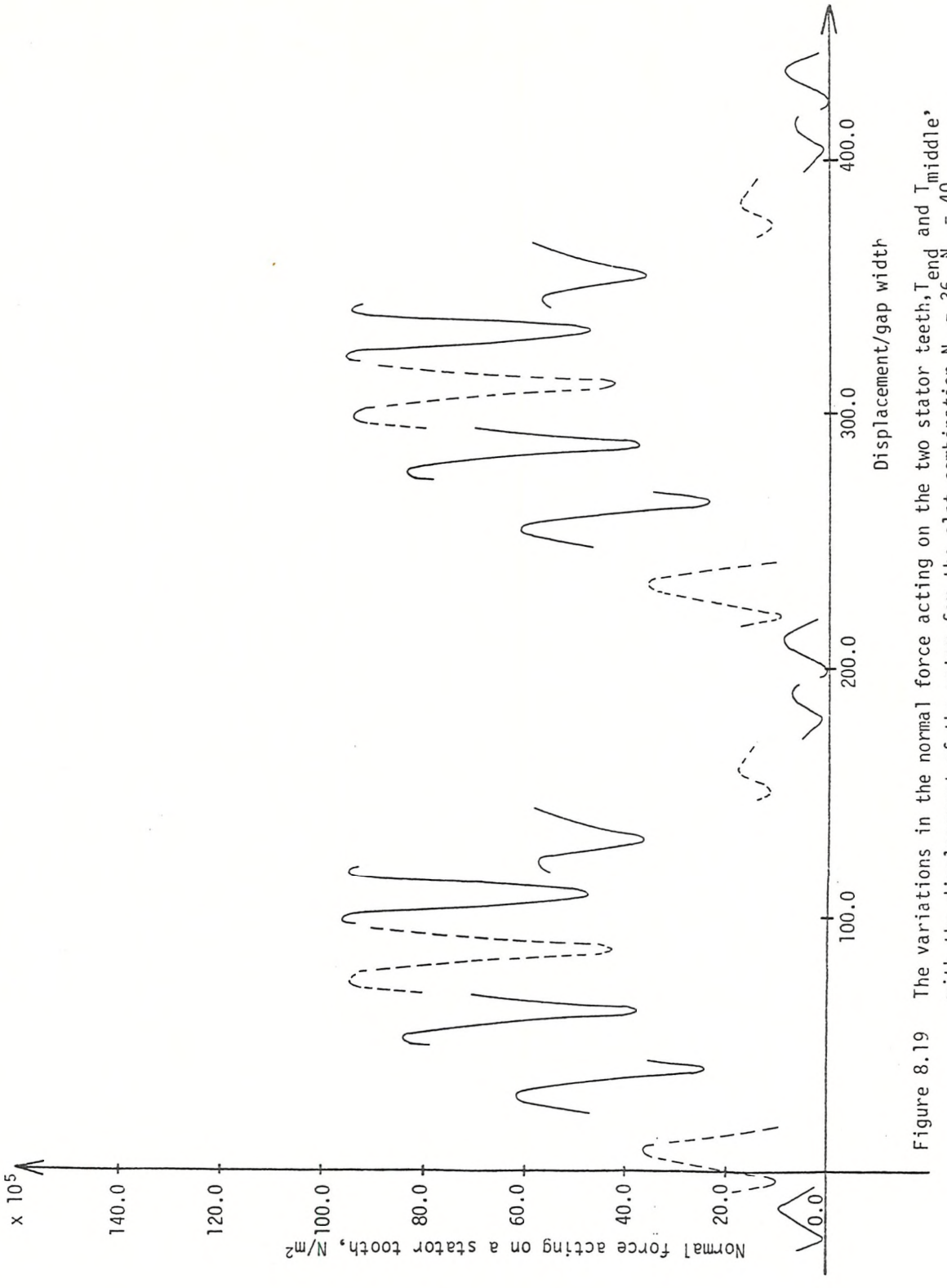

Figure 8.19 The variations in the normal force acting on the two stator teeth, T_{end} and T_{middle}, with the displacement of the rotor for the slot combination $N_S = 36$, $N_R = 40$

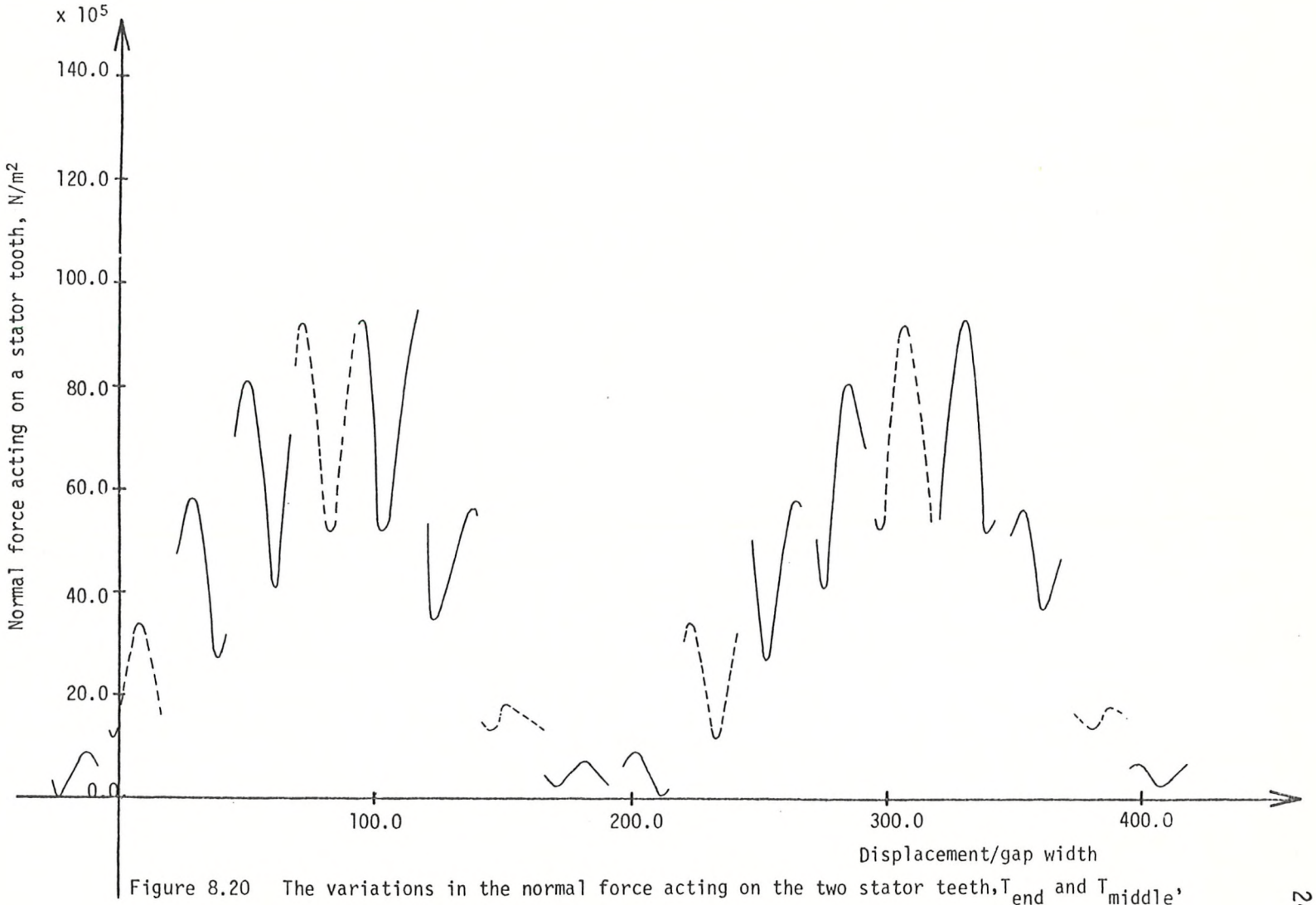

Figure 8.20 The variations in the normal force acting on the two stator teeth, T_{end} and T_{middle}, with the displacement of the rotor for the slot combination $N_S = 36$, $N_R = 42$

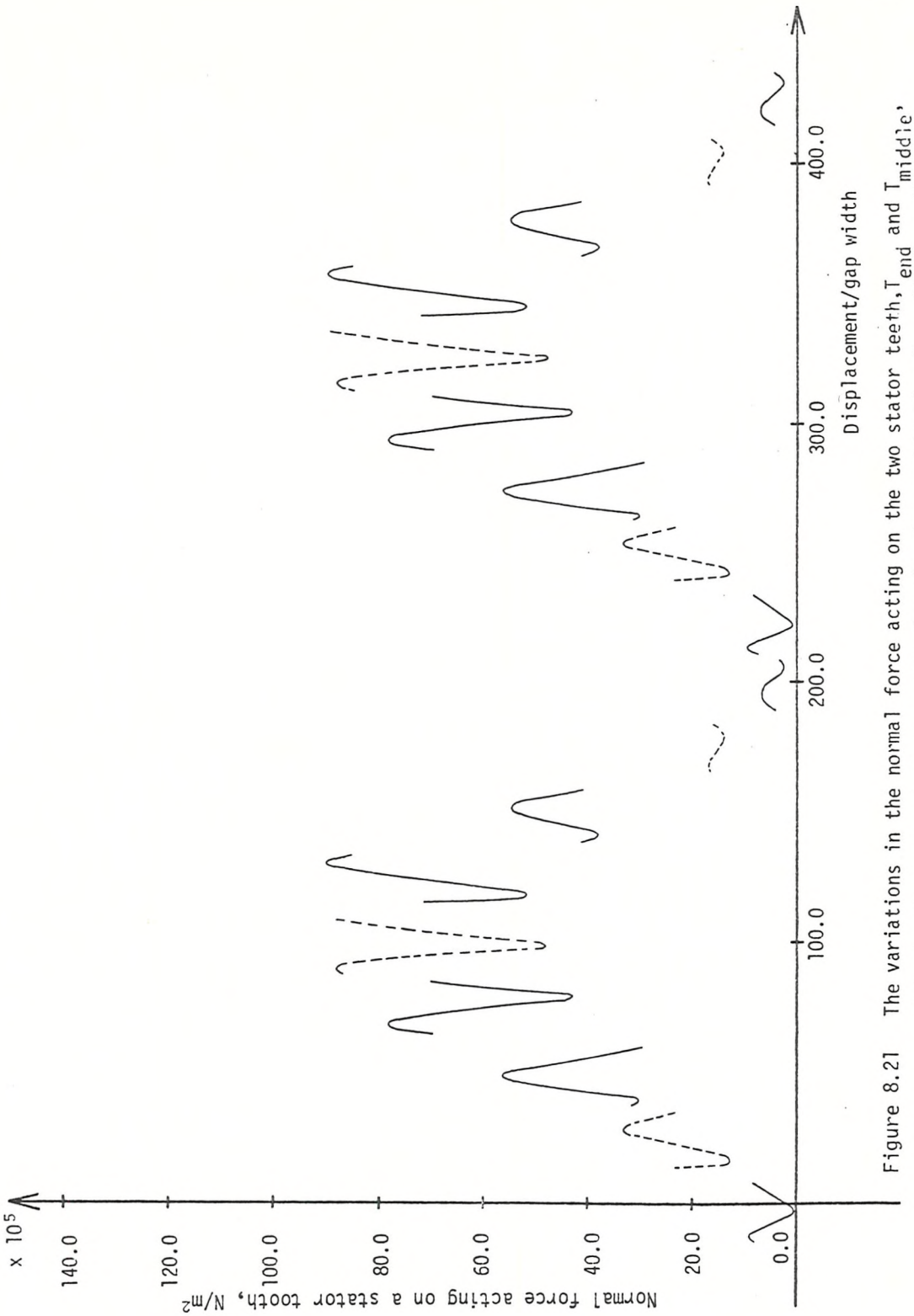

Figure 8.21 The variations in the normal force acting on the two stator teeth, T_{end} and T_{middle}, with the displacement of the rotor for the slot combination $N_S = 36$, $N_R = 44$

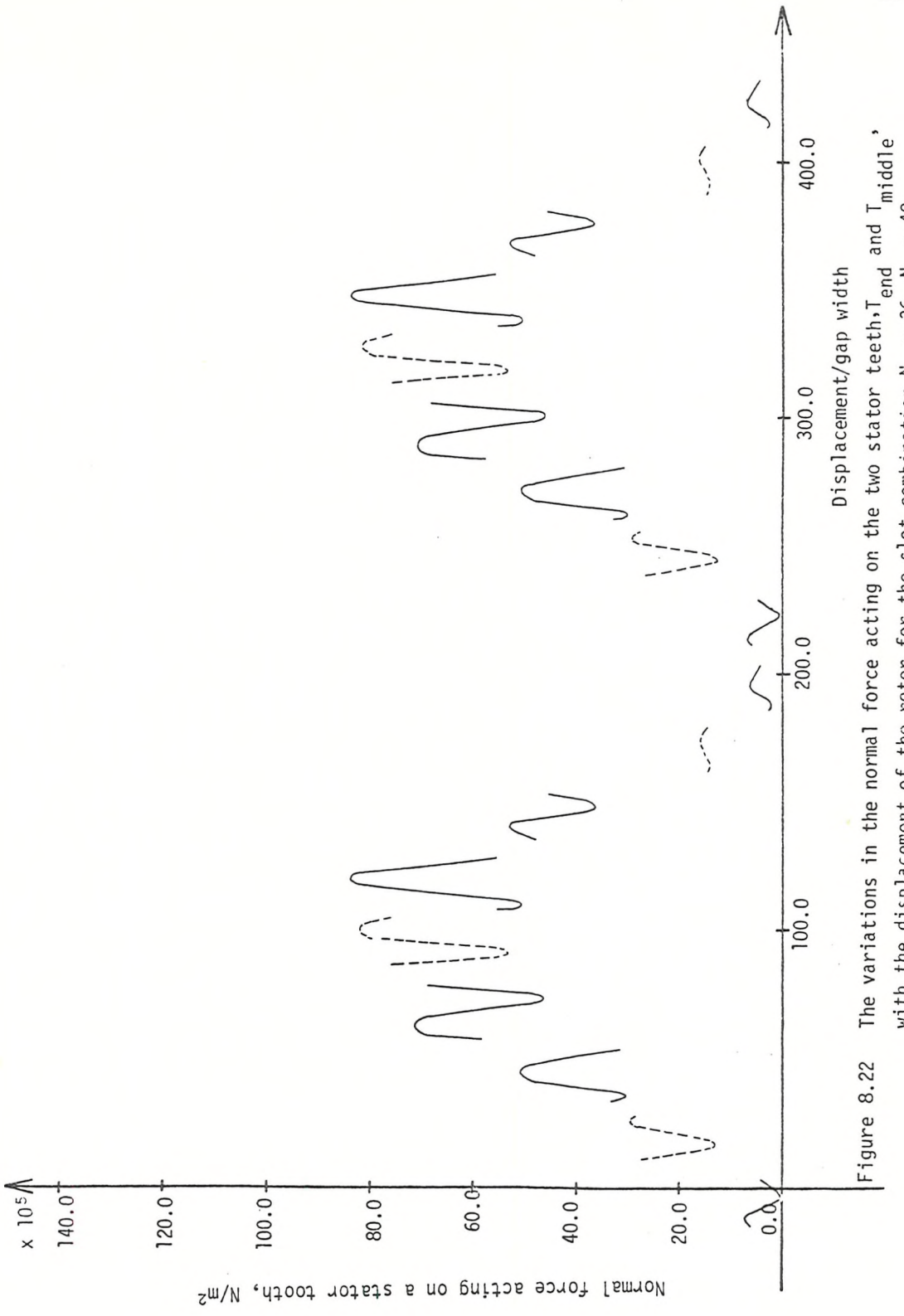

Figure 8.22 The variations in the normal force acting on the two stator teeth, T_{end} and T_{middle}, with the displacement of the rotor for the slot combination $N_S = 36$, $N_R = 48$

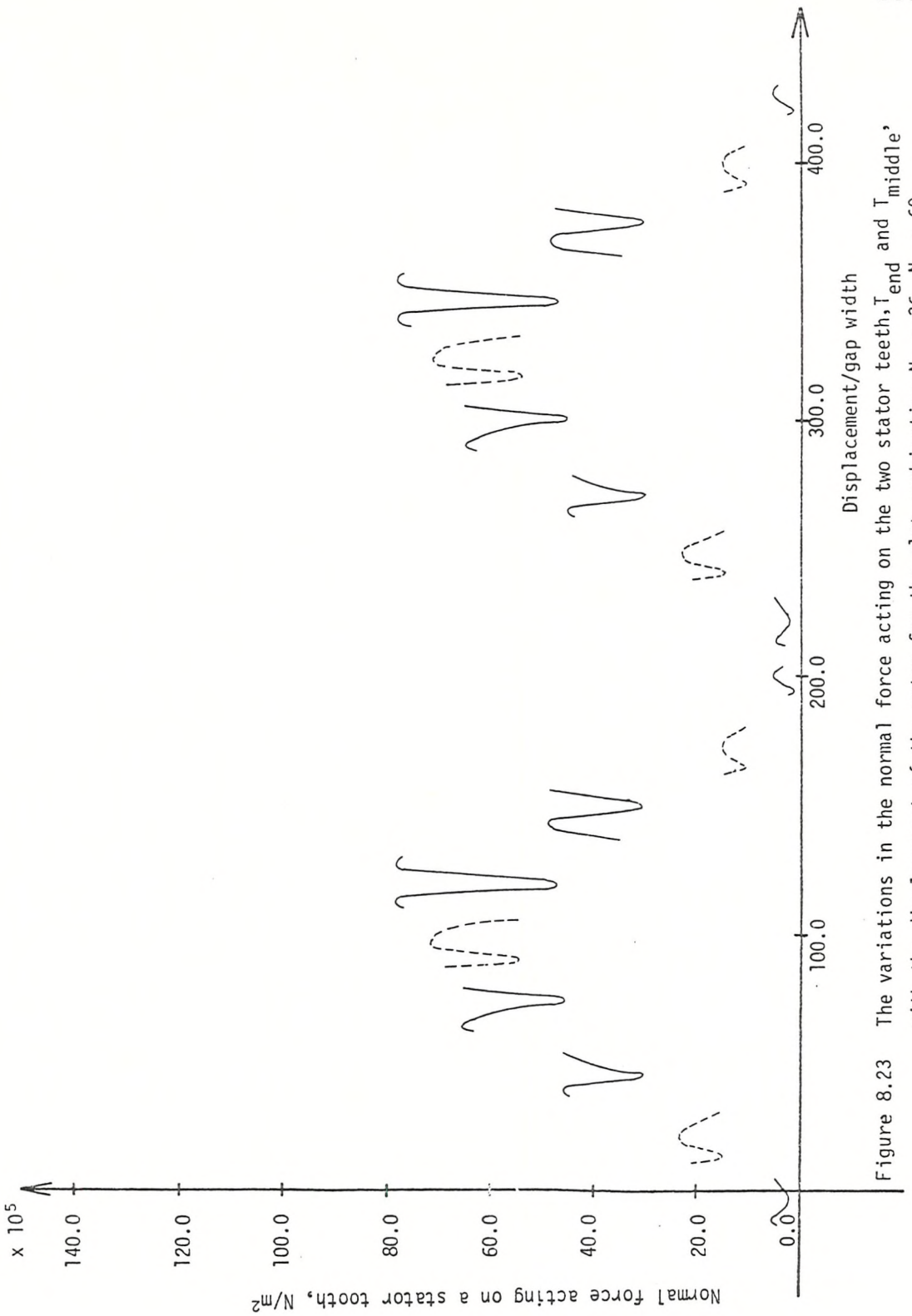

Figure 8.23 The variations in the normal force acting on the two stator teeth, T_{end} and T_{middle}, with the displacement of the rotor for the slot combination $N_S = 36$, $N_R = 60$

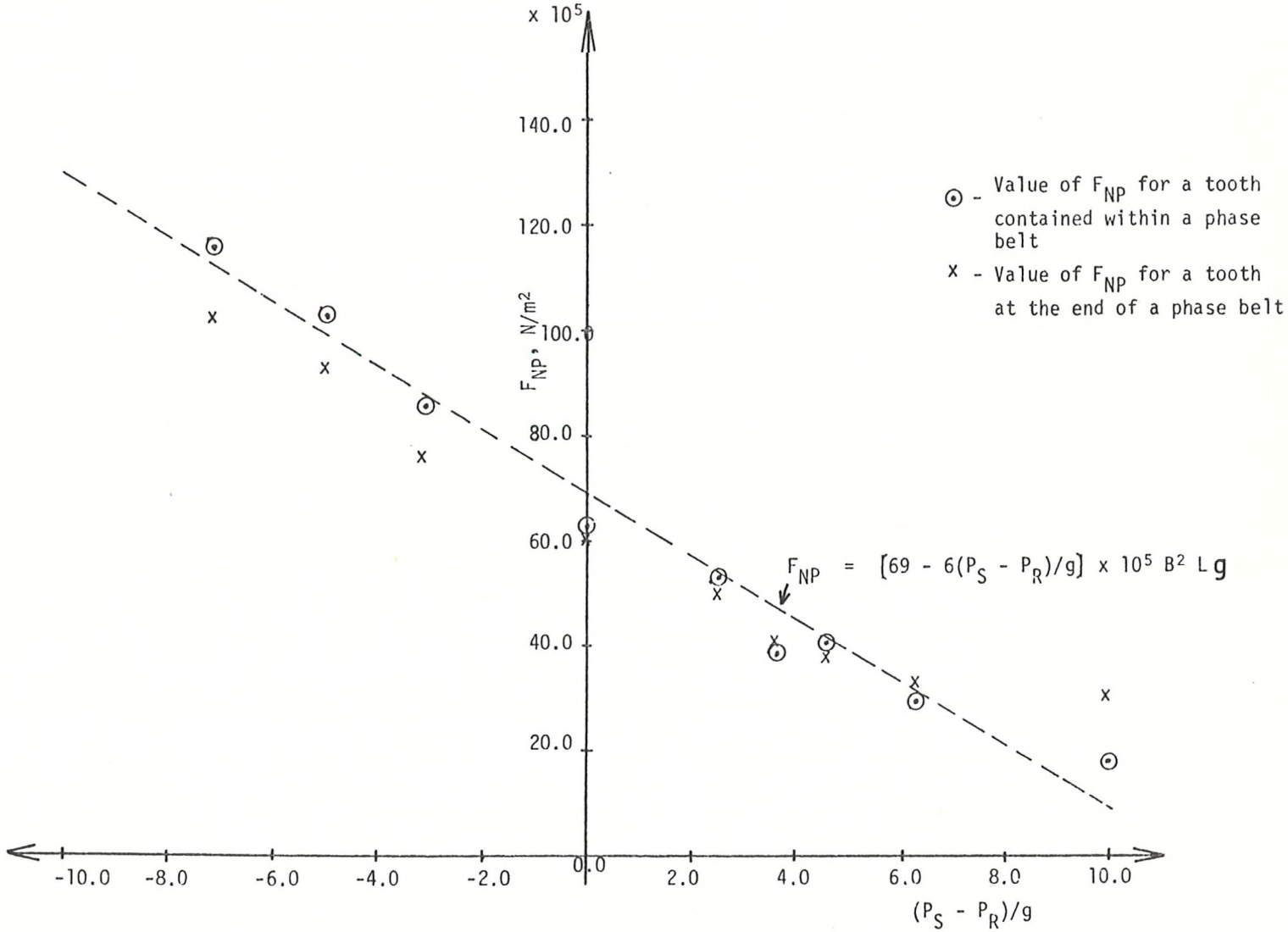

Figure 8.24 The variations in the peak to peak values of the largest normal force pulsation acting on the two stator teeth (T_{end}, T_{middle}) with the difference in slot pitches.

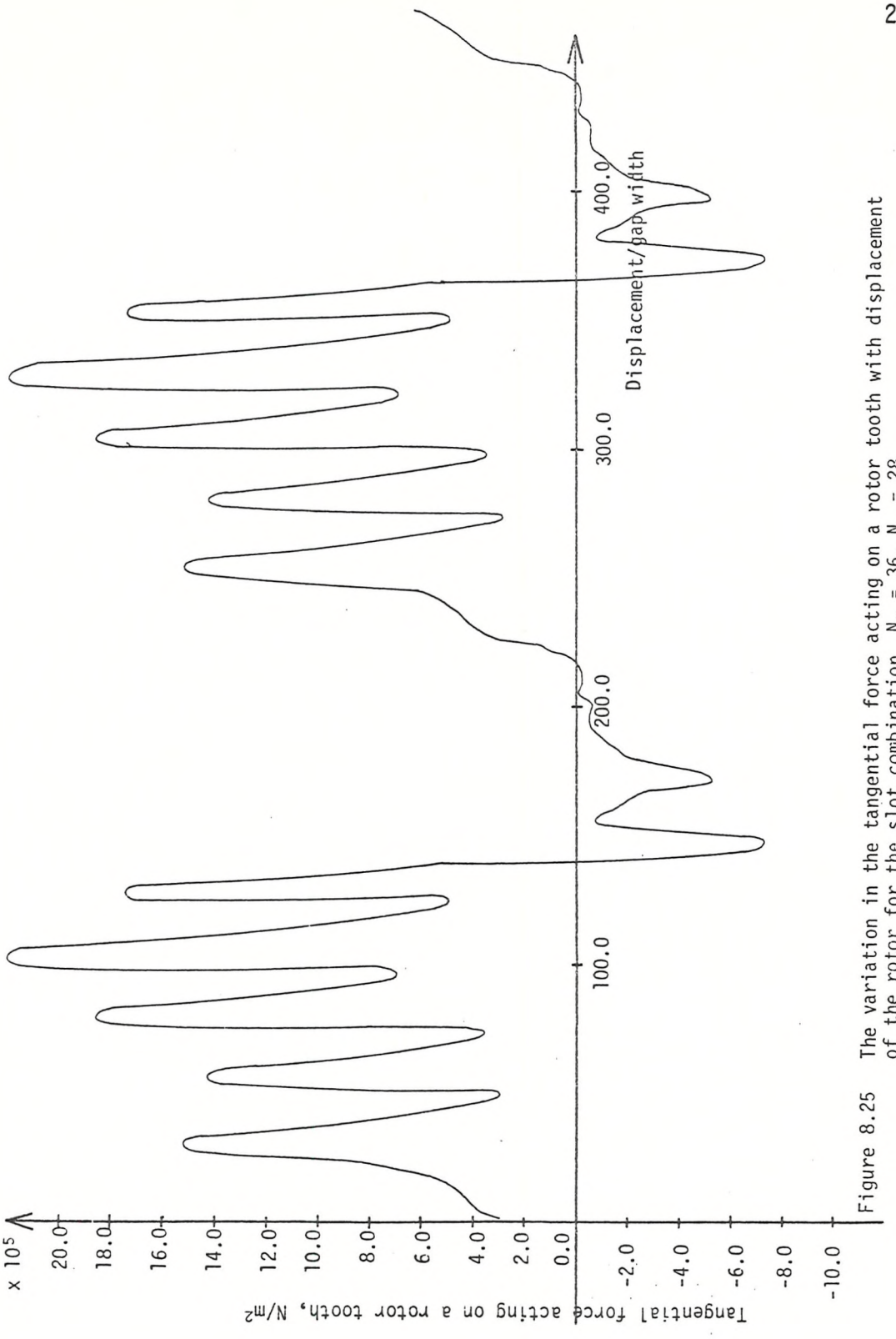

Figure 8.25 The variation in the tangential force acting on a rotor tooth with displacement of the rotor for the slot combination $N_S = 36$, $N_R = 28$

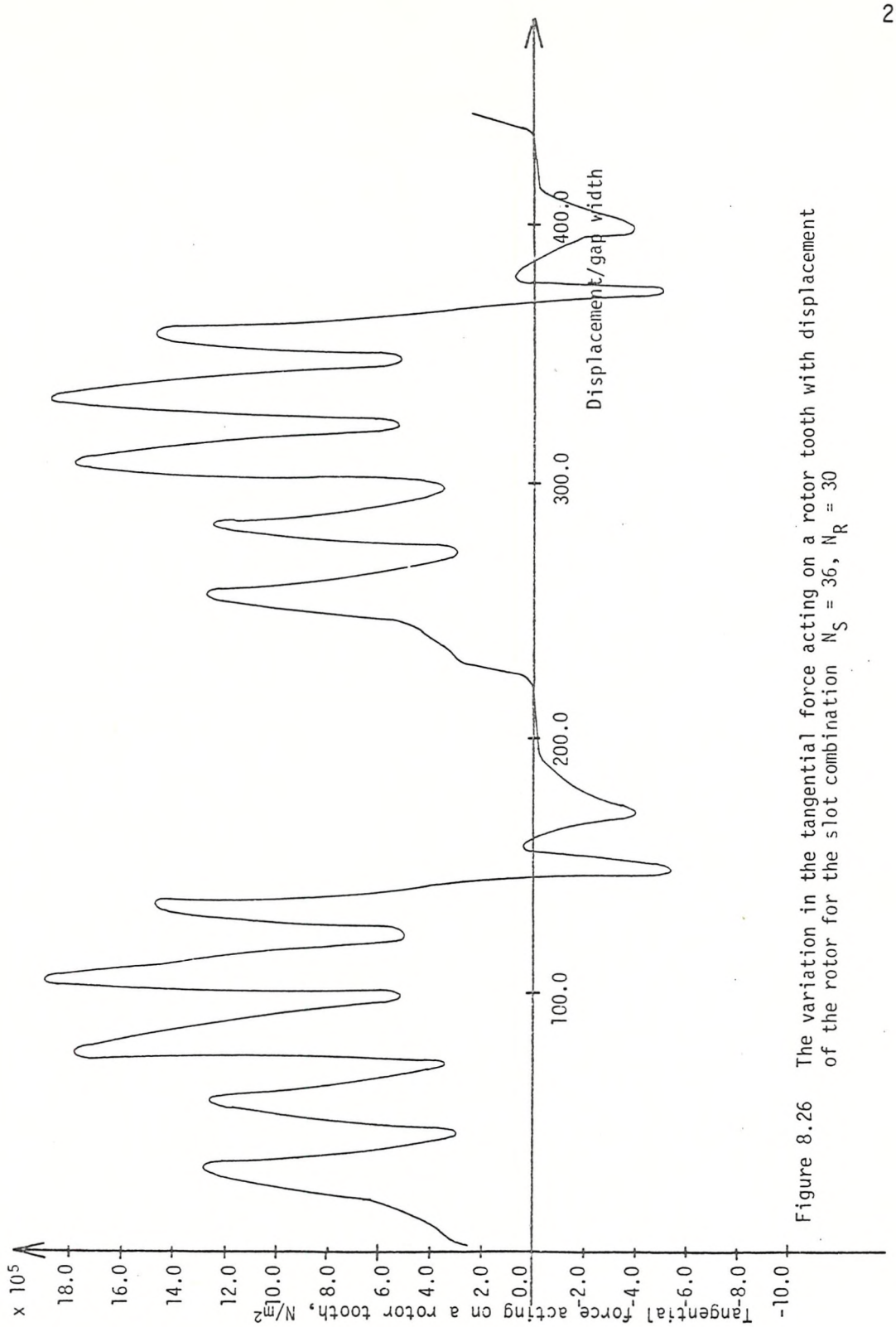

Figure 8.26 The variation in the tangential force acting on a rotor tooth with displacement of the rotor for the slot combination $N_S = 36$, $N_R = 30$

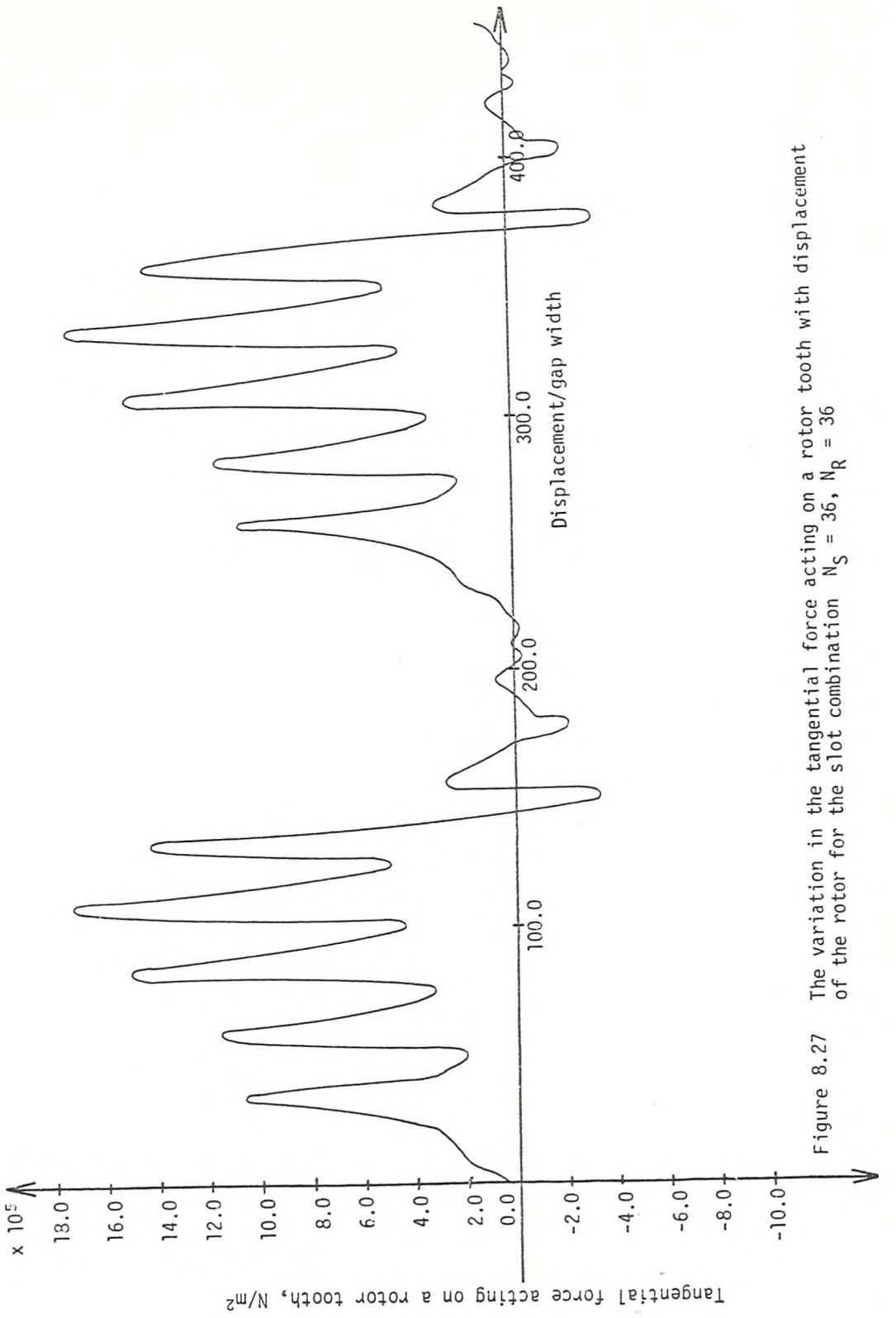

Figure 8.27 The variation in the tangential force acting on a rotor tooth with displacement of the rotor for the slot combination $N_S = 36$, $N_R = 36$

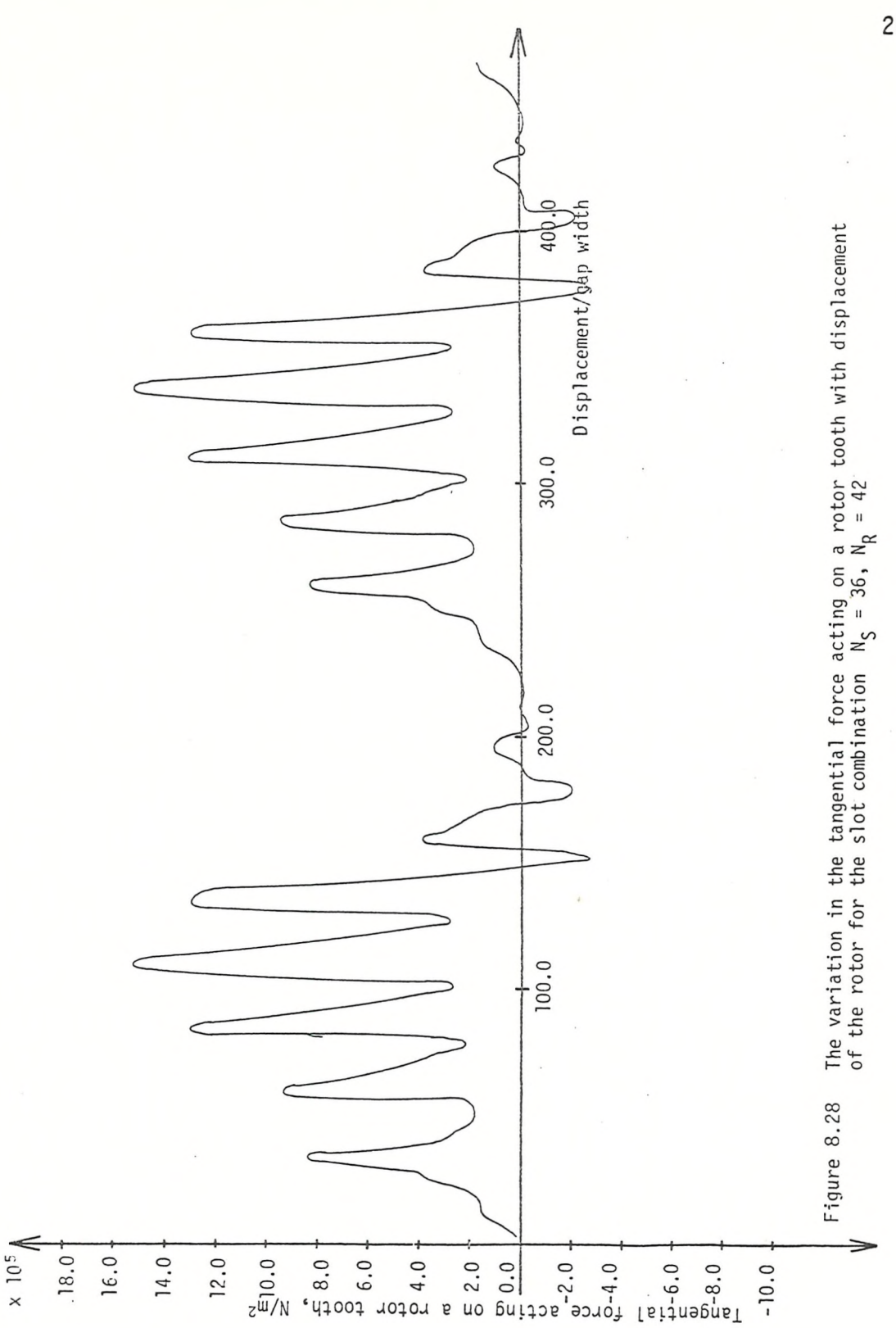

Figure 8.28 The variation in the tangential force acting on a rotor tooth with displacement of the rotor for the slot combination $N_S = 36$, $N_R = 42$

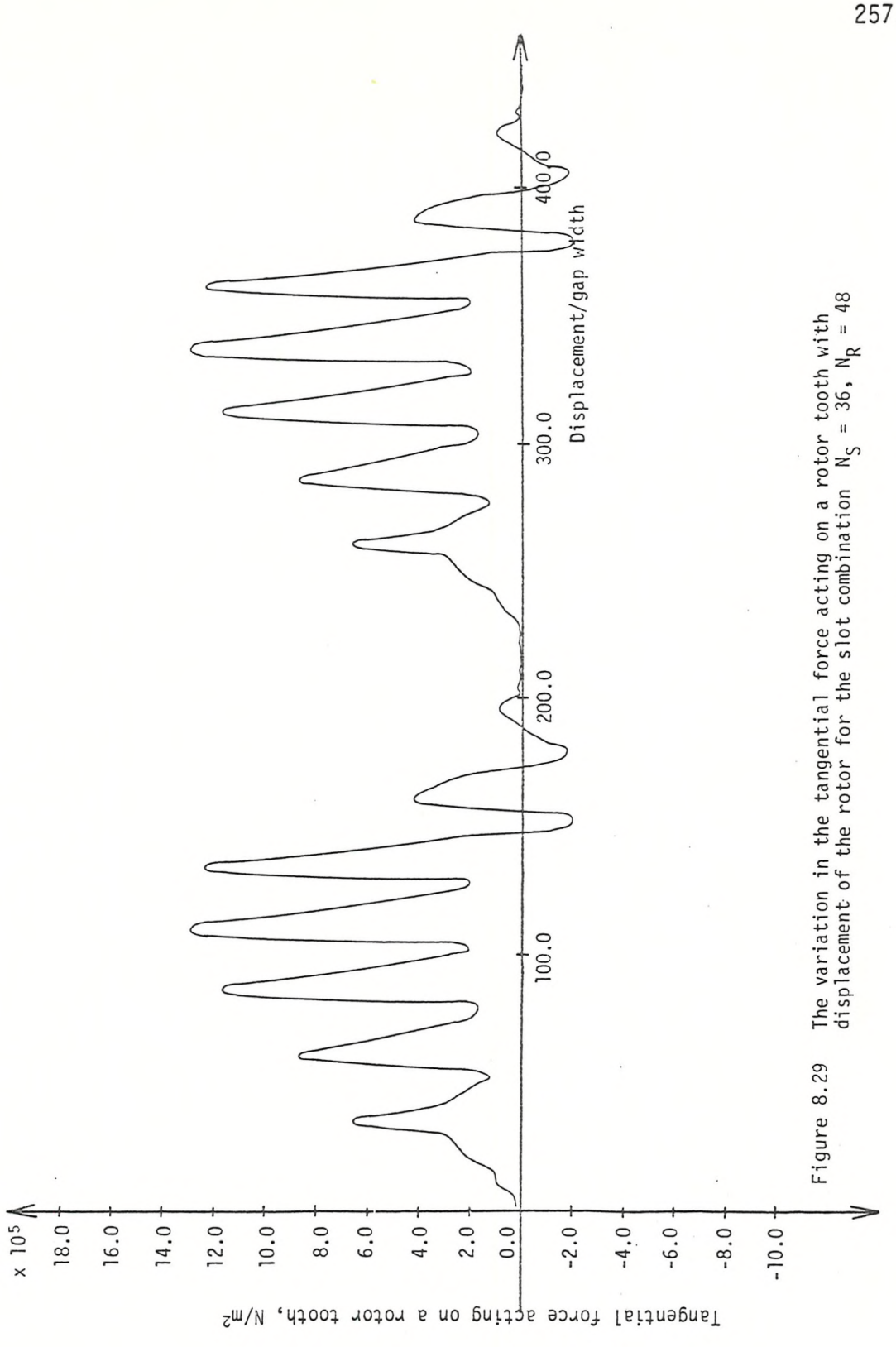

Figure 8.29 The variation in the tangential force acting on a rotor tooth with displacement of the rotor for the slot combination $N_S = 36$, $N_R = 48$

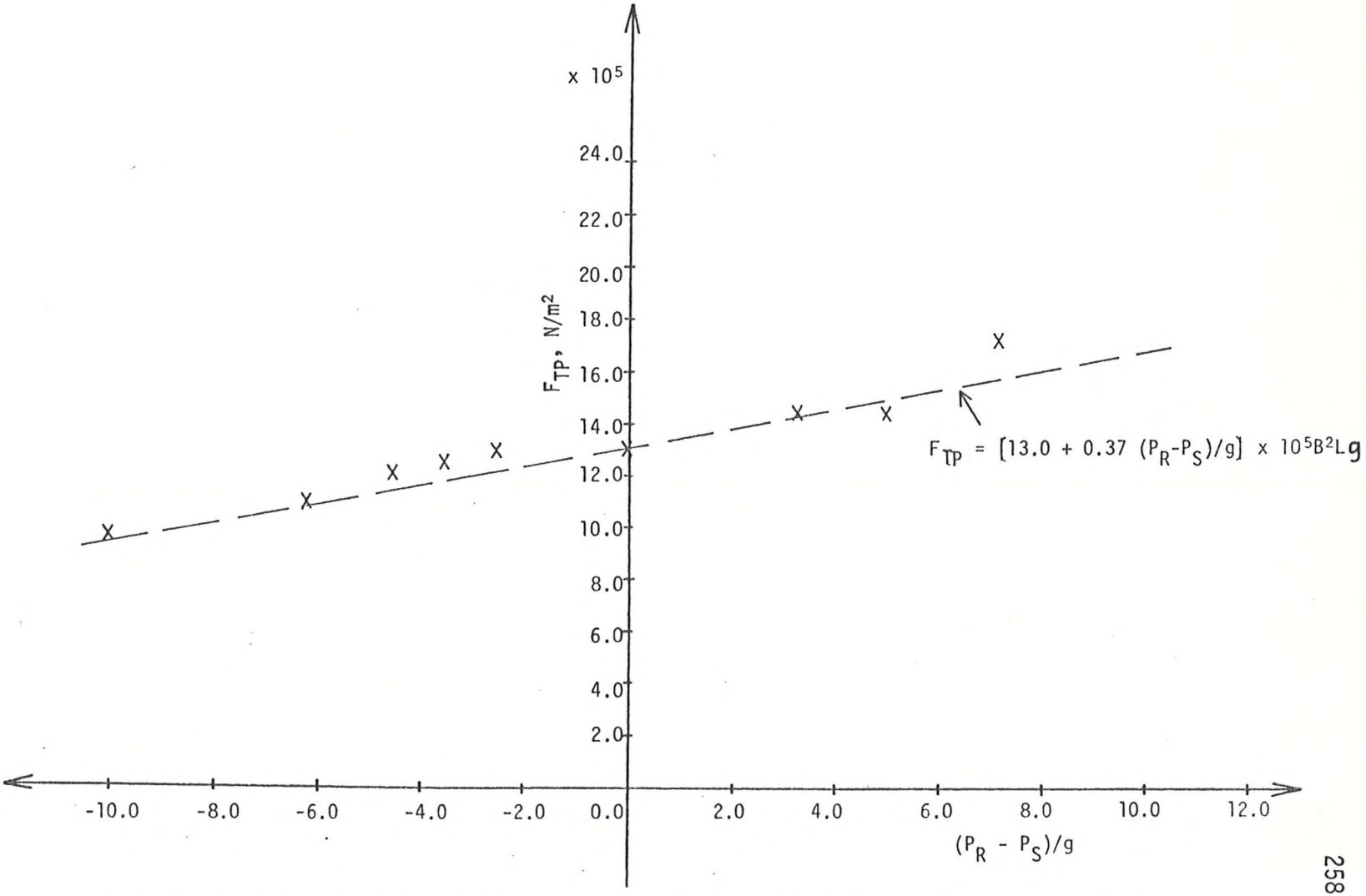

Figure 8.30 The varaition in the peak to peak value of the largest tangential force pulsation acting on a rotor tooth with the difference in slot pitches

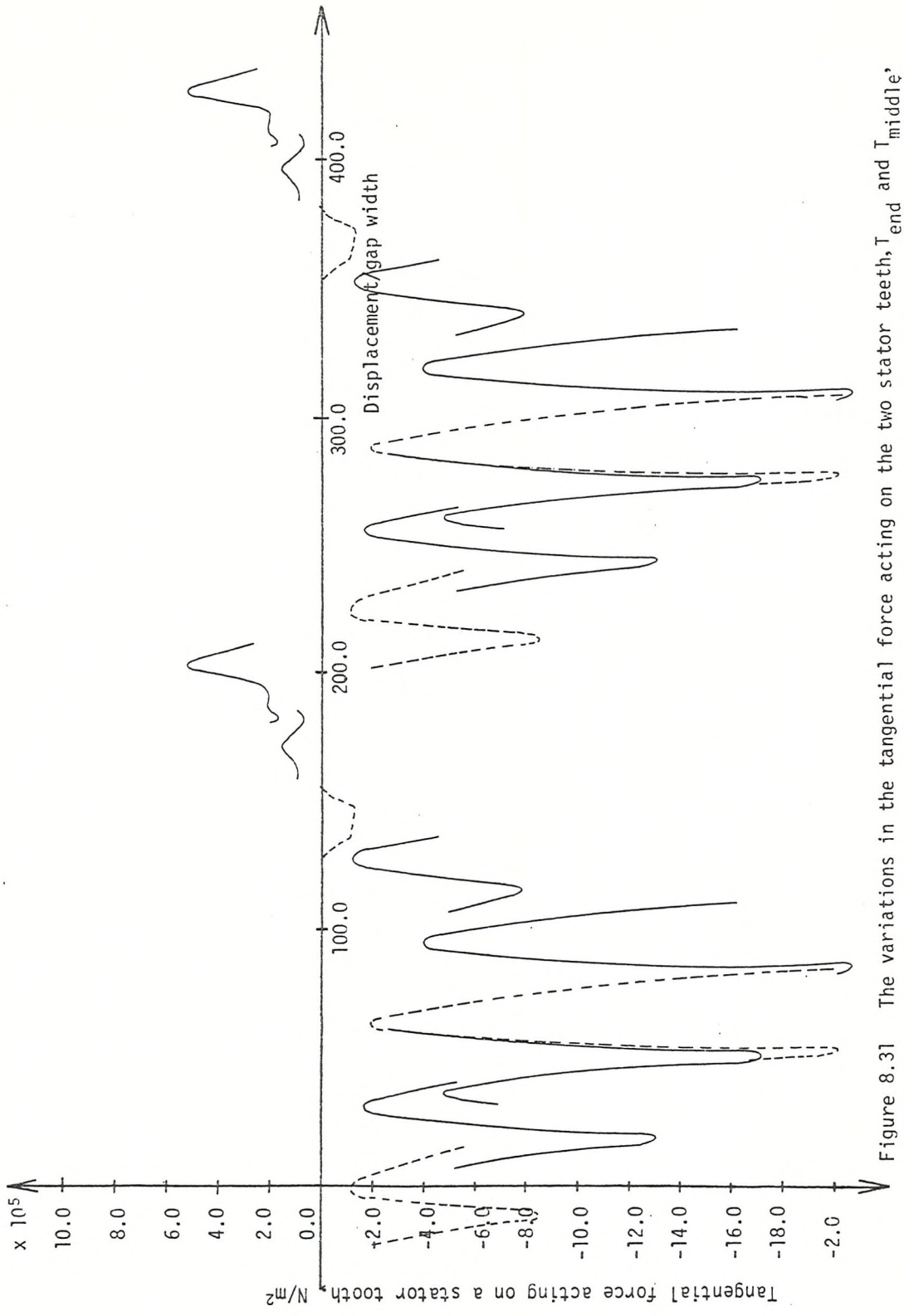

Figure 8.31 The variations in the tangential force acting on the two stator teeth, T_{end} and T_{middle}, with displacement of the rotor for the slot combination $N_S = 36$, $N_R = 28$

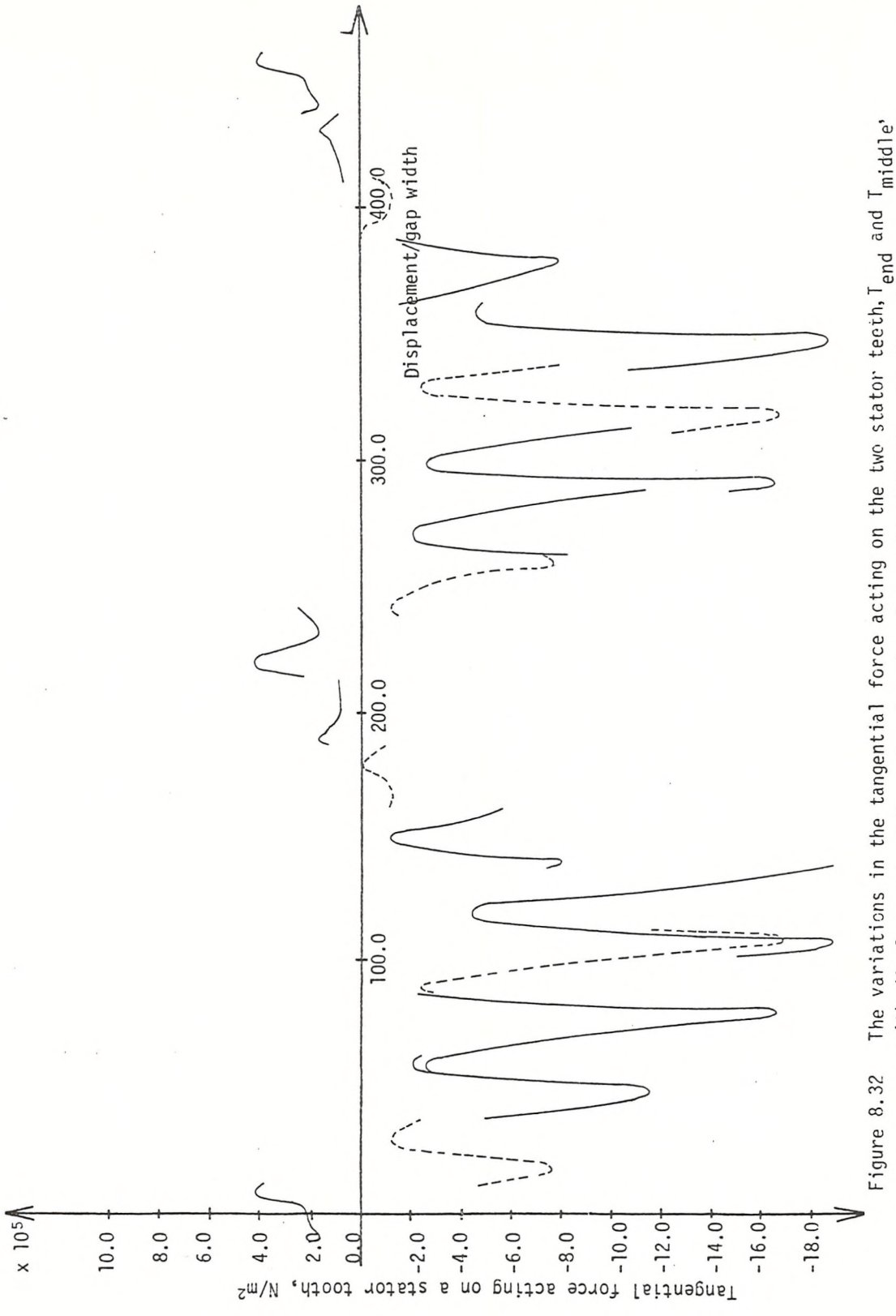

Figure 8.32 The variations in the tangential force acting on the two stator teeth, T_{end} and T_{middle}, with displacement of the rotor for the slot combination $N_S = 36$, $N_R = 30$.

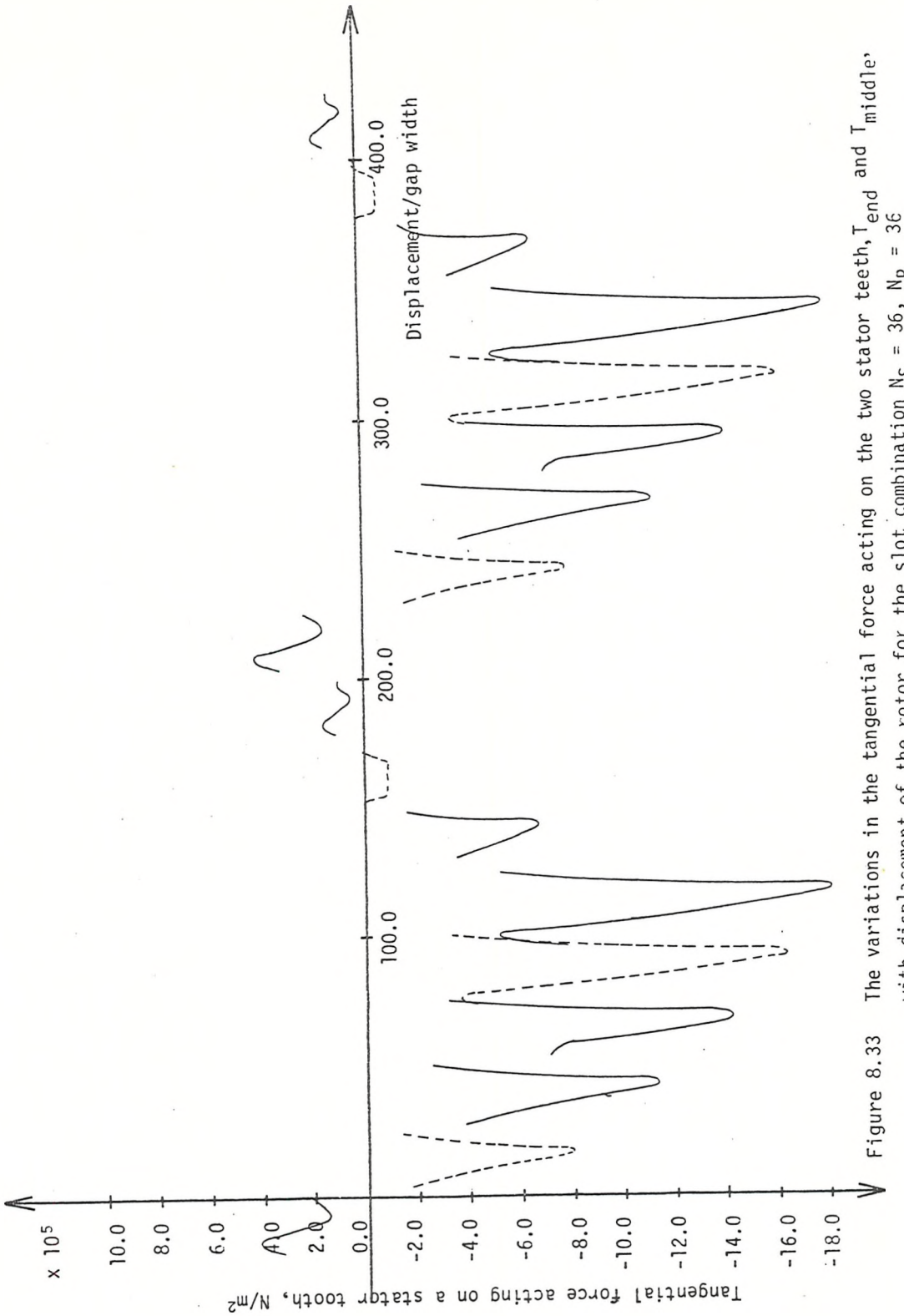

Figure 8.33 The variations in the tangential force acting on the two stator teeth, T_{end} and T_{middle}, with displacement of the rotor for the slot combination $N_S = 36$, $N_R = 36$

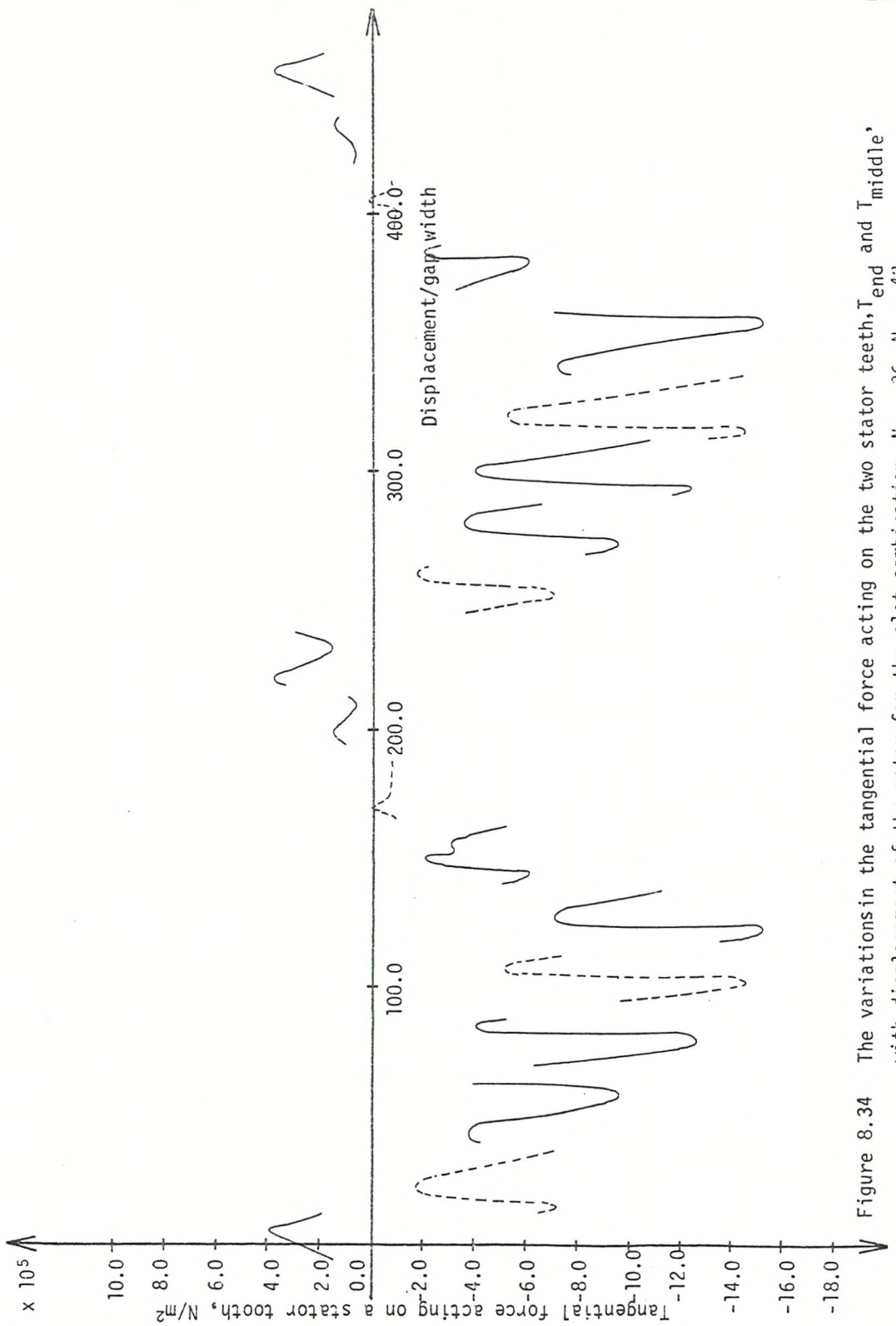

Figure 8.34 The variations in the tangential force acting on the two stator teeth, T_{end} and T_{middle}, with displacement of the rotor for the slot combination $N_S = 36$, $N_R = 42$

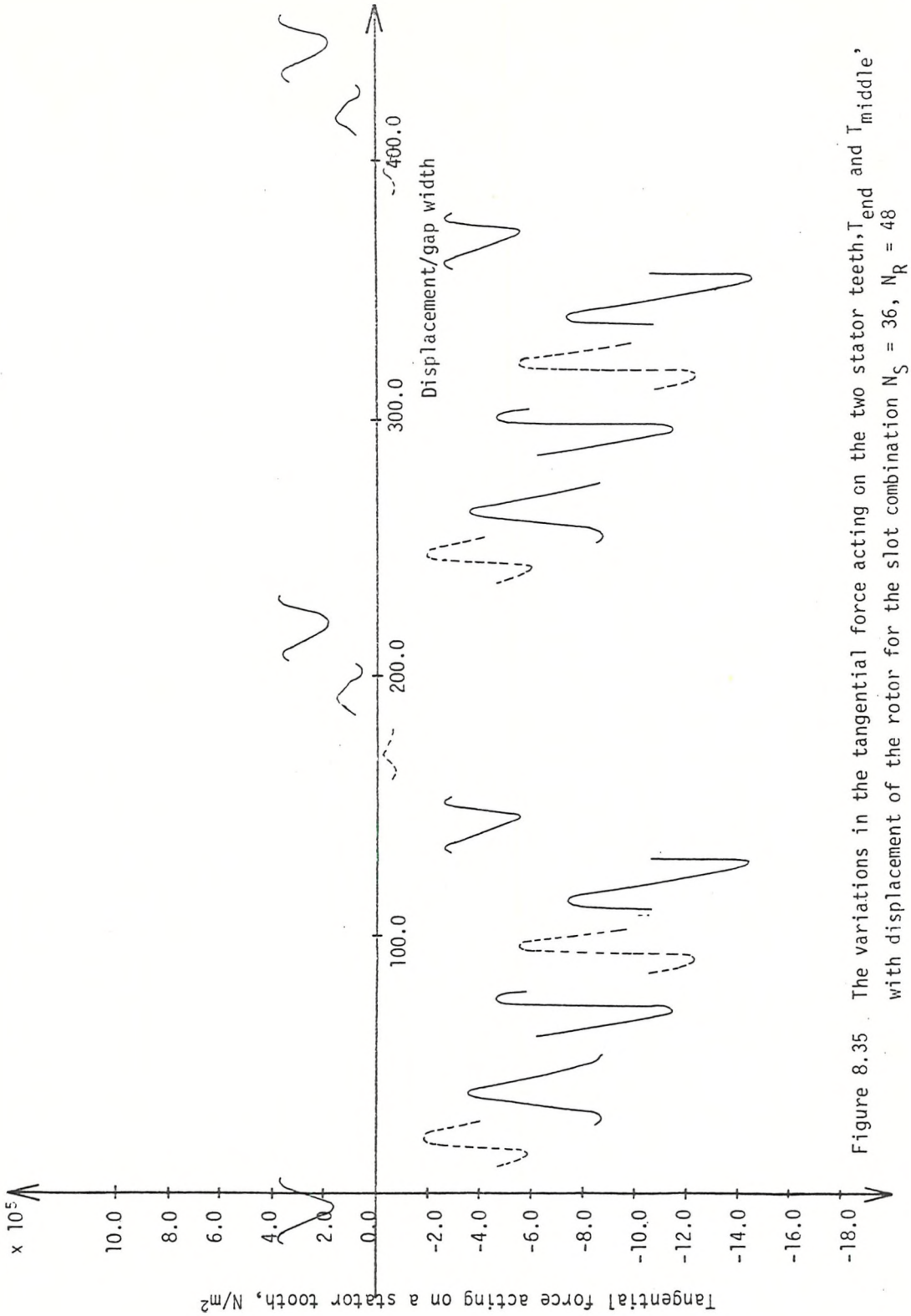

Figure 8.35 The variations in the tangential force acting on the two stator teeth, T_{end} and T_{middle}, with displacement of the rotor for the slot combination $N_S = 36$, $N_R = 48$

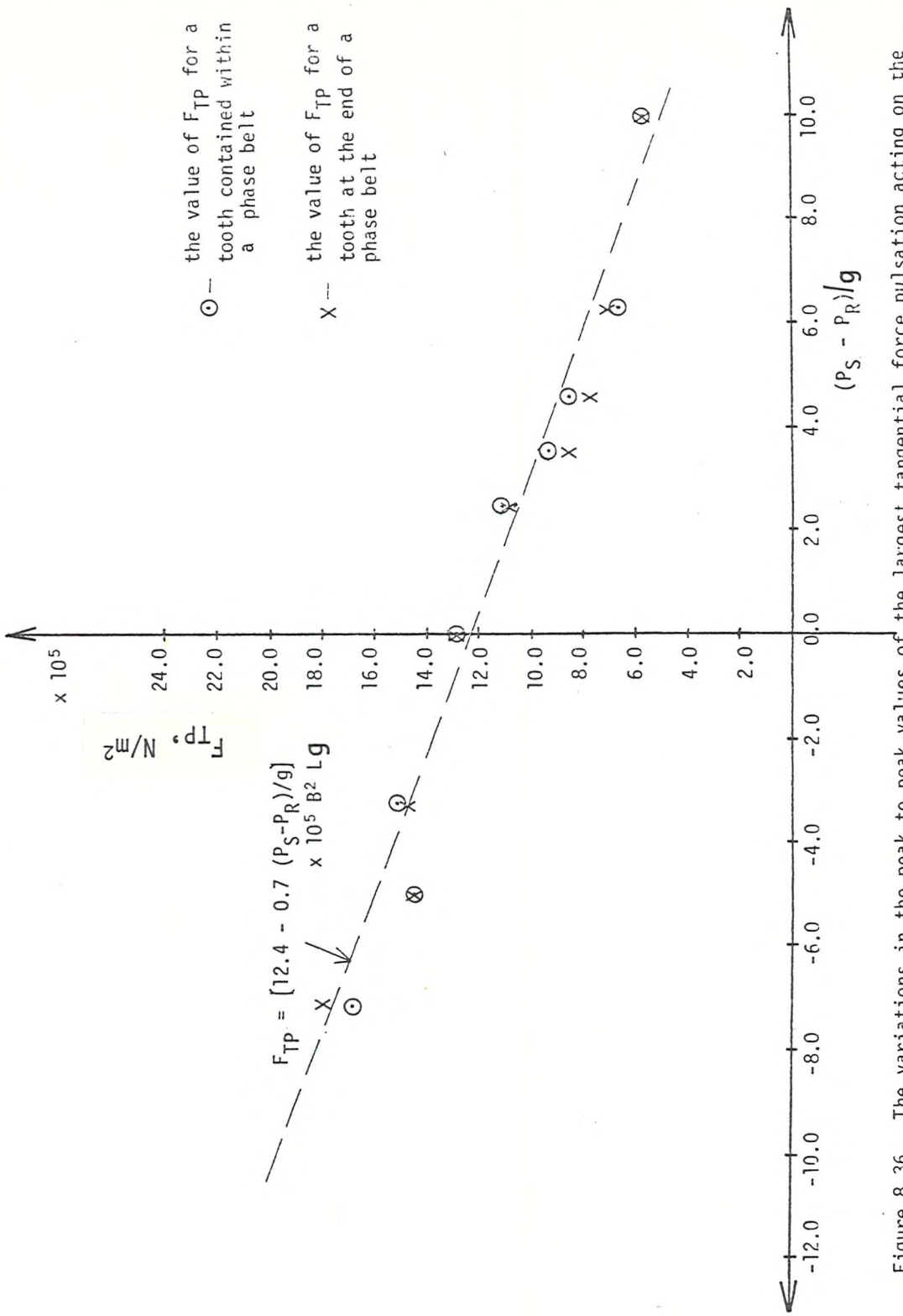

Figure 8.36 The variations in the peak to peak values of the largest tangential force pulsation acting on the two stator teeth (T_{end}, T_{middle}) with the difference in slot pitches

CHAPTER 9

HARMONIC TOOTH-RIPPLE TORQUES ON LOAD

9. Introduction

9.1 Discussion of Results

9.2 Conclusions

9. Introduction

In the previous chapter the tangential forces acting on the stator or rotor teeth, in any rotor position, were represented as a discrete set of parameters distributed in space. In this form, these tangential force distributions were used to obtain the tangential force pulsations acting on a rotor or stator tooth. In addition to obtaining these pulsations, it is also possible, for any rotor position, to use the distribution of tangential forces acting on the stator or rotor teeth to calculate the instantaneous value of torque. Furthermore, the variation of torque with rotor displacement (over a rotor slot pitch) can be investigated by calculating the torque at a number of positions within a rotor slot pitch. The useful and the fundamental tooth-ripple componentsof torque can be extracted from these torque variations using Fourier analysis.

In Section 9.1, the variations of torque with rotor displacement associated with the ten slot combinations are presented.* In addition, the value of the useful torques and the fundamental tooth-ripple components of torque are calculated and these results are discussed. In Section 9.2, some conclusions are drawn about the relationship between the torque variations and slot combination.

9.1 Discussion of Results

Figures 9.1 to 9.10 show the variation of torque with rotor position for each of the ten slot combinations. The useful torque and the fundamental tooth-ripple component of torque are also shown on these figures. The second, third and higher order tooth-ripple components have not been calculated because there are not enough torque values to calculate these components to a sufficiently high accuracy. The values

*All torque values are calculated per double pole pitch.

of the useful torque, the peak value of the fundamental tooth-ripple components of torque and the ratio of the two are presented in Table 9.1 for the ten slot combinations.

Slot Combination	Useful Torque of the Machine (T_m) x 10^5 N/m^3	Peak Value of Fund Tooth-Ripple Torque (T_s) x 10^5 N/m^3	$\frac{T_s}{T_m}$ %
36/24	81.60	8.09	10
36/28	81.77	8.65	11
36/30	79.53	0.00	0
36/32	81.40	36.52	45
36/36	79.53	45.40	57
36/40	78.64	15.72	20
36/42	78.72	0.00	0
36/44	78.09	5.26	7
36/48	77.01	1.10	1
36/60	72.86	1.59	2

Table 9.1

The ten graphs and the results presented in the table are now examined. It is convenient to consider together those slot combinations for which the modulus of the difference in stator and rotor slot number divided by the number of poles is the same.

a) $N_S = 36, \quad N_R = 36 \quad \left| \frac{N_S - N_R}{N_P} \right| = 0$

This slot combination has the largest torque variation as expected. The fundamental tooth-ripple component of torque is very large and there are also significant higher harmonic tooth-ripple components present. The large variation in torque is due to nearly all the tangential force pulsations being in phase with each other, as shown in Figure 9.11. The numbers on the figure denote the positions of the rotor at which the tangential forces were computed.

b) $N_S = 36, \quad N_R = 32 \quad \text{and} \quad N_S = 36, \; N_R = 40 \quad \left| \frac{N_S - N_R}{N_P} \right| = 1$

There are large torque variations associated with both these slot combinations. The fundamental tooth-ripple components of torque are large, but it is significant that the value of this component for the overslotted case is less than half that for the underslotted case. It is clear from Figures 9.4 and 9.6 that the higher harmonic tooth-ripple components are negligible, that is, the variation in torque with rotor position is nearly sinusoidal.

c) $N_S = 36$, $N_R = 30$ and $N_S = 36$, $N_R = 42$ $\left| \frac{N_S - N_R}{N_P} \right| = 1.5$

The torque variations associated with both these slot combinations are small. Furthermore, the nature of these slot combinations are such that the field distribution (and tangential force) associated with any tooth, is the same as that of a tooth a pole pitch away after a rotor displacement of half a rotor slot pitch. This condition arises partly because of the way in which the current distributions are calculated. It results in the torque being periodic in half a rotor slot pitch, so that there is no fundamental tooth-ripple component of torque. It is clear, from Figures 9.3 and 9.7, that the second harmonic tooth-ripple component of torque is small. Thus, whilst the torque is periodic in half a rotor slot pitch, it is significant that the variation over half a slot pitch is small. The phase of the tangential force pulsations are such as to give an almost constant torque (see Figure 9.12).

d) $N_S = 36$, $N_R = 28$ and $N_S = 36$, $N_R = 44$ $\left| \frac{N_S - N_R}{N_P} \right| = 2$

These two slot combinations have relatively small torque variations in comparison with case (b). The fundamental tooth-ripple components of torque are, however, relatively large when compared with

the useful torque (approx. 10%). It is apparent from Figures 9.2 and 9.8 that the higher harmonic tooth-ripple components of torque are small.

e) $N_S = 36$, $N_R = 24$ and $N_S = 36$, $N_R = 48$ $\left| \frac{N_S - N_R}{N_P} \right| = 3$

The slot combination $N_S = 36$, $N_R = 24$ has a large torque variation and a relatively large fundamental tooth-ripple component of torque when compared with the useful torque (10%). It is apparent from Figure 9.1 that there are also significant higher harmonic tooth-ripple components of torque present.

The slot combination $N_S = 36$, $N_R = 48$ has a small torque variation and a small fundamental tooth-ripple component of torque. It is also evident, from Figure 9.9, that there are only small higher harmonic tooth-ripple torques present.

f) $N_S = 36$, $N_R = 60$ $\left| \frac{N_S - N_R}{N_P} \right| = 6$

In this case the torque variation is small and so are all the harmonic torque components.

9.2 Conclusions

(i) The peak value of the fundamental tooth-ripple component of torque can be of the order of 50% of the useful torque for those slot combinations for which the difference between the number of rotor and stator slots is small. On the other hand, this torque component can be small (1%), when compared with the useful torque, for those slot combinations for which the difference between the number of stator and rotor slots is large.

(ii) The magnitude of the torque variation, over a rotor slot pitch, is largely dependent on the relative phases of the tangential force pulsations. A large variation will occur when most of these force

pulsations are in phase with each other. This particularly occurs for those slot combinations for which the difference between the number of stator and rotor slots is small.

(iii) The designer should avoid choosing those slot combinations for which the difference in the number of stator and rotor slots is small, and especially the combination which has an equal number of stator and rotor slots, since these slot combinations have large torque variations and fundamental tooth-ripple components of torque.

(iv) To avoid large harmonic torques, a slot combination should be chosen where the phases of the tangential force pulsations are such as to give an almost constant torque (case c).

(v) The criteria for minimising harmonic tooth-ripple torques and stray load losses associated with the stator and rotor tooth-ripple fluxes are incompatible.

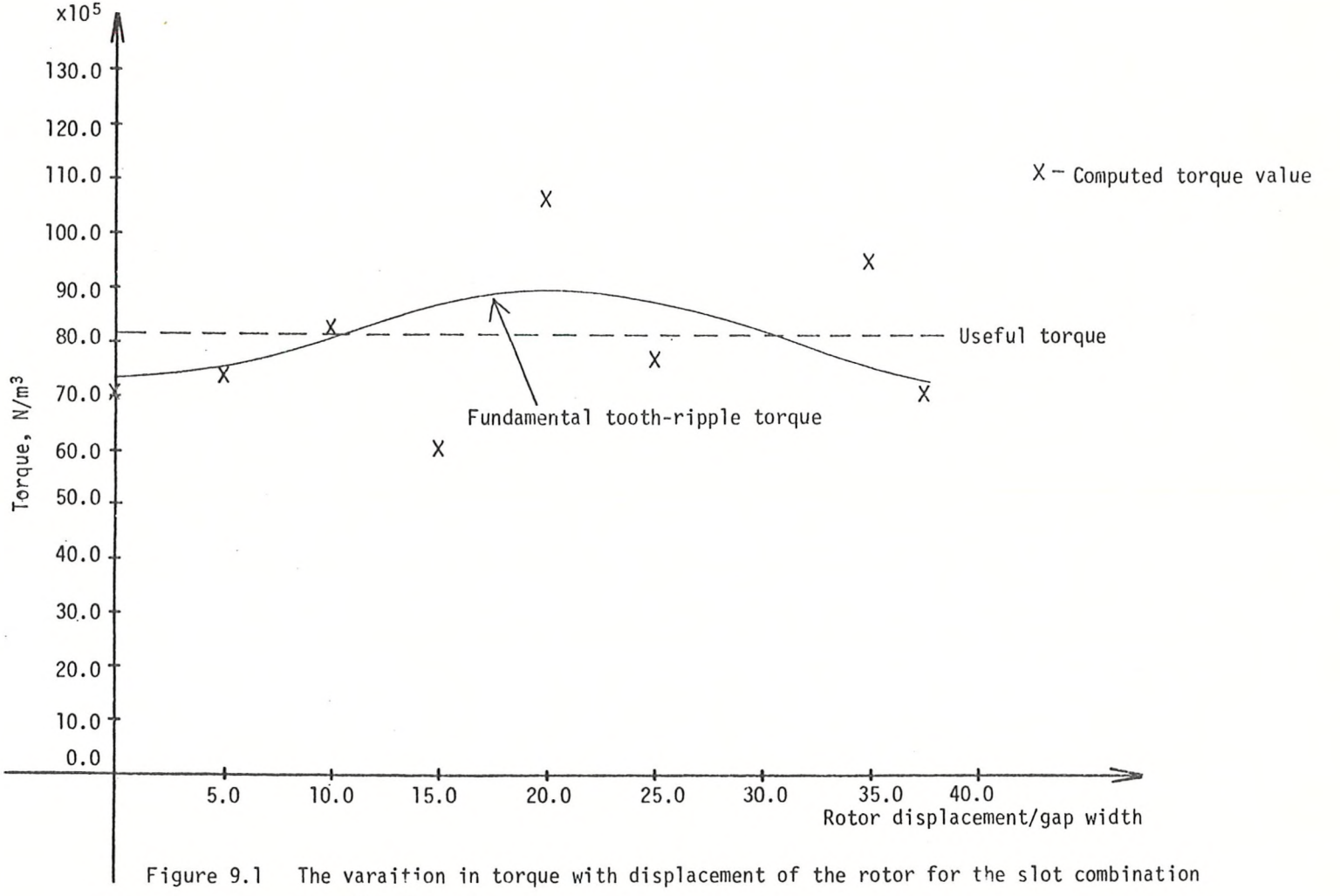

Figure 9.1 The varaition in torque with displacement of the rotor for the slot combination $N_S = 36$, $N_R = 24$

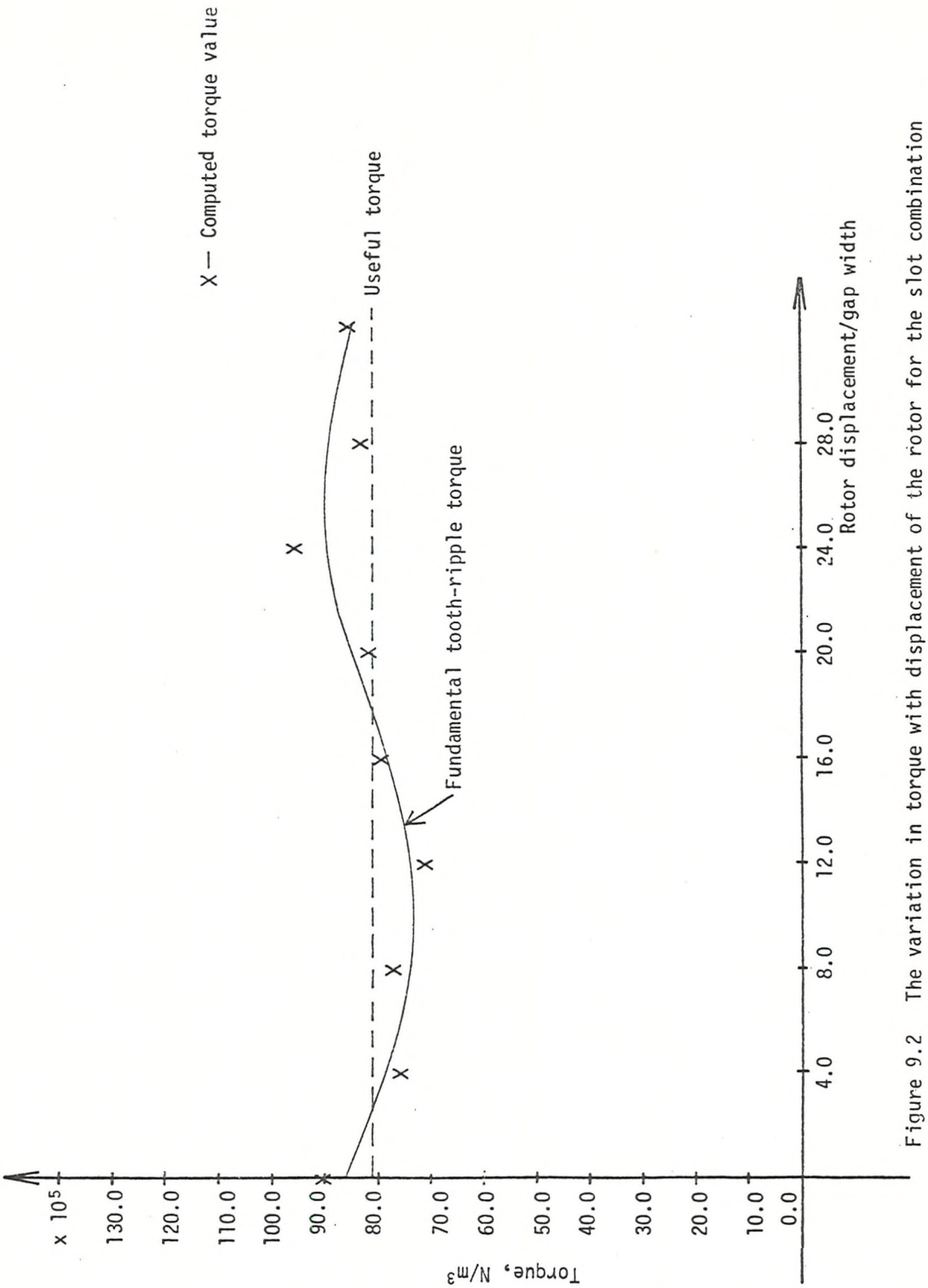

Figure 9.2 The variation in torque with displacement of the rotor for the slot combination $N_S = 36$, $N_R = 28$

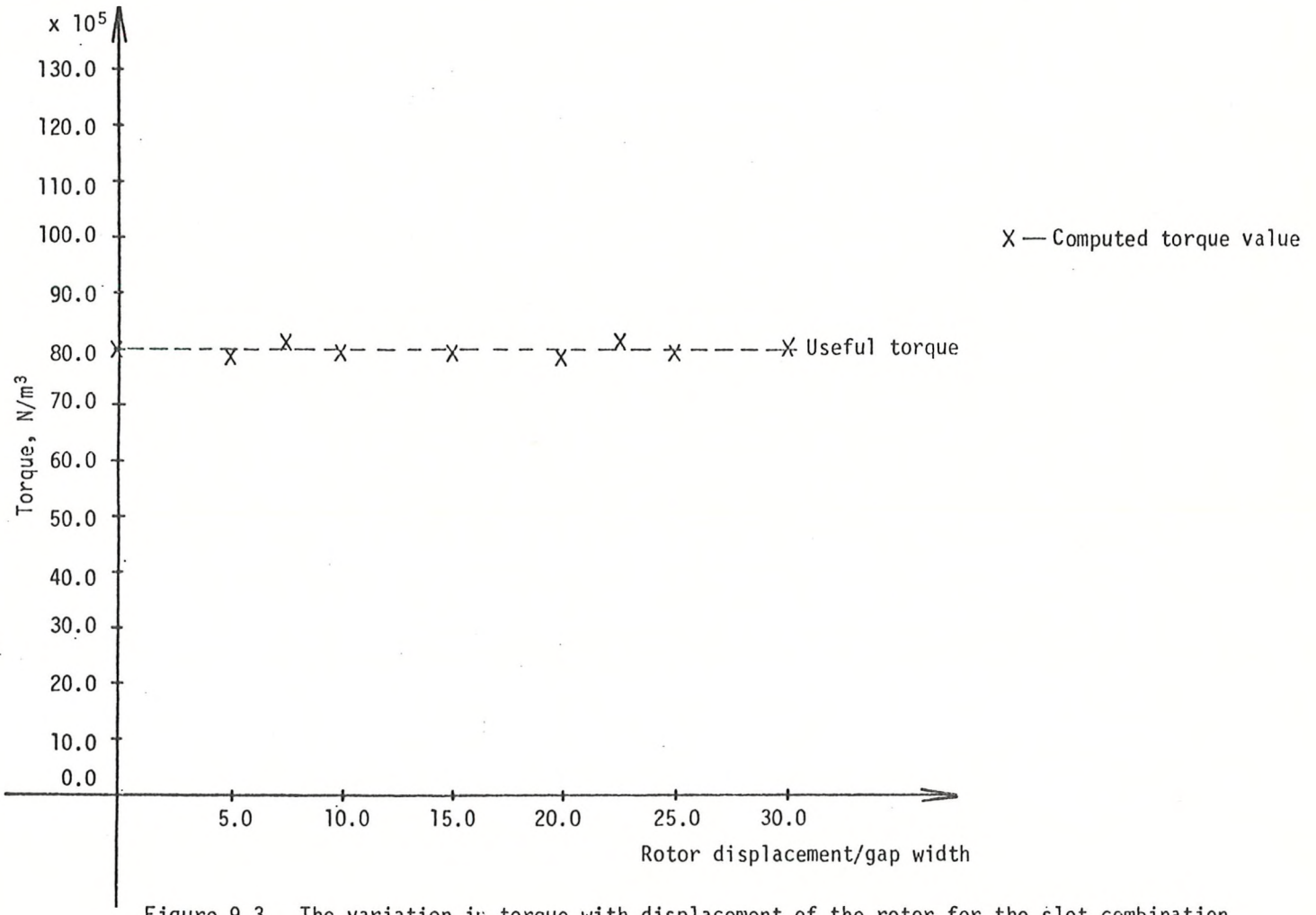

Figure 9.3 The variation in torque with displacement of the rotor for the slot combination $N_S = 36$, $N_R = 30$

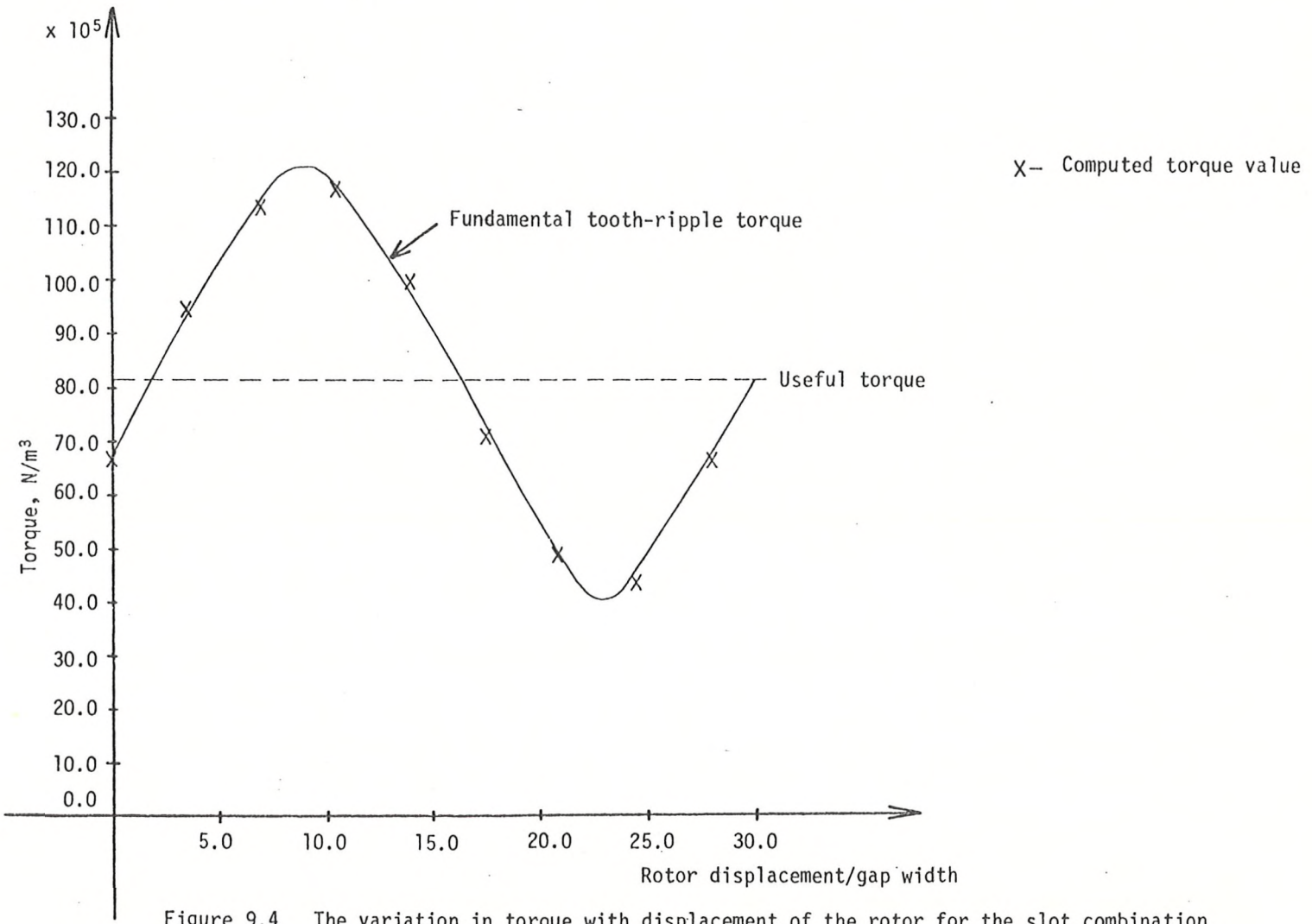

Figure 9.4 The variation in torque with displacement of the rotor for the slot combination $N_S = 36$, $N_R = 32$

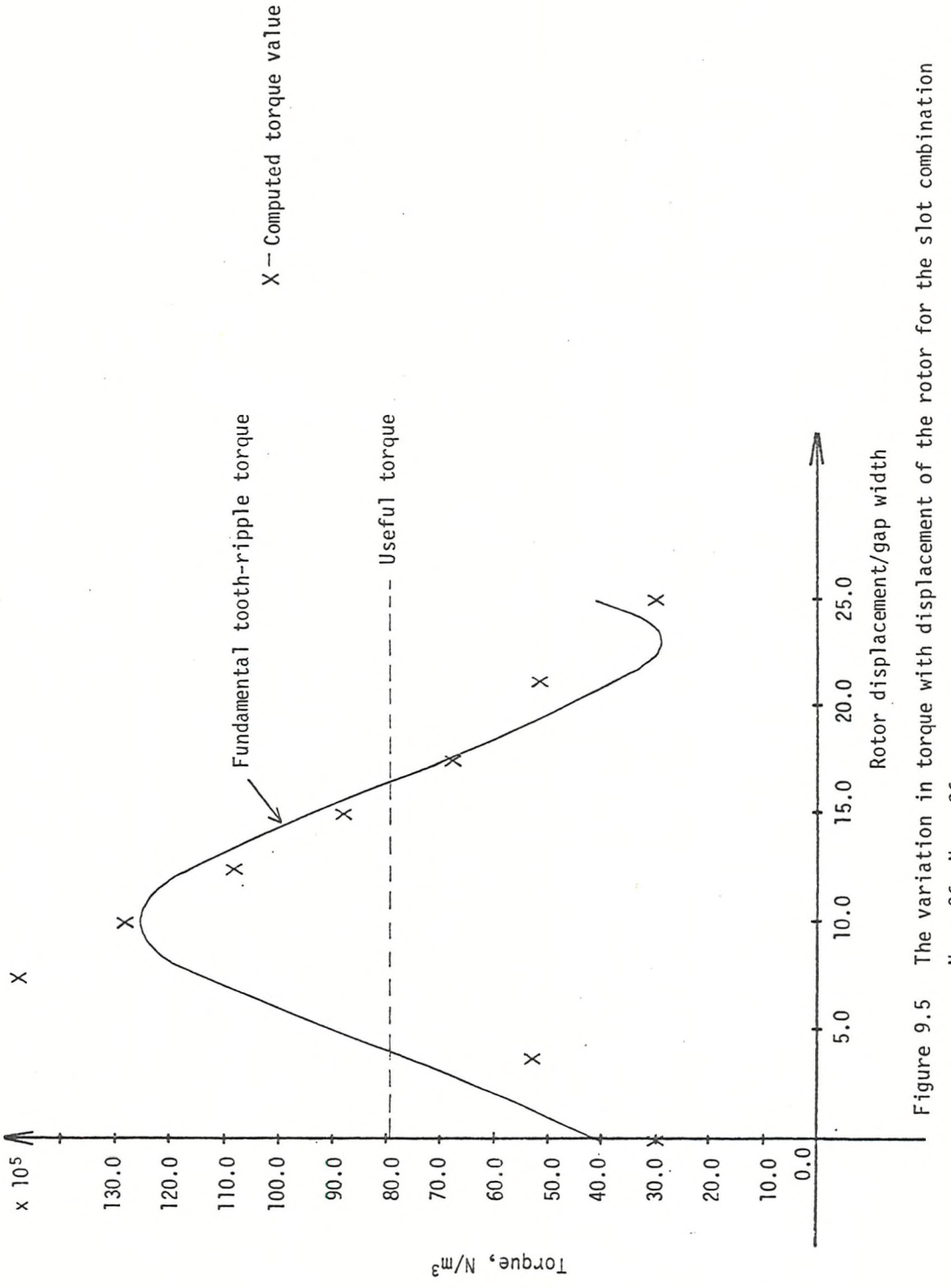

Figure 9.5 The variation in torque with displacement of the rotor for the slot combination $N_S = 36$, $N_R = 36$

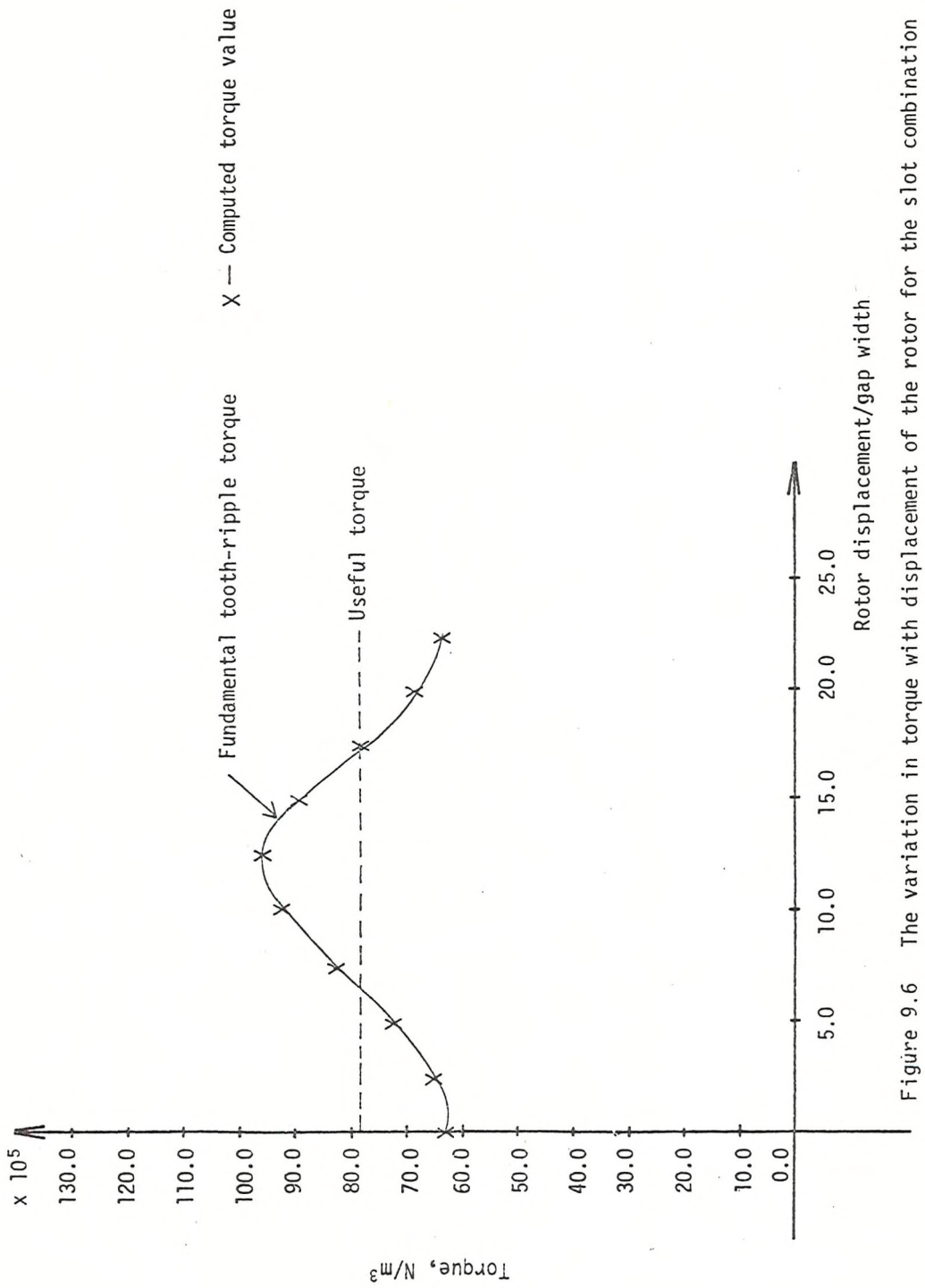

Figure 9.6 The variation in torque with displacement of the rotor for the slot combination $N_S = 36$, $N_R = 40$

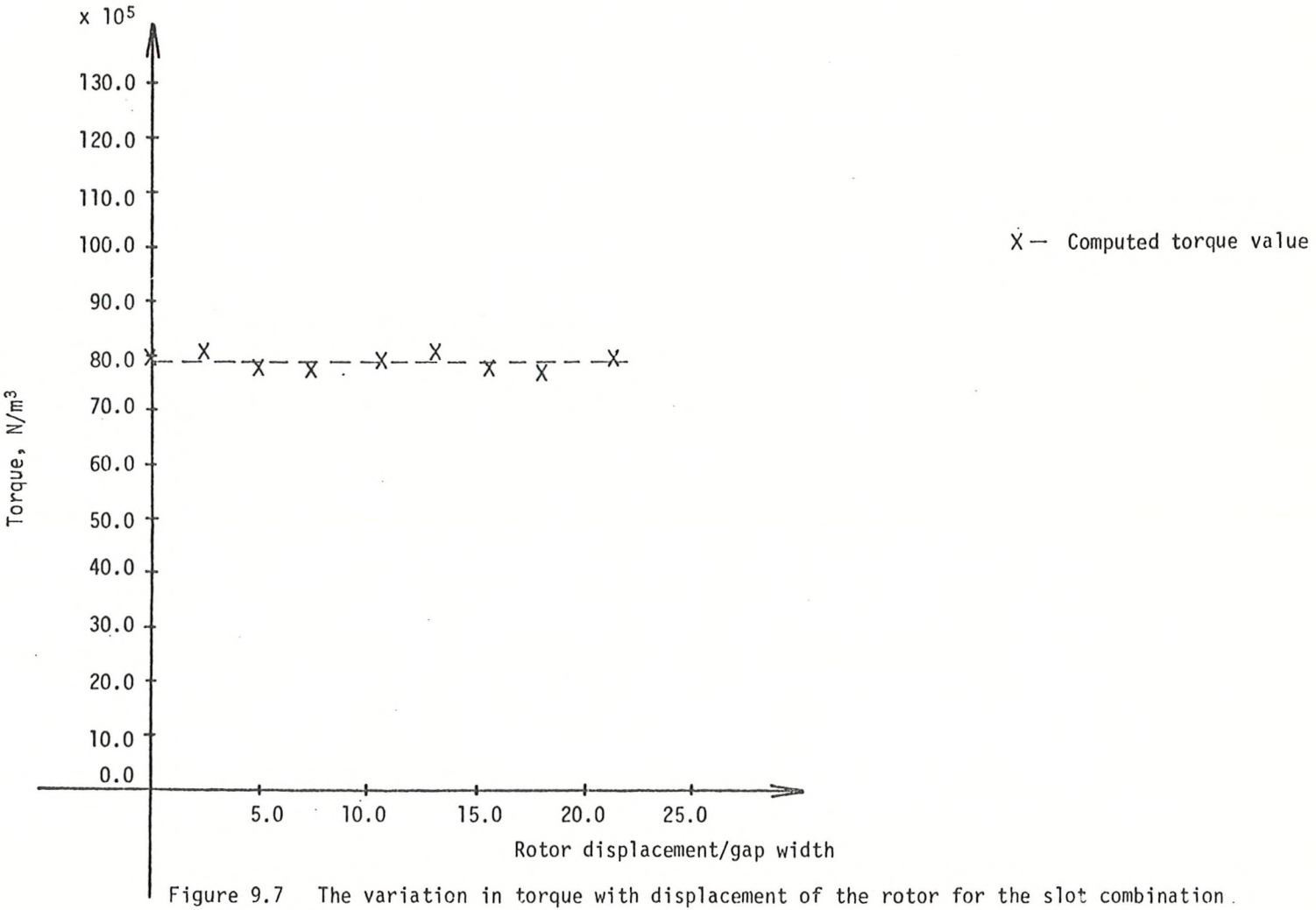

Figure 9.7 The variation in torque with displacement of the rotor for the slot combination $N_S = 36$, $N_R = 42$

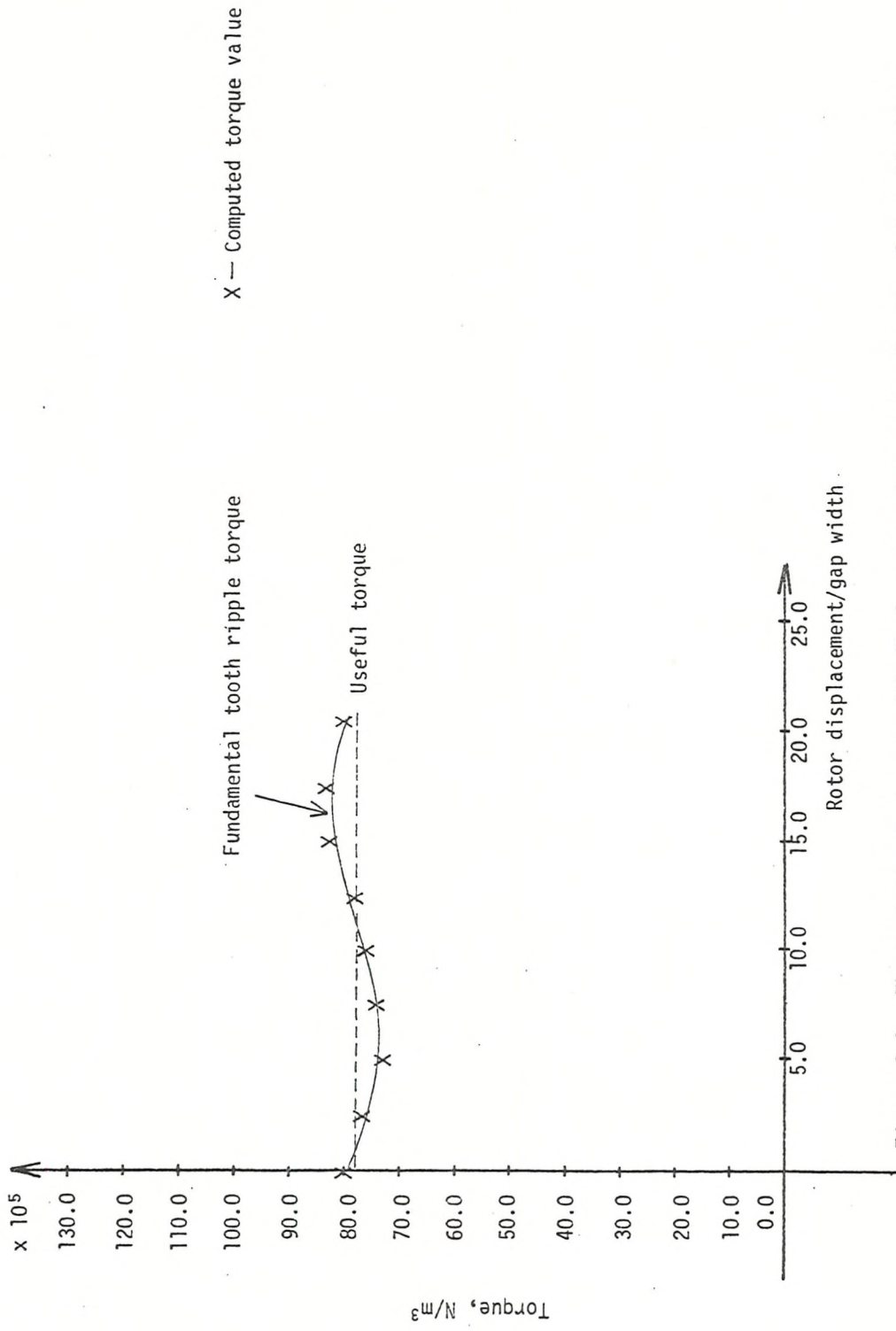

Figure 9.8 The variation in torque with displacement of the rotor for the slot combination $N_S = 36$; $N_R = 44$

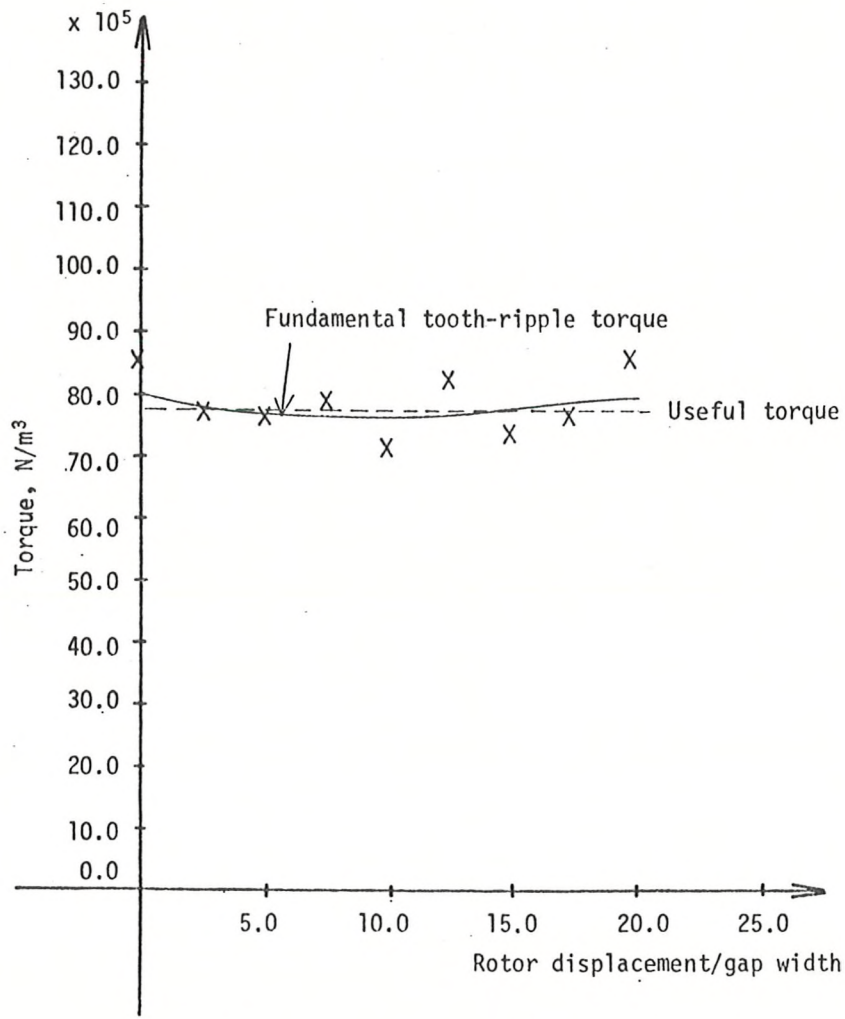

Figure 9.9 The variation in torque with displacement of the rotor for the slot combination $N_S = 36$, $N_R = 48$

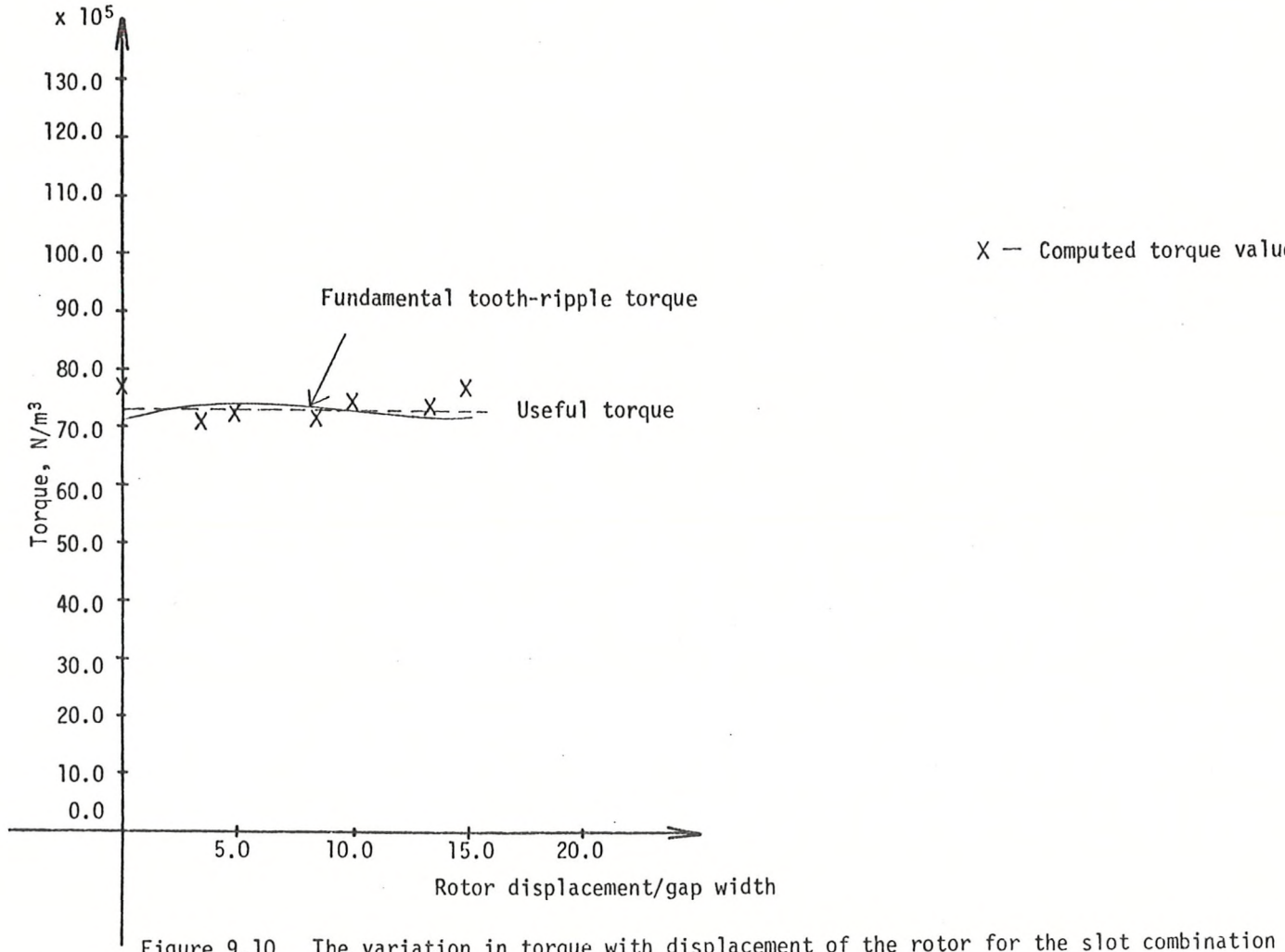

Figure 9.10 The variation in torque with displacement of the rotor for the slot combination $N_S = 36$, $N_R = 60$

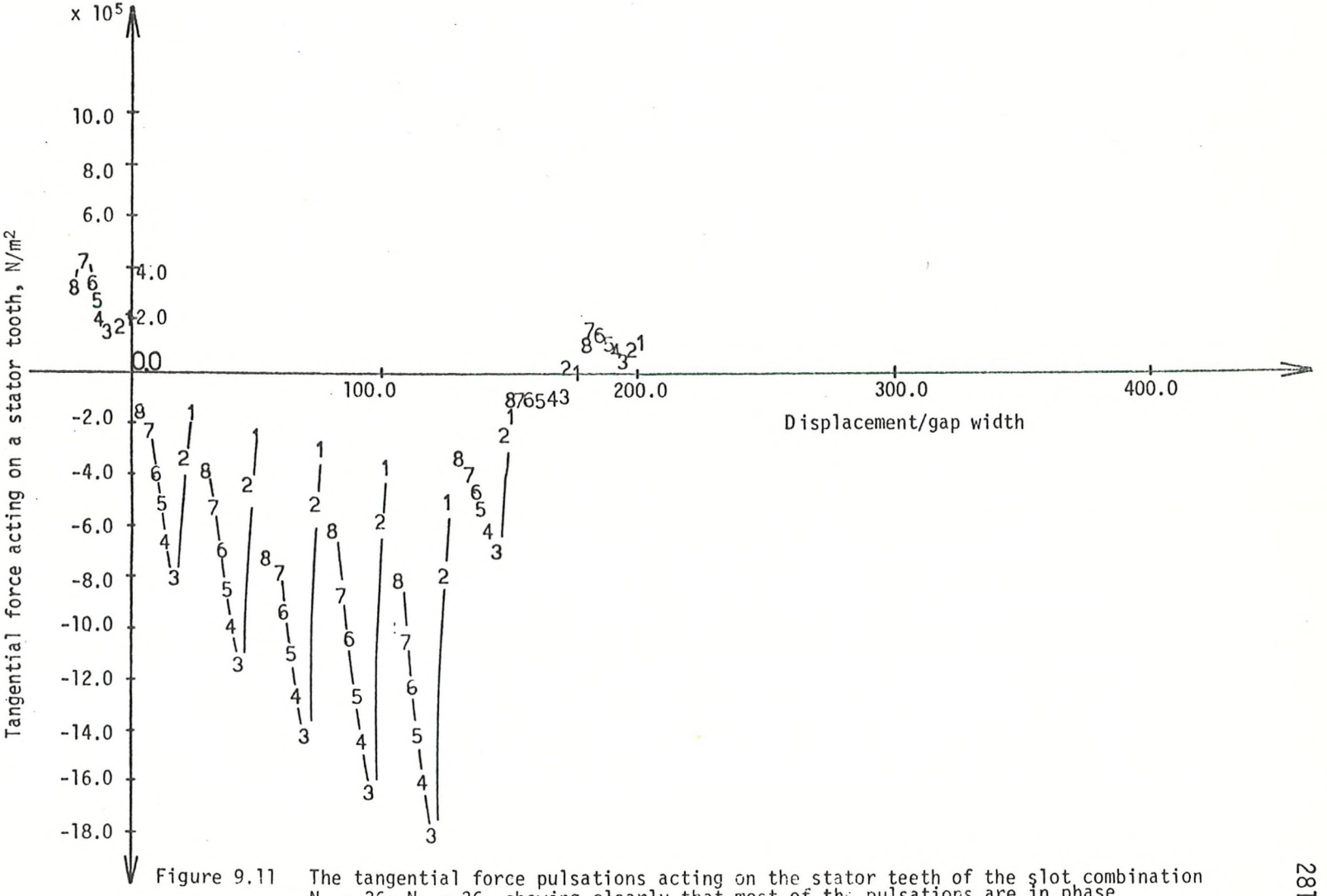

Figure 9.11 The tangential force pulsations acting on the stator teeth of the slot combination $N_S = 36$, $N_R = 36$ showing clearly that most of the pulsations are in phase with each other.

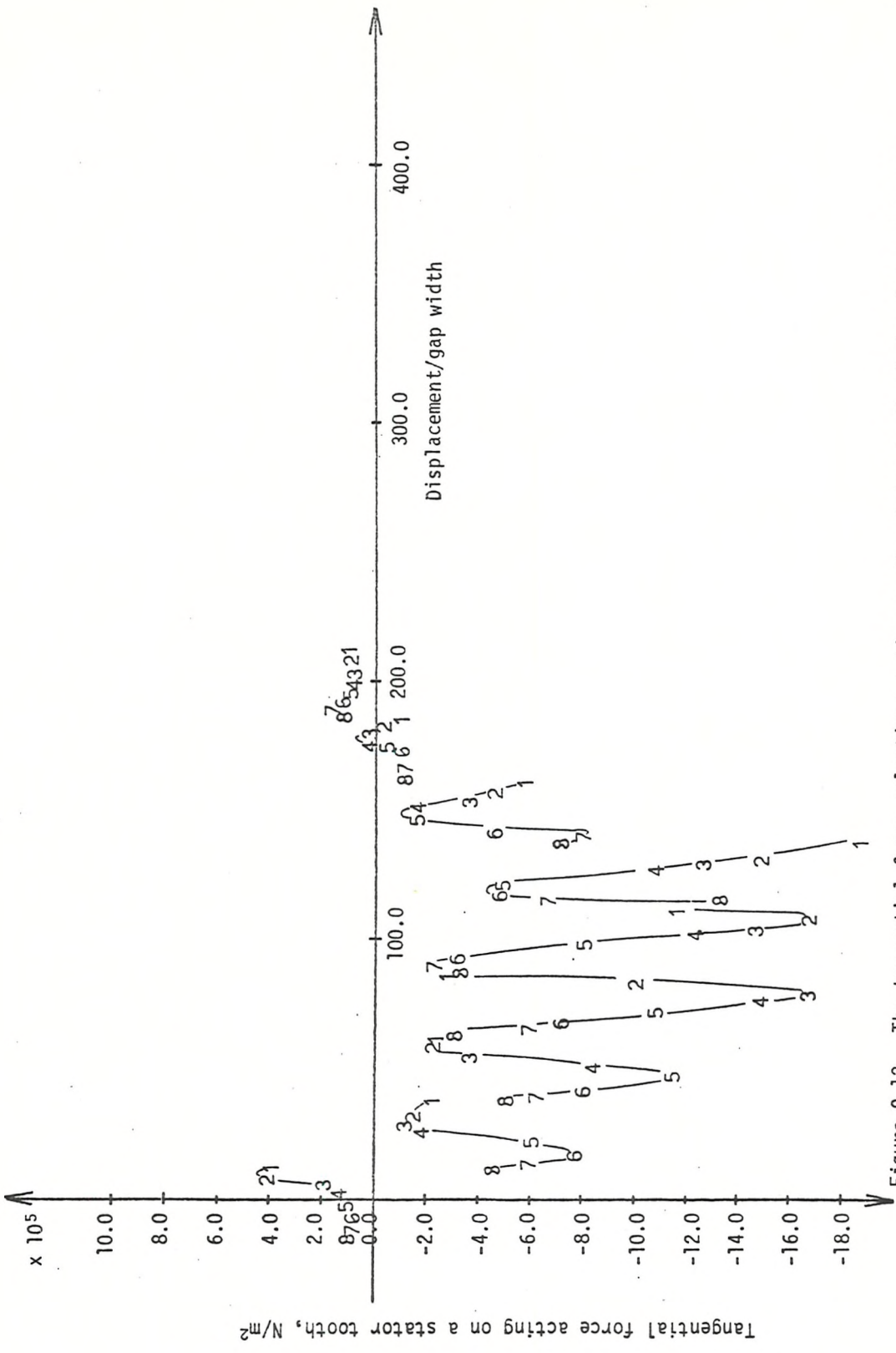

Figure 9.12 The tangential force pulsations acting on the stator teeth of the slot combination $N_S = 36$, $N_R = 30$ showing that the pulsations are not in phase with each other

CHAPTER 10

CONCLUSIONS

10. Introduction

10.1 Summary of Detailed Conclusions

10.1.1 Numerical Evaluation of the Integrals Associated with Conformal Transformation

10.1.2 Tooth-Ripple Flux Pulsations

10.1.3 Normal Tooth-Ripple Force Pulsations

10.1.4 Tangential Tooth-Ripple Force Pulsations

10.1.5 General Conclusion Relating to the Force Pulsations

10.1.6 Harmonic Tooth-Ripple Torques

10.2 Discussion

10.3 Suggestions for Further Work

10.4 Reference

10. Introduction

This thesis is concerned with an examination of tooth-ripple fluxes and forces under load conditions. In addition, the fundamental harmonic tooth-ripple component of torque has been computed for a range of slot combinations. Throughout this research the method of conformal transformation has been used extensively and several ways of improving the accuracy and efficiency of the numerical techniquesassociated with this method have been found. In this chapter, the important conclusions, obtained from the preceding chapters, are summarised and suggestions are made for further research. However, before considering these conclusions, it is useful to review certain aspects of the work discussed in the previous chapters.

When using the method of conformal transformation to solve a Laplacian field in a region having a complicated boundary, it is often necessary to use numerical methods to find the constant terms of the transformation equations. These constant terms are the solution of a set of non-linear simultaneous equations. These equations are formulated by relating the transformation equation to the dimensions of the boundary. The set of non-linear equations are evaluated by using a direct-search routine based on Peckham's method. A full description of the constant finding process is given in Chapter 3. In this process, and when using conformal transformation to evaluate force quantities, it is necessary to evaluate integrals which contain singularities. These integrals are of two types; the first has critical points at both limits of integration, and the second has, in addition to critical points at both limits, a simple pole within the range of integration. This second type of integral is called a Cauchy Principal

Value. In Chapter 4 a number of methods are described for the numerical evaluation of both types of integral. The techniques described in Chapters 3 and 4 should enable any problem involving a Laplacian field and a complicated polygonal boundary to be solved successfully.

In Chapter 5, the method of conformal transformation is used to calculate the flux entering, and the tangential and normal forces acting on, any induction motor tooth under load. The assumptions underlying the use of this method are clearly stated. However, it is important to emphasise that the flux distribution around a tooth and the tangential and normal force acting on it are obtained by a combination of the solutions of the air-gap fields in three separate regions. The first region contains two displaced slots (doubly-slotted boundary) and it is important to note that the gap flux density becomes almost uniform at a point on the tooth surface remote from the slot openings because the air-gap is narrow. The second region contains one slot (singly-slotted boundary) and the gap flux density is uniform at a point on the tooth surface remote from the slot opening. The third region has no slots and the gap flux density is assumed uniform everywhere. The field solutions in these separate regions can be combined because, for all practical air-gap dimensions, points can be found on the teeth surfaces (where the teeth overlap) sufficiently remote from the slot openings for the gap flux density to be assumed uniform.

The tangential and normal forces acting on a tooth are obtained by integrating the Maxwell stress function over the appropriate surfaces. It is not possible by this or any other method to determine uniquely how the the stress is distributed over the tooth, since it is not possible to represent the iron by a unique set of magnetic sources. The use of the Maxwell stress function has the advantages that the

force can be obtained as a function of the complex potential function and that it is economic in computer time and storage.

The analysis described in Chapter 5 is incorporated into a computer program which can be used to calculate the flux entering, and the tangential and normal forces acting on, any induction motor tooth under load. This program has been used extensively in the calculation of tooth-ripple fluxes, forces and harmonic torques. It is believed that it is one of the fastest programs available for calculating the two-dimensional air-gap field in an induction motor.

In calculating the air-gap field, under load conditions, there are some additional parameters not present in the no-load case. For example, under no-load conditions, the air-gap field is main flux dominated so that the field may be calculated by assuming a simple potential difference to exist across the gap. The exact type of stator winding is unimportant under these conditions. Under load conditions, however, there are additional leakage flux components associated with both the stator winding and the rotor cage, and these must be considered in the calculation of the air-gap field under load. With regard to the stator winding it is neither practical nor necessary to consider all types of stator winding in the analysis. The main object is to determine conditions under which the flux and force pulsations in the stator and rotor teeth are minimal. Each m.m.f. harmonic will modulate the fundamental and harmonic tooth-ripple frequencies, but, if the fundamental carrier is small, so will the resultant effect be small. The tooth-ripple carrier is critically dependent on the slot dimensions, and these are fixed by the designer, when he chooses the rotor slot number.

Another important parameter under load conditions is the load current level. This can be conveniently expressed in terms of the

stator magnetising current. The value of this ratio is dependent on the actual size of the machine. Its value is close to unity for a small machine and quite large for a machine of megawatt rating. However, undesirable effects, such as flux and force pulsations due to load, begin gradually and increase as the load is increased. This is important because different machine sizes do not have to be considered in isolation except for small machines which are stator winding resistance dominated.

It should be emphasised that the damping effect of the cage on the flux and force pulsations has been neglected. To include this effect it would be necessary to specify the type of cage used so that the appropriate resistances and reactances can be calculated. From a practical point of view only a few cages can be considered, but it is known that the relative merits of different slot combinations are not critically dependent on cage design. Whilst the damping influence of the cage is beneficial in reducing flux and force harmonics, it does not critically effect the choice of slot combination. In short, a bad choice of slot combination can only be slightly improved by cage design; its relative merits compared to other choices remain largely the same.

In Chapter 6, a method is described for calculating, for a set of imposed stator currents, an approximate rotor current distribution. In all but very small machines, the magnetising flux is constant, for a given terminal voltage, and consequently the resultant air-gap m.m.f. is also constant as load changes. Furthermore, in large induction motors, the air-gap m.m.f. is remarkably sinusoidal because of the damping action of the cage. Therefore, an approximate rotor m.m.f. distribution can be obtained by subtracting the sinusoidal air-gap m.m.f. from the stator m.m.f. associated with the stator load current. From this rotor m.m.f. distribution, the currents can be obtained for any

rotor position relative to the stator.

The tooth-ripple flux pulsations in a rotor and stator tooth, for a range of slot combinations, are presented in Chapter 7. These flux pulsations are obtained by computing the flux distributions at a number of rotor positions within a rotor slot pitch. Under quasistatic field conditions, the flux and force distributions associated with a tooth are the same after a rotor displacement of a rotor slot pitch. Therefore, the flux pulsations in all the rotor teeth over a rotor slot pitch, can be combined to give the complete time history of the tooth-ripple flux in a single rotor tooth as the tooth is displaced through a double pole pitch. In the case of the stator, leakage fluxes produce additional effects dependent upon the position of the tooth relative to the phase belt. These additional effects are superimposed on the travelling air-gap field. It is necessary, therefore, to compute separately the time history of the tooth-ripple flux in a tooth at the end of a phase belt and a tooth contained within a phase belt.

It is shown in Chapter 7 that the most important defining quantity for both the stator and rotor is the peak to peak value of the largest flux pulsation relative to the fundamental flux wave. This quantity is related to the slot pitch difference, for both the stator and rotor, by two simple equations. These equations are used to determine conditions under which the tooth-ripple flux pulsations are minimal.

The variations in the normal and tangential forces acting on a rotor and a stator tooth for a range of slot combinations are presented in Chapter 8. The peak to peak value of the largest normal and tangential force pulsations acting on a rotor and stator tooth are related to the slot pitch difference by four simple equations. These equations are used to determine the conditions under which the normal and tangential force pulsations acting on the rotor and stator teeth are minimal.

In Chapter 9 the variations in torque, over a rotor slot pitch, are obtained for a range of slot combinations. From these torque variations the fundamental component of tooth-ripple torque is extracted using Fourier analysis. A comparison is made of the torque variations and fundamental tooth-ripple torques produced by the various slot combinations.

The above paragraphs briefly describe the work and the important conclusions made in the previous chapters. The detailed conclusions that can be drawn from this work are given in Section 10.1. These are discussed in Section 10.2 and general recommendations about the choice of slot combination are made. Finally, in Section 10.3 suggestions are made for further work.

10.1 Summary of Detailed Conclusions

10.1.1 Numerical Evaluation of the Integrals Associated with Conformal Transformation

In Chapter 4, a number of numerical methods for the evaluation of the definite and improper integrals encountered in the use of conformal transformation methods are described and compared.

Four methods are described for the evaluation of the definite integral with critical points at both limits of integration. Results of reasonable accuracy can be obtained, for a number of problems, by displacing the limits of integration from the singularities and using Simpson's quadrature. The definite integral may also be evaluated by a simple change of variable. The Gauss-Jacobi method can be used to obtain results of high accuracy but this is a difficult method to program. The method of Branders and Piessens is particularly suitable for the evaluation of the definite integral because results of high accuracy can be obtained. Furthermore, a computer package exists for this method which allows the user to specify the degree of accuracy required.

Cauchy Principal Values arise with boundaries having parallel sides. Two methods have been developed for the evaluation of this type of integral. The first is an extension of the Clenshaw-Curtis method to include integrals with critical points at both limits of integration and a simple pole within the range of integration. The second method is based on the technique of subtracting out the singularity. Both methods can give results of high accuracy but the latter method is more efficient in computer time and storage.

10.1.2 Tooth-Ripple Flux Pulsations

The calculation of the tooth-ripple flux pulsations under load is described in Chapter 7. The following conclusions can be drawn from this analysis.

(i) The peak to peak value of the largest flux pulsation into a rotor tooth as a fraction of the fundamental flux wave is closely related to the slot pitch difference by the equation

$$\frac{\Phi_{TP}}{\Phi_{FP}} = -0.068\ (P_R/g - P_S/g) + 0.21 \quad \text{if } P_S/g > P_R/g$$

and

$$\frac{\Phi_{TP}}{\Phi_{FP}} = 0.21 \quad \text{if } P_R/g \geq P_S/g$$

for constant rotor and stator slot widths of 5.0/g and 7.5/g respectively. This choice of slot widths was made because together with the slot pitches, these dimensions represent practical air-gap dimensions. However, it should be noted that the influence of slot openings on the flux and force pulsations does not significantly effect the choice of slot pitches, but simply makes these pulsations more or less acute. Therefore, it is reasonable to choose any practical slot widths in the examination of tooth-ripple flux and force pulsations on load.

(ii) The peak to peak value of the largest flux pulsation into a stator tooth as a fraction of the fundamental flux wave is closely related to the slot pitch difference by the equation

$$\frac{\Phi_{TP}}{\Phi_{FP}} = -0.068\ (P_S/g - P_R/g) + 0.10 \qquad \text{if } P_R/g > P_S/g$$

and

$$\frac{\Phi_{TP}}{\Phi_{FP}} = 0.10 \qquad \text{if } P_S/g \geq P_R/g$$

for constant rotor and stator slot widths of 5.0/g and 7.5/g respectively.

(iii) It is clear from the equations in (i) and (ii) that the stator and rotor tooth-ripple flux pulsations obey equations of a similar form.

(iv) The criteria for minimising stator and rotor flux pulsations on load are incompatible.

(v) Tooth losses inevitably become large, but in one member only, if the slot number difference is very large.

(vi) The criterion for minimising tooth flux pulsations on load is similar to that for no-load operation.

10.1.3 Normal Tooth-Ripple Force Pulsations

The calculation of tooth-ripple normal force pulsations is described in Chapter 8. The following conclusions emerge from this work.

(i) The peak to peak value of the largest normal force pulsation acting on a rotor tooth is closely related to the slot pitch difference by the equation

$$F_{NP} = \left(69 + (P_R - P_S)/g\right) \times 10^5\ B^2\ L\ g$$

for constant rotor and stator slot widths of 5.0/g and 7.5/g respectively.

(ii) The peak to peak value of the largestnormal force pulsations acting on a stator tooth is closely related to the slot pitch difference by the

equation

$$F_{NP} = \left(69 - 6\ (P_S - P_R)/g\right) \times 10^5\ B^2\ L\ g$$

for constant rotor and stator slot widths of 5.0/g and 7.5/g respectively.

(iii) The normal force pulsations acting on the stator and rotor teeth increase on load with an increase in $(P_R - P_S)$ but the relationship is more sensitive for the stator teeth.

(iv) The criterion for low stator force pulsations is similar to the no-load case $(P_S > P_R)$

(v) In the case of the rotor, the effect of slot combination on the normal force pulsations is not very significant and the effect of load (leakage flux) is to change the relative amplitudes for load and no-load.

10.1.4 Tangential Tooth-Ripple Force Pulsations

The calculation of the tangential tooth-ripple force pulsations is presented in Chapter 8. The following conclusions can be drawn from this work:

(i) The peak to peak value of the largest tangential force pulsation acting on a rotor tooth is closely related to the slot pitch difference by the equation

$$F_{TP} = \left(13.0 + 0.37\ (P_R - P_S)/g\right) \times 10^5\ B^2\ L\ g$$

for constant rotor and stator slot widths of 5.0/g and 7.5/g respectively.

(ii) The peak to peak value of the largest tangential force pulsation acting on a stator tooth is closely related to the slot pitch difference by the equation

$$F_{TP} = \left(12.4 - 0.7\ (P_S - P_R)/g\right) \times 10^5\ B^2\ L\ g$$

for constant rotor and stator slot widths of 5.0/g and 7.5/g respectively.

(iii) As in the case of the normal force pulsations, the tangential force

pulsations acting on the stator and rotor teeth increase with an increase in $(P_R - P_S)$. This relationship is more sensitive for the stator teeth.

(iv) The tangential force pulsations acting on the rotor and stator teeth are small when compared with the normal force pulsations. This conclusion is the same as for the no-load case.

(v) As regards the stator, the criterion for low tangential force pulsations on load ($P_S > P_R$) differs from that of the no-load case. However, the effect of a change in slot combination on the tangential force pulsations is not very significant when compared with the effect on the normal force pulsations.

(vi) In the case of the rotor, the effect of slot combination on the tangential force pulsations is not very significant.

10.1.5 General Conclusions Relating to the Force Pulsations

(i) Since stator normal force pulsations are a basic cause of 'magnetic noise', attention should be concentrated on the reduction of this cause of core vibration and the choice of rotor slotting is critical in this respect.

(ii) It is unlikely that the stator tangential force pulsations make a significant contribution to core vibration. However, it is possible that they can cause the teeth in a large machine to vibrate, if the resonant frequency of such teeth lies within the tooth-ripple frequency range.

10.1.6 Harmonic Tooth-Ripple Torques

The calculation of the harmonic tooth-ripple torques is presented in Chapter 9. The following conclusions emerge from this analysis.

(i) The peak value of the fundamental tooth-ripple component of torque can be of the order of 50% of the useful torque for those slot combinations for which the difference between the number of rotor and stator slots is small. On the other hand, this torque component can be small, compared with the useful torque, for those slot combinations in which the difference between the number of stator and rotor slots is large.

(ii) The magnitude of the torque variation, over a rotor slot pitch, is largely dependent on the relative phases of the tangential force pulsations. A large variation will occur when most of these force pulsations are in phase with each other. This occurs particularly for those slot combinations in which the difference in stator and rotor slot number is small.

(iii) The designer should obviously avoid choosing those slot combinations for which the difference in the number of stator and rotor slots is small, and especially the combination which has an equal number of stator and rotor slots, since these slot combinations have large torque variations and fundamental tooth-ripple components of torque.

(iv) To avoid large harmonic torques, a slot combination should be chosen in which the phases of the tangential force pulsations are such as to give an almost constant torque.

(v) The criterion for minimising harmonic tooth-ripple torques and stray losses associated with stator and rotor tooth-ripple fluxes are incompatible.

10.2 Discussion

The occurrence of parasitic fluxes, forces and torques associated with the slotting in induction motors is strongly dependent on the rotor and stator slot numbers.

It is clear from the rules in Sections 10.1.2 to 10.1.6 that there is no overall optimum since specific criteria are incompatible. However, when a choice of rotor slotting is available, the balance between excessive stray loss, vibration producing forces and harmonic tooth-ripple torques can be changed in the light of these criteria.

It has been shown that the criteria for minimising the losses associated with stator and rotor flux pulsations are incompatible. An effort should be made to keep the difference in stator and rotor slot numbers as small as possible consistent with satisfying other design criteria. This condition is the same as that obtained for the no-load case.

The amplitude of the normal force pulsations can be minimised by making $P_S/g > P_R/g$, that is, by making $N_R > N_S$. However, it is also important to recognise that the relative phases of the pulsations are important in noise studies, since even in machines in which the force pulsations are small, the phase of the pulsations can be such as to produce a force wave having a long wavelength. Such a force wave can produce significant core vibration. In this thesis it has been shown how the applied electromagnetic force pulsations can be computed under complex load conditions. The method described here for computing these force pulsations can be applied to any machine and used in a study of noise and vibration associated with the stator core of that machine.

In a similar manner, the method described here for computing the tangential force pulsations can be applied to large machines in a study of the vibration of a single tooth.

It is clearly important to avoid slot combinations for which the stator and rotor slot numbers are close in value, as such a machine has a large torque variation and fundamental tooth-ripple component of

torque. It has been shown that the magnitude of the harmonic torque is largely dependent on the relative phases of the tangential force pulsation. A large torque variation occurs when most of these force pulsations are in phase with each other.

Conformal transformation has proved to be a most suitable method for the investigation of tooth-ripple fluxes, forces and torques in induction motors.

10.3 Suggestions for Further Work

Subjects for further research on parasitic effects under load are suggested below;

(i) Investigation of the effect of varying the stator and rotor slot widths on the tooth-ripple fluxes, forces and harmonic torques. As discussed in Section 6.2, the designer has only a limited choice of stator and rotor slot openings. For example, the stator slot openings must be large enough to allow the stator to be wound, although it is well-known that if the stator slot openings are too large this gives rise to excessive tooth losses in the rotor. Of course, these losses may be reduced by inserting magnetic wedges into the slot mouths. There is little point in considering either a very small or large stator slot opening when examining flux or force pulsations. In the case of the rotor, large stator flux pulsations will occur if the rotor slot openings are too large. To avoid this, semi-closed slots are normally used, so that there is little point in considering a large rotor slot opening.

(ii) Calculation of the high frequency damping currents caused by the relative motion of the slotted surfaces and examination of the effects these currents have on the tooth-ripple fluxes, forces and torques. These currents may be obtained for a specific cage, by first calculating the

change in flux in all the rotor teeth for a small rotor displacement (for example, half a rotor slot pitch). These flux values can, of course, be computed using the program described in Chapter 5. The e.m.f. associated with each tooth can be calculated simply as the change in flux entering the tooth divided by the time taken to displace the rotor. The damping currents can be found by using the e.m.f. values to solve the circuit equations associated with the rotor winding. The resistances and reactances of the bars can either be obtained using an appropriate model[10.1] or by direct measurement.

(iii) The applied electromagnetic normal force pulsations can be used in a study of core vibration. The choice of a suitable model to represent the stator core, frame and windings is clearly of great importance in obtaining realistic results. The tangential force pulsations can be used in a study of noise and vibration produced by a single tooth.

(iv) Determination of the equivalent open slot widths of a range of commercially used slot profiles. It has been shown in Chapter 4 that the method of conformal transformation can be applied to complicated slot shapes. It is hoped to extend this analysis to other slot profiles. Clearly, it will be important to account for the effects of saturated tooth tips on the local flux density distribution.

(v) Refinement of the computer program described in Chapter 5 so that the user has only to specify the air-gap dimensions (slot widths and pitches) and the load current level.

10.4 Reference

10.1 SWANN, S. A. and SALMON, J. W. : 'Effective resistance and reactance of a rectangular conductor placed in a semi-closed slot', Proc. I.E.E., 1963, 110, (9), pp.1656-1662.

APPENDIX 1

THE ANALYTICAL SOLUTION OF AN ELLIPTIC INTEGRAL

The object of this appendix is to obtain an analytical solution to the integral

$$Z = K \int \frac{\sqrt{(t+t_0)(t+t_1)(t-t_2)(t-t_4)}\, dt}{t\,(t+1)(t-t_3)} \qquad (A1.1)$$

This integral can be expressed in the following form

$$Z = K \int \frac{(t+t_0)(t+t_1)(t-t_2)(t-t_4)}{t\,(t+1)(t-t_3)} \frac{dt}{\sqrt{Q}} \qquad (A1.2)$$

where $Q = (t+t_0)(t+t_1)(t-t_2)(t-t_4)$. The polynomial Q may be expressed in terms of even powers only by using the transformation $t = (a+bz)/(1+z)$. Then $dt/\sqrt{Q}$ becomes of the form

$$\frac{C}{\sqrt{(z^2 - A^2)(z^2 - B^2)}} \qquad (A1.3)$$

where A, B and C are constants.

The rational part of equation (A1.2) can be expressed in partial fractions of the form

$$A_1 + \frac{A_2}{(a_1 + a_2 z)} + \frac{A_3}{(a_3 + a_4 z)} + \frac{A_4}{(a_5 + a_6 z)} + \frac{A_5}{(a_7 + a_8 z)} \qquad (A1.4)$$

where A_1, A_2, A_3, A_4, A_5, a_1, a_2, a_3, a_4, a_5, a_6, a_7 and a_8 are constants. Thus equation (A1.1) can be expressed in the following form

$$Z = K.C \left(\int \frac{A_1\, dz}{\sqrt{(z^2-A^2)(z^2-B^2)}} + \int \frac{A_2\, dz}{(a_1+a_2z)\sqrt{(z^2-A^2)(z-B)}} \right.$$
$$\left. + \text{the 3 remaining terms which are of the same form as the second term} \right) \qquad (A1.5)$$

Let $x = Az$, then the first term in equation (A1.5) becomes

$$A \int \frac{dx}{\sqrt{(1-x^2)(1-K'^2x^2)}} \qquad \text{(A1.6)}$$

where A is a constant and $K' = A/B$. This term is an elliptic integral of the first kind to modulus K' and is equal to $F(x,K')$.

Consider the second term in equation (A1.5), which after applying the transformation $x = Az$ becomes

$$A'_1 \int \frac{dx}{(a_1+a_2Ax)\sqrt{(1-x^2)(1-K'^2z^2)}} \qquad \text{(A1.7)}$$

By multiplying the numerator and denominator of the integrand by $(a_1 - a_2 Ax)$, equation (A1.7) can be separated into the following two integrals

$$A'_1 \left(\int \frac{a_1\, dx}{(a_1^2-a_2^2A^2x^2)\sqrt{(1-x^2)(1-K'^2x^2)}} + \int \frac{a_2 A x\, dx}{(a_1^2-a_2^2A^2x^2)\sqrt{(1-x^2)(1-K'^2x^2)}} \right) \qquad \text{(A1.8)}$$

The first term in equation (A1.8) is an elliptic integral of the third kind to modulus K' and is equal to $\pi(x, k, k').B_1$ where $K_1 = a_2A/a_1$ and $B_1 = a_1A'_1$. The second term in equation (A1.8) can be integrated in terms of elementary functions by substituting $y = x^2$, which makes the term under the root sign a quadratic, and then y - (a constant) $= 1/v$, which converts the integral to the form

$$C_1 \int \frac{dv}{\sqrt{[(v-s)^2 + \ell^2]}} = C \sinh^{-1} \frac{v-s}{\ell} \qquad \text{(A1.9)}$$

where C_1, s and ℓ are constants.

The remaining three terms in equation (A1.5) can be treated in exactly the same way as the second. The analytical solution of equation (A1.1) is thus given by

$$Z = K \left[A\, F(x, k') + \sum_{i=1}^{4} B_i\, \Pi\, (x, k_{1i}, k') + \sum_{i=1}^{4} C_i \sinh^{-1} \frac{(v_i - \ell_i)}{s_i} \right] \qquad \text{(A1.10)}$$

The numerical evaluation of the third elliptic integral is most easily performed in Jacobian notation, by putting $x = \mathrm{sn}u$ and $k_1 = k'\mathrm{sn}\alpha$. The Jacobian form of the third elliptic integral, π_j, is given by

$$\pi(x,k_1,k') = u + \frac{\mathrm{sn}\alpha}{\mathrm{cn}\alpha\ \mathrm{dn}\alpha}\ \pi_j(u,\alpha) \qquad \text{(A1.11)}$$

and it can be shown that

$$\pi_j(u,\alpha) = \tfrac{1}{2}\log \frac{\Theta(u-\alpha)}{\Theta(u+\alpha)} + u\,Z(\alpha) \qquad \text{(A1.12)}$$

The theta function can be evaluated from a Fourier series

$$\Theta(\alpha) = 1 + 2\sum_{n=1}^{\infty}(-1)^n q^n \cos\frac{n\pi\alpha}{k} \qquad \text{(A1.13)}$$

in which $q = e^{-\pi k'/k}$. Also, $Z(\alpha)$ is defined as $E(\alpha) - F(\alpha)\,E/k'$.

In this way, the integral as a whole can be expressed in terms of elliptic integrals of the first and second kind, which have been tabulated or which can be evaluated from well-known series.

BIBLIOGRAPHY

The literature referred to in this thesis is listed below in alphabetical order. Following each reference is the chapter or chapters in which it appears.

ALGER, P. L. : 'The nature of induction machines',(Gordon and Breach, 1965). Chapters 1, 2 and 7.

BINNS, K. J. : 'Calculation of some basic flux quantities in induction and other doubly slotted electrical machines', Proc. I.E.E., 1964, 111, (11), pp.1847-1858. Chapters 1 and 2.

BINNS, K. J. : 'Cogging torques in induction machines', Proc. I.E.E., 1968, 115, (12), pp.1783-1790. Chapter 2.

BINNS, K. J. : 'The magnetic field and centring force of displaced ventilating ducts in machine cores', Proc. I.E.E., 1961, 108C, pp.64-70. Chapters 1 and 2.

BINNS, K. J. : 'Numerical methods of conformal transformation', Proc. I.E.E., 1971, 118, (7), pp.909-910. Chapter 4.

BINNS, K. J., KAHAN, P. A., REES, G. R., SIMKIN, J. and TROWBRIDGE, C. W. : 'A comparison of two methods of field solution for slotted boundary shapes in two dimensions', Proc. Compumag, Oxford, 1978. Chapters 1 and 2.

BINNS, K. J. and LAWRENSON, P. J. : 'Analysis and computation of electric and magnetic field problems', (Pergamon, 1973). Chapters 2, 3, 4 and 5.

BINNS, K. J. and ROWLANDS-REES, G. : 'Main flux pulsations and tangential tooth-ripple forces in induction motors', Proc. I.E.E., 1975, 122, (3), pp.273-277. Chapters 1, 2, 6, 7 and 8.

BINNS, K. J. and ROWLANDS-REES, G. :'Radial tooth-ripple forces in induction motors due to the main flux', Proc. I.E.E., 1978, 125, (11), pp.1227-1231. Chapters 1, 2 and 8.

BINNS, K. J., ROWLANDS-REES, G. and KAHAN, P. A. : 'The evaluation of improper integrals encountered in the use of conformal transformation', Journal of Numerical Methods in Engineering, Vol. 14, pp 567-580, 1979. Chapters 2 and 3.

BINNS, K. J. and SCHMID, E. : 'Some concepts involved in the analysis of the magnetic field in cage induction machines', Proc. I.E.E., 1975, 122, (2), pp.169-175. Chapters 1, 6 and 7.

BRANDERS, M. and PIESSENS, R. : 'An extension of Clenshaw-Curtis Quadrature', J. Comp. and Appl. Maths., 1, 1975, pp.55-57. Chapter 4.

CARPENTER, C. J. : 'Surface-integral methods of calculating forces on magnetised iron parts', Proc. I.E.E., 1960, 107C, pp.19-28. Chapters 1 and 2.

CARTER, F. W. : 'The magnetic field of the dynamo-electric machine', Journal I.E.E., 1926, pp.1115-1138. Chapter 5.

CARTER, F. W. : 'Magnetic noise in dynamo-electric machines', Engineering, 1932, pp.548-551. Chapter 1.

CLENSHAW, C. W. and CURTIS, A. R. : 'A method for numerical integration on an automatic computer', Num. Maths., 1962, 2, pp.197-205. Chapter 4.

COHEN, A. M., CUTTS, J. F., FIELDER, R., JONES, D. E., RIBBANS, J. and STUART, E. : 'Numerical analysis', (McGraw Hill, 1973), Chapter 3.

DAVIS, P. J. and RABINOWITZ, P. : 'Methods of Numerical Integration', (Academic Press, 1975). Chapter 4.

DVORACEK, A. I. : 'Forces on the teeth in d.c. machines', Trans. A.I.E.E., 1962-63, 81, pp.1054-1061. Chapter 1.

EASTHAM, J. F. and BALCHIN, M. J. : 'Pole-change windings for linear induction motors', Proc. I.E.E., 1975, 122, (2), pp.154-160. Chapter 1.

EASTHAM, J. F. and WILLIAMSON, S. : 'Generalised theory of induction motors with asymmetrical air-gap and primary windings', Proc. I.E.E., 1973, 120, (7), pp.767-775. Chapter 1.

ELLISON, A. J. and MOORE, C. J. : 'Acoustic noise and vibration of rotating electric machines', Proc. I.E.E., 115, (11), pp.1633-1640. Chapters 1 and 8.

FOX, L. and MAYER, D. G. : 'Computing Methods for Scientists and Engineers', (Clarendon Press, Oxford, 1968). Chapter 4.

FOX, L. and PARKER, I. B. : 'Chebyshev Polynomials in Numerical Analysis', (Oxford University Press, London, 1968). Chapter 4.

FREEMAN, E. M. : 'The calculation of harmonics due to slotting in the flux-density waveform of a dynamo-electric machine', Proc. I.E.E., 1962, 109C, p.581. Chapter 4.

FREEMAN, E. M. : 'Travelling waves in induction machines, input impedance and equivalent circuits', Proc. I.E.E., 1968, 115, (12), pp.1772-1776. Chapter 4.

FREEMAN, E. M. and LOWTHER, D. A. : 'Normal force in single sided linear induction motors', Proc. I.E.E., 1973, 120, (12), pp.1499-1505. Chapter 1.

GIBBS, W. J. : 'Conformal transformation in electrical engineering', (Chapman and Hall, 1958). Chapter 2.

HAMMOND, P. : 'Applied electromagnetism', (Pergamon Press, 1971). Chapter 2.

HELLER, B. and HAMATA, V. : 'Additional fields, forces and losses in the induction machine', Publishing House of the Czechoslovakia Academy of Science, NCSAV, 1961. Chapter 1.

HELLER, B. and HAMATA, V. : 'Harmonic Field Effects in Induction Machines', (Elsevier Scientific Publishing Company, 1977). Chapter 7.

HELLER, B. and JOKL, A. L. : 'Tangential forces in squirrel-cage induction motors', I.E.E.E. Trans, 1969, PAS-88, pp.484-492. Chapter 1.

HOWE, D. : 'The application of numerical methods to the conformal transformation of polygonal boundaries', J. Inst. Maths. Applics., 1973, 12, pp.125-136. Chapter 4.

IMHOF, J. P. : 'On the method for numerical integration of Clenshaw and Curtis', Num. Maths., 1963, 5, p.138. Chapter 4.

JABBAR, M. A. : 'Analysis of the performance of a permanent-magnetic a.c. machine', Ph.D. Thesis, University of Southampton, 1977. Chapter 1.

JAWSON, M. A. : 'Integral equation methods in potential theory 1', Proc. Roy. Soc. A., 1963, 275, pp.23-32. Chapter 1.

KRYLOV, V. I. : 'Approximate calculation of integrals', (London and New York, Macmillan, 1962). Chapter 4.

LAWRENSON, P. J. and GUPTA, S. K. : 'Conformal transformation employing direct-search techniques of minimisation', Proc. I.E.E., 1968, 115, (3), pp.427-431. Chapters 3 and 4.

LEHMANN, T. H. : 'The calculation of magnetic attraction', Trans. A.I.E.E., 1926, 45, pp.383-394. Chapter 1.

LIEBMANN, G. : 'The change in air-gap flux in electrical machines due to the displacement of opposed slots', Proc. I.E.E., 1957, 104C, pp.102-118. Chapter 1.

LIWSCHITZ, M. M. : 'Field harmonics in induction motors', Trans. Am. Inst. Elec. Eng., 1942, 61, pp.797-803. Chapters 1 and 7.

LIWSCHITZ-GARIK, M. and WHIPPLE, C. : 'A.C. machines', (Van Nostrand, 1961, 2nd Edition). Chapter 1.

MURTHY VAMARAJU, S. R. : 'Improvements in numerical techniques for conformal transformation with particular reference to electromagnetic fields', I.E.E.E. Transaction on Magnetics, 1978, 14 (4), pp.233-240. Chapter 4.

NORRIE, D. H. and VRIES, G. : 'The finite element method', (Academic Press, 1973). Chapter 1.

OBERRETL, K. : 'New facts about parasitic torques in induction motors', Bulletin Oerlikon, 1962, 348, pp.130-155. Chapter 1.

OBERRETL, K. : 'The field harmonic theory of the squirrel cage motor, taking multiple armature reaction and parallel winding branches into account', Arch. Elektrotech., 1965, 49, pp. 343-364 (in German). Chapter 1.

O'HARA, H. and SMITH, F. J. : 'Error estimation in the Clenshaw-Curtis quadrature formula', Comp. Journal, 1968, 11, pp.213-219. Chapter 4.

PATTERSON, T. N. L. :' The optimum addition of points to quadrature formulae', Maths. Comp., 1968, 22, pp.847-856. Chapter 4.

PECKHAM, G. : 'A new method for minimising a sum of squares without calculating gradients', The Computer Journal, 1970, 13, pp.418-420. Chapter 3.

PHILLIPS, G. M. and TAYLOR, P. J. : 'Theory and Application of Numerical Analysis', (Academic Press, 1973). Chapter 5.

POWELL, M. J. D. : 'A method for minimising a sum of squares of non-linear functions without calculating derivatives', The Computer Journal, 1965, 7, pp.303-307. Chapter 3.

RICHTER, R. : 'Elektrische Maschinen, Vol. 4 - Die Induktions machinen', (Verlag Birkhaüser, 1954). Chapter 1.

ROBERTSON, B. L. and TERRY, J. A. : 'Analytical determination of magnetic fields', Trans. Am. Inst. Elect. Engrs., 1929, 48, pp.1242-69. Chapter 5.

ROBINSON, A. C. : 'Harmonics in a.c. rotating machines', Proc. I.E.E., 1962, 109C, pp.380-387. Chapter 1.

ROWLANDS-REES, G. : 'Analysis of no -load force pulsations and cogging torques in induction machines', Ph.D. Thesis, University of Southampton, 1978. Chapters 1, 2, 3, 4 and 5.

SAY, M. G. : 'Alternating current machines', (Pitman, 1976). Chapter 2.

SCHWARZ, K. K. : 'Survey of basic stray losses in squirrel cage induction motors', Proc. I.E.E., 1964, 111, (9), pp.1565-1574. Chapter 1.

SELBY, S. M. : 'Standard Mathematical Tables', (C.R.C., 1973). Chapter 5.

SILVESTER, P. and CHARI, M. V. K. : 'Finite element solution of saturable magnetic field problems', I.E.E.E. Trans., 1970, PAS-89, pp.1642-1651. Chapters 1 and 2.

SIMKIN, J. and TROWBRIDGE, C. W. : 'Magnetostatic fields computed using an integral equation derived from Green's theorem', Proc. Compumag, Oxford, 1976. Chapter 1.

SMITH, F. J. : 'Quadrature methods based on the Euler-Maclaurin formula and on the Clenshaw-Curtis method of integration', Num. Maths., 1965, 7, pp.406-411.

STOLL, R. L. and HAMMOND, P. : 'Calculation of the magnetic field of rotating machines - Pt. 4, Approximate determination of the field and losses associated with eddy currents in conducting surfaces', Proc. I.E.E., 1965, 112, (11), pp.2083-2094. Chapter 1.

STROUD, A. H. and SECREST, D. : 'Gaussian quadrature formulae', (New Jersey, Prentice Hall, 1966). Chapter 4.

SWANN, S. A. and SALMON, J. W. : 'Effective resistance and reactance of a rectangular conductor placed in a semi-closed slot', Proc. I.E.E., 1963, 110, (9), pp.1656-1662. Chapter 10.

WILLIAMSON, S. : 'The anisotropic layer theory of induction machines and induction devices', J. Inst. Maths. Applics., 1976, 17, No. 1, pp.69-84. Chapter 1.

WILLIAMSON, S. and SMITH, A. C. : 'Layer theory analysis for integral-bar induction devices', 2nd Compumag Conference, Grenoble, September 1978. Chapter 1.

WILLIAMSON, S. and SMITH, A. C. : 'Field analysis for rotating induction machines and its relationship to the equivalent-circuit method', Proc. I.E.E., 1980, 127, Pt. B, 2, pp.83-90. Chapter 1.